

UNCLASSIFIED

AD 669 121

**BEHAVIOR OF MISSILE SILO CLOSURES DESIGNED TO RESIST
HIGH OVERPRESSURES**

Robert M. Iten, et al

Illinois University
Urbana, Illinois

March 1968

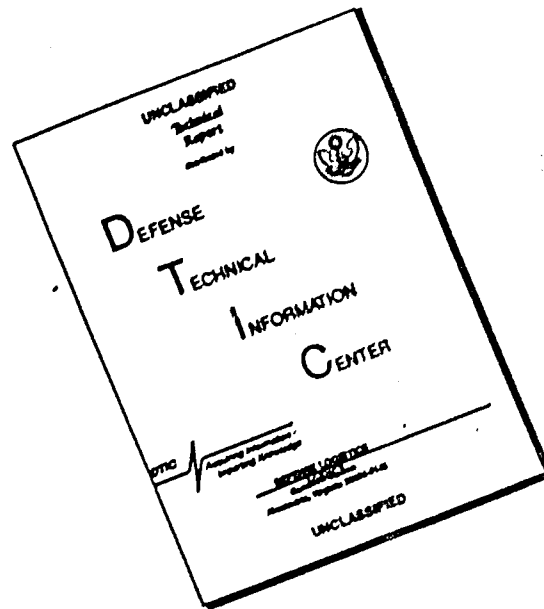
Processed for . . .

**DEFENSE DOCUMENTATION CENTER
DEFENSE SUPPLY AGENCY**



U. S. DEPARTMENT OF COMMERCE / NATIONAL BUREAU OF STANDARDS / INSTITUTE FOR APPLIED TECHNOLOGY

DISCLAIMER NOTICE



THIS DOCUMENT IS BEST QUALITY AVAILABLE. THE COPY FURNISHED TO DTIC CONTAINED A SIGNIFICANT NUMBER OF PAGES WHICH DO NOT REPRODUCE LEGIBLY.

SAMSO-TR-68-72

AD669121

BEHAVIOR OF MISSILE SILO CLOSURES
DESIGNED TO RESIST HIGH OVERPRESSURES

by

R. M. Iten, Major, USAF

W. L. Gamble

DEPARTMENT OF CIVIL ENGINEERING
UNIVERSITY OF ILLINOIS
URBANA, ILLINOIS
MARCH, 1968

SPACE AND MISSILE SYSTEMS ORGANIZATION
AIR FORCE SYSTEMS COMMAND
UNITED STATES AIR FORCE
NORTON AIR FORCE BASE
Contract No. AF04-694-796

UNCLASSIFIED

DISTRIBUTION OF THIS DOCUMENT IS UNLIMITED

Reproduced by the
CLEARINGHOUSE
for Federal Scientific & Technical
Information Springfield Va. 22151



250

SPECIAL NOTICE

DISTRIBUTION OF THIS DOCUMENT IS UNLIMITED

ACCESSION for	
CFSTI	WRITE SECTION <input checked="" type="checkbox"/>
DDC	DIFF SECTION <input type="checkbox"/>
UNANNOUNCED	<input type="checkbox"/>
JUSTIFICATION.....	
.....	
BY	
DISTRIBUTION/AVAILABILITY CODES	
DIST.	AVAIL. and/or SPECIAL
/	

SAMSO-TR-68-72

BEHAVIOR OF MISSILE SILO CLOSURES
DESIGNED TO RESIST HIGH OVERPRESSURES

by

R. M. Iten, Major, USAF

W. L. Gamble

DEPARTMENT OF CIVIL ENGINEERING
UNIVERSITY OF ILLINOIS
URBANA, ILLINOIS
MARCH, 1968

SPACE AND MISSILE SYSTEMS ORGANIZATION
AIR FORCE SYSTEMS COMMAND
UNITED STATES AIR FORCE
NORTON AIR FORCE BASE
Contract No. AF04-694-796

UNCLASSIFIED

DISTRIBUTION OF THIS DOCUMENT IS UNLIMITED

FORWARD

This report contains information useful for the design or review of thick reinforced concrete slabs which are suitable for use as closures for missile launch facilities which must resist high overpressures resulting from nuclear detonations.

The work was done by the Department of Civil Engineering, University of Illinois, Urbana, Illinois, 61801, under Air Force Contract No. AF04-694-796.

The work was sponsored by the Space and Missile Systems Organization (SMNP-1), Air Force Systems Command, United States Air Force, Norton Air Force Base, California, 92409. John M. Comalli, Captain, U.S.A.F., and George W. Barnes, Captain, U.S.A.F., acted as technical monitors, and were assisted by Craig R. Smith, Aerospace Corporation.

The work reported was conducted between 16 June 1967 and 31 January 1968. The draft of this report was submitted for review in February, 1968, and the final printing date was March, 1968.

Distribution of this document is unlimited.

This technical report has been reviewed and is approved.

George W. Barnes, Captain, U.S.A.F.
Project Officer
Space and Missile Systems Organization

ABSTRACT

Nuclear weapons effects pertinent to the design of closure systems for missile emplacements are briefly reviewed. The relationships between design overpressure, weapon yield, attacking weapon accuracy and probability of survival are discussed.

A method of designing closure structures, based on the yield-line method of analysis, is described. Prototype closures designed to resist nominal overpressure loads of 1000 and 2000 psi are presented. A method of determining allowable loads, required number and optimum spacing of shear connectors for composite steel-concrete slabs is described.

Designs for a series of model closure slabs are presented. A total of 34 models are described. Design loads ranging from 300 to 2000 psi and span/thickness ratios from 2.35 to 5.6 are included. Fabrication techniques and the materials used are described, as are the test fixtures and measuring instruments employed.

Results of the tests are presented in narrative form. In addition, results in the form of load-deflection curves, deflection profiles, load-strain curves and photographs are presented for the latest (G-Series) group of model closures. The results are analyzed, and shear stress data is normalized in several ways in order to find a design expression which best fits all the data. A formula for the design of closure structures is presented, with an accompanying recommendation regarding bearing stress limitations and a stipulation regarding its range of validity.

Conclusions drawn from the study are enumerated and recommendations for further testing and analytical study are presented.

TABLE OF CONTENTS

	Page
LIST OF TABLES.	v
LIST OF FIGURES	vi
NOTATION.	xii
1. INTRODUCTION.	1
1.1. General	1
1.2. Objective	2
1.3. Scope	2
1.4. Arrangement of Report	3
1.5. Analytical Studies.	4
1.6. Other Investigations.	5
1.7. Acknowledgments	7
2. WEAPONS EFFECTS	8
2.1. General	8
2.2. Air Blast	8
2.3. Ground Shock.	10
2.4. Nuclear Radiation	10
2.5. Electromagnetic Pulse	12
2.6. Cratering and Debris.	13
3. PRELIMINARY DESIGN STUDIES.	20
3.1. General	20
3.2. Basic Design Procedure.	20
3.3. Bar-Reinforced Slabs.	22
3.4. Plate-Reinforced Slabs.	23
3.5. Shear Reinforcing	27
3.6. Dynamic Load Considerations	28
4. MODEL TEST SERIES	41
4.1. General	41
4.2. Scaling Relationships	42
4.3. Test Device for 1/14th-Scale Models	43
4.4. Test Device for 1/5th-Scale Models.	44
4.5. K-Series Models	45
4.6. J-Series Models	47
4.7. G-Series Models	48
4.8. Materials	54
4.9. Fabrication	57
4.10. Instrumentation	59

TABLE OF CONTENTS (Continued)

	Page
5. TEST RESULTS.	97
5.1. General	97
5.2. Bar-Reinforced Slabs.	100
5.3. Plate-Reinforced 1000-psi Slabs	102
5.4. Plate-Reinforced 300-psi Slabs, 1/14th Scale.	105
5.5. Plate-Reinforced 300-psi Slabs, 1/5th Scale	106
5.6. Plate-Reinforced 2000-psi Slabs	109
5.7. Plate-and-Bar-Reinforced Slabs.	113
5.8. Miscellaneous Slabs	115
5.9. Randomly-Reinforced Slabs	119
6. DISCUSSION OF TEST RESULTS.	195
6.1. General	195
6.2. Friction Forces	196
6.3. Bearing Capacity.	198
6.4. Shear Strength.	201
6.5. Ductility	208
6.6. Confinement	210
6.7. Recommended Design Procedure.	211
7. CONCLUSIONS AND RECOMMENDATIONS	224
7.1. Conclusions	224
7.2. Recommended Additional Tests.	225
7.3. Analytical Study.	228
LIST OF REFERENCES.	230

LIST OF TABLES

Number		Page
2.1	Miss Distances for Various Yields and Peak Overpressures.	15
2.2	Crater Dimensions in Dry Soil	15
2.3	Crater Ejecta Depths for $\alpha = 1.0$	15
3.1	Variation of P_m/Q_y With Ductility Ratio	32
4.1	Properties of Model Closure Slabs, K and J-Series	63
4.2	Sheet Metal and Wire Gages.	64
4.3	Properties of Model Closure Slabs, G-Series	65
4.4	Concrete Compressive Strength Data.	66
4.5	Concrete Tensile Strength Data.	67
4.6	Strength Properties of Reinforcing Materials.	68
5.1	Stiffness and Ductility of Model Slabs.	122
5.2	Effect of Shear Reinforcement on Stiffness.	123
5.3	Effect of Shear Reinforcement on Ductility.	124
5.4	Effect of Shear Reinforcement on Maximum Load	125
5.5	Tests on 1/5-th Scale Slabs	126
6.1	Bearing Stresses at Failure	213
6.2	Ultimate Shear Stresses on Sections t in Thickness, K and J-Series Models	214
6.3	Ultimate Shear Stresses on Section t in Thickness, G-Series Models	215
6.4	Ultimate Shear Stresses at Support in Terms of p , (L/t) and $\sqrt{f'_c}$	216
6.5	Ultimate Shear Stresses at Support in terms of \sqrt{p} , $\sqrt{L/t}$ and $\sqrt{f'_c}$	217
7.1	Variations of Material Property and Geometric Parameters.	229

LIST OF FIGURES

Number		Page
2.1	Peak Overpressure vs. Shock Radius for a 1 MT Surface Burst.	16
2.2	Probability of Survival vs. CEP for Various Yield-Overpressure Combinations	17
2.3	Thickness Requirements for Radiation Shielding.	18
2.4	Crater Ejecta Distribution Model.	19
3.1	Effective Depth of Section vs Load.	33
3.2	Silo Closure Slab 60-B.	34
3.3	Silo Closure Slab 40-A.	35
3.4	Silo Closure Slab 40-B.	36
3.5	Silo Closure Slab 36-A.	37
3.6	Silo Closure Slab 36-B.	38
3.7	Silo Closure Slab 36-C.	39
3.8	Shear Reinforcement	40
4.1	Cross-Section of Slab Testing Device.	69
4.2	Seal Details, 1/14th Scale Slab Testing Device.	70
4.3	Partly Dismantled Slab Testing Device	71
4.4	Cross-Section of Specimen Tank and Slab Support	72
4.5	Details of Seal and Support Area, 1/5th Scale Models.	73
4.6	Bar Reinforced Slabs.	74
4.7	Model Slabs with Plate Reinforcement.	75
4.8	Shear Reinforcement in Model Slabs.	76
4.9	Model Slab Reinforced with Retaining Ring, K-9.	77
4.10	Slab Models J-1 and J-2	78

LIST OF FIGURES (Continued)

Number		Page
4.11	Slab Models J-5 to J-8.	79
4.12	Slab Model G-5.	80
4.13	Slab Models G-7 and G-10.	81
4.14	Shear Reinforcement for Models G-7 and G-10	82
4.15	Slab Model G-12 Prior to Casting.	82
4.16	Slab Models G-6 and G-8	83
4.17	Slab Model G-11	84
4.18	Slab Model G-12	85
4.19	Aggregate Gradation Curves.	86
4.20	Typical Stress-Strain Curve, 1/8" x 1/8" Reinforcing Bars	87
4.21	Typical Stress-Strain Curve, 16 Gage Plate.	88
4.22	Typical Stress-Strain Curve, 24 Gage Plate.	89
4.23	Typical Stress-Strain Curve, K-Series Vertical Steel. . .	90
4.24	Locations of Deflection Gages	91
4.25	Deflection Instrumentation, 1/14th Scale Models	92
4.26	Lateral Deflection Gage, G-Series Models.	93
4.27	Strain Gage Locations and Numbering	94
4.28	Arrangement of Deflection Gages 1/5th Scale Models. . . .	95
4.29	Locations and Numbering of Strain Gages, 1/5th Scale Models.	96
5.1	Load-Deflection Curve, Slab G-1	127
5.2	Deflection Profiles, Slab G-1	128
5.3	Load-Strain Curves, Slab G-1.	129
5.4	Load-Strain Curves, Slab G-1.	130

LIST OF FIGURES (Continued)

Number		Page
5.5	Load-Strain Curves, Slab G-1.	131
5.6	Load-Deflection Curve, Slab G-2	132
5.7	Deflection Profiles, Slab G-2	133
5.8	Load-Strain Curves, Slab G-2.	134
5.9	Load-Strain Curves, Slab G-2.	135
5.10	Load-Strain Curves, Slab G-2.	136
5.11	Load-Strain Curves, Slab G-2.	137
5.12	Load-Deflection Curve, Slab G-3	138
5.13	Deflection Profiles, Slab G-3	139
5.14	Load-Strain Curves, Slab G-3.	140
5.15	Load-Strain Curves, Slab G-3.	141
5.16	Load-Deflection Curve, Slab G-4	142
5.17	Deflection Profiles, Slab G-4	143
5.18	Load-Deflection Curve, Slab G-5	144
5.19	Deflection Profiles, Slab G-5	145
5.20	Load-Strain Curves, Slab G-5.	146
5.21	Load-Strain Curves, Slab G-5.	147
5.22	Load-Strain Curves, Slab G-5.	148
5.23	Load-Deflection Curve, Slab G-6	149
5.24	Deflection Profiles, Slab G-6	150
5.25	Load-Strain Curves, Slab G-6.	151
5.26	Load-Strain Curves, Slab G-6.	152
5.27	Load-Strain Curves, Slab G-6.	153
5.28	Load-Deflection Curve, Slab G-7	154

LIST OF FIGURES (Continued)

Number		Page
5.29	Deflection Profiles, Slab G-7	155
5.30	Load-Strain Curves, Slab G-7.	156
5.31	Load-Strain Curves, Slab G-7.	157
5.32	Load-Strain Curves, Slab G-7.	158
5.33	Load-Deflection Curve, Slab G-8	159
5.34	Deflection Profiles, Slab G-8	160
5.35	Load-Strain Curves, Slab G-8.	161
5.36	Load-Strain Curves, Slab G-8.	162
5.37	Load-Strain Curves, Slab G-8.	163
5.38	Load-Deflection Curve, Slab G-9, Cycles 1-5	164
5.39	Load-Deflection Curve, Slab G-9, Cycles 6 and 7	165
5.40	Deflection Profiles, Slab G-9	166
5.41	Load-Strain Curves, Slab G-9.	167
5.42	Load-Deflection Curve, Slab G-10.	168
5.43	Deflection Profiles, Slab G-10.	169
5.44	Load-Strain Curves, Slab G-10	170
5.45	Load-Strain Curves, Slab G-10	171
5.46	Load-Deflection Curve, Slab G-11.	172
5.47	Deflection Profiles, Slab G-11.	173
5.48	Load-Strain Curves, Slab G-11	174
5.49	Load-Deflection Curve, Slab G-12.	175
5.50	Deflection Profiles, Slab G-12.	176
5.51	Load-Strain Curves, Slab G-12	177
5.52	Load-Strain Curves, Slab G-12	178

LIST OF FIGURES (Continued)

Number		Page
5.53	Slab G-1, Deformation of Top Surface.	179
5.54	Slab G-1, Deformation of Bottom Surface	179
5.55	Slab G-1, Profile	180
5.56	Slab G-2, Deformation of Top Surface.	180
5.57	Slab G-2, Deformation of Bottom Surface	181
5.58	Slab G-3, Deformation of Top Surface.	181
5.59	Slab G-3, Deformation of Bottom Surface	182
5.60	Slab G-4, Deformation of Top Surface.	182
5.61	Slab G-4, Deformation of Bottom Surface	183
5.62	Slab G-4, Profile	183
5.63	Slab G-5, Deformation of Top Surface.	184
5.64	Slab G-5, Deformation of Bottom Surface	184
5.65	Slab G-5, Profile	185
5.66	Slab G-6, Deformation of Top Surface.	185
5.67	Slab G-6, Deformation of Bottom Surface	186
5.68	Slab G-6, Profile	186
5.69	Slab G-7, Deformation of Top Surface.	187
5.70	Slab G-7, Deformation of Bottom Surface	187
5.71	Slab G-7, Profile	188
5.72	Slab G-8, Deformation of Top Surface.	188
5.73	Slab G-8, Deformation of Bottom Surface	189
5.74	Slab G-8, Profile	189
5.75	Slab G-9, Deformation of Top Surface.	190
5.76	Slab G-9, Deformation of Bottom Surface	190

Number		Page
5.77	Slab G-10, Deformation of Top Surface	191
5.78	Slab G-10, Deformation of Bottom Surface.	191
5.79	Slab G-10, Profile.	192
5.80	Slab G-11, Deformation of Top Surface	192
5.81	Slab G-11, Deformation of Bottom Surface.	193
5.82	Slab G-12, Deformation of Top Surface	193
5.83	Slab G-12, Deformation of Bottom Surface.	194
5.84	Slab G-12, Profile.	194
6.1	Variation of Support Friction with Load (Gamble's Method)	218
6.2	Variation of Support Friction with Load (Iten's Method) .	218
6.3	Variation of Normalized Shear Stress with Span/Thickness Ratio.	219
6.4	Variation of Normalized Shear Stress with Reinforcement Ratio	220
6.5	Ultimate Shear Stress vs. Span/Thickness Ratio.	221
6.6	Variation of Q_y/Q_m with Ductility for Model Test Series .	222
6.7	Variation of P_m/Q_m with Ductility	223

NOTATION

Each symbol is defined where it is first introduced in the text. In the following summary, some of the most important symbols are defined for the convenience of the reader. Symbols used only in a limited portion of the text, and not important in subsequent considerations, are not included.

a	radius of plate (in computing period of vibrator, Eq. (3.10))
a	area tributary to a single shear stud, shear stud spacing
A	constant in Eq. (6.2)
A _s	area of tension reinforcement
A _v	area of shear reinforcement
b	chord distance (for shear stud layout)
b _o	periphery of critical section
C	CEP, in Eq. (2.2)
C	constant in Eq. (6.7)
d	crater depth, in Ch. 2
d	distance from extreme compression fiber to centroid of tension reinforcement
D	diameter of crater, Ch. 2
D	slab diameter
D	plate stiffness, $D = Et^3/(1-\nu^2) 12$
D _i	inside diameter
D _o	outside diameter
D _s	shear stud diameter
D _γ	total dose of gamma radiation

e	base of the Napierian logarithms
E	Young's modulus
f_b	bearing stress
f'_c	compressive strength of concrete
f_v	tensile stress in shear reinforcement
f_y	yield strength of reinforcement
f_r	"relative" coefficient of friction, Eq. (6.2)
g	acceleration of gravity
h	height of crater lip, Ch. 2
I	gamma radiation dose penetrating shield, Ch. 2
j	ratio of distance between centroid of compression and centroid of tension to the depth, d
l	crater dimension defined on Fig. 2.4
ln	logarithm to the base e
L	width of crater lip, Ch. 2
L	clear span diameter, Ch. 6
m_y	unit yield moment
n	number of shear studs
n	coefficient of σ , standard deviation, in Eq. (6.8)
N	attenuated neutron dose, Ch. 2
N_o	total neutron dose, Ch. 2
p	ratio of area of tension reinforcement to effective area of concrete
P_m	maximum applied dynamic load (for response analysis)
P_s	probability of survival
Q	allowable load on shear stud
Q_m	maximum static resistance (in response analysis)

Q_y	yield resistance (in response analysis)
R	shock radius, or "miss distance," Ch. 2
R	radius to row of shear studs
R_v	radius of vulnerability, Ch. 2
t	height of slab
t	hoop thickness, Eq. (4.4)
t_d	duration of loading pulse
t_∞	duration of effective triangle which preserves initial decay rate of pressure pulse
t_{50}	duration of effective triangle which preserves time to one-half peak pressure
t_i	duration of effective triangle which preserves total impulse
T	period of vibration
u	bond stress
v_u	ultimate shear stress
V	total shear
V'	portion of total shear carried by shear reinforcement
V_c	volume of crater, Ch. 2
V_l	volume of crater lip
w	applied uniformly distributed load
w'	portion of applied load taken by shear reinforcement
W	weapon yield, Ch. 2
x	shield thickness, Ch. 2
x_o	arbitrary offset, in ductility calculations, Ch. 5
α	volume expansion factor, Ch. 2
α	coefficient in Eq. (2.6)
γ	density, Eq. (3.10)

λ	coefficient in Eq. (2.6)
μ	ductility, defined as maximum deflection divided by yield deflection
ν	Poisson's ratio
ρ	air density, Eq. (2.3)
σ	standard deviation
σ_1	major principal stress
σ_3	minor principal stress
Σ	neutron attenuation factor, Ch. 2
Σ_0	perimeter of reinforcement crossing section

CHAPTER 1
INTRODUCTION

1.1. General

This report describes portions of a program of research into the behavior of reinforced concrete missile silo closures under the application of high overpressure loadings. The program was sponsored by the U. S. Air Force Space and Missile Systems Organization (SAMSO). The overall program was directed, for the University of Illinois, by Professor William L. Gamble. **The Illinois analysis and test program** included static tests of closures designed for 1000 psi, dynamic tests of closures designed for 300 psi, an analytical study of flat plate and plug type closures, an investigation of failure criteria for concrete and rock, and prototype closure design studies. Professors A. J. Hendron, Jr., J. H. Rainer and W. C. Schnobrich collaborated on the project (1).*

An **addition** to the **Illinois schedule of research** called for an additional series of static tests of models designed for nominal overpressures of 2000 psi. The design and testing of these models were conducted by the writer. This report covers the entire model test program, in order to arrive at conclusions regarding closure slab behavior. The discussion of the dynamic tests is as brief as continuity allows, and the reader is referred to Ref. 1 for further detail. The reader is also referred to Ref. 1 for test data in the form of

* A number in parentheses following a reference to a publication or an author's name refers to an entry in the List of References.

deflection profiles, load-deflection curves, and load-strain curves for the original series of 1000 psi and 300 psi model tests, as this volume supplies only the data from the final series of twelve models.

The research reported and discussed in the sections and paragraphs that follow includes all of the closure slab model testing conducted at the University of Illinois.

1.2. Objective

The objective of the research was to demonstrate that silo closure slabs can be built to withstand overpressures as high as one wishes. In this study, models were designed to resist overpressures of 1000 psi and 2000 psi from weapons of 100 KT, 1 MT, and 10 MT yield. The ability of the model slabs to withstand more than design overpressure was demonstrated so early in the program that the determination of the highest overpressure load that could be resisted became an unstated objective. The ultimate aim, of course, was to obtain an understanding of the behavior of the closure structures, which are, necessarily, very deep slabs. A desired end product was an expression, or method, which the sponsoring agency can use for the design of closures for future missile emplacements.

1.3. Scope

As stated in Chapter 2, this study considers the effects of blast loadings of 1000 and 2000 psi from attacking weapons of C.1, 1 and 10 MT. Only the overpressure load on the surface of the closure is taken into account, though it is recognized that the air and

ground shock-induced motions of the structure supporting the closure may significantly affect the response of the closure.

The inside diameter of the prototype closure was selected as 15 feet, the average of the dimensions furnished by SAMSO. An outside diameter of 19 feet was chosen to limit the average bearing stress, at an applied load of 1000 psi, to an acceptable value. All of the model tests were conducted at the diameter ratio 19/15. No other geometry was considered.

This study was limited to the consideration of the behavior of closures supported on rigid, motionless bearing structures, comparable in strength and rigidity (relative to the closure) to the test fixtures. Certain assumptions are implied by the limitations of the study. The supporting structure, for instance, is assumed to be capable of resisting the large friction-induced radial horizontal forces which were found in the model tests to exist and to result in high flexural strengths. It is assumed that practical problems can somehow be overcome. Gamble (1, Ch. 6) has treated the problem of providing an opening mechanism for a massive closure which may be surcharged with an accumulation of blast-borne debris.

1.4. Arrangement of Report

The remaining sections of this introductory chapter supply brief discussions of the analytical work done in connection with the silo closure problem, as well as the experimental work of other investigators. The second chapter describes some of the nuclear weapons effects of importance in the design of closures. A discussion

of the studies which led to the design of several prototype structures which were modeled and tested appears in Chapter 3. The design, fabrication, materials and instrumentation of the model test series are described in the fourth chapter. Chapter 5 presents the results of the model tests. The results are discussed in the sixth chapter, and a design expression is suggested. In Chapter 7 conclusions from the study are listed and recommendations are presented.

Figures and tables in this report are found at the end of the chapter in which they are first referenced. Publications cited in the text are listed in the List of References that follows Chapter 7.

1.5. Analytical Studies

Rainer (1, Ch. 3) has modeled the silo closure as a plate, simply supported over the clear span, using the discrete lumped parameter model developed by Ang and Rainer (2) and applied to a variety of problems by Ang, Rainer and others. The method proceeds from a physical analogy to obtain a set of equations identical to those obtained by a finite difference approach. Rainer applied the model to flat plate closures of several span/thickness ratios, under both static and dynamic loadings, as well as to closure types with which this report is not concerned. Rainer's results are thoroughly reported and discussed in SAMSO TR-67-15 (1).

Unfortunately, Rainer modeled only the simply-supported plate with no overhang. The structures of interest in this study are supported over an annular bearing area with a ratio of outside diameter to inside diameter of 19/15. The differences in support

configuration are great enough to render Rainer's results less valuable than they might otherwise be.

1.6. Other Investigations

In order to better define the shear strength of deep slabs, the results of the few existing tests of slabs, and of some tests of deep beams, were reviewed. In most investigations the test structures were appreciably different from those in this program, so that the results are not directly applicable. Some of the results are discussed in the following paragraphs.

Brotchie, et al (3), tested groups of square slabs with span/thickness ratios of 5, 10 and 20, tension steel ratios of 0 to 3 percent, and five conditions of edge restraint. Eleven specimens with span/thickness ratio of five and edges restrained at the level of the reinforcement are somewhat comparable to the models tested at the University of Illinois. All of these models failed in shear. Average shear stresses at the face of the support were calculated for the eight of those specimens that were provided with tension reinforcement, using Eq. (6.8) from this report. The observed average shear stresses were then divided by the calculated values. The average of the quotients was found to be 1.01, and the coefficient of variation for the eight tests was 0.188. Thus, it appears that the failure loads for deep, square slabs are influenced by the same parameters as those for circular slabs, when the conditions of edge restraint are comparable.

Brotchie tested one model with the edge restrained at mid-depth and two models with simply supported edges. All three structures had span/thickness ratios of five. Two failed in flexure, and one failed in shear, at average shear stresses about one-third as high as those predicted by Eq. (6.8).

Tests of 18 square or rectangular slabs and one circular slab were conducted at Southwest Research Institute (4). All were simply supported. The mean value of the average shear stresses at the face of the support for seven square slabs and the single circular slab, divided by the stresses computed by Eq. (6.8), is 0.62, with a coefficient of variation of 0.139 for the array of eight values. The ratio of observed stress to calculated stress for the circular slab was 0.48, but this slab had not failed at the maximum reported load.

Beadle, et al (5) tested six thick circular slabs with very thick steel plates used at the lower surfaces. An additional thirteen tests have been conducted, using the same apparatus, by cadets of the U. S. Air Force Academy under the direction of Professor (Lt. Col.) Wallace E. Fluhr. Loads as high as 7800 psi were obtained with base plates 1.3 inches thick and confining rings 0.2 and 0.25 inches thick. It should be noted that, if a scale factor of 12 is assumed, the prototype thicknesses represented by these models are 15.6 inches and 3 inches for base plate and hoop, respectively, and each closure requires 107 tons of steel.

The experimental work at the Air Force Academy has been briefly reported by Menza (6). A semi-empirical equation for computing

the apparent yield load of these structures has been derived by Burgess (7). The Air Force Academy structures are entirely different from those tested at the University of Illinois, and fail in a completely different manner. Therefore, no comparison has been attempted.

The results of a large number of tests of reinforced concrete deep beams have been reported. References 8, 9, 10 and 11 contain or review much of the basic information available. Though the strength properties of deep beams may not be directly applicable to deep slabs, deep beam strengths should form a lower bound to the strengths of deep slabs. In Chapter 6, it is shown that Eq. (6.8) derived from the results of the University of Illinois tests, yields shear stress values (at the face of the support) comparable to those predicted by Albritton's (8) simple equation for uniformly loaded deep beams.

1.7. Acknowledgments

The project was under the direction of Professor G. K. Sinnamon from its beginning, 1 July 1965, until March, 1966. From that time to the completion of the project, Professor W. L. Gamble has been the Project Director, and Professor Sinnamon has acted as a consultant to the project. Professor N. M. Newmark, Head of the Department of Civil Engineering, has overseen all of the work.

Valuable assistance was given by Research Assistant Steve Katz and Student Assistant Larry Newman.

Captains John Comalli and George Barnes monitored the program for the Space and Missile Systems Organization. They were assisted by Mr. Craig Smith of the Aerospace Corporation.

CHAPTER 2
WEAPONS EFFECTS

2.1. General

The weapon effect of primary concern to this study is the air blast, which is treated as a uniform, static overpressure loading the structure. An understanding of the overall design problem, however, requires at least a recognition of those other weapons effects which accompany the air blast. These are discussed or mentioned in this chapter. The discussions that follow refer always to a surface burst at sea level.

2.2. Air Blast

The exploding nuclear weapon produces a pressure wave that varies with time and with distance from ground zero, the point of detonation. At a given distance from ground zero, the pressure rises almost instantaneously to a peak, decays with time to zero and is followed by a negative pressure phase. Thorough descriptions of this phenomenon are given in Refs. 12, 13 and 14. For many purposes it is sufficient to know only the relation between yield, distance and peak pressure. The variation of peak overpressure with distance is plotted in Fig. 2.1 for a weapon yield of 1 MT. For a given overpressure, distances corresponding to other yields are obtained from the relation

$$R = R_{1MT} W^{1/3} \quad (2.1)$$

where W is expressed in MT. Data for Fig. 2.1 are taken from Ref. 12.

Although statistical limitations are seldom presented with weapon effects data, it should be recognized that variations in these data must exist.

If we assume that a structure designed for a particular overpressure will fail at any larger overpressure and survive at any lesser overpressure, then the distance associated with that overpressure is the "radius of vulnerability" of the structure. The probability of the structure surviving an incoming weapon then coincides with the probability of the weapon impacting at a distance from the structure greater than the radius of vulnerability. The latter probability is given by M. S. Aghabian (23) as

$$F_s = 0.5 \left(\frac{R_v}{C} \right)^2 = e^{-0.693 \left(\frac{R_v}{C} \right)^2} \quad (2.2)$$

where R_v is the radius of vulnerability and C is the "circular error probable" (CEP), defined as the radius, about the structure, of the circle into which half of all weapons aimed at the structure will fall. Equation (2.2) and the value of C define the assumed error of the attacking delivery system.

Radii of vulnerability of interest to this study are tabulated in Table 2.1. Probability of survival versus CEP is plotted for each of these radii in Fig. 2.2. The variation of F_s with CEP for any other radius may be added to Fig. 2.2 by plotting a single point and extending a line between the plotted point and the upper-right corner of the figure.

The probabilistic aspects of designing protective structures are certainly not as simple as implied in the foregoing paragraphs. Charts such as Fig. 2.2 serve to point out, however, the importance of enemy CEP as a design parameter.

2.3. Ground Shock

Ground shock effects occur both as the result of direct coupling of a part of the weapon's energy to the soil, and as a result of the air blast passing over the soil. Under certain conditions a ground shock wave may "outrun" and precede the air blast wave to the structure. In this study ground shock effects have been ignored and the structure supporting the closure has been assumed to remain rigid and motionless.

2.4. Nuclear Radiation

One of the functions of the closure is to shield the missile from nuclear radiation effects. Exact shielding requirements cannot be calculated because tolerance criteria have not been furnished for the missile. Some educated guesses can be made, however, to illustrate the general conclusion that concrete thicknesses required for radiation protection are about the same as those required for structural purposes.

Let us first consider neutrons. Brode (12) gives us the formula

$$N_o = \frac{2 \times 10^{22} W_{MT}}{R^2 \text{ ft}} \exp(-\rho R/780) \quad (2.3)$$

where N_0 is the total dose, neutrons/cm², R the distance from ground zero and ρ the air density, which can be taken as 1.1 at sea level.

Brode (2.1) also gives the attenuation relation

$$\frac{N_0}{N} = e^{\Sigma x} \quad (2.4)$$

where N_0 is the total dose, N the attenuated dose, Σ the attenuation factor, given as 0.09 cm⁻¹ for concrete, and x the shield thickness in centimeters. From this we can obtain, for the shield thickness in inches, the expression

$$x = 4.37 \ln \left(\frac{N_0}{N} \right) \text{ inches} \quad (2.5)$$

where ln is the logarithm to the base e and the remaining terms have been previously defined. Brode (12) suggests a tolerance of 10¹¹ to 10¹² n/cm² for solid state electronic components. Taking the more severe requirement, 10¹¹ n/cm², as representative of missile tolerance, concrete shield requirements have been calculated for the yields and overpressures of interest in this study and plotted as Fig. 2.3. The thicknesses obtained are similar to those required for structural purposes, as later sections of this report will show.

For gamma radiation, Brode (12) supplies the formula

$$D_\gamma = \frac{3 \times 10^{13} W_{MT}}{R^2 \text{ ft}} \alpha \exp(-\rho R/\lambda) \quad (2.6)$$

where D_γ is the dose (roentgens) and the other variables not previously

defined are given by

$$\begin{aligned}\alpha &= 1 + 0.005W^2 \\ \lambda &= 1300 + 30W + 3W^2\end{aligned}\tag{2.7}$$

For attenuation of polyenergetic gamma radiation, Brode (12) suggests the expression

$$\frac{D_\gamma}{I} = e^{0.021 \rho x}\tag{2.8}$$

where ρ is the density of the shield, gm/cc, x its thickness in cm, and I the dose penetrating. For concrete with a density of 2.4 gm/cc, we obtain, for the required thickness in inches,

$$x = 7.8 \ln \left(\frac{D_\gamma}{I} \right) \text{ inches}\tag{2.9}$$

A gamma dose of 100 roentgens is tolerable by humans and should represent a conservative tolerance for missile equipment, where no other criterion is available. Concrete shield thicknesses required to reduce the initial gamma dose to 100 roentgens have been computed for the yields and overpressures considered in this study. The results are plotted on Fig. 2.3. Thicknesses for gamma shielding are greater than thicknesses required for blast resistance, but are of the same order of magnitude.

2.5. Electromagnetic Pulse

A continuous steel liner, 1/4 inch or more in thickness, is believed to be sufficient to protect the missile and associated

equipment from electromagnetic pulse (EMP) effects. The extension of the EMP shield over the lower surface of the closure will serve also to protect the missile from spalling of the concrete closure and will serve as all or part of the tension reinforcement for the closure.

2.6. Cratering and Debris

The most recent and accurate work done on cratering and debris (crater ejecta) depths is not available in unclassified form. However, some conclusions regarding the magnitude of these effects can be drawn from the information available in the open literature. Reference 14 gives crater dimensions for a 1 KT burst and suggests cube root scaling to obtain dimensions for other yields. Values of these dimensions for 100 KT, 1 MT and 10 MT are presented in Table 2.2. Since we have also assumed cube-root scaling for miss-distances, this assumption for crater dimensions implies that the edge of the crater and the edge of the crater lip will occur at the same overpressures regardless of yield. These overpressures are, at the crater edge, about 13000 psi, and at the edge of the crater lip, about 1700 psi. According to these data there will be no debris at the 1000 psi level.

An estimate of the magnitude of debris depths that might be expected at pressure levels greater than 1700 psi may be obtained by assuming an ejecta distribution pattern, as in Fig. 2.4, and accounting for the volume of material removed from the crater. For example, assume the crater is a paraboloid of revolution, with volume equal to

$$V_c = \frac{\pi d D^2}{8} \quad (2.10)$$

where V_c , d , and D are the volume, depth and diameter, respectively, of the crater. Further assume that the slope of the inner face of the crater lip is constant and equal to the slope of the crater at its edge (which gives a slope of about 1:1 for all yields). If the crater lip is assumed to be triangular in section, its volume is given by

$$V_L = \frac{\pi d l}{6D(L-l)} \left\{ 12lD(L-l) + (D+2L)^2 - (D+2l)^2(D+6L-4l) \right\} \quad (2.11)$$

where V_L is the volume of the crater lip and the other variables are identified on Fig. 2.4. The maximum height of the lip can now be found by setting

$$V_L = \alpha V_c \quad (2.12)$$

where α is a factor allowing for volumetric expansion of the material removed from the crater. If Eq. (2.10) and (2.11) are substituted into Eq. (2.12) and the result is solved for l ($\alpha = 1.0$), l is found to be almost exactly equal to one-tenth of the crater diameter. The maximum lip height, h , is equal to $0.4d$. Debris depths at various yields and overpressures for a surface burst are shown in Table 2.3. Though the model used is an oversimplified representation of a complex problem, the results are believed to be indicative of the magnitude of the debris problem that might be encountered.

TABLE 2.1. MISS DISTANCES FOR VARIOUS YIELDS AND PEAK OVERPRESSURES

W-MT	Miss Distance, feet		
	300 psi	1000 psi	2000 psi
0.1	1070	696	557
1	2250	1500	1200
10	4950	3230	2580

TABLE 2.2. CRATER DIMENSIONS IN DRY SOIL

	100KT	1MT	10MT
Crater Diameter, D, feet	600	1300	2790
Crater Depth, d, feet	140	300	645
Lip Width, L, feet	280	600	1290

TABLE 2.3. CRATER EJECTA DEPTHS FOR $\alpha = 1.0$

Overpressure	100KT	1MT	10MT
1,700 (Lip Edge)	0	0	0
2,000	5.35	11.4	24.6
3,000	21.3	45.8	98.5
4,000	32.0	69.0	148.0
5,000	44.3	82.3	177.0
9,000 (Lip Crest)	56.0	120.0	258.0

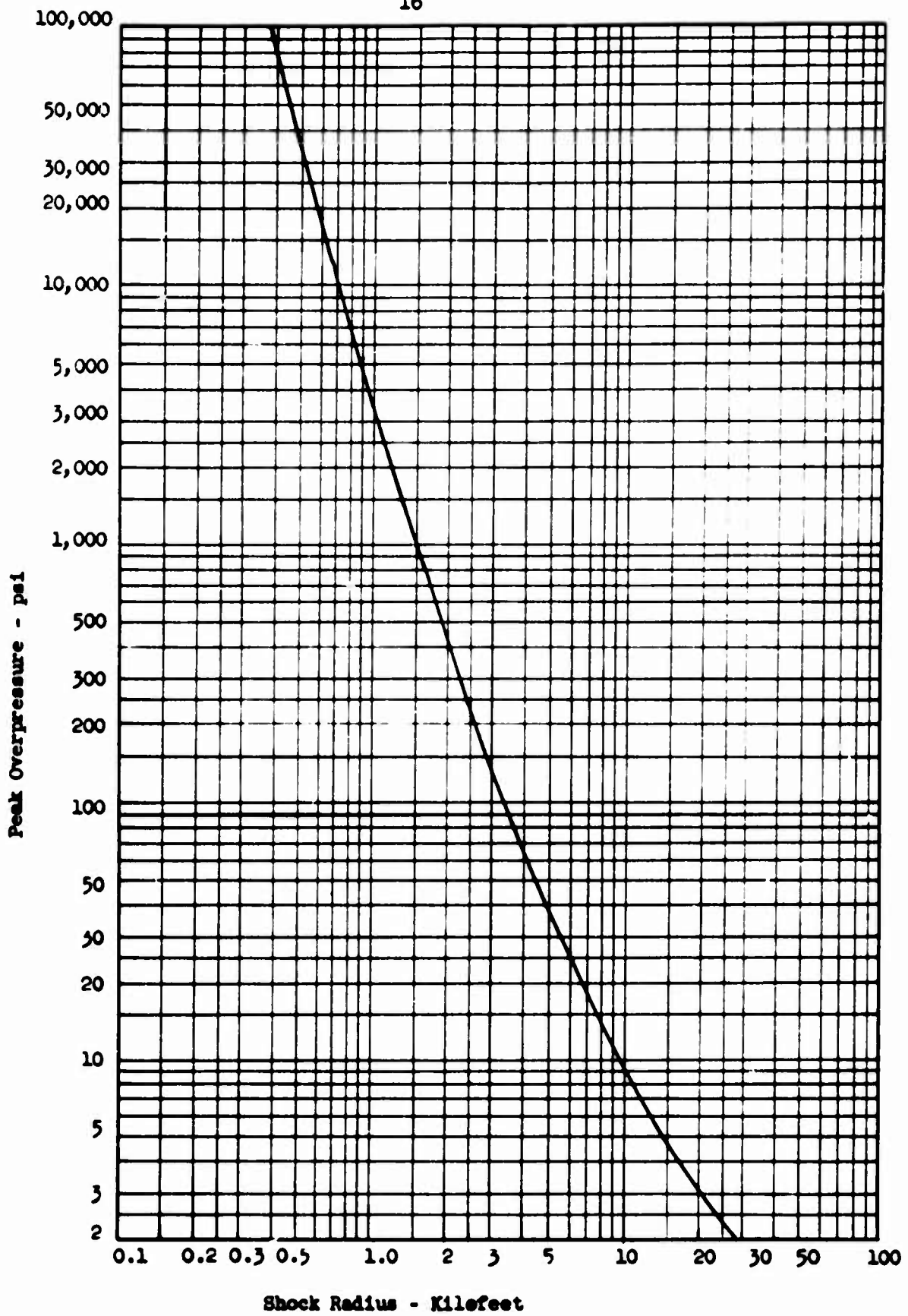
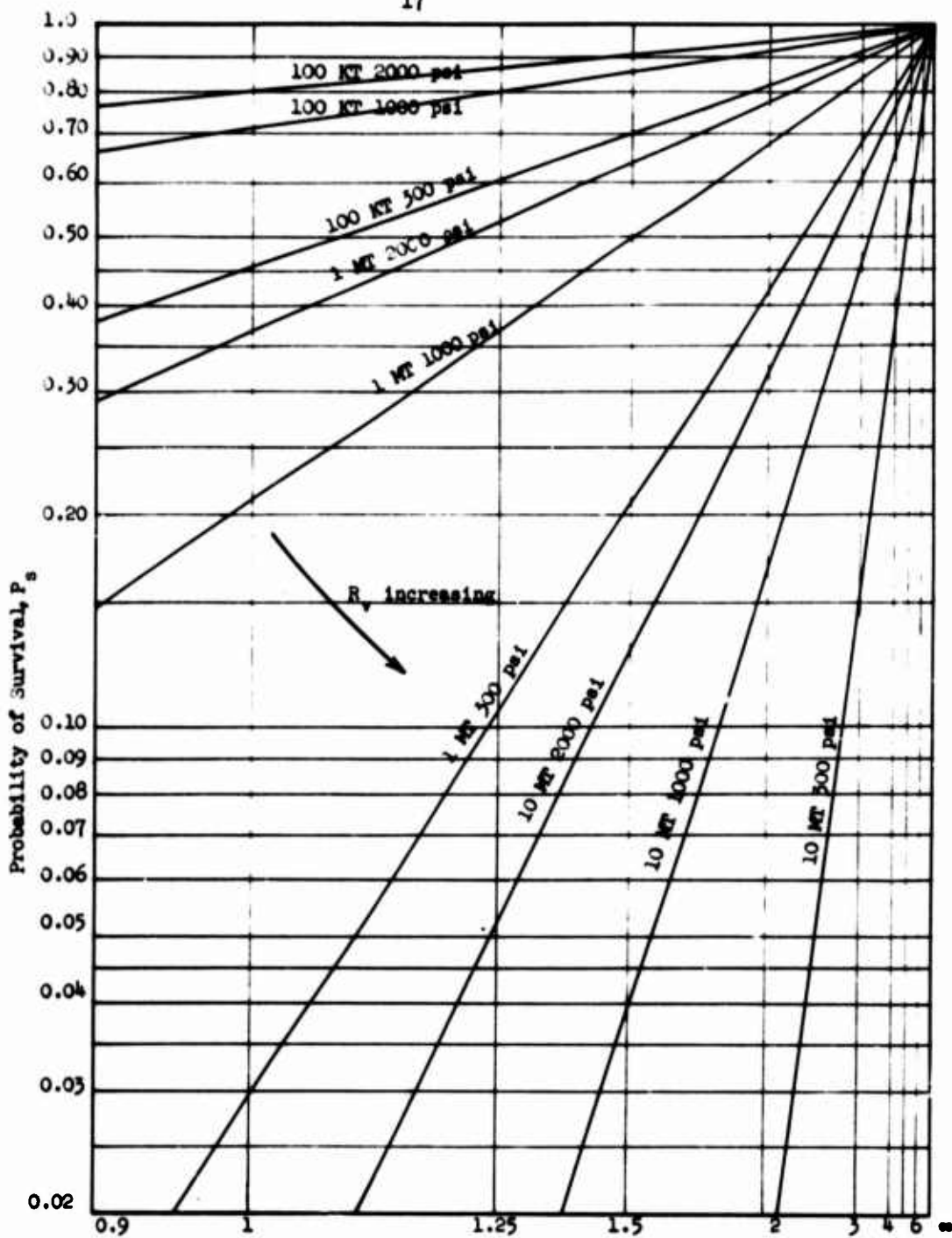


Fig. 2.1 Peak Overpressure vs. Shock Radius for a 1 MT Surface Burst



Circular Error Probable (CEP) - Kilofeet
 Fig. 2.2 Probability of Survival vs CEP at Various Yields and Overpressures

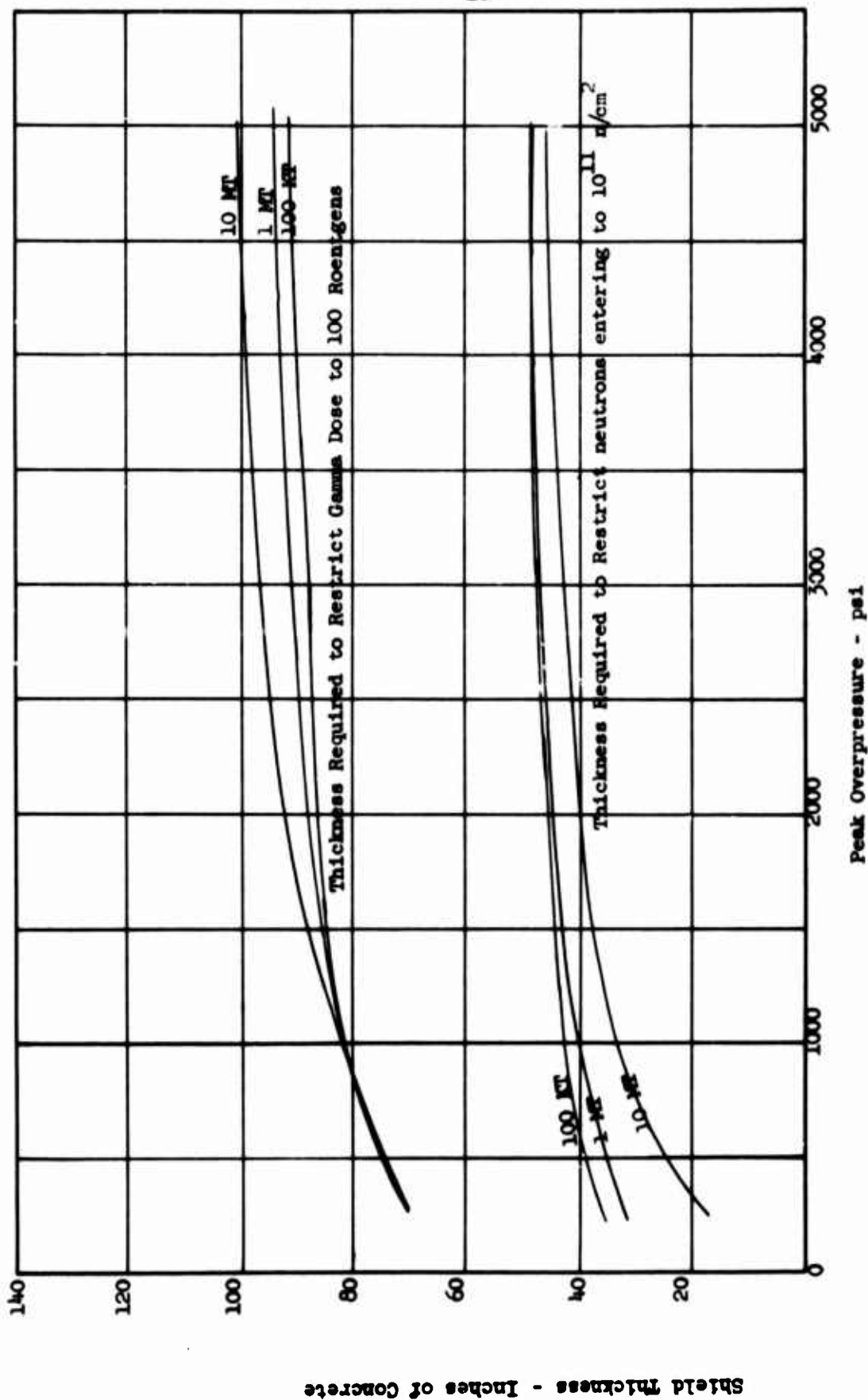


Fig. 2.3 Thickness Requirements for Radiation Shielding

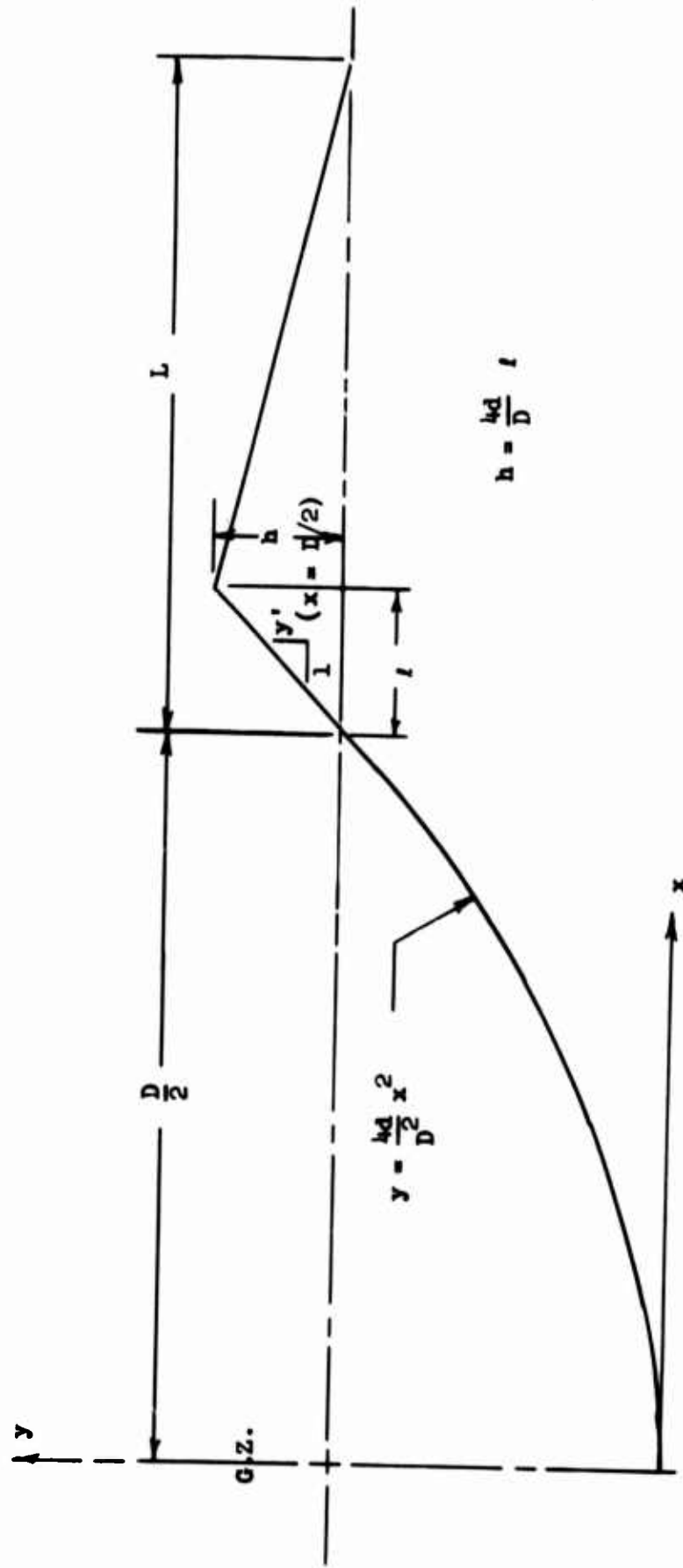


Fig. 2.4 Crater Ejecta Distribution Model

CHAPTER 3
PRELIMINARY DESIGN STUDIES

3.1. General

In order to obtain a basis for designing the series of model test experiments which were the essential part of this research, it was necessary to develop a design procedure and select representative prototype sizes for the overpressure loads considered. The prototype design studies are discussed in this chapter.

In accordance with the rationale developed in Section 3.6 below, the load is assumed to be uniform and static. The structure is assumed to be simply supported over the clear span, and is analyzed by the yield-line method. Thus, no advantage is taken of either the restraining effect of friction on the bearing surface or of the moment reduction due to the clamping effect of the load acting on the supported portion of the slab. Further, material yield strengths have not been increased beyond their static values in these studies.

3.2. Basic Design Procedure

The yield moment in a simply supported, uniformly loaded circular plate is given by Wood (15) as

$$m_y = \frac{wD^2}{24} \quad (3.1)$$

where m_y is the unit moment (kip-in/in), w is the uniform load, ksi, and D the clear span diameter, inches. The resisting moment at yield is found from the expression

$$m_y = f_y A_s j d = f_y p j d^2 \quad (3.2)$$

for a one-inch section, where

f_y = the yield stress of the reinforcing, ksi

p = the tension reinforcing steel ratio

$j d$ = the effective lever arm of the section, and

d = distance from the top surface to the center of the tension reinforcing steel.

Equating expressions (3.1) and (3.2), we can solve for the required effective depth, d , obtaining

$$d = 0.204D \left(\frac{w}{f_y p j} \right)^{1/2} \quad (3.3)$$

For the single span (180 inches) considered, and letting $j = 0.9$, Eq. (3.3) becomes

$$d = \frac{38.7w^{1/2}}{\sqrt{f_y p}} \quad (3.4)$$

which can be plotted as a family of parallel lines, representing various combinations of f_y and p , on log-log paper. The variation of d with w is plotted for a few such combinations in Fig. 3.1.

An outside diameter of 19 feet was chosen to insure bearing stresses of less than 3000 psi at a design load of 1000 psi. The bearing stress for the selected geometry becomes

$$f_b = 2.65w \quad (3.5)$$

Compression steel equal to one-half the tension steel is added to all designs to resist rebound effects from dynamic loading, as recommended by the Air Force Design Manual (13).

The design studies assume a flexural failure mode and reinforcement ratios of 2 percent or less. For these assumptions the ultimate moments are insensitive to concrete strength. Therefore, $f'_c = 5000$ psi was adopted for the design and model studies.

3.3. Bar-Reinforced Slabs

In the early phases of the study, consideration was given to the use of high-strength reinforcing steel. Line No. 1, Fig. 3.1, represents the combination of 60 ksi steel with a reinforcement ratio of 0.0133. The resulting effective depth is about 45 inches for a design load of 1,000 psi. The steel area required is $(0.0133)(45) = 0.60$ in.²/in., which can be provided by two layers of No. 11 bars spaced at 5-1/4 inches each way. By spreading the steel over the entire 19-ft span of the slab, the spacing can be increased by $(19/15)$ to 6-1/2 inches. The addition of 6 inches to the effective depth to account for the steel and provide 3 inches cover brings the total thickness to 51 inches. The design just described is designated 60-B and is illustrated in Fig. 3.2. The thickness selected for closure 60-B was retained as a standard prototype thickness for the 1000-psi series of models tested in this program.

High-strength steel reinforcing bars present problems in field fabrication due to the difficulty in welding these bars satisfactorily without lowering their strength and ductility. Consequently, the use

of high-strength reinforcing steel is not recommended. A design equivalent to 60-B, using intermediate grade reinforcing steel with a 40 ksi yield point, is obtained by increasing the percentage of steel:

$$p = \frac{60}{40} (0.0133) \approx 0.02$$

The steel required is $(0.02)(45) = 0.9 \text{ in.}^2/\text{in.}$, which is supplied by two layers of No. 11 bars spaced at $4\text{-}3/8"$ each way, when advantage is taken of the full 19-ft span of the slab. This design, designated 40-A, is illustrated in Fig. 3.3.

The basic prototype for the 2000-psi series of model tests was designed using line 2 of Fig. 3.1, where $p = 0.015$ and $f_y = 40 \text{ ksi}$. The effective depth is found to be 70.5 inches for a 2000-psi load. The total thickness is taken as 78 inches to allow for adequate cover over No. 14S bars. This design, shown in Fig. 3.4 is designated 40-B.

Figures 3.2 and 3.3 show the reinforcing bar ends welded to a circular steel plate to provide mechanical anchorage. An alternate method of obtaining anchorage is to weld the bar ends to one or more crossing bars. This method, which may be preferable from the standpoint of field fabrication, is shown in Fig. 3.4.

3.4. Plate-Reinforced Slabs

As discussed in Chapter 2, the silo closure will require a steel plate over its inner surface for EMP shielding and to protect the missile from spallation. This plate can be made to serve a third purpose by providing the necessary tension reinforcing for the closure.

Let us consider A-36 steel plate and let $t = d$ for design purposes. Equation (3.4) can be rewritten, for $f_y = 36$ ksi, as

$$p = 41.6 w/d^2 \quad (3.6)$$

where w is expressed in ksi. For the 1000 psi design, with $d = t = 51$ inches, we obtain $p = 41.6/(51)^2 = 0.016$. The plate thickness required is then $(0.016)(51) = 0.815$, or about $13/16$ ". We will designate this design as closure 36-A.

For the 2000-psi design, with $d = t = 78$ inches, we obtain $p = (41.6)(2)/(78)^2 = 0.0137$. The plate thickness required is then $(0.0137)(78) = 1.07$, or about $1-1/16$ inches. This closure is designated No. 36-B.

We will also require a 300 psi plate-reinforced prototype. Let p for this design by 0.012 and work directly from Eq. (3.4) to obtain

$$t = d = \frac{(38.7)(0.3)^{1/2}}{(6)(0.012)} = 32.3, \text{ say } 32.5 \text{ inches}$$

This closure is designated 36-C.

In order to utilize the strength of the plate, it is necessary to transfer the tension load to it. This can be accomplished by welding shear connectors to the plate, as described by Casillas, et al (16). If the shear connectors are round bars, such as Nelson studs, design forces can be determined from the formulae proposed by Viest (17). For studs larger than one inch in diameter, Viest suggests the expression

$$Q = 5 D_s f'_c \sqrt{\frac{4000}{f'_c}}$$

where Q is the load per stud in pounds and D_s the stud diameter in inches. This expression can be made more convenient by expressing Q in kips and f'_c in ksi and writing it

$$Q = 10 D_s \sqrt{f'_c} \text{ (kips)} \quad (3.7)$$

For 5000 psi concrete, we have $Q = 22.4D$; and for 1.5-inch studs, the load per stud is $Q = 33.6$ kips.

Spacing for the shear connectors will depend on bond stress, which in turn is a function of shear, which varies from zero at the center of the closure to a maximum at the support. The unit shear, kips/in., at a distance R from the center, is

$$V = \frac{wR}{2} \text{ kips/in.}$$

The unit bond stress, u is given by

$$u = \frac{V}{\sum_o jd} = \frac{wR}{2jd} \text{ for } \sum_o = 1 \text{ inch}$$

where \sum_o is unity because V is expressed in kips/in. The plate area tributary to a single stud can be taken as a square, such that

$$a^2 = \frac{Q}{u} = \frac{2Qjd}{wR}$$

and it follows that

$$a = \left(\frac{23.1d}{w}\right)^{1/2} R^{-1/2} \quad (3.8)$$

The method followed by the writer in determining shear spacing consists of plotting a vs. R (Eq. 3.8), and working inward from the edge of the support with a trial-and-error procedure, adjusting a after each step so that the number of studs in the row is an integer. At the smaller radii, where the chord distance differs significantly from the arc distance, the chord distance, designated b , is computed for layout purposes as

$$b = 2R \sin\left(\frac{\pi}{n}\right) \quad (3.9)$$

where n is the number of studs in the row.

Stud spacing in the supported portion of the slab is arbitrary. The writer has worked outward from the edge of the support, maintaining a mirror image of the row spacing inside the support and either the number of studs in the row or the stud spacing. If the number of studs in the row is reflected in the supported area, a good approximation for the total number of studs required can be obtained by working outward from the center and assuming a continuous distribution. Thus, for the geometry of these designs we obtain

$$n = \frac{1,225,000w}{Qd} \quad (3.9)$$

Where w and Q must be in compatible units. Using 1.5-inch studs this yields, for the 1,000 psi design, where $d = 51$ inches, $n = 795$. For the 2,000 psi design with $d = 78$ inches, $n = 1,040$. For

the 300 psi design with $d = 32.5$ inches, $n = 375$. The 1,000, 2,000 and 300 psi plate-reinforced slabs, designated 36-A, 36-B and 36-C, respectively, are illustrated in Figs. 3.5, 3.6 and 3.7.

3.5. Shear Reinforcing

It seemed reasonable to assume that a shear failure, if it occurred, would result in a truncated 45-degree cone of concrete being punched out of the slab. Shear reinforcement could then be conveniently provided by supplying vertical steel bars in concentric circles over the region of the crack. The added shear resistance available for each ring of bars **intersecting the crack would be**

$$V' = A_v f_v$$

Where V' is the force taken by the shear reinforcement, A_v is the area of steel cut by the shear crack and f_v is the shear steel stress. The shear steel will be assumed to yield, so that $f_v = f_y$.

Gamble, et al (1) have computed the extra load capacity contributed by three rings of shear reinforcement located as shown in Fig. 3.8. The reinforcing is welded wire fabric with 1/2-inch vertical bars at 6-inch spacing and horizontal 1/4-inch bars to provide anchorage. The total steel area for the configuration shown is 40.8 in^2 . The welded wire fabric has $f_y = 64 \text{ ksi}$, so that $V' = (40.8)(64) = 260 \text{ kips}$.

The shear steel carries only the load on the upper surface of the truncated cone. For the 51-inch slab, this surface has a diameter equal to $180 - 102 = 78$ inches and an area equal to $(0.785)(78)^2 =$

4770 in². Letting $4770w' = 2610$, we obtain $w' = 0.547$ ksi = 547 psi for the extra load capacity contributed by the shear reinforcement. (Gamble used a loaded diameter of 90 inches, i.e., $D-2d$, and obtained $w' = 405$ psi.)

Other methods of anchoring the shear reinforcing steel are available. One of the simplest is to use rods welded to the bottom plate or EMP shield. For a plate-reinforced slab the shear reinforcing rods need only be longer shear connectors.

3.6. Dynamic Load Considerations

In order to check the propriety of treating a complex dynamic response problem as a static problem, one can begin by considering a relatively simple substitute dynamic case. Melin, et al (18) have studied in detail the problem of an elasto-plastic single-degree-of-freedom system subjected to an initially-peaked triangular load pulse. Test results from the closure study have shown that an assumption of elasto-plastic behavior is not unreasonable. The true pressure pulse from a nuclear burst can be, and frequently is (13, Ch. 3) represented as an initially-peaked triangle without an intolerable loss of accuracy. All that remains, then, is to investigate the period of the structure and its relation to the rise time and duration of the load.

Timoshenko (19) gives the fundamental period of a thin, elastic, simply-supported circular plate as

$$T = \frac{2\pi a^2}{5.25} \sqrt{\frac{\gamma t}{gD}} \quad (3.10)$$

in which a = radius of plate, $\frac{\gamma t}{g}$ = mass per unit area of plate and

$$D = \frac{Et^3}{12(1-\nu^2)}$$

where E = Young's modulus, t = plate thickness and ν = Poisson's ratio, which is assumed to be zero for concrete. If we let $\gamma = 0.087 \text{ lbs/in}^3$ and $E = 4,000,000$ for concrete, Eq. (3.10) becomes

$$T = (3.11 \times 10^{-5}) \frac{a^2}{t} \quad (3.11)$$

which yields a period of 4.94 msec for the 51-inch closure and 3.23 msec for the 78-inch closure. These calculations are approximate, since the closures considered do not meet the requirements of the assumptions that led to Eq. (3.11). For the sake of argument, suppose these results are no more than an order of magnitude too great or too small. Considering an average for the two structures of 4 msec, then the actual value is at least 0.4 msec but not more than 40 msec.

The rise time of the pressure pulse will be one or two msec. If the period of the closure is less than computed, the assumption of zero rise time will be conservative in the sense that the closure response will be smaller than predicted. If the period is greater than the computed value, the assumption is essentially correct.

We may now consider extremes of the ratio t_d/T , where t_d is the duration of the loading pulse and T the period of the structure. For the upper bound, consider the shorter period, 0.4 msec. The maximum response should occur early in the pressure history and the appropriate value for t_d is the t_∞ value, which preserves the initial

decay rate of the actual pressure curve, as recommended by the Air Force Design Manual (13). We choose $t_{\infty} = 32$ msec for a 10 MT weapon and 1000 psi pressure, obtaining $t_d/T = 80$.

For the lower bound consider the longer period of 40 msec, and assume that maximum response will occur after the pressure pulse has passed. For this case the Air Force Design Manual recommends an effective triangle with duration t_i , preserving the impulse of the actual pressure-time curve. We choose $t_i = 55.5$ msec for a 100 KT weapon and 1000 psi pressure, obtaining $t_d/T = 1.39$.

We might have assumed that the maximum response of the closure with period of 40 msec occurs neither after the pressure pulse has passed, nor early in the pressure history, but at some intermediate time. In that case, the Air Force Design Manual recommends using $t_d = t_{50}$, conserving the time to one-half peak pressure of the actual pressure-time curve. For 100 KT and 1000 psi, we use $t_{50} = 13$ msec and obtain $t_d/T = 0.325$ as a lower lower bound.

Melin, et al (18) have computed P_m/Q_y vs ductility for t_d/T between 0.1 and 80. Values of P_m/Q_y for t_d/T of 0.3, 1.4 and 80 have been extracted from Ref. 18 and listed in Table 3.1 for ductilities from 1.3 to 20. P_m may be considered the peak dynamic load and Q_y the static yield load. It is apparent that for ductilities of 5 or more, $P_m \geq 0.9 Q_y$, and for ductilities of 10 or more $P_m \geq Q_y$ throughout the range of t_d/T considered. If account is taken of the increased strength of materials under dynamic loading, one could probably safely conclude that $P_m \geq Q_y$ for ductilities of 5 or more.

The results of the model tests conducted in this study indicate that the required ductilities are obtainable, as shown in Chapter 5.

The prototype designs developed in this chapter established the basic sizes and configurations for the scale models tested in this study.

TABLE 3.1. VARIATION OF P_m/Q_y WITH DUCTILITY RATIO

Ductility Ratio μ	Values of P_m/Q_y		
	$t_d/T = 0.3$	$t_d/T = 1.4$	$t_d/T = 80$
1.3	1.45	0.75	0.61
1.5	1.65	0.81	0.66
2.0	2.0	0.95	0.74
3.0	2.6	1.1	0.83
4.0	3.0	1.2	0.88
5.0	3.5	1.3	0.90
6.0	3.8	1.37	0.92
7.0	4.2	1.44	0.93
8.0	4.5	1.5	0.94
9.0	4.8	1.55	0.95
10.0	5.0	1.6	0.955
15.0	6.0	1.8	0.98

(Values from Chart I, Ref. 18)

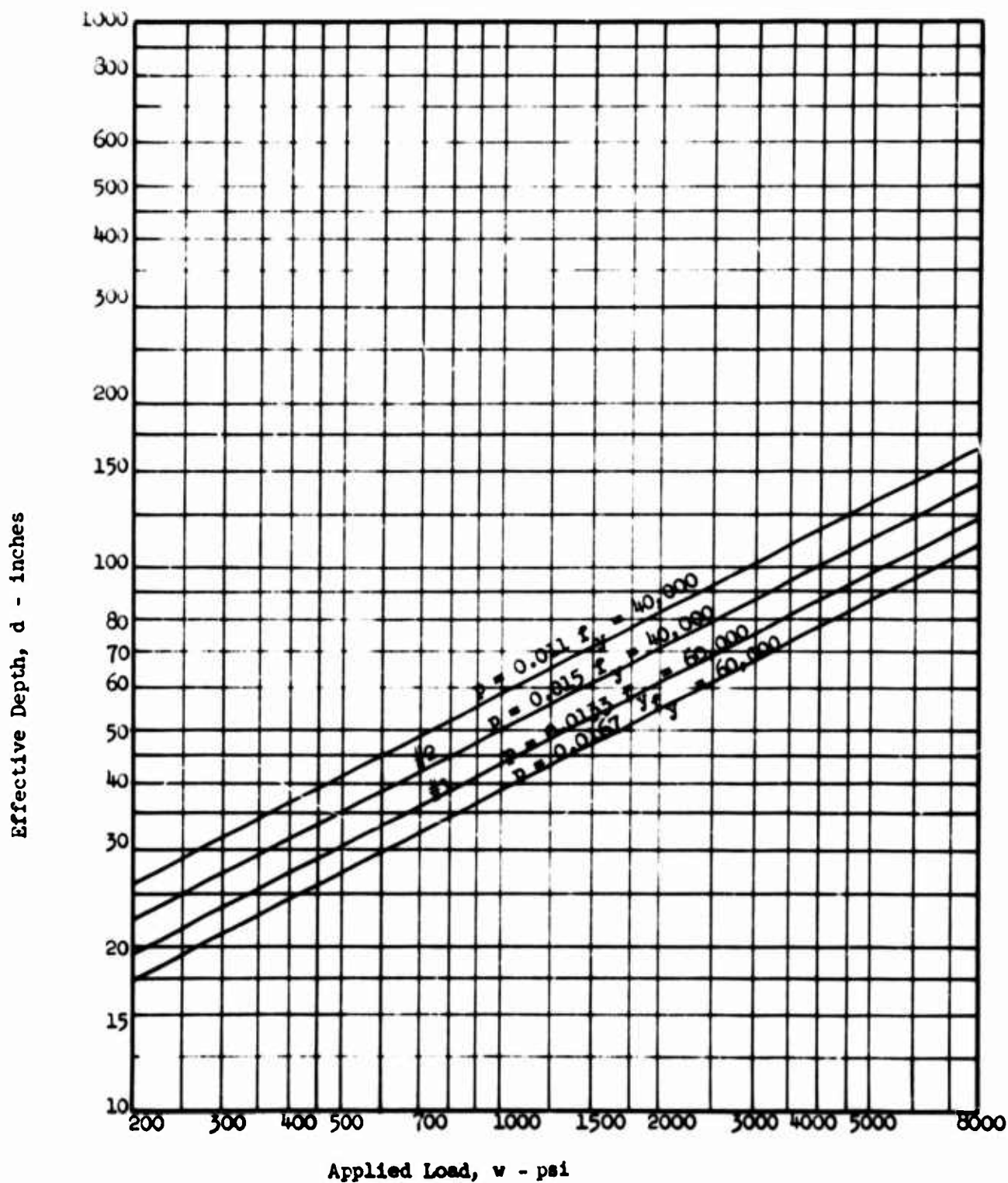


Fig. 3.1 Effective Depth of Section vs. Load

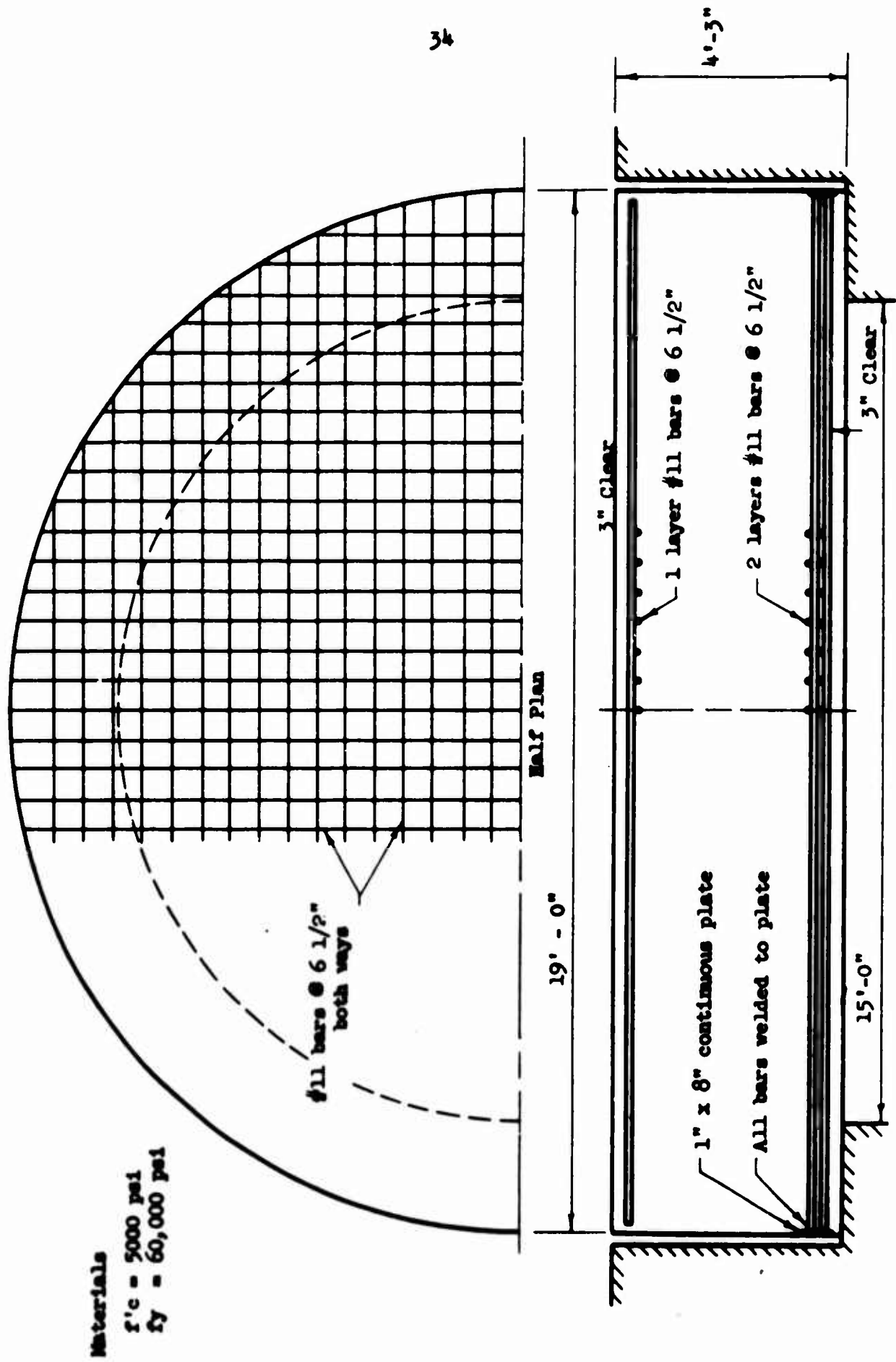


Fig. 3.2 Silo Closure Slab 60-B

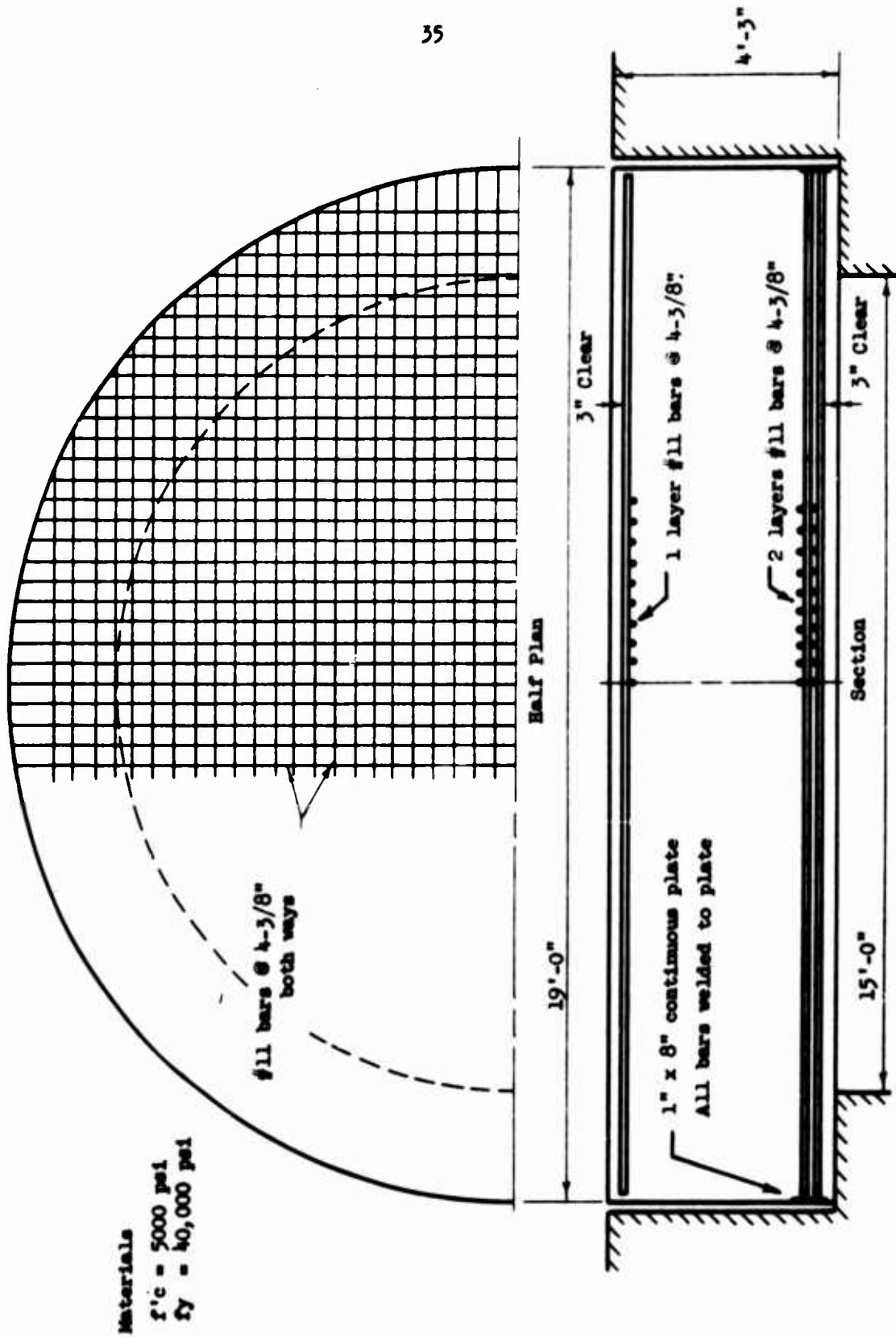


Fig. 3.3 Silo Closure Slab 40-A

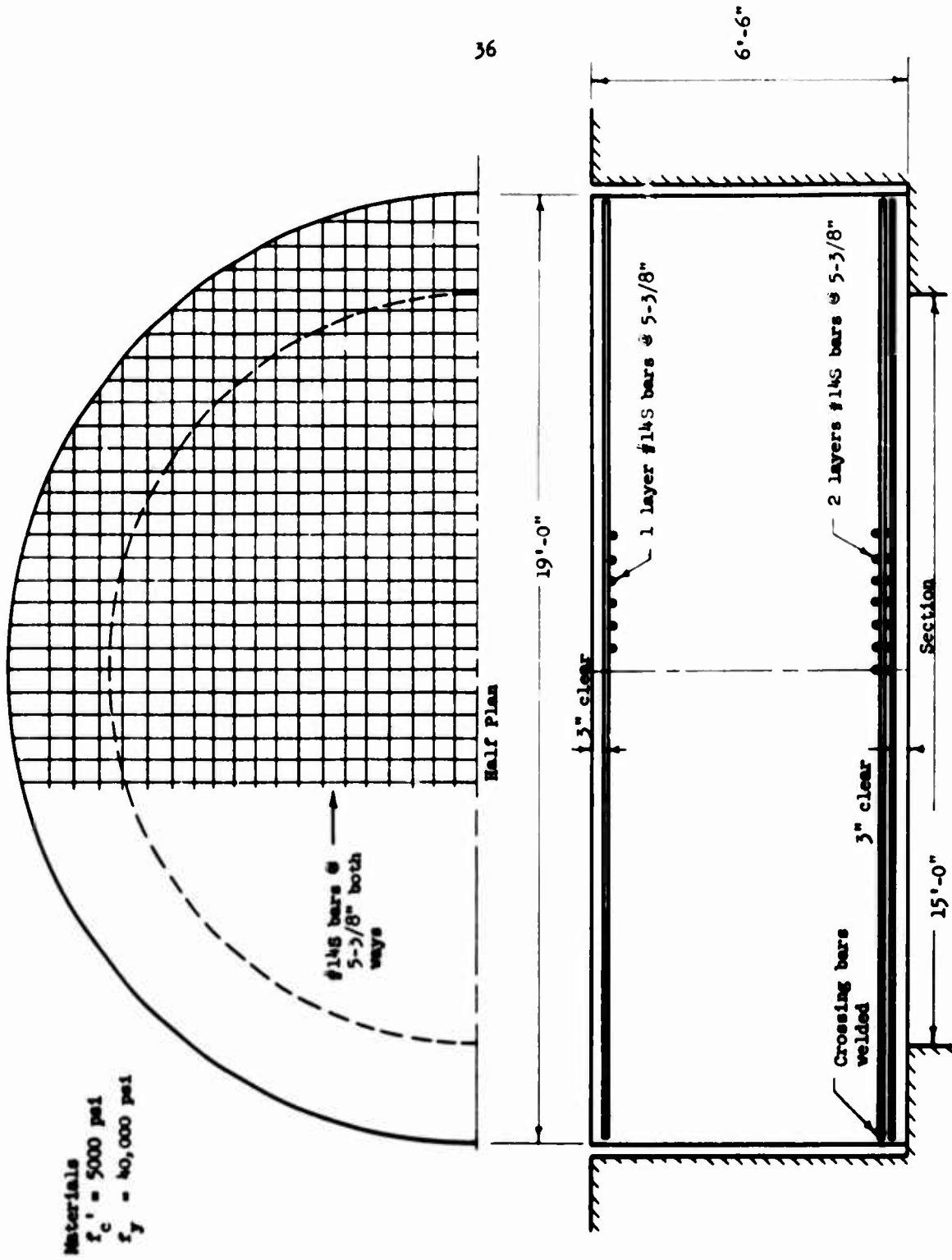


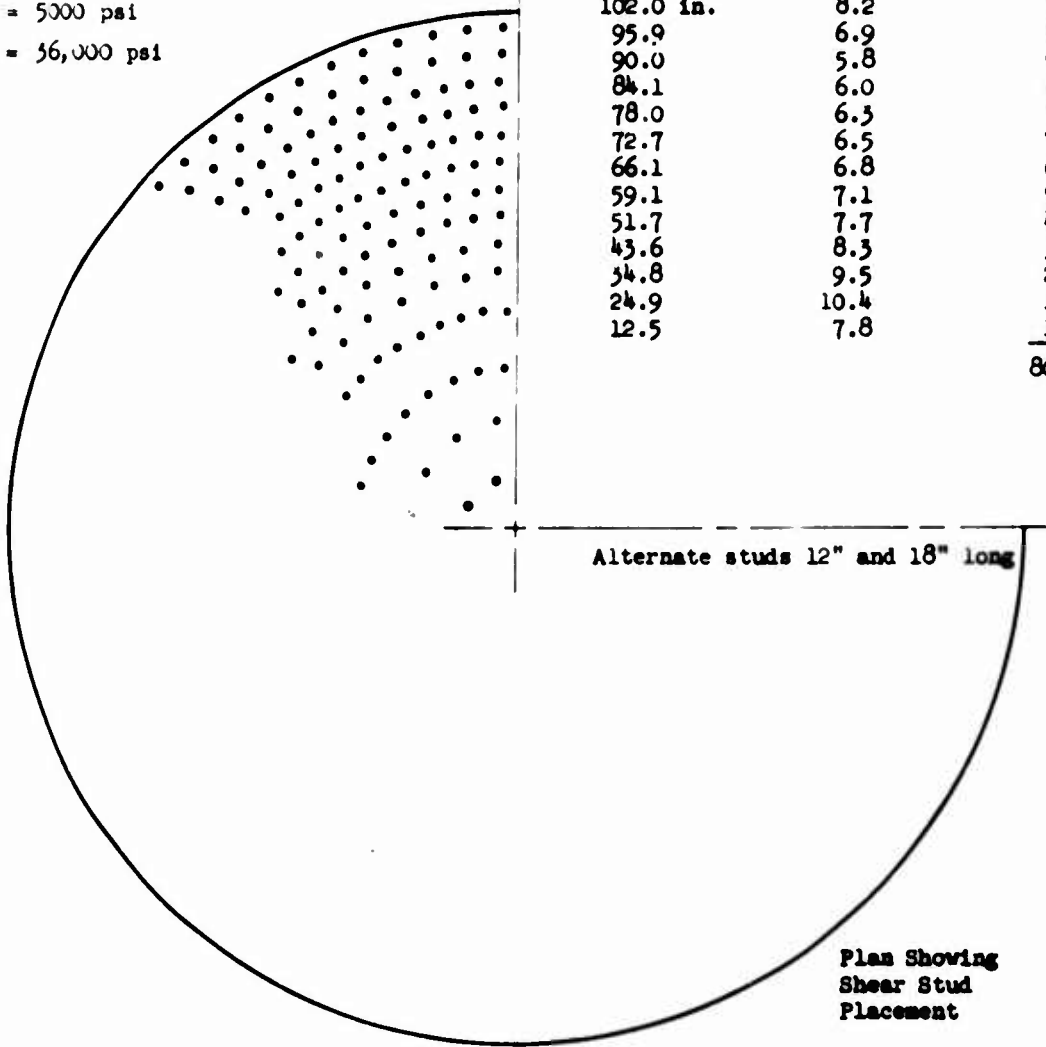
Fig. 3.4 Silo Closure Slab 40-B

37

Materials

$f_c' = 5000$ psi
 $f_y = 36,000$ psi

Radius to Row	Spacing Along Row	Number
108.4 in.	9.7 in.	70
102.0 in.	8.2	78
95.9	6.9	88
90.0	5.8	97
84.1	6.0	88
78.0	6.5	78
72.7	6.5	70
66.1	6.8	61
59.1	7.1	52
51.7	7.7	42
43.6	8.3	33
34.8	9.5	23
24.9	10.4	15
12.5	7.8	10
		<hr/>
		805



Plan Showing Shear Stud Placement

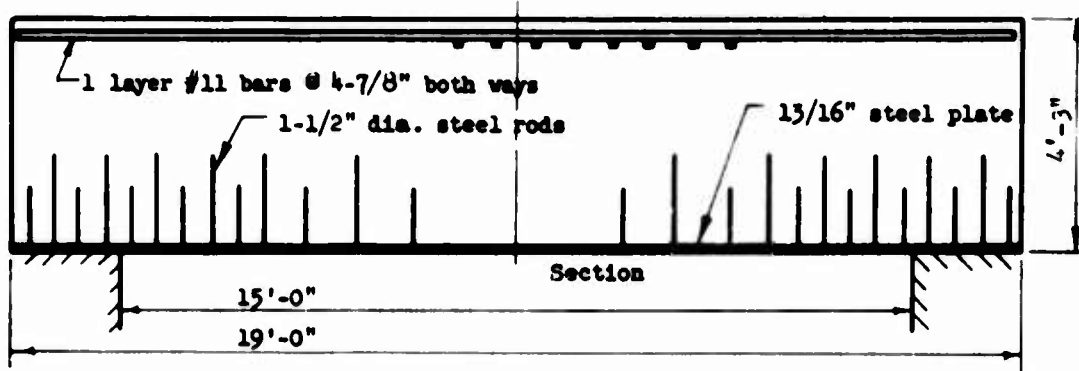
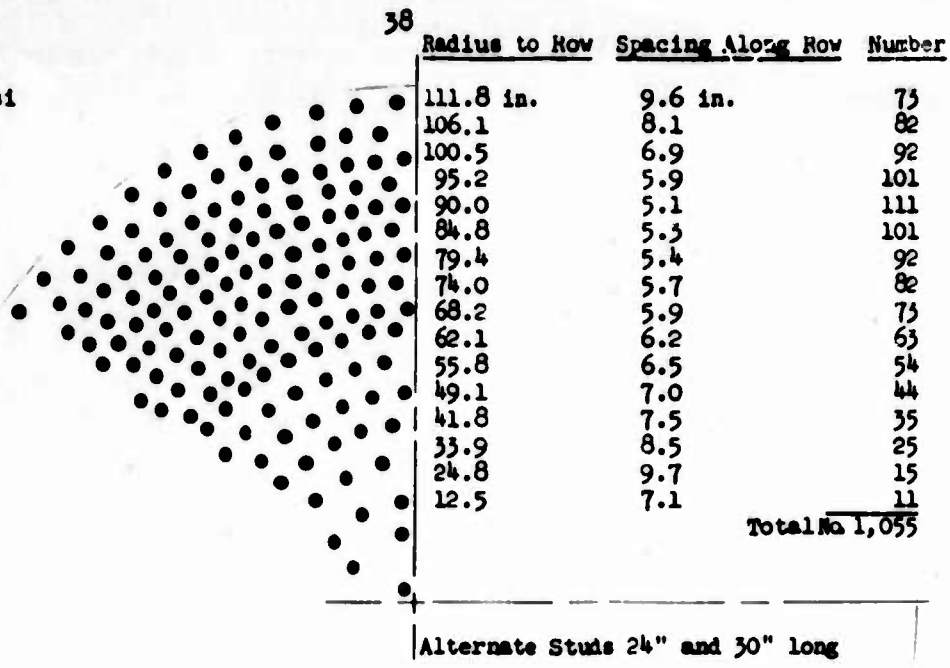


Fig. 3.5 Silo Closure Slab 36-A

Materials
 $f'_c = 5000$ psi
 $f_y = 36,000$ psi



Plan Showing
 Shear Stud
 Placement

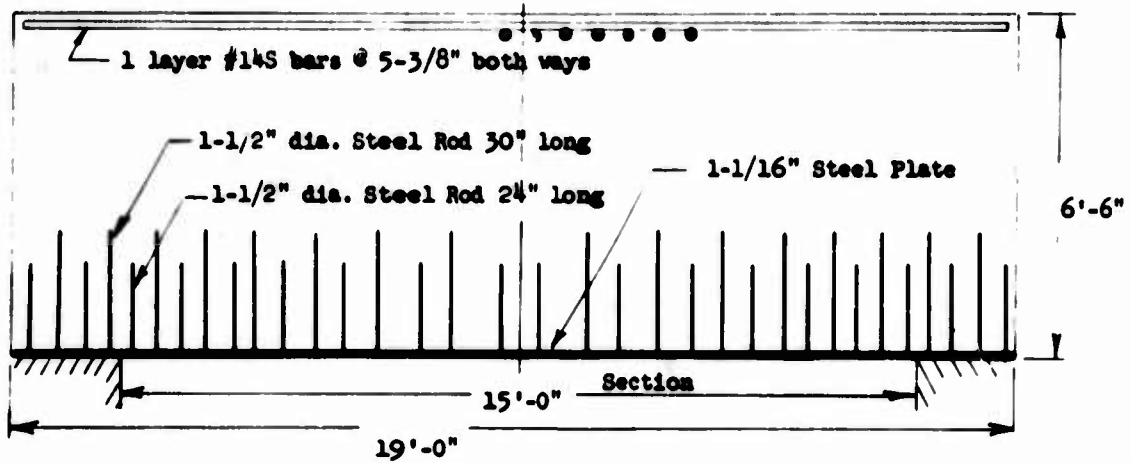


Fig. 3.6 Silo Closure Slab 36-B

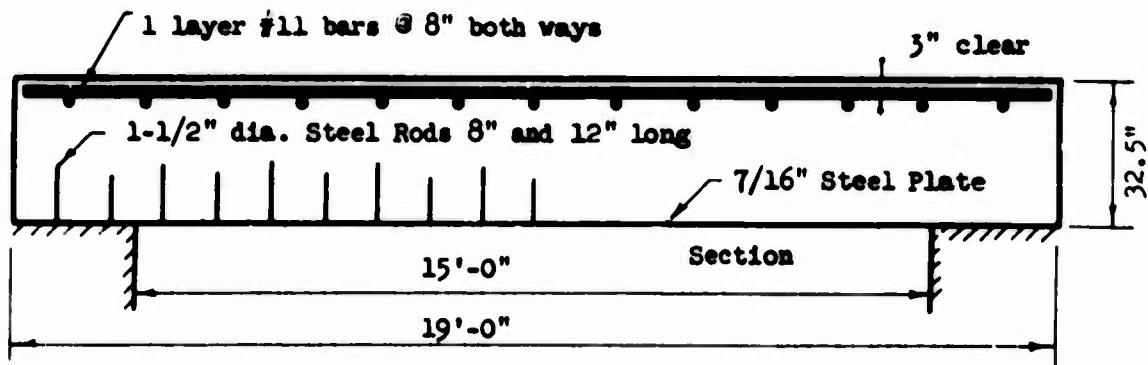
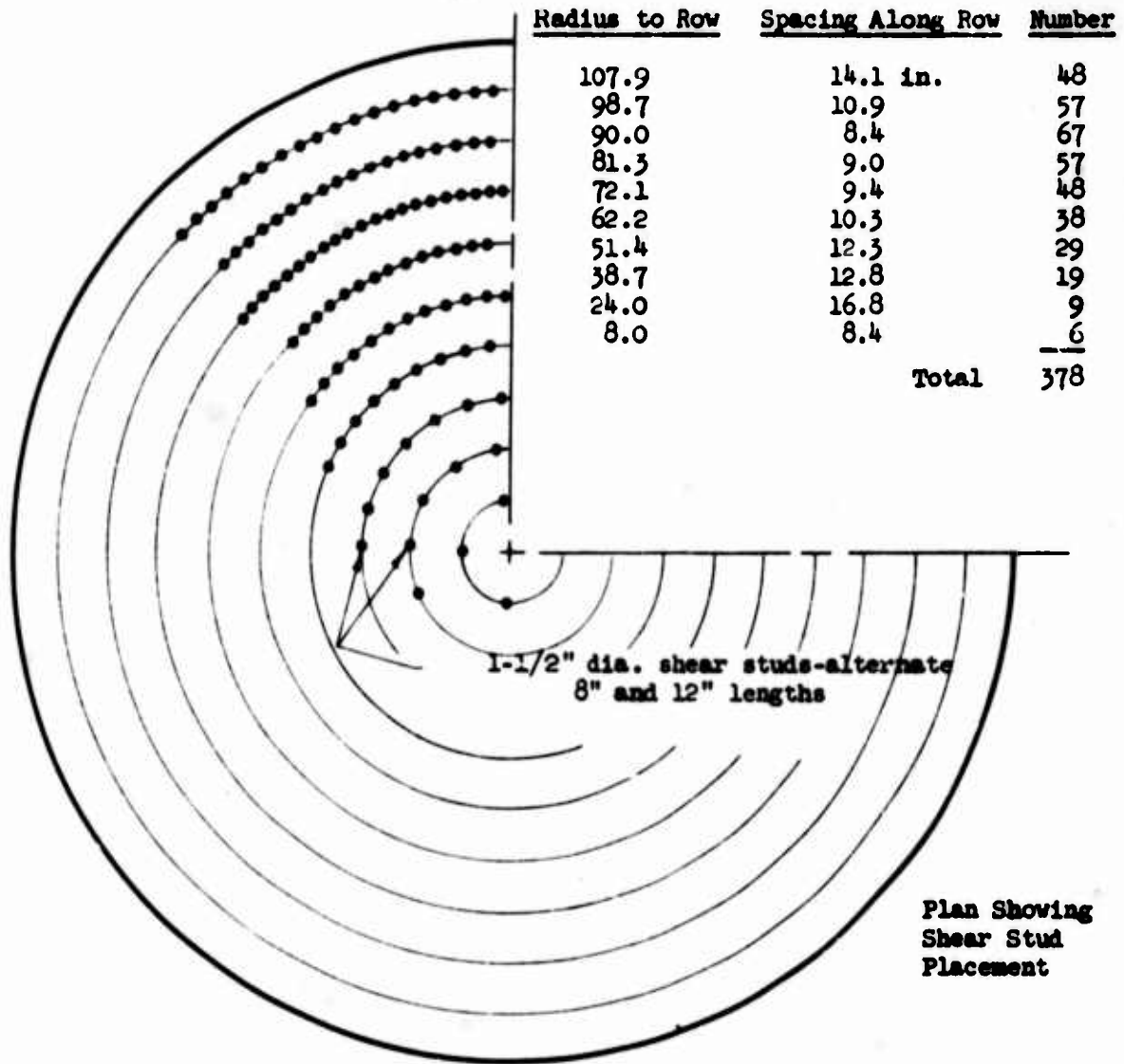


Fig. 3.7 Silo Closure Slab 36-C

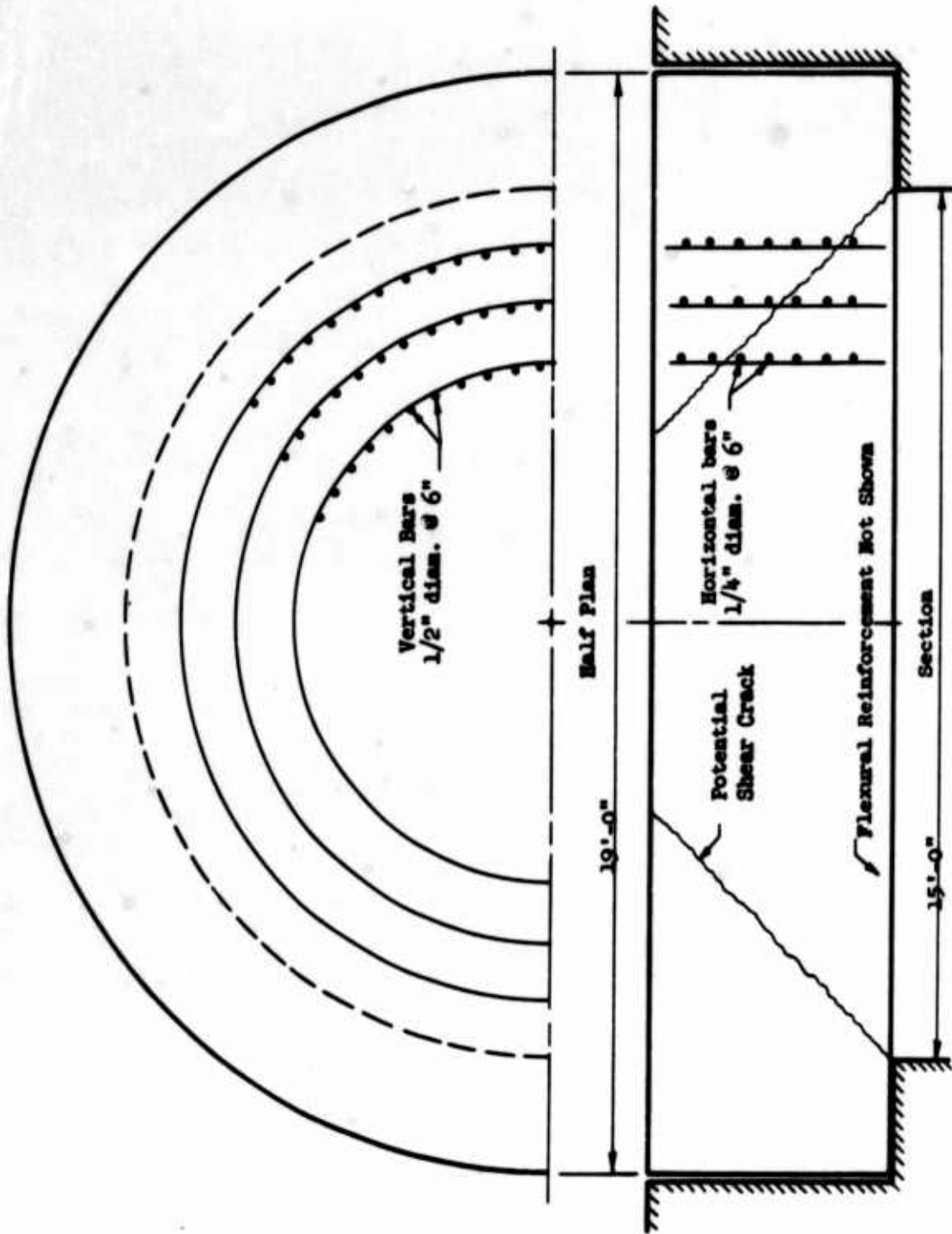


Fig. 3.8 Shear Reinforcement

CHAPTER 4
MODEL TEST SERIES

4.1. General

In order to determine the actual loads at failure and modes of failure of closures similar to those proposed in the design study (Chapter 3), a group of models was constructed and tested. Since the force required for testing to a given pressure varies with the square of the model diameter, it was necessary to use relatively small models. This consideration, and the possibility of coupling the test device to an existing dynamic loader, led to the adoption of a model scale factor of $1/14$ th.

Three series of models were tested. The first series (Series K) consisted of 17 models, all $1/14$ th scale. The models were 16.29 in. outside diameter, 3.68 in. thick, and were supported on a 12.85-inch clear span. Most were variations of scale models of the 1000-psi prototypes described in Chapter 3.

The second series (Series J) consisted of models of closure prototype 36-C, nominally designed for 300 psi. Two of the models were $1/14$ th scale and 2.30 in. thick. The remaining four models were $1/5$ th scale, 47.5 in. in diameter, 6.5 in. thick and tested over a 36-in. clear span. Two of the latter slabs were tested dynamically.

The third series (Series G) comprised twelve models of $1/14$ th scale. The series included models 3.68 in. and 5.47 in. thick, representing variations of scale models of the 1000-psi and 2000-psi

prototypes, respectively; and two 4.47-in. thick, 2000-psi models for which no prototype had been designed.

The following sections describe the scaling relationships, testing devices, model designs, material properties and instrumentation.

4.2. Scaling Relationships

The model dimensions were scaled linearly from the dimensions of the prototype structures. The physical properties of the materials, i.e., moduli of elasticity, steel yield strength and concrete tensile and compressive strength, were maintained as close to those of the prototype as possible.

So long as the physical properties of model and prototype are the same for a given distributed load intensity, the stresses and strains at corresponding points in the model and the prototype will be the same. According to Mattock (20), this is a sufficient requirement to guarantee that the strength and behavior of the prototype will be reproduced by the model even for large inelastic deformations.

In order to properly represent the shear strength of the prototype, which was expected to be governed by diagonal tension stresses, small-aggregate concrete was not used. For a given compressive strength, the small-aggregate, or "micro" concrete generally has a higher tensile strength than a normal mix, leading to deceptively high shear strengths for small-scale models. The models in this study were cast with normal-aggregate concrete, with a maximum coarse-aggregate size of $3/8$ in. Materials are discussed further in Section 4.8.

4.3. Test Device for 1/14th-Scale Models

The 1/14th-scale models were loaded hydraulically, using the fixture shown in cross-section in Fig. 4.1. The device consists of a base plate, model support ring, spacer rings for the several model thicknesses, and the pressure head. A supporting stand provides floor clearance and a mounting base for the dial gages used to measure model displacements. The gap between the spacer ring and the model is bridged by an aluminum ring 1/16 in. thick; and a 3/32-in. thick fabric-reinforced neoprene membrane covers the aluminum ring and the entire upper surface of the model. A butyl rubber O-ring completes the oil seal, as shown in the detail of Fig. 4.2. Figure 4.3 is a photo of the partly dismantled loader and supporting stand with a slab in place.

The loading device was made of ASTM A-212, grade B, steel. After assembly, the base plate, support ring, spacer rings and pressure head are bolted together with 24 1-1/4-in. high strength ($f_y = 100$ ksi) steel studs. The pressure head and studs were designed to yield at a loading pressure of 5000 psi. The uniformly distributed oil pressure for testing is obtained by supplying oil to the pressure head with a hand pump of 10,000 psi capacity.

Figure 4.1 shows the loading device as it was arranged for the 3.68-in. thick slabs. When the 2.30-in. slabs were tested, an auxiliary support ring 1.38 in. thick, 16.29 in. outside diameter and 12.85 in. inside diameter, was placed on top of the regular support ring and secured with countersunk screws. When the 4.47-in. G-Series models

were tested, an auxiliary spacer ring, 0.79 in. thick, was placed between the support ring and the regular spacer ring. An additional 1-in. thick spacer ring was used for testing the 5.47-in. thick G-Series models.

4.4. Test Device for 1/5th-Scale Models

The tests of the 1/5th-scale J-Series models were conducted in the Structural Dynamics Testing Facility of the University of Illinois Department of Civil Engineering. The testing device used is a gas-operated loader capable of producing an 800-psi gas pressure over an area four feet in diameter. The rise time of the loading pulse can be controlled to provide a minimum time to peak pressure of 2.5 milliseconds. The decay rate can be controlled to approximate the portion of a nuclear detonation from peak pressure to one-half peak pressure. The operation of the loading device is briefly discussed in Ref. 1.

Each closure model tested was supported so that its upper surface was flush with the top edge of the four-ft diameter specimen tank shown in Fig. 4.4. The slabs were supported around the outer edge by means of a cylindrical support which extended to the bottom of the specimen tank. The gap between the specimen tank wall and the model was bridged by a 3/16-in. thick steel ring, and a clamped 3/32-in. thick fabric-reinforced neoprene membrane covered the steel ring and the entire upper surface of the model. Rubber O-rings were used to complete the seal, as shown in Fig. 4.5.

4.5. K-Series Models

The K-Series of models consisted of 17 slabs which were 1/14th-scale reproductions of prototype closures 40-A, 60-B or 36-A, as described in Chapter 3, or variations of them. The models were 16.29 in. outside diameter and 3.68 in. thick. Those models that were direct reproductions of the design study prototypes were all designed to resist 1000 psi overpressure.

The 17 models of K-Series fall into five groups: (1) A group of four 1000 psi models, (2) A group of four models identical to those of the first group except that each contains 3 rings of shear reinforcement, (3) A pair of models identical to two of the models of the first group except for the addition of 6 rows of shear reinforcement, (4) A group of four "miscellaneous" models, and (5) A group of three models containing "random" reinforcement. Some of the properties of the K and J-Series of model slabs are listed in Table 4.1.

Slab K-1 was the scaled replica of prototype 40-A. The bottom reinforcement consisted of two layers of 1/8-in. square bars spaced at 5/8 in. center-to-center in the two perpendicular directions. One such layer, or mat, was provided for top reinforcement. The ends of each bar of the bottom mats were welded to a 16-gage hoop to insure anchorage. (For the readers' convenience, the thicknesses in inches of the sheet metal and wire gages used in model construction in this study are listed in Table 4.2.) Model K-1 is shown in cross-section in Fig. 4.6.

Model slab K-2 was similar to K-1 except that anchorage of the tension steel was obtained by welding the end two intersections of every bar.

Model K-3 was the scaled reproduction of prototype 36-A, the basic plate-reinforced closure. The tension reinforcement was provided by a 16-gage plate, and a single mat of 1/8 x 1/8-in. square bars supplied the compression reinforcement. The model shear connectors were 12-gage "Insul-pins," one and 1-1/2 in. long, made by Omark Industries and welded to the plate with an Omark stud welding machine. The model cross-section and shear stud arrangement are shown in Fig. 4.7.

Model K-10 was the last model of the first group of four. Tension reinforcement was provided by a 24-gage plate and one mat of 1/8 x 1/8-in. square bars. A single mat provided the compression reinforcement, as in the other model slabs. The shear stud arrangement for model K-10 is shown in Fig. 4.7. The shear studs were 12-gage "Insul-pins," one and 1-1/2 in. long.

The second group of four models included K-6, K-5, K-8 and K-11, which repeated K-1, K-2, K-3 and K-10, respectively. Each of the models in this group was supplied with three rings of shear reinforcement as shown in Fig. 4.8. The shear reinforcement was proportioned so that the force provided by each ring was equivalent to that provided by welded wire fabric ($f_y = 64$ ksi) having vertical 0.5-in. diameter bars at 6-in. spacing in the prototype slab.

Models K-3 and K-1 were reproduced a second time as K-12 and K-13, respectively, each with six rings of shear reinforcement. The location of the shear steel was as shown in Fig. 4.8.

The "miscellaneous" group of models included slabs K-7, K-4, K-9 and K-14. Model K-7 was a plain concrete specimen, included to establish a lower limit of strength and ductility.

Model K-4 was reinforced with a 24-gage plate only and had the lowest steel ratio of any of the models. Its nominal design load was 500 psi. The shear stud arrangement for K-4 is shown in Fig. 4.7.

Model K-9 was reinforced with a circular angle retaining ring at the lower edge of the slab and by a single compression mat near the top surface. The plan and cross-section are shown in Fig. 4.9.

Model K-14 was identical to K-3. Test conditions were changed, though, by polishing the lower surface of the slab and the upper surface of the support ring and by greasing these surfaces prior to testing.

Models K-15, K-16, and K-17, fabricated of randomly reinforced concrete, composed the final group of the K-Series of models. Chopped wire concrete is of interest because of its high tensile strength, high cracking resistance and resistance to shattering under impact or explosive loading conditions. Unfortunately, no practical way of making a full size closure slab is now known. The material mixes are discussed further in Section 4.8.

4.6. J-Series Models

The J-Series included six models. All were scaled from prototype 36-C, which was designed for a nominal 300-psi overpressure.

Slabs J-1 and J-2 were identical 1/14th-scale models, each reinforced with a 24-gage plate at the bottom and a single mat of 1/8 x 1/8-in. square bars at 1-1/4-in. centers each way at the top. These slabs were 2.30 in. thick. Figure 4.10 shows the cross-section

and a plan view with a shear stud layout. The shear connectors were 12-gage "Insul-pins" one and 1-1/2 in. long.

Slabs J-5 through J-8, (numbers J-3 and J-4 were not used), were 1/5th-scale models of closure 36-C. The slabs were 47.5 in. outside diameter, 6.5 in. thick and supported on a 36-in. diameter clear span. The outside diameter was slightly greater than the scaled dimension to simplify sealing in the existing 4-ft specimen tank. Tension reinforcement was provided by a 16-gage plate. One mat of No. 3 deformed bars at 3-1/2 in. centers each way supplied the compression reinforcement. The shear connectors were 3/16-in. diameter round bars, two and 2-1/2 in. long. The slab cross-section and shear stud arrangement are shown in Fig. 4.11. Model J-7 was defective and was not tested.

4.7. G-Series Models

The G-Series included twelve 1/14th-scale models of 1000 and 2000-psi prototypes. Model thicknesses of 3.68 in., 4.47 in. and 5.47 in. were represented and concrete strengths were varied in several cases. Properties of the G-Series model closure slabs are listed in Table 4.3.

Models G-1, G-2 and G-3 were identical to each other and to model K-3, except that concrete strengths were varied. Cylinder strengths for these models were 7050, 5130 and 3030 psi, respectively. The purpose of this group of models was to demonstrate a relation between shear stress at failure and concrete compressive strength.

The scaled thickness of the 2000-psi prototypes 40-B and 36-B is 5.57 in. Variations of the 2000-psi models were to be cast at 4.57 in. thick. Due to an error in dimensioning, however, the models produced were 5.47 in. and 4.47 in. thick. Models G-4 and G-5 were tested with test fixture spacers totaling 5.57 in. thickness. The error was discovered and 0.1 in. was removed from the 0.89-in. spacer ring. The test machine was then compatible with model slab thickness for the remainder of the tests, though the prototype thicknesses were not exactly scaled.

Model G-4 was a plain concrete slab 5.47 in. thick, intended to provide a lower strength limit for the thicker slabs.

Model G-5 was a 5.47-in. thick reproduction of prototype closure 36-B except that the 2-in. long "Insul-pins" used for the longer shear studs were 10 gage rather than 12 gage, as designed. The 1-1/2-in. long "Insul-pins" were of 12-gage material. Tension reinforcement was provided by a 14-gage plate and compression reinforcement by a single mat of 1/8 x 1/8-in. square bars at 5/8-in. spacing each way. Model G-5 was the last of the plate-reinforced models in which the number of shear studs in the prototype was reproduced exactly with "Insul-pins" of scaled diameter. The remaining G-Series models were designed directly, using Viest's (17) equation for shear connectors of diameter less than one inch, which results in fewer studs required. A plan and cross-section of the model slab are shown in Fig. 4.12.

Model G-7 was roughly equivalent to a G-5 model with shear reinforcement added, although there were actually several significant differences. Tension and compression reinforcement were identical, but

the shear studs were 10-gage "Insul-pins" two and 2-1/2 in. long. Allowable loads per shear connector were computed from Viest's formula for rods smaller than one inch in diameter:

$$Q = 5.25D_s^2 \sqrt{4000f'_c} \quad (4.1)$$

For units of kips and ksi this can be conveniently rewritten as

$$Q = 10.5D_s^2 \sqrt{f'_c} \text{ kips} \quad (4.2)$$

For studs 0.135 in. in diameter, the allowable load per stud for $f'_c = 5$ ksi, is 0.428 kips. For the model dimensions, one can derive the following formula for number of shear studs:

$$n = \frac{446}{Q_j d} \quad (4.3)$$

which is equivalent to Eq. (3.9) derived for the prototype dimensions. For the 10-gage studs and $d = 5.47$ inches, $n = 424$ studs. This compares with about 820 studs that would have been required for a prototype designed for studs 1.89 in. in diameter, i.e., 14×0.135 in., using the method of Chapter 3.

Alternate shear connectors in three rings were replaced with 11-gage annealed wires which were welded to the steel plate and extended to the bottom of the compression bars. Anchorage at the top of the shear reinforcement was supplied by horizontal 11-gage wire hoops, welded to each of the vertical wires. A plan and cross-section of the model are shown in Fig. 4.13. Figure 4.14 is a photograph of the shear reinforcement.

Model G-10 was identical to G-7 except that one mat of $1/8 \times 1/8$ -in. square bars spaced at $13/16$ in. each way provided additional tension reinforcement.

In order to obtain data at one additional L/d ratio, two models 4.47 in. thick were tested. Model G-6 was supplied with tension reinforcement in the form of a 14-gage plate and one mat of $1/8 \times 1/8$ -in. square bars at $13/16$ in. spacing. The compression reinforcement was one mat of $1/8 \times 1/8$ -in. square bars at $5/8$ in. on centers. Shear connectors were 10-gage "Insul-pins," two and $2-1/2$ in. long. About 350 pins were required. The cross-section, plan and shear stud arrangement for G-6 are shown in Fig. 4.16.

Model G-8 was identical to G-6 except that the nominal concrete compressive strength was 7000 psi rather than 5000 psi.

Models G-9, G-11 and G-12 compose a miscellaneous group of models, each constructed for a specific purpose. Model G-9 was identical to K-3 and was built to test the ability of the K-3 (or prototype 36-A) design to withstand repeated loadings.

Model G-11 was also identical to K-3, except that alternate shear studs in one ring were replaced by vertical shear reinforcement consisting of $1/4$ -in. threaded rods. The threaded rods were anchored at the bottom by standard $1/4$ - 20 nuts welded to the plate and at the top by specially manufactured nuts, $3/4 \times 3/4 \times 1/4$ in. thick. This scheme was designed to facilitate assembly of the model and to avoid the loss of anchorage which may have occurred due to weld failures in other attempts at providing shear reinforcement. In the prototype, deformed bars welded directly to the bottom plate and hooked

at the top would supply the shear reinforcing. The cross-section and plan of model G-11 are shown in Fig. 4.17. Figure 4.15 is a photograph of model G-12 prior to casting which illustrates the threaded rod shear reinforcement common to G-11 and G-12.

The final model of the series, G-12, represented an attempt to gain additional strength by confining the concrete in a steel shell in a manner similar to that used successfully by IIT Research Institute (5) and the Air Force Academy (6). The model was reinforced with an 11-gage plate at the bottom and by two mats of 1/8 x 1/8 in. square bars at 5/8 in. on centers at the top. Shear connectors were 10-gage "Insul-pins," two and 2-1/2-in. long, in the same pattern as for G-7 and G-10. Shear reinforcement was provided by 1/4-in. threaded rods as in G-11. The model was encased in an 11-gage steel sleeve which extended from the top of the steel plate to the upper surface of the slab. The model is shown in Fig. 4.18 and 4.15.

The thickest steel that can be rolled into a 16-in diameter hoop in the University of Illinois shops is 11 gage. Model G-12 was designed on the basis of this limitation. A simple hoop-stress analysis was used to determine the improvement in bearing stress capacity resulting from confinement by an 11-gage hoop. The confining stress, or minor principal stress when the hoop yields, is given approximately by

$$\sigma_3 = \frac{2f_y t}{D_o} \quad (4.4)$$

where t is the thickness of the hoop and D_o its outside diameter.

The bearing stress, which is the major principal stress in the support area, is obtained from the formula of Richart, et al (21):

$$\sigma_1 = 4.1\sigma_3 + f'_c \quad (4.5)$$

which in this case becomes

$$\sigma_1 = \frac{8.2f_y t}{D_o} + f'_c \quad (4.6)$$

From Eq. (3.5) and (4.6) the allowable load based on bearing is found to be

$$w = \frac{3.1f_y t}{D_o} + \frac{f'_c}{2.65} \quad (4.7)$$

For $f_y = 40$ ksi, $t = 0.1196$ in. and $f'_c = 5$ ksi, w is found to be 2.8 ksi. With no confinement the load w is only 1.9 ksi.

Shear reinforcement was provided to resist 800 psi of the total load applied to a truncated cone with upper surface 5.5 in. in diameter. Each 1/4-in. threaded rod was capable of resisting a load P_y of 0.8 kip after annealing, and the number of rods required was computed as

$$n = \frac{\pi D^2 w}{4 P_y} = \frac{(0.7854)(5.5)^2(0.8)}{0.8} \approx 24$$

The tension plate thickness was chosen to carry the 2800-psi load computed above. Equation (3.6) may be rewritten for the model dimensions as

$$p = 0.213 w/d^2 \quad (4.8)$$

and for $w = 2.8$ ksi, $d = 5.47$ in., the proportion of steel is found to be $p = 0.02$. The plate thickness required is then $t = (0.02)(5.47) = 0.1094$ in. An 11-gage plate, $t = 0.1196$ in., was chosen.

4.8. Materials

The materials used in the construction of the models are described in the following paragraphs.

The concrete used in all models except slabs G-1, G-3, G-8 and the randomly reinforced specimens had a nominal cylinder strength of 5000 psi. Type III Portland cement was used so that the required strength could be obtained after seven days of moist curing and seven days of drying. The 1/14th-scale slabs were moist cured in the Talbot Laboratory fog room and the 1/5th-scale slabs were cured under damp burlap and polyethylene. In all cases the test cylinders received the same curing conditions as the models.

The coarse aggregate was pea gravel with a maximum size of 3/8 in. Grain-size distributions for the aggregates are shown in Fig. 4.19. The cement:sand:gravel ratio for the 5000 psi concrete was 1:3.2:3.5 by weight and the nominal water-cement ratio was 0.69 by weight. The model concrete was not "micro-concrete," but a material with the strength and deformation characteristics of ordinary high-strength concrete.

Stress-strain properties were obtained for cylinders from an initial trial batch. For a group of three cylinders with an average f'_c of 5500 psi, the initial modulus of elasticity was 3.8×10^6 psi,

the secant modulus to $0.5f'_c$ was 3.4×10^6 psi, and the maximum stresses were reached at strains between 0.0025 and 0.0027.

The concrete for model slab G-3 was identical to the 5000-psi concrete described above. The 3000-psi cylinder strength for G-3 was obtained by curing for only three days. The 7000-psi concrete for model slabs G-1 and G-8 utilized a cement:sand:gravel ratio of 1:2.52:2.76 and a nominal water:cement ratio of 0.545 by weight. The cement and aggregates used in G-1 and G-8 were the same as those used in the 5000-psi specimens.

The randomly reinforced slabs, K-15, K-16 and K-17, were cast from concrete containing short pieces of wire. No coarse aggregate was used. The cement:sand ratio was 1:2.5 and the water:cement ratio was 0.5, both by weight. The concrete contained 2.98 percent of wire by volume. Short lengths of 0.017 in. diameter steel wire were used. Pieces of smooth, wavy wire 1.0 in. long were used in K-15. Smooth, straight pieces 1.2 in. long were used in K-16. Straight, crimped pieces were used in model slab K-17.

In the mixing process, the mortar was mixed, and the wire was then gradually added to the running mixer.

The compression strengths of the concrete in each slab model are shown in Table 4.4. The strengths shown for the 4 x 8-in. cylinder are the average of four cylinders and are assumed to be representative of the 1/14th-scale slabs. The strengths reported for the 6 x 12-in. cylinder are the average of two cylinders tested, and are assumed to be representative of the concrete in the 1/5th-scale slabs.

The tensile strengths of the concrete are shown in Table 4.5. These were obtained from split cylinder tests of 4 x 8-in. and 6 x 6-in. cylinders. At least three 4 x 8-in. and two 6 x 6-in. cylinders were tested from each batch.

Strength properties of the reinforcement used in the various models are shown in Table 4.6. The yield and ultimate stress values shown are the averages of several tests. Additional information concerning the various reinforcing materials is contained in the following paragraphs.

The 1/8-in. square bars were of AISI B-1118 steel, annealed at 1300°F. for three hours and washed in hot, dilute hydrochloric acid before use. A typical stress-strain curve is shown in Fig. 4.20.

The 11, 14, 16 and 24-gage sheets were of black, hot-rolled steel obtained from the University sheet metal shop. The material did not exhibit a sharply defined yield point, but did have a yield plateau. In some cases the yield strength in two perpendicular directions differed by one to two ksi. In such cases the averages are reported. Typical stress-strain curves for 16 gage and 24 gage specimens are shown in Figs. 4.21 and 4.22, respectively.

The 16-gage wire used as shear reinforcement in K-Series slabs was cut to length, stretched in a frame and annealed for two hours at 1150°F. in an electric oven. Several batches of the steel were annealed, and the yield strengths were slightly different, as indicated in the table. A typical stress-strain curve is shown in Fig. 4.23.

The 11-gage wire used as shear reinforcement in model slabs G-7 and G-10 was cut to length and annealed in the electric oven for two hours at 1200°F.

The 1/4-in. threaded rods used for shear reinforcement in models G-11 and G-12 were cut to length and annealed at 1500°F for one hour in the electric oven.

4.9. Fabrication

Procedures used in constructing the model slabs are discussed in this section.

The 1/14th-scale models, except G-12, were cast in a steel form. The form consisted of a steel bottom plate and a side section made by cutting a slice from a piece of thick-walled pipe, clamping the gap shut, and machining the inner surface to the proper diameter. In use, releasing the clamp allowed the pipe to open slightly and facilitated removal of the model. Two side pieces were constructed for 3.68-in. and 5.47-in. high models. Plywood fillers, 1.38 in. and 1.0 in. thick, were used with these forms to make 2.30-in. and 4.47-in. high models.

In general, the fabrication sequence was: (1) Assemble the reinforcing steel. (2) Place the tension reinforcement in the form. (3) Pour concrete to the level of the compression steel, and place the compression steel. (4) Pour the remaining concrete and finish the top surface. Variations from this sequence and additional notes on construction of the models are discussed in the paragraphs following.

The 10-gage, 12-gage and 3/16-in. shear studs were electrically welded to the bottom steel plates with an Omark stud welding gun. This device was also modified and used to attach the 11-gage wires

used as vertical reinforcement in model slabs G-7 and G-10. The shortest studs were always welded first.

The stresses built up during the stud-welding process deformed the steel plates into a dish shape. To hold the plate flat for casting, eight threaded studs were welded to the underside of the plate and used to bolt it securely to the form.

The outside steel confining ring for model G-12 was tack-welded to the finished bottom plate and the concrete was then placed directly in the assembled steel shell, with no other form required.

The K-Series models with 16-gage wire shear reinforcement required a variation in the usual casting procedure. Since the shear steel extended through the compression steel mats in these models, all of the reinforcing was assembled before any concrete was placed. This required that the concrete be filtered through the 1/2-in. square openings in the compression steel. To facilitate this operation the slump was increased to five or six inches and the curing time was extended to compensate for the expected change in strength.

The reinforcing assembly procedure for models G-11 and G-12 was: (1) The 1/4-in. standard nuts were welded in place on the steel plate. (2) Shear studs were attached using the Omark welder. (3) The 1/4-in. threaded rod shear reinforcement was screwed into the nuts on the bottom plate and the 3/4 by 3/4-in. nuts were attached at the upper ends. The need for an assembly procedure which would eliminate interference between the shear studs and the longer vertical rods dictated the use of threaded rods for these models.

The 1/5th-scale models were cast in a form having 16-gage sheet metal sides and a plywood base. The models were large enough to allow ordinary concrete placement and vibration procedures.

4.10. Instrumentation

The instrumentation for measuring deflection, strain and pressure is described in this section. The instrumentation used for the 1/14th-scale slabs is discussed first, and a description of the 1/5th-scale instrumentation follows.

The deflections of the bottom surface of each 1/14th-scale slab were measured at five points along a single diameter. The locations of these points are shown in Fig. 4.24(a). Measurements were made with dial gages, sensitive to 0.001 in., attached to the supporting stand and actuated by push rods as illustrated in Fig. 4.25. An additional gage measured the deflection of the test device support ring relative to the supporting stand.

Lateral movement of the G-Series of 1/14th-scale models was measured at a single point by a dial gage mounted as shown in Fig. 4.26.

Strain gages were placed on the reinforcing of all of the model slabs except K-1. Four gages were placed on the bottom steel, and four on the top steel. The gages on the top steel were located as shown in Fig. 4.27(a). The gages on the bottom steel were in similar locations on the bar-reinforced models. The gages on the plate-reinforced models were located as shown in Fig. 4.27(b). The gages on bars were always placed on the bars nearest the slab surface. Gages on plates were placed on the lower surface of the plate.

In addition to the gages on the compression steel of K-9, two gages were placed on the outside vertical surface of the steel retaining ring to measure the horizontal strain in the ring. The gages were located 0.5 in. and 1.2 in. above the lower surface of the slab.

Model slab G-12 was also equipped with two additional gages, one located on the outside confining ring, about $1/4$ in. above the lower surface of the model, and the other placed at mid-length on one of the $1/4$ -in. threaded shear reinforcing rods.

The gages were Budd Metalfilm foil gages, type C6-111B or C6-121B, except that in some cases SR-4, type A-7 paper backed gages were substituted for application to the exterior of the model. The foil gages were attached with an epoxy-resin cement. Eastman 910 or Budd GA-1 contact cement was used to bond the SR-4 gages.

Gages placed on reinforcing bars were waterproofed with two or three coats of Gagekote No. 2 waterproofing compound and then given two coats of Petrolastic. Gages placed on the outside of the slab were treated with Gagekote only.

The strains were read with a Baldwin SR-4 strain indicator and were recorded manually.

The hydraulic pressures were read by means of Bourdon tube gages. Gages of 2000, 3000, 5000 and 10,000 psi capacity were used at different times as the project progressed. The gages were calibrated with the aid of a dead-loading calibrating device.

The $1/5$ th-scale tests required different instrumentation. The two dynamic tests required automatic data recording and the

inaccessible location of the slab surfaces in the test fixture demanded remote readout of the deflection gages.

Deflections were measured at five locations along a single diameter on the lower surface, as shown in Fig. 4.24(b). Slide-wire electrical deflection gages with a total travel of 2.0 in. were mounted on an 8-in. wide flange section and actuated by push-rods. Figure 4.28 shows the actuating assembly. The gages were connected so that each formed two active arms of a four-armed bridge measuring circuit.

The strain gages on the 1/5th-scale slabs were located as shown in Fig. 4.28. The four gages on the compression reinforcement were installed and waterproofed, as described earlier, before the concrete was cast. The lead wires from these gages were brought out through a hole in the steel plate. Budd Metafilm Model gages, type C6-141B, were attached to the compression reinforcement by means of an epoxy cement. Similar gages were attached to the lower surface of the slab with Eastman 910 cement after the concrete had cured. In addition, supplementary paper-backed gages were attached to the plate near gage points 1 and 3, in order to compare the behavior of the different gages.

During the static test of slab J-5, the pressures in the chamber above the slab and in the tank below the slab were measured with CEC Model 4-313 pressure gages, which employ electrical resistance sensing elements. The gages were calibrated against Bourdon tube gages, which were also used to monitor the pressures. During the dynamic tests, pressures were measured with Kistler Model 601

piezoelectric pressure transducers which had been calibrated against Bourdon tube gages.

The data from the deflection, strain and pressure gages were recorded on magnetic tape during each of the tests. Data stored on magnetic tape at the University of Illinois Structural Dynamics Laboratory can be recovered in several forms. In this investigation only graphical output has been used.

This completes the discussion of the design, construction and instrumentation of the model slabs. Test results are presented in the chapter following.

TABLE 4.1. PROPERTIES OF MODEL CLOSURE SLABS, K AND J SERIES

Slab No.	Date Cast	Date Tested	f'_c psi	Max. Load psi	Reinforcement
K-1	2-25-66	4-13-66	5870	2460	2 mats welded to band
K-2	3-18-66	4-21-66	6400	2450	2 mats welded at ends
K-3	4-12-66	4-28-66	5720	2150	16 ga. plate
K-4	4-15-66	5-5-66	5260	1735	24 ga. plate
K-5	4-26-66	5-12-66	5650	2710	2 mats welded at ends, 3 rings shear steel
K-6	5-5-66	5-19-66	5030	2310	2 mats welded to band, 3 rings shear steel
K-7	5-12-66	6-16-66	5420	2120	None
K-8	5-17-66	6-17-66	4800	2150	16 ga. plate, 3 rings shear steel
K-9	5-20-66	6-23-66	5000	2140	Angle retaining ring
K-10	6-9-66	6-28-66	5970	2160	24 ga. plate, 1 mat welded at ends
K-11	6-23-66	7-7-66	4050	1655	24 ga. plate, 1 mat welded at ends, 3 rings shear steel
K-12	6-29-66	8-2-66	5970	2200	16 ga. plate, 6 rings shear steel
K-13	7-7-66	7-28-66	5650	2610	2 mats welded to band, 6 rings shear steel
K-14	7-8-66	8-12-66	6560	2170	16 ga. plate (Greased support)
J-1	7-13-66	8-17-66	5540	785	24 ga. plate (2.3" thick x 12.85" span)
J-2	7-19-66	8-18-66	6220	720	24 ga. plate
J-5	8-3-66	1-10-67	5560	560	16 ga. plate (6.5" thick x 36" span)
J-6	8-9-66	2-27-67	5760	592	16 ga. plate
J-7	8-15-66		Not tested		16 ga. plate
J-8	8-16-66	5-12-67	6430	675	16 ga. plate
K-15	----	8-26-66	5890*	2100	Random - smooth, wavy wire 1" long
K-16	----	8-29-66	7120*	1205	Random - smooth, straight wire 1.2" long
K-17	----	8-29-66	7240*	2850	Random - straight, crimped wire 1" long

* 2" x 4" cylinders

TABLE 4.2. SHEET METAL AND WIRE GAGES

Gage No.	United States Standard Gage (Sheet Metal)	United States Steel Wire Gage
	Thickness, Inches	Diameter, Inches
10	-----*	0.135
11	0.1196	0.1205
12	-----	0.1055
14	0.0747	-----
16	0.0598	0.0625
18	0.0478	-----
24	0.0239	-----

* Only those sizes used in model fabrication are tabulated.

TABLE 4.3. PROPERTIES OF MODEL CLOSURE SLABS, G-SERIES

Slab No.	Date Cast	Date Tested	f'_c psi	Max. Load psi	Thickness Inches	Reinforcement
G-1	2-22*	5-17	7050	2280	3.68	16 ga. plate (identical to K-3)
G-2	2-23	3-21	6130	2175	3.68	16 ga. plate (identical to K-3)
G-3	3-5	3-8	3030	1575	3.68	16 ga. plate (identical to K-3)
G-4	5-18	6-5	5400	1940	5.47	None
G-5	6-20	7-11	5600	2800	5.47	14 ga. plate
G-6	7-6	7-27	5750	2775	4.47	14 ga plate and 1/8" sq. bars at 13/16"
G-7	7-24	8-7	4670	2925	5.47	14 ga. plate, 11 ga. shear reinf. (3 rows)
G-8	8-2	8-17	7030	3400	4.47	Identical to G-6
G-9	8-14	8-29	5250	2300	3.68	16 ga. plate (identical to K-3)
G-10	8-22	9-8	5500	3400	5.47	14 ga. plate and 1/8" sq. bars at 13/16" also 11 ga. shear reinf. (3 rows)
G-11	9-7	9-25	5100	2480	3.68	14 ga. plate and 1/4" threaded rod shear reinf. (1 row)
G-12	9-7	9-22	5100	4100	5.47	11 ga. plate, 11 ga. confining ring and 1/4" threaded rod shear reinf.

* All dates in 1967.

TABLE 4.4. CONCRETE COMPRESSIVE STRENGTH DATA

Slab No.	Date Cast	Date Tested	Slump in.	f' _c - psi	
				4 x 8 in.	6 x 12 in.
K-1	25 Feb. 1966	13 April 1966	6 1/2	5870	5985
K-2	18 March	21 April	1 1/2	6400	5500
K-3	12 April	28 April	2 1/2	5720	5190
K-4	15 April	5 May	2	5260	5200
K-5	26 April	12 May	2 1/2	5650	5060
K-6	5 May	19 May	2	5030	4760
K-7	12 May	16 June	5 1/2	5420	5330
K-8	17 May	17 June	6	4800	4930
K-9	20 May	23 June	6 1/2	5000	5230
K-10	9 June	28 June	1	5970	5470
K-11	23 June	7 July	6 1/2	4050	4010
K-12	29 June	2 Aug.	3	5970	5700
K-13	7 July	28 July	2 1/4	5650	5460
K-14	8 July	12 Aug.	1	6560	6520
J-1	13 July	17 Aug.	3	5540	6030
J-2	19 July	18 Aug.	2	6220	5850
J-5	3 Aug.	11 Jan. 1967	3 1/4	5130	5560
J-6	9 Aug.	27 Feb. 1967	2 1/2	5440	5760
J-7	15 Aug.	Not Tested	3/4	--	--
J-8	16 Aug.	12 May 1967	I 1/2**	6430	5720
			II 1	5430	5310
G-1	22 Feb. 1967	17 May 1967	3/4	7050	6580
G-2	23 Feb.	21 Mar.	3	6130	5650
G-3	5 Mar.	8 Mar.	4	3030	2910
G-4	18 May	5 June	2 1/2	5400	5520
G-5	20 June	11 July	--	5600	4860
G-6	6 July	27 July	--	5750	5200
G-7	24 July	7 Aug.	--	4670	4912
G-8	2 Aug.	17 Aug.	1/4	7030	6730
G-9	14 Aug.	29 Aug.	1/2	5250	5990
G-10	22 Aug.	8 Sept.	2	5500	5750
G-11*	7 Sept.	25 Sept.	--	5100	--
G-12	7 Sept.	22 Sept.	--	5100	--
				2 x 4 in., Mortar	6 x 12 in. With Wire
K-15		26 Aug. 1966		5890	6320
K-16		29 Aug.		7120	6660
K-17		29 Aug.		7240	7030

* G-11 and G-12 were cast from same batch. Strength reported is average of 8 cylinders.

** Batch II represents compression zone and most of critical shear region.

TABLE 4.5. CONCRETE TENSILE STRENGTH DATA

Slab No.	f_t - psi	
	4 x 8 in.	6 x 6 in.
K-1	520*	495
K-2	334	465*
K-3	414	354
K-4	525	469
K-5	552	471
K-6	497	437
K-7	573	458
K-8	477	477
K-9	543	497
K-10	507	434
K-11	403	478
K-12	512	587
K-13	497	576
K-14	549	625
J-1	476	370
J-2	495	552
J-5	421	358
J-6	430	424
J-7	---	---
J-8	498	I 450
	487	II 425
G-1	615	532
G-2	578	470
G-3	354	276
G-4	545	529
G-5	605	550
G-6	592	478
G-7	510	416
G-8	568	487
G-9	528	433
G-10	605	513
G-11	568**	---
G-12	568	---
	6 x 6 in.	
	1st Crack	2nd Crack
K-15	592	678
K-16	612	707
K-17	675	705

* 1 cylinder only

** G-11 and G-12 were cast from same batch. Strength reported is average of 4 cylinders.

TABLE 4.6. STRENGTH PROPERTIES OF REINFORCING MATERIALS

Description	Slab	Yield Stress (ksi)	Ultimate Stress (ksi)	Percent Elongation At Ultimate
1/8" x 1/8" Reinforcing bars	All except K-0, K-7	40.8	57.0	--
16 ga. Steel plate	K-3, K-8, K-12, K-14	44.4	54.2	24.1
16 ga. Steel plate	J-5	36.2	44.5	18.1
16 ga. Steel plate	J-6	37.8	46.7	20.6
16 ga. Steel plate	J-7	36.1	44.9	22.5
16 ga. Steel plate	J-8	37.4	46.1	21.3
16 ga. Steel plate	G-1, G-2, G-3, G-9	38.6	47.5	20.8
14 ga. Steel plate	G-5, G-6, G-7, G-8, G-10, G-11	38.4	53.3	29.0
11 ga. Steel plate	G-12	40.2	51.3	--
24 ga. Steel plate	K-4, K-10, K-11	42.0	52.1	--
24 ga. Steel plate	J-1, J-2	36.0	45.4	25.4
24 ga. Steel plate	K-9	38.5	59.8	30.6
Retaining Ring	J-5, J-6, J-7, J-8	44.8	69.0	18.0
#3 Reinforcing Bars	K-5, K-6	36.2	46.1	--
Vertical Steel, 16 ga. wire	K-8	35.9	48.3	--
Vertical Steel, 16 ga. wire	K-12	34.1	51.5	--
Vertical Steel, 16 ga. wire	K-13	34.7	47.5	--
Vertical Steel, 11 ga. wire	G-7, G-10	38.0	--	--
Vertical Steel, 1/4" Threaded rod	G-11, G-12	16.8	27.0	--
12 ga. "Insul-pin" shear studs (1")	K-3, K-4, K-8, K-10, K-11, K-12, K-14, J-1, J-2	34.6	50.2	--
12 ga. "Insul-pin" shear studs (1-1/2")	K-3, K-4, K-8, K-10, K-11, K-12, K-14, J-1, J-2, G-5	31.6	46.6	--
3/16" Shear studs	J-5, J-6, J-7, J-8	31.2-50.7	45.7-62.0	--

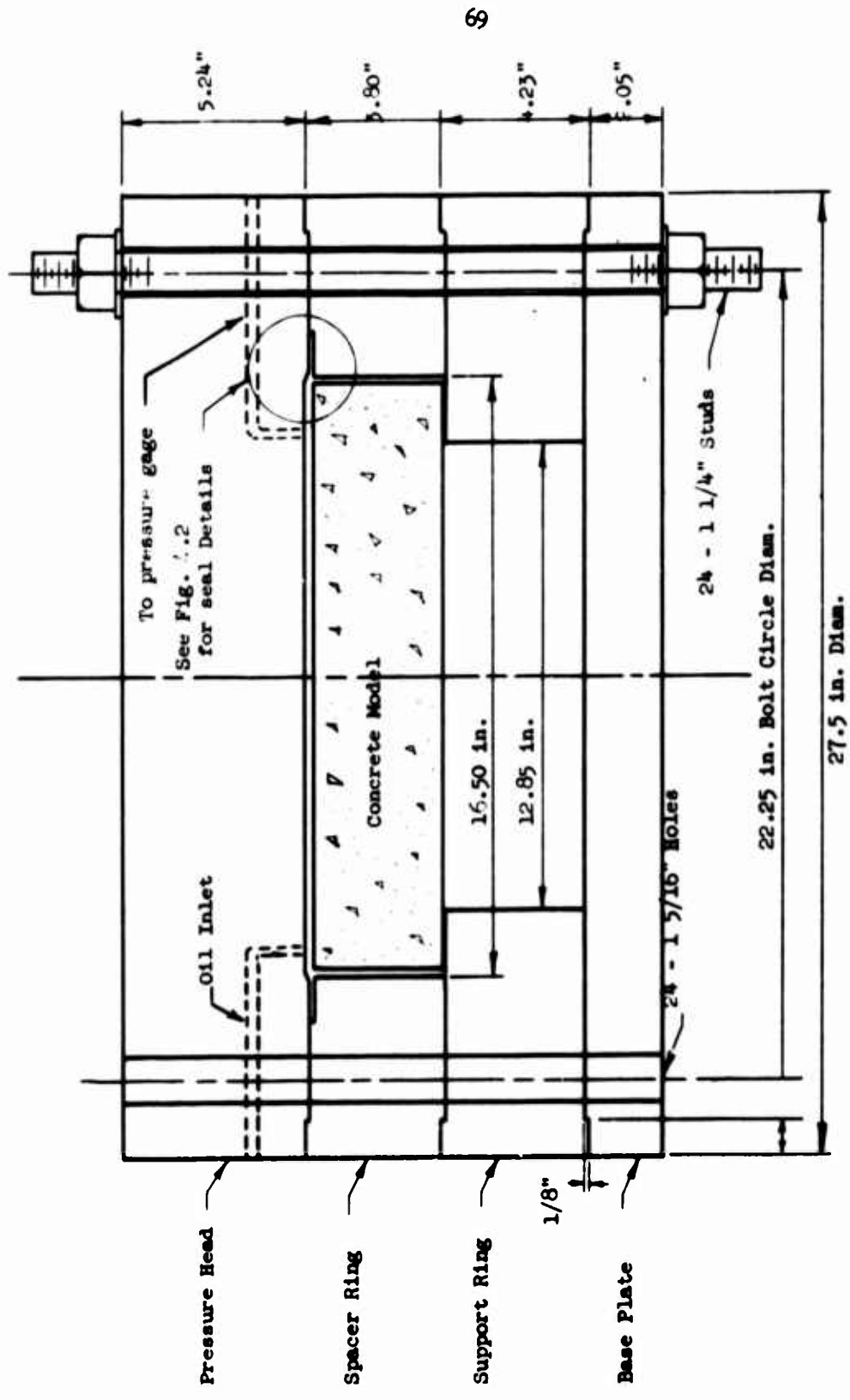


Fig. 4.1 Cross Section of Slab Testing Device

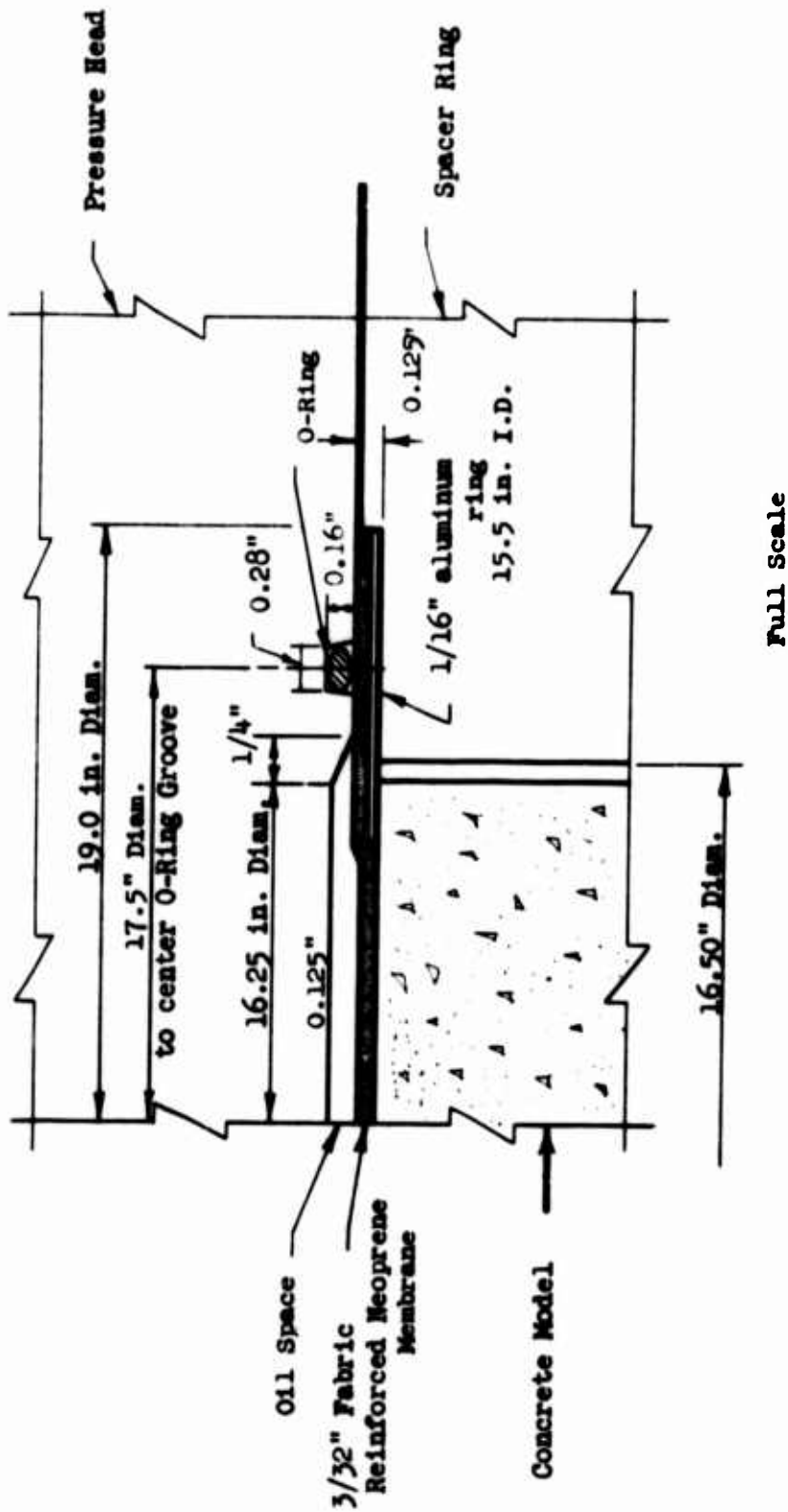


Fig. 4.2 Seal Details, 1/14th scale slabs



Fig. 4.3 Partly Dismantled Slab Testing Device

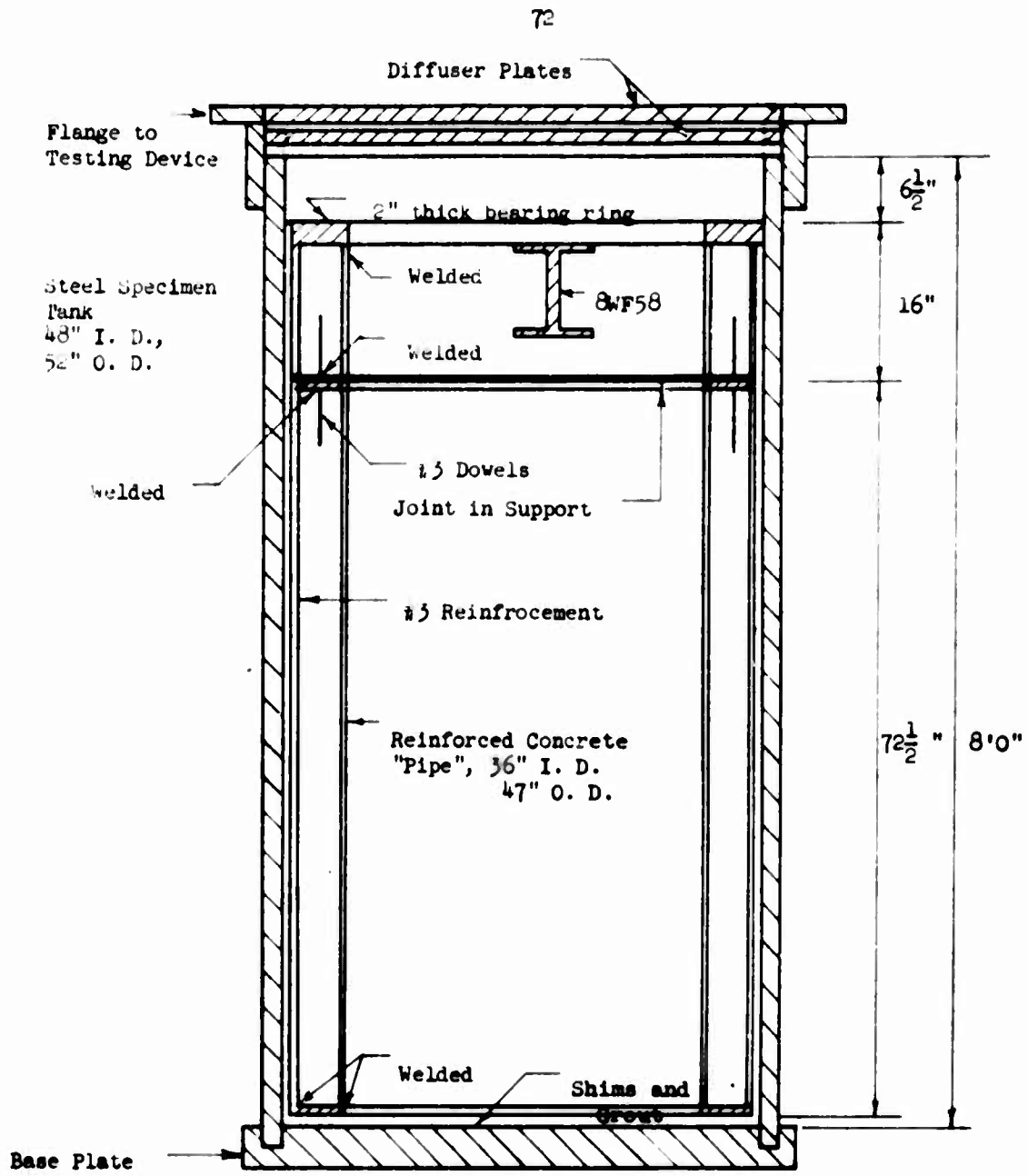


Fig. 4.4 Cross-Section of Specimen Tank and Slab Support

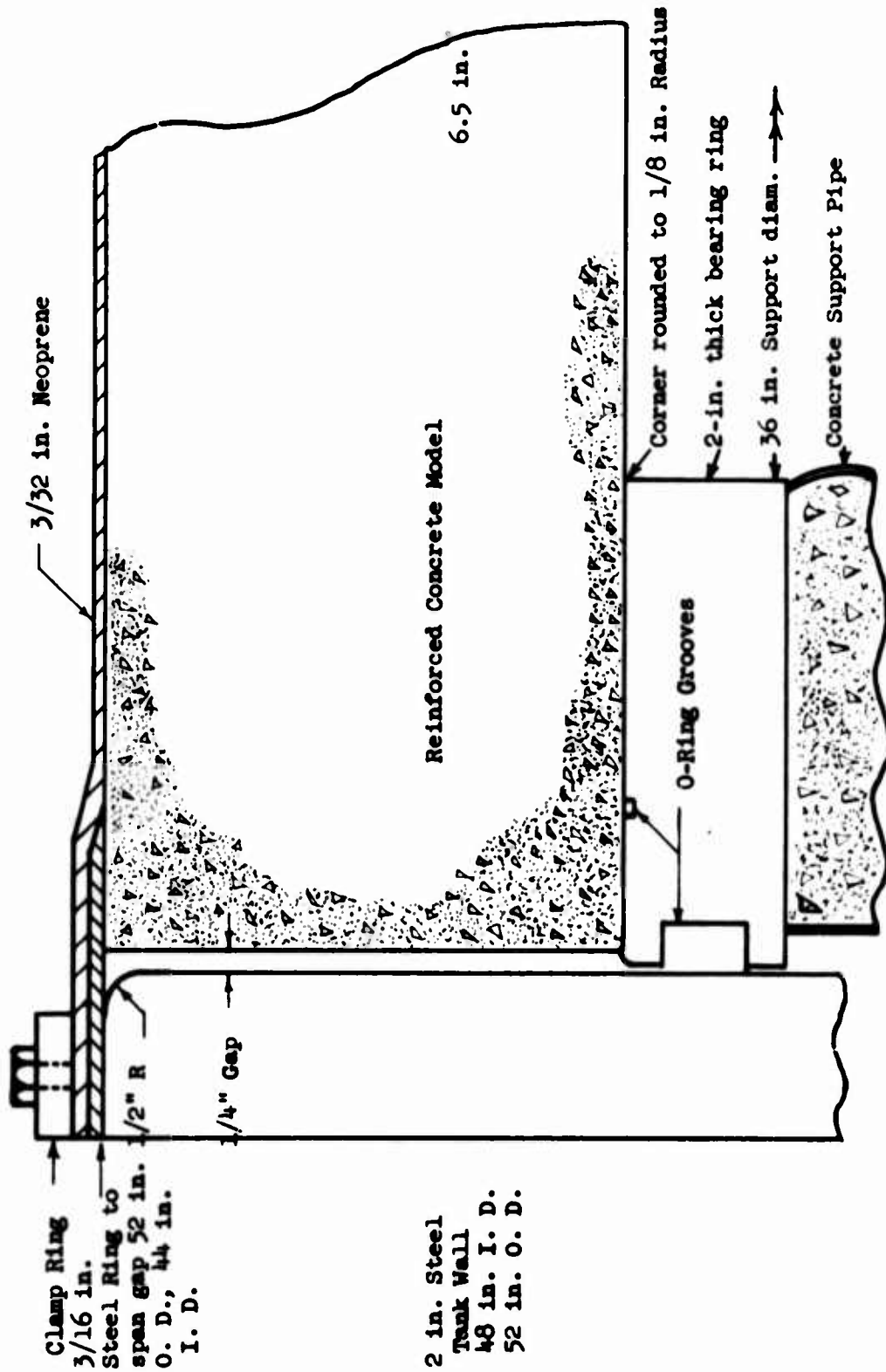


Fig. 4.5 Details of Seal and Support Area, 1/5-th Scale Models

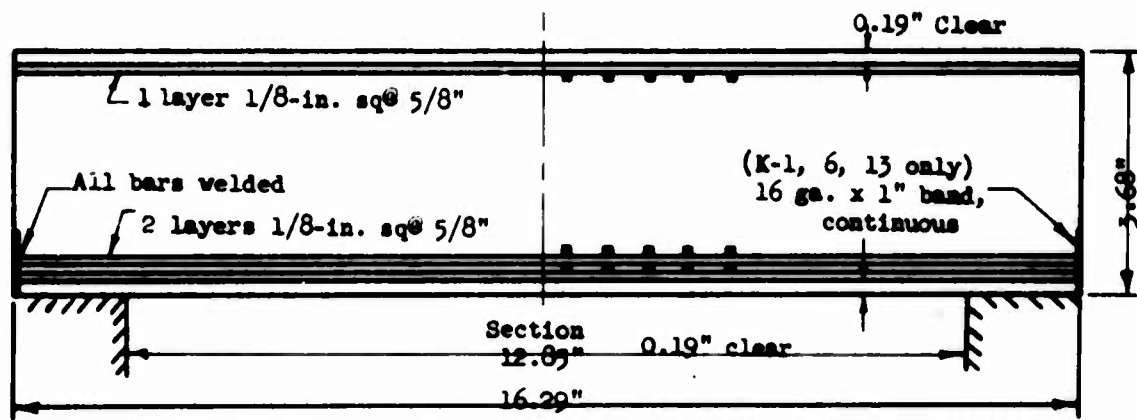
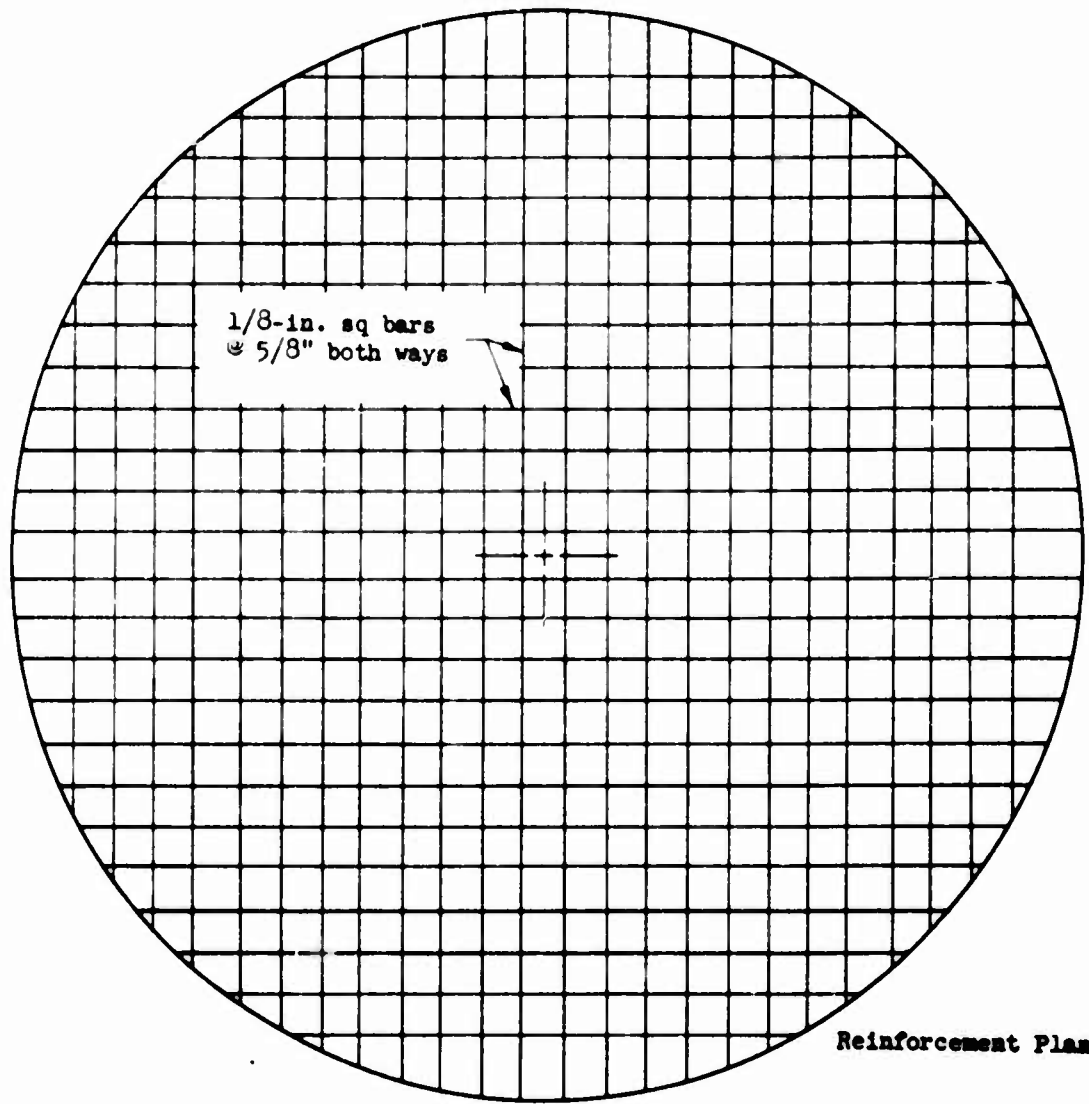


Fig. 4.6 Bar Reinforced Slabs

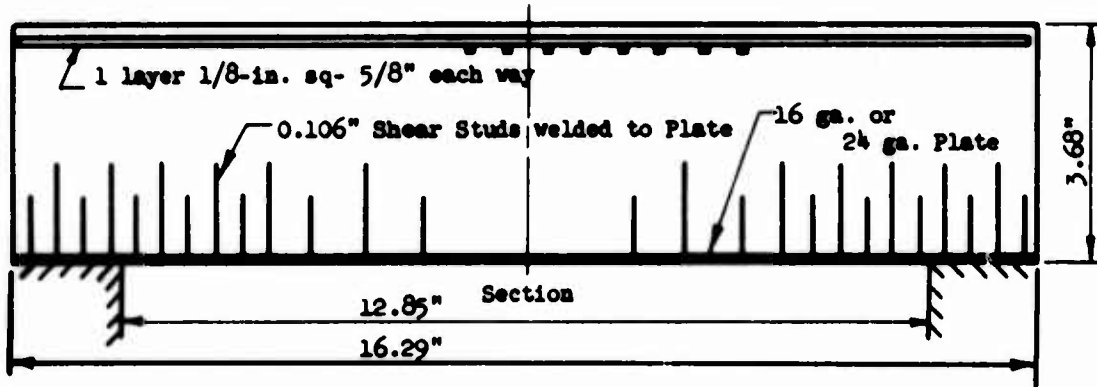
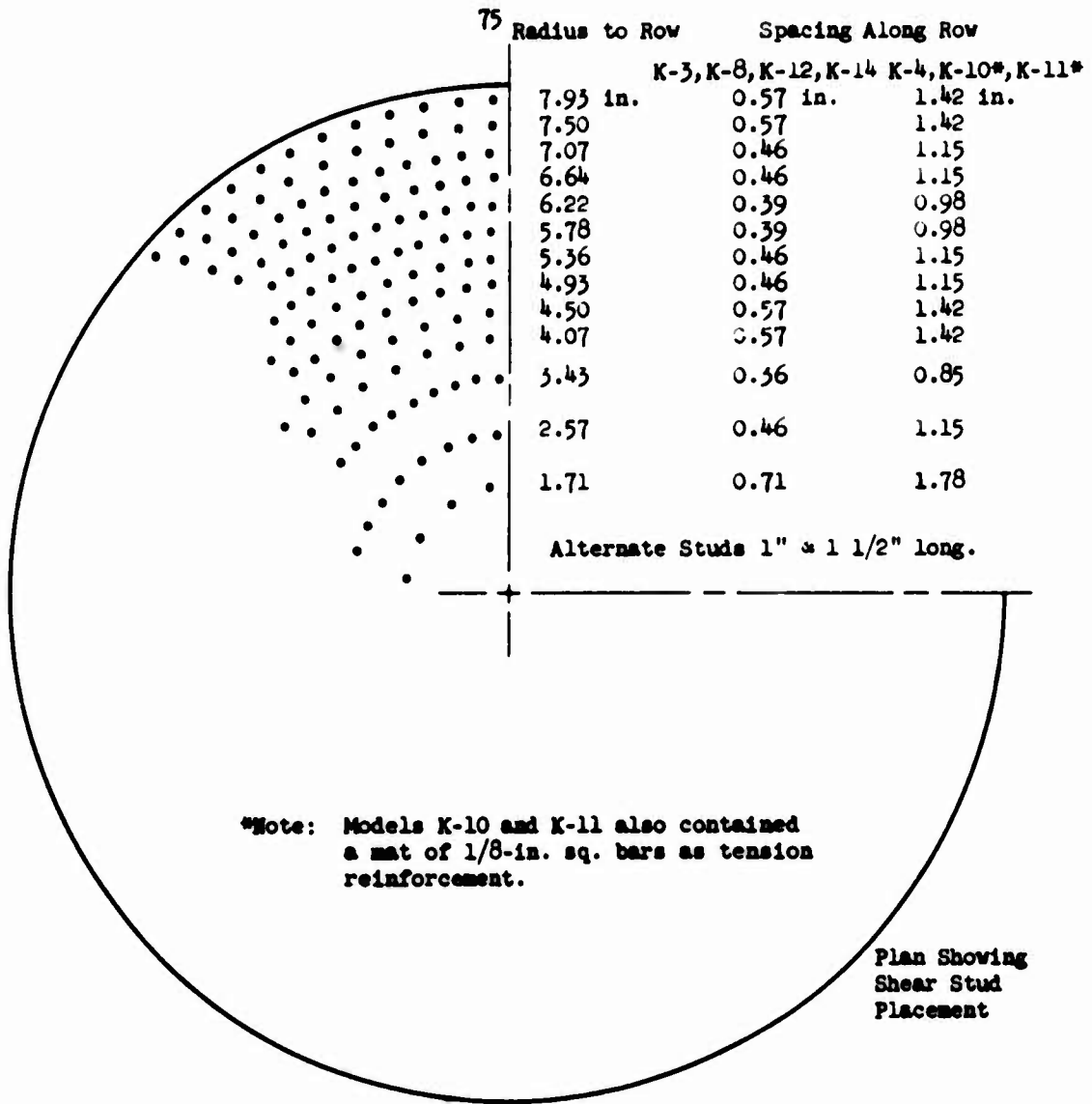


Fig. 4.7 Model Slabs With Plate Reinforcement

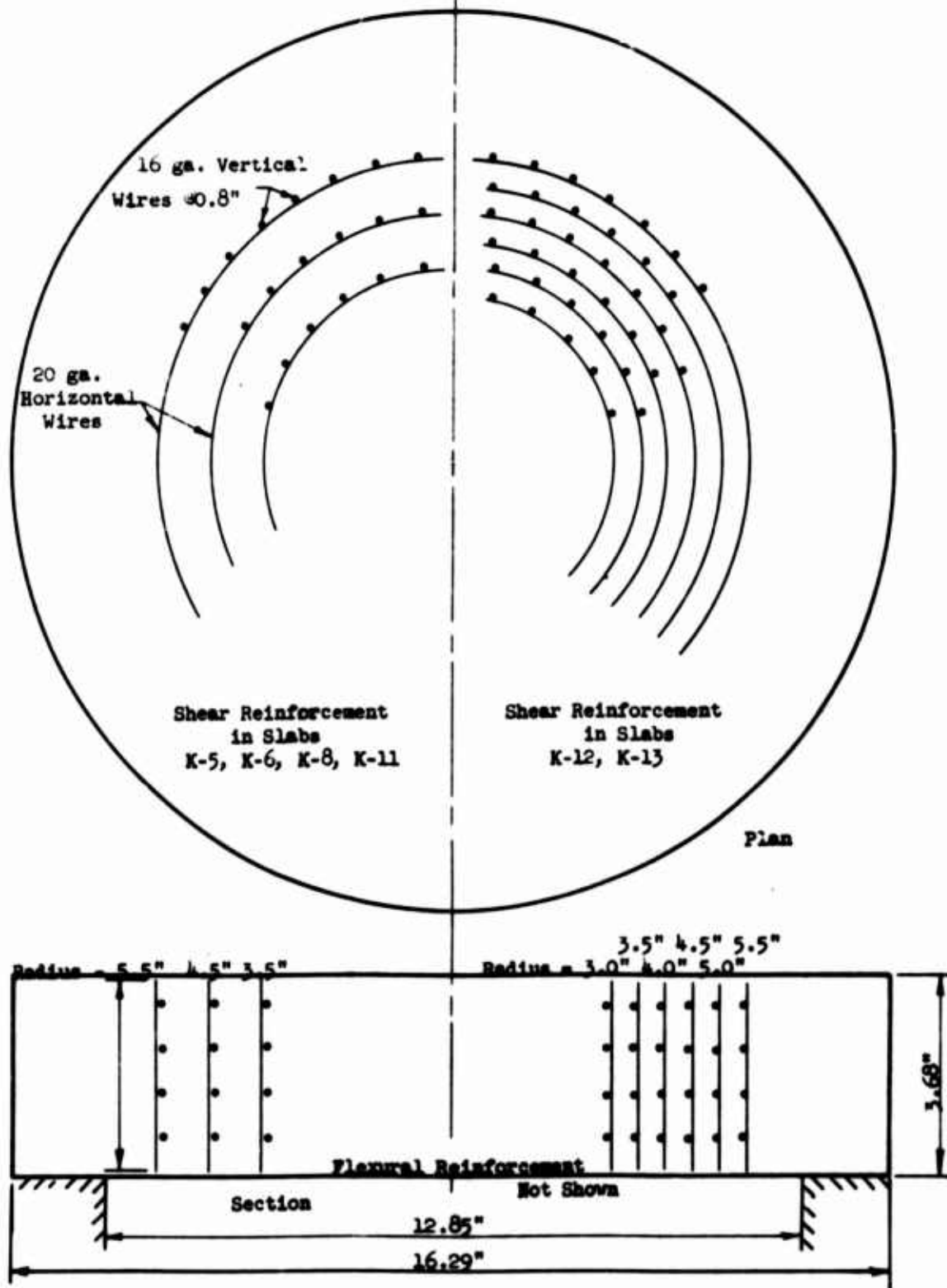


Fig. 4.8 Shear Reinforcement in Model Slabs

77

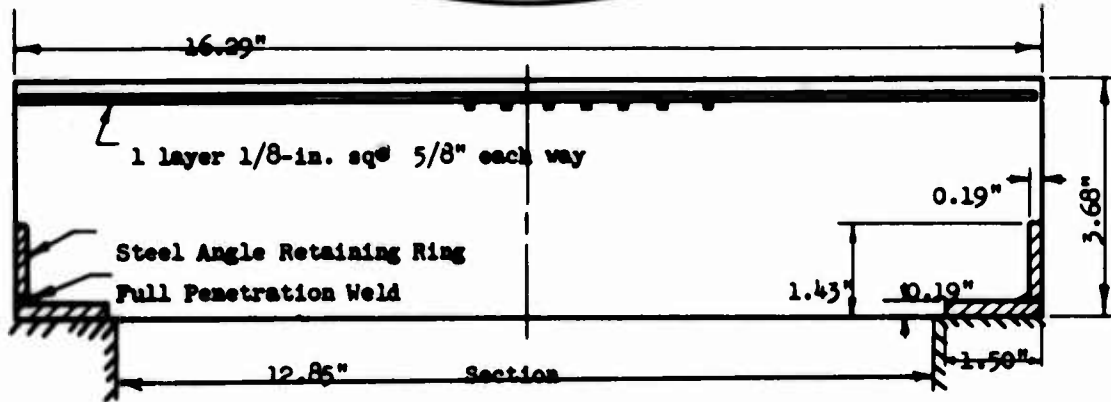
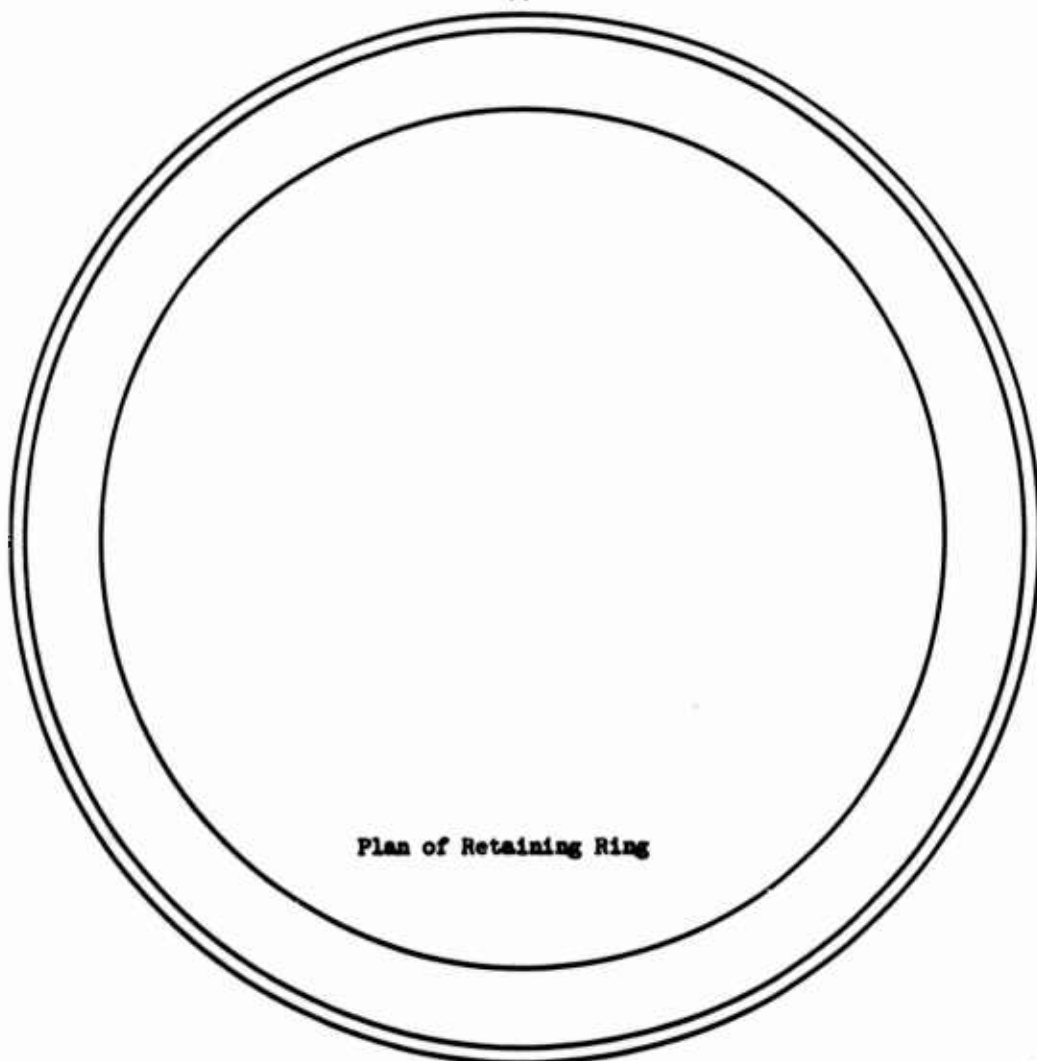


Fig. 4.9 Model Slab Reinforced With Retaining Ring, K-9

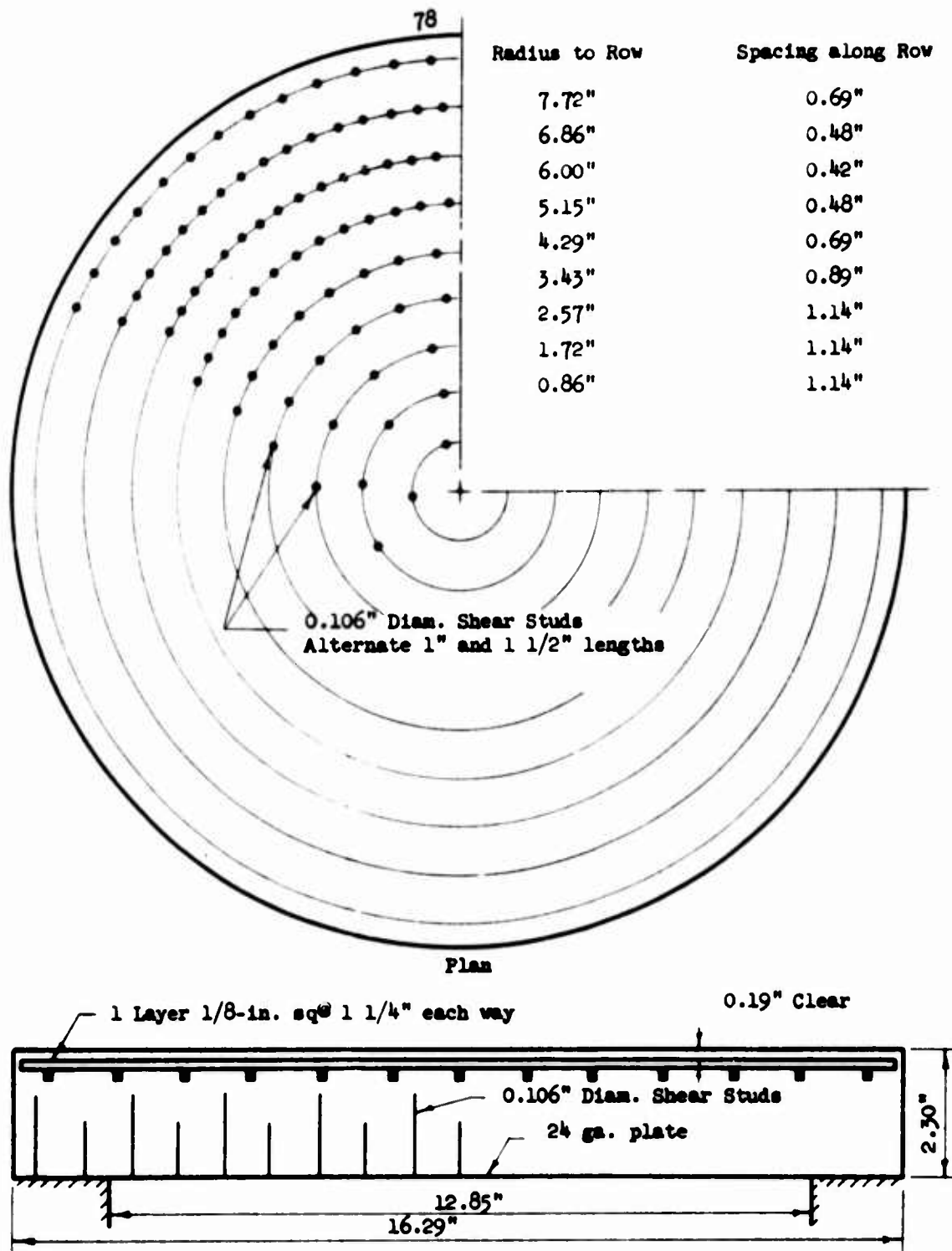


Fig. 4.10 Slab Models J-1 and J-2

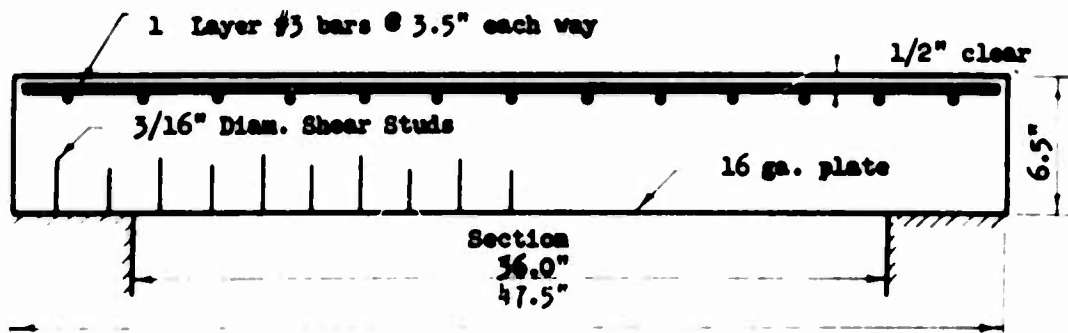
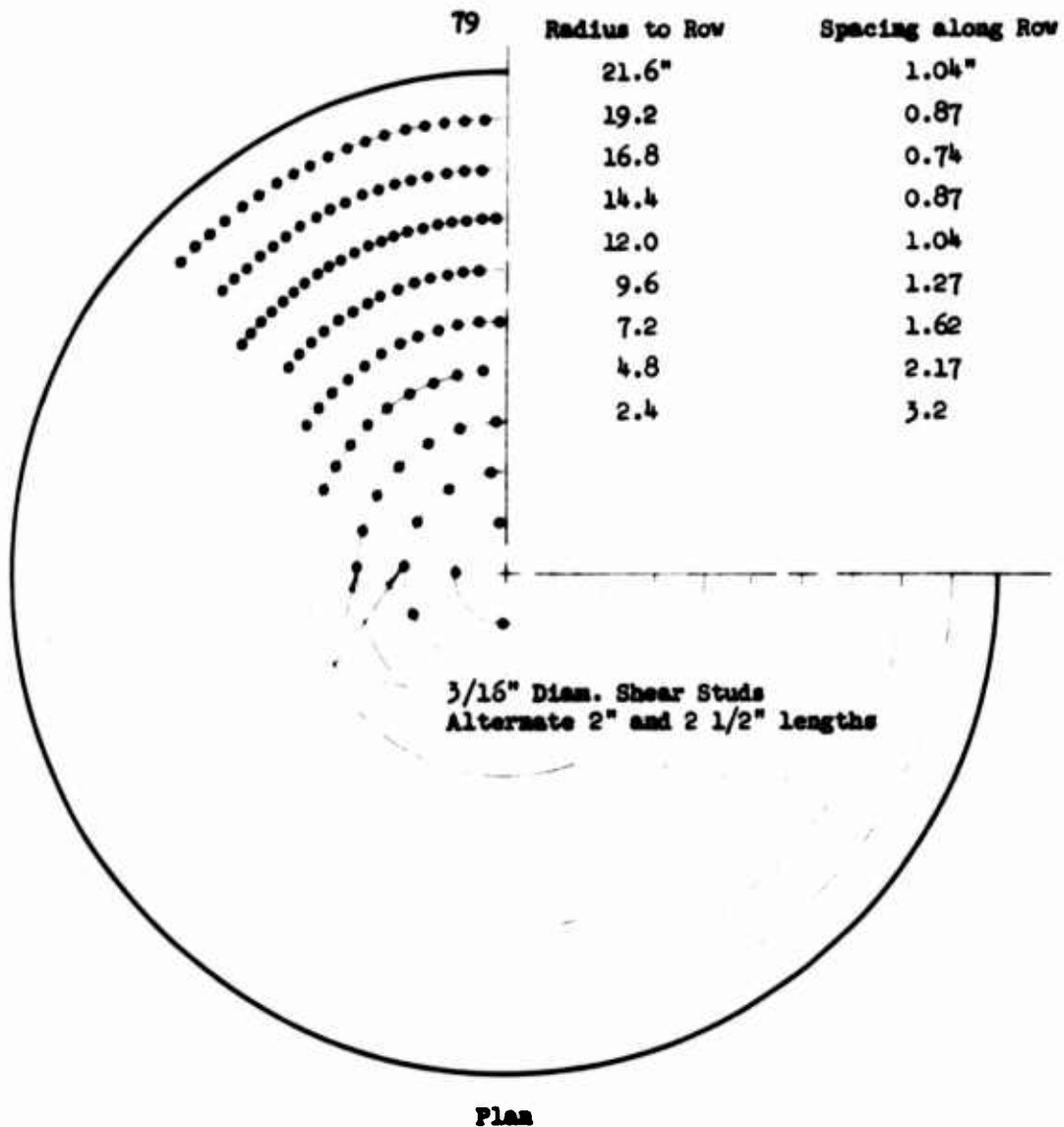


Fig. 4.11 Slab Models J-5 to J-8

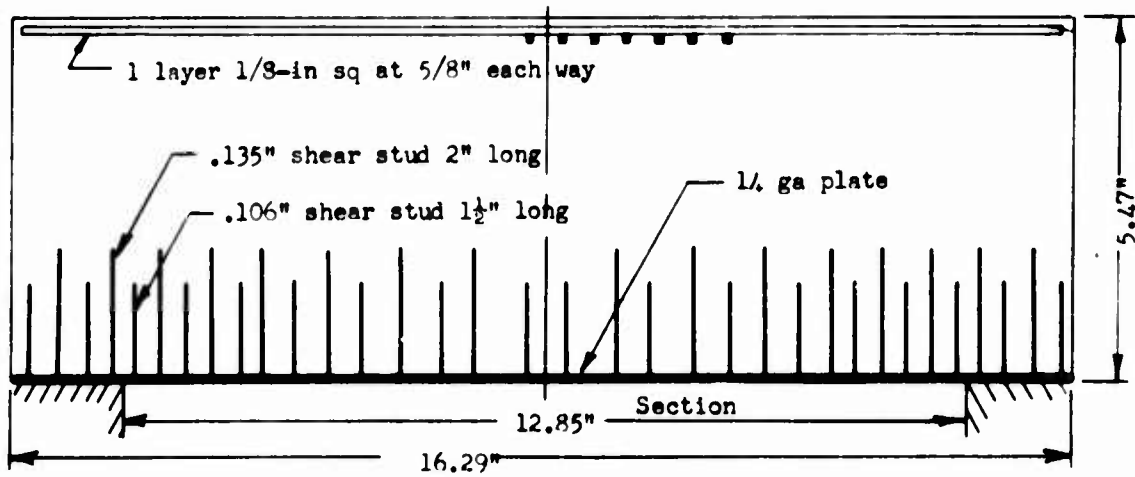
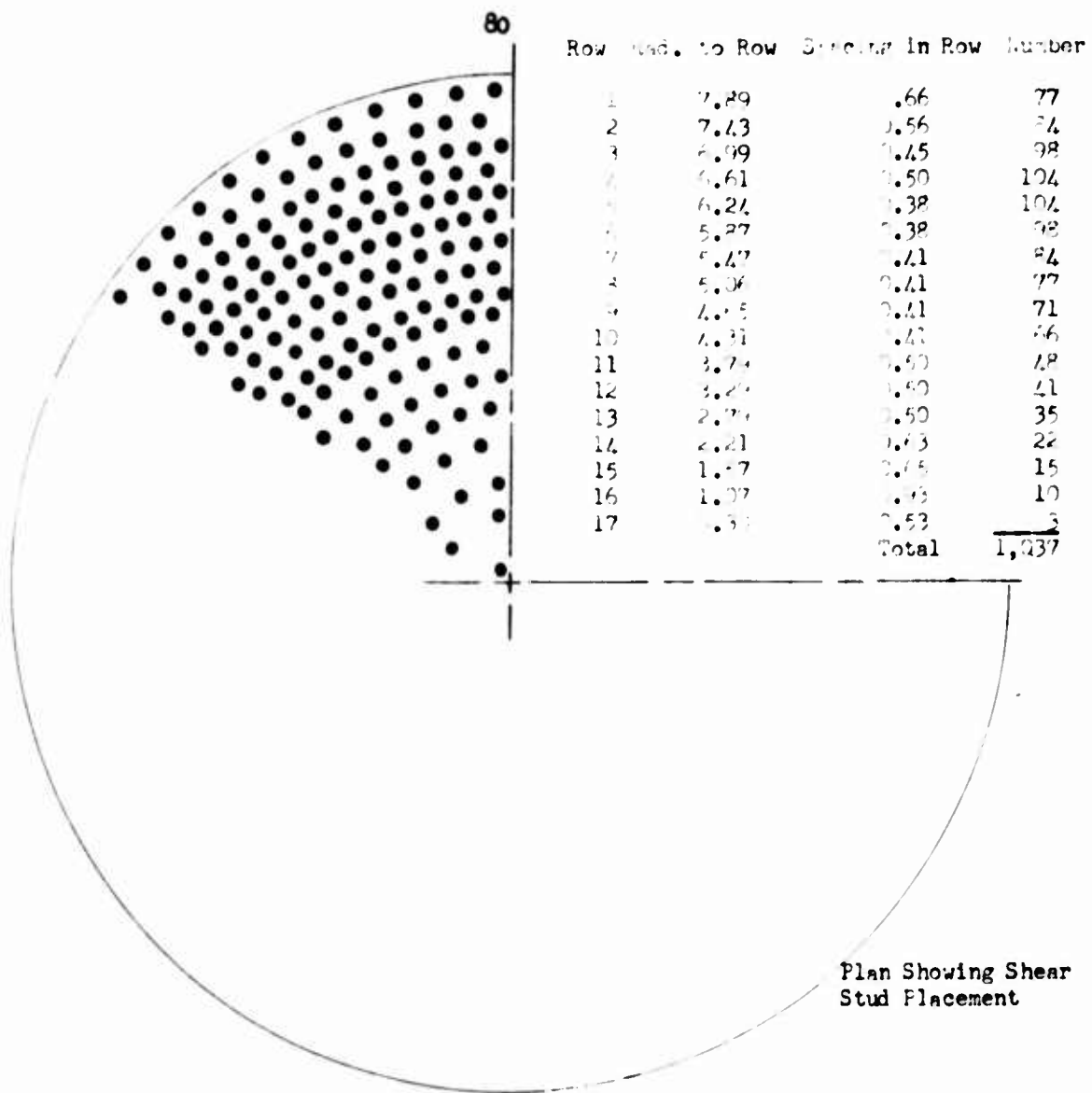
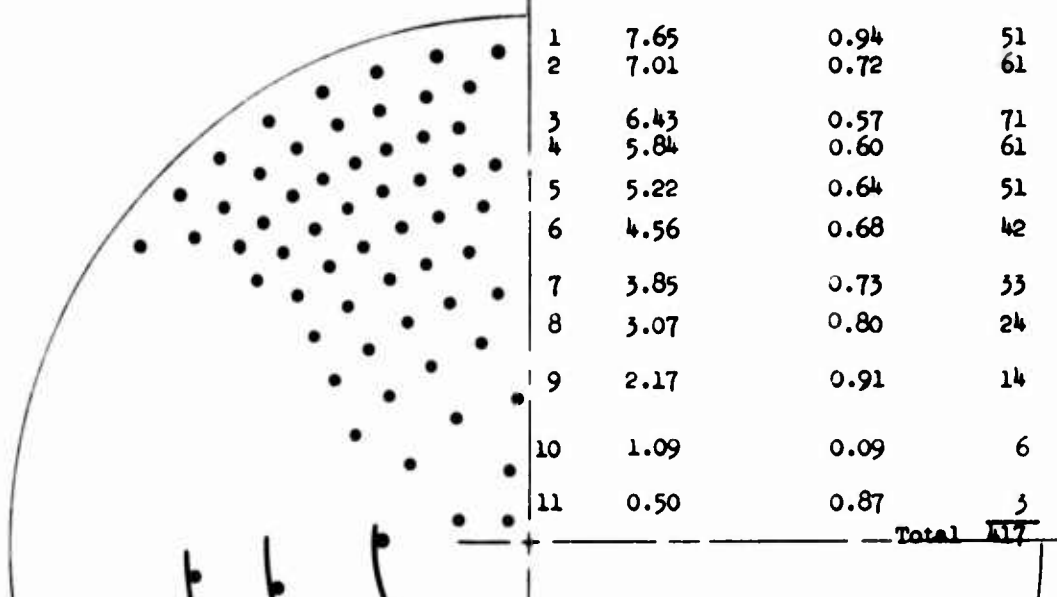


Fig. 4.12 Model Slab G-5

Row Rad. to Row Spacing in Row Number



Shear reinforcing
11 ga x 4-7/8" long

Note: Model G-10 also contained a mat of 1/8 in sq bars at 13/16" spacing each way as tension reinf.

Plan showing Shear Stud and Shear Reinforcing Placement

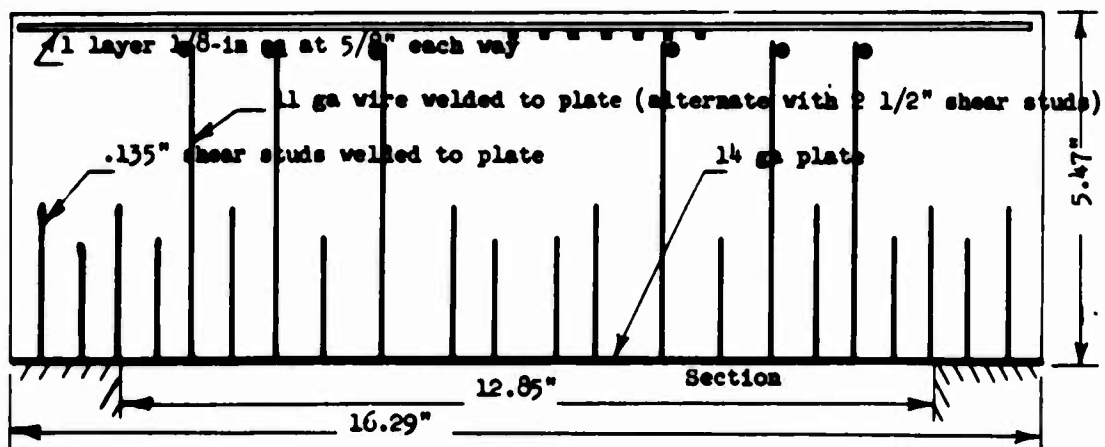


Fig. 4.13 Model Slabs G-7 and G-10

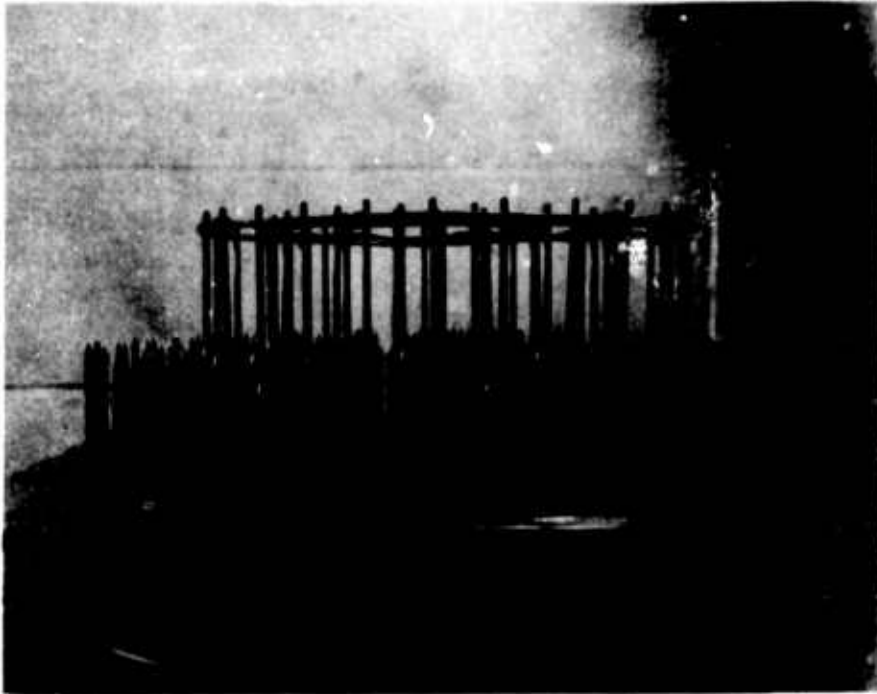


Fig. 4.14 Shear Reinforcement for Models G-7 and G-10

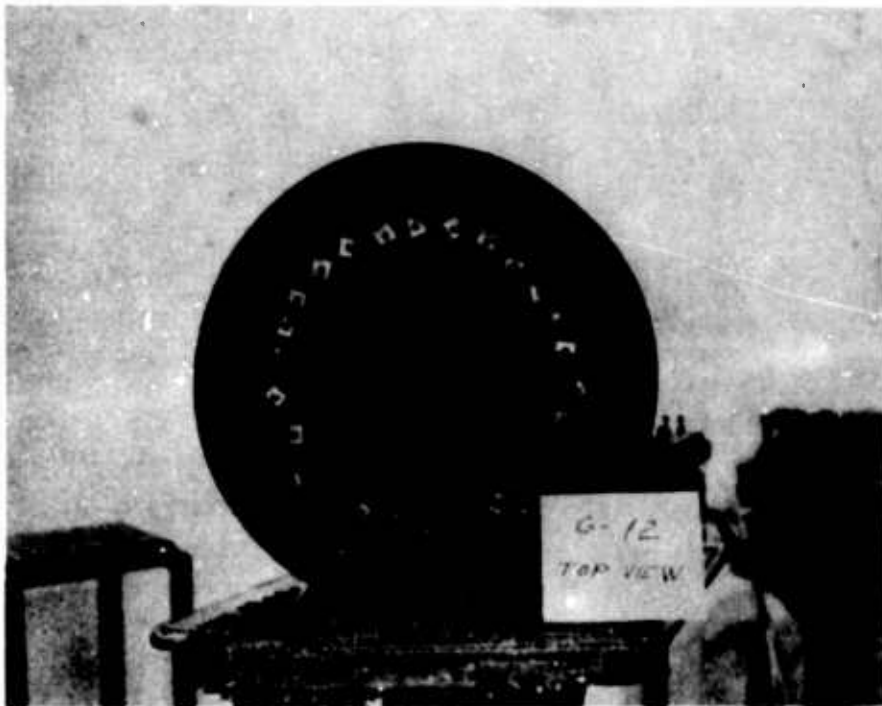


Fig. 4.15 Slab Model G-12 Prior to Casting

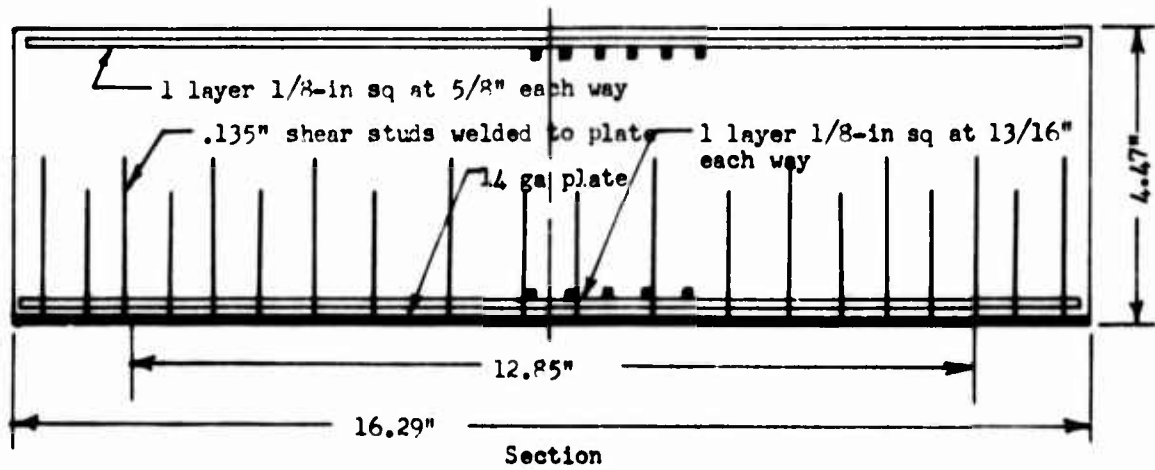
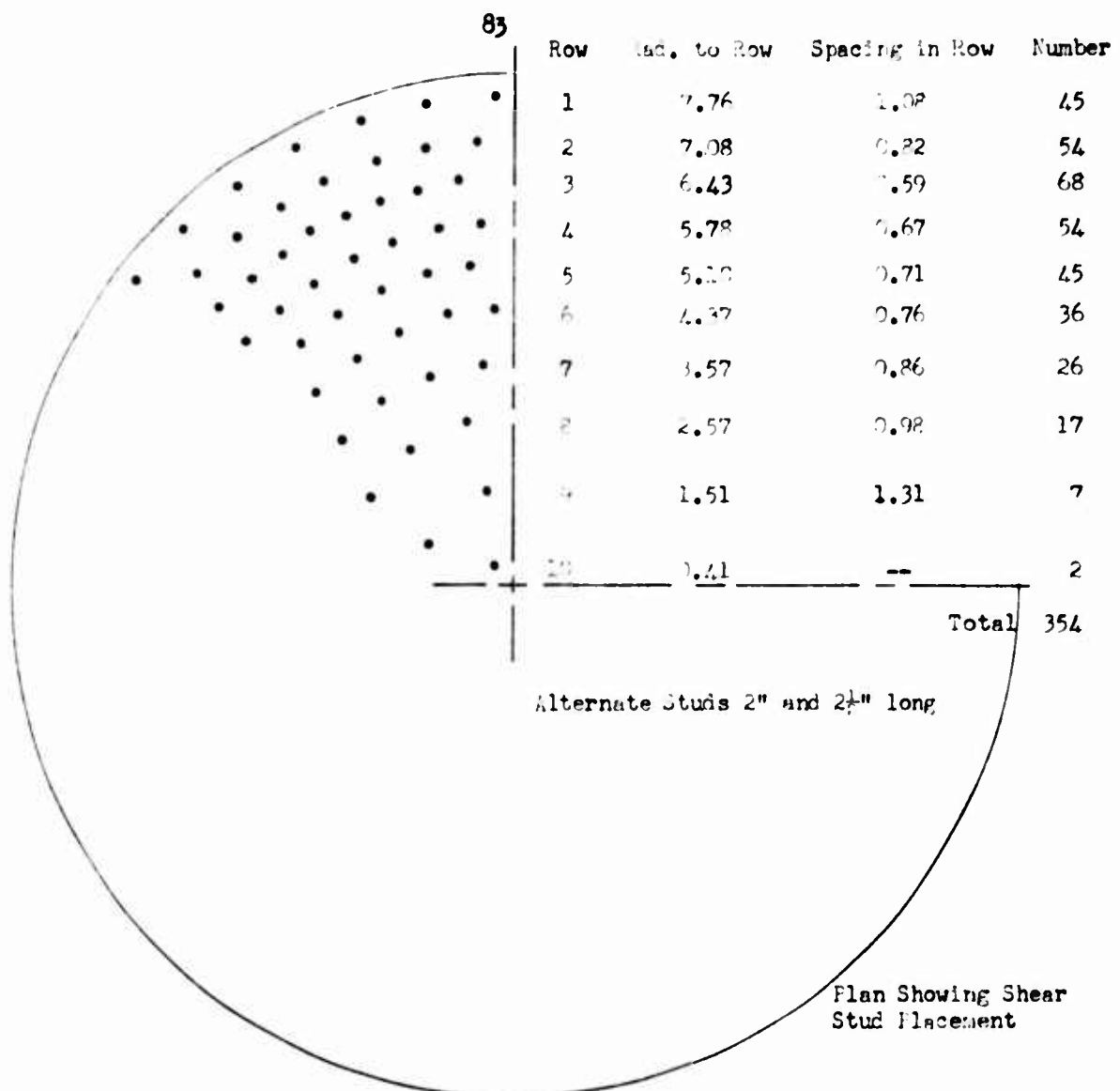


Fig. 4.16 Model Slabs G-6 and G-8

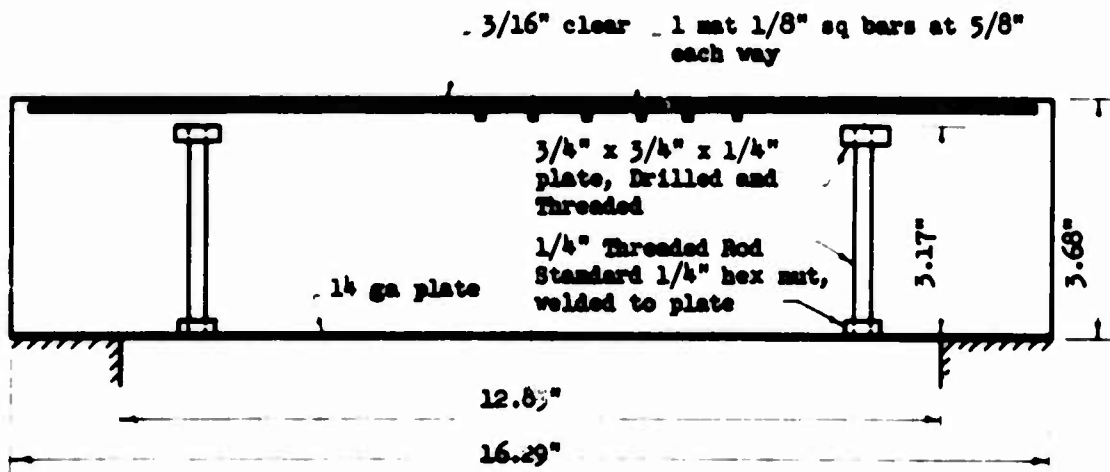
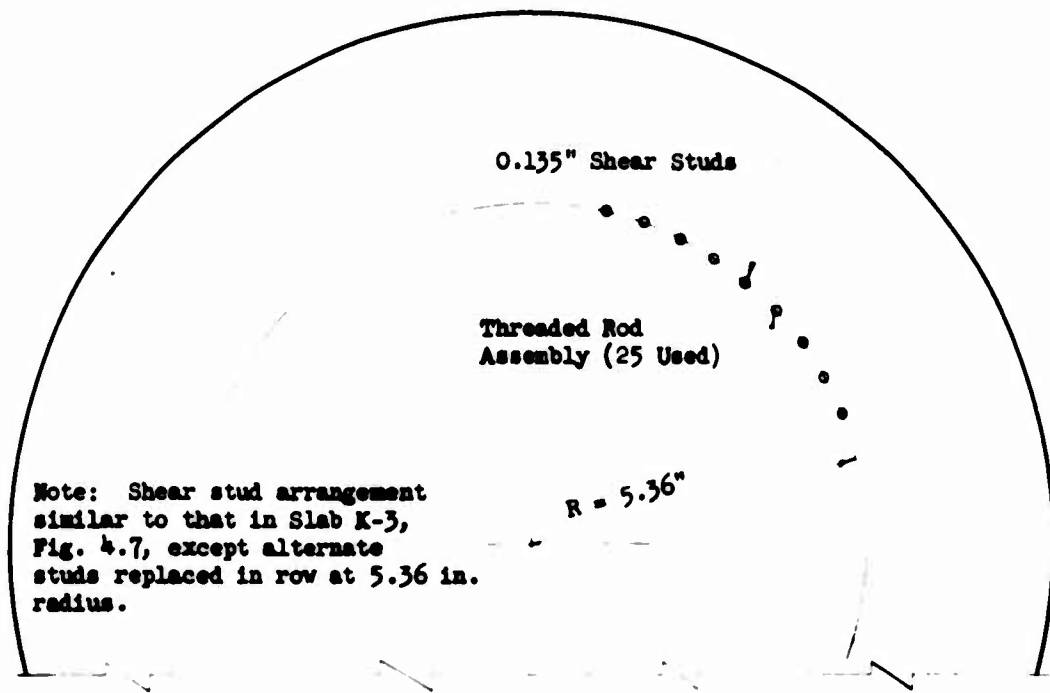
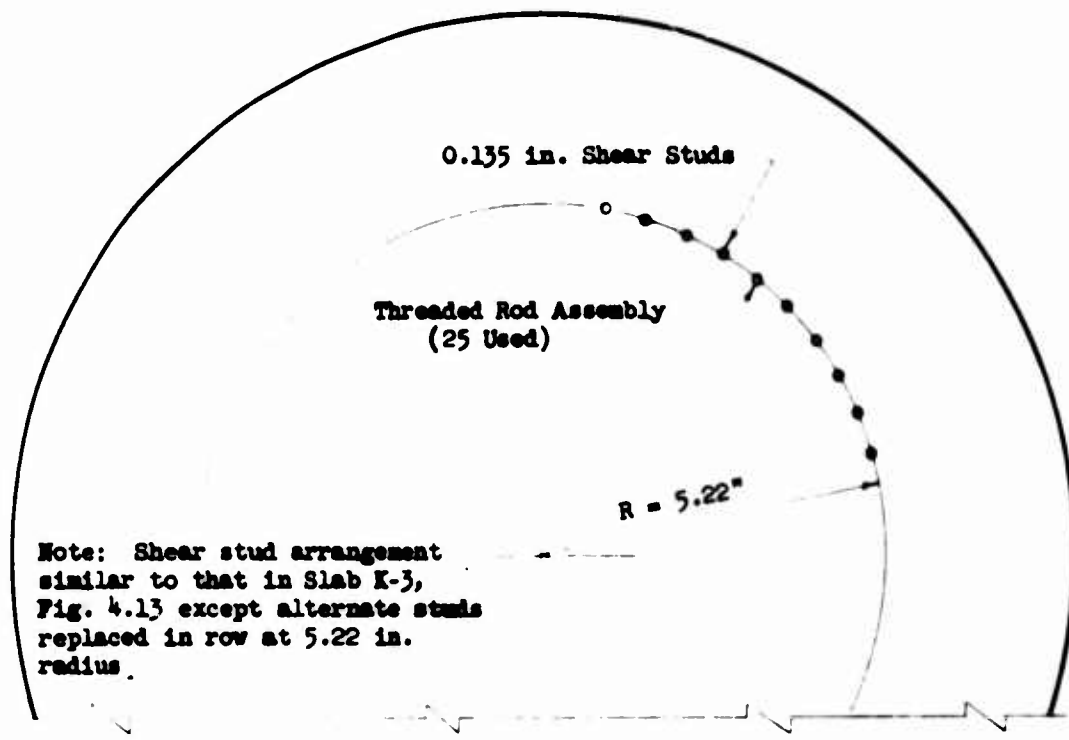


Fig. 4.17 Slab Model G-11



Note: Shear stud arrangement similar to that in Slab K-3, Fig. 4.13 except alternate studs replaced in row at 5.22 in. radius.

Partial Plan

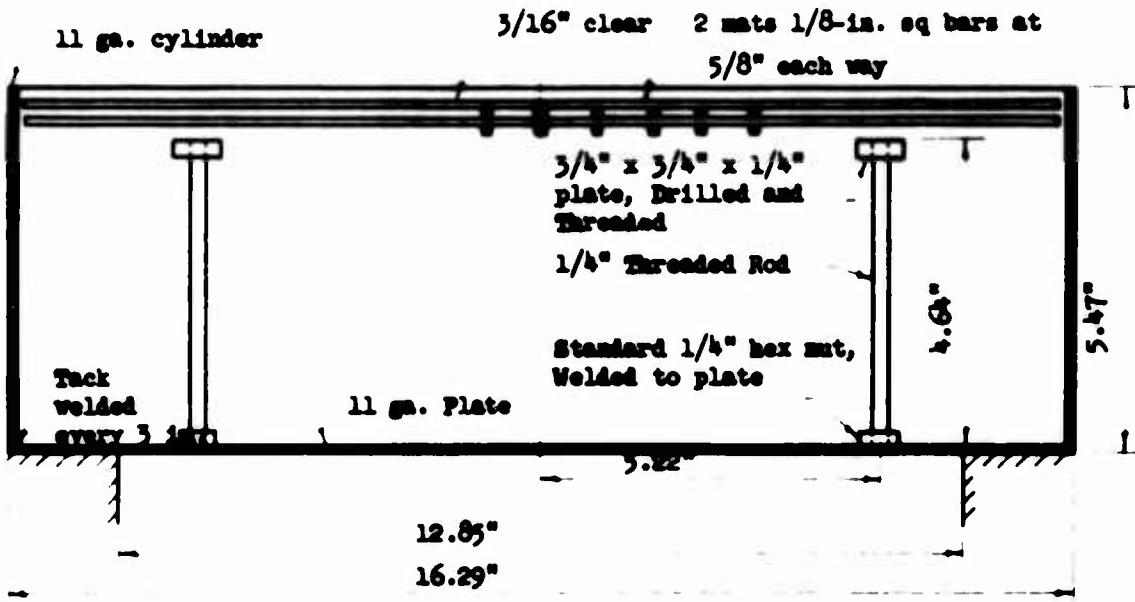


Fig. 4.18 Slab Model G-12

PER CENT COARSER

U. S. STANDARD SIEVE SIZE

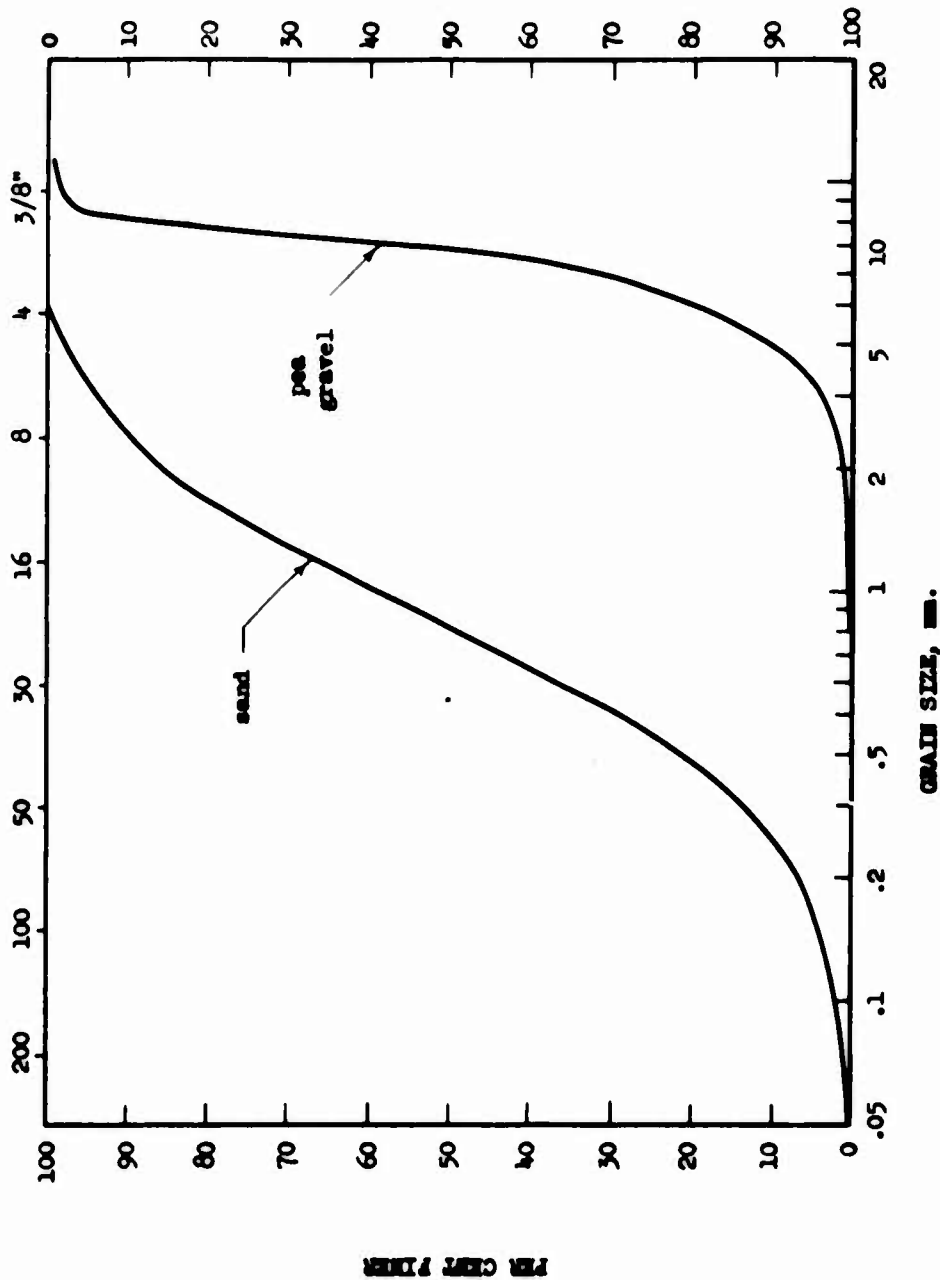


Fig. 4.19 AGGREGATE GRADATION CURVES

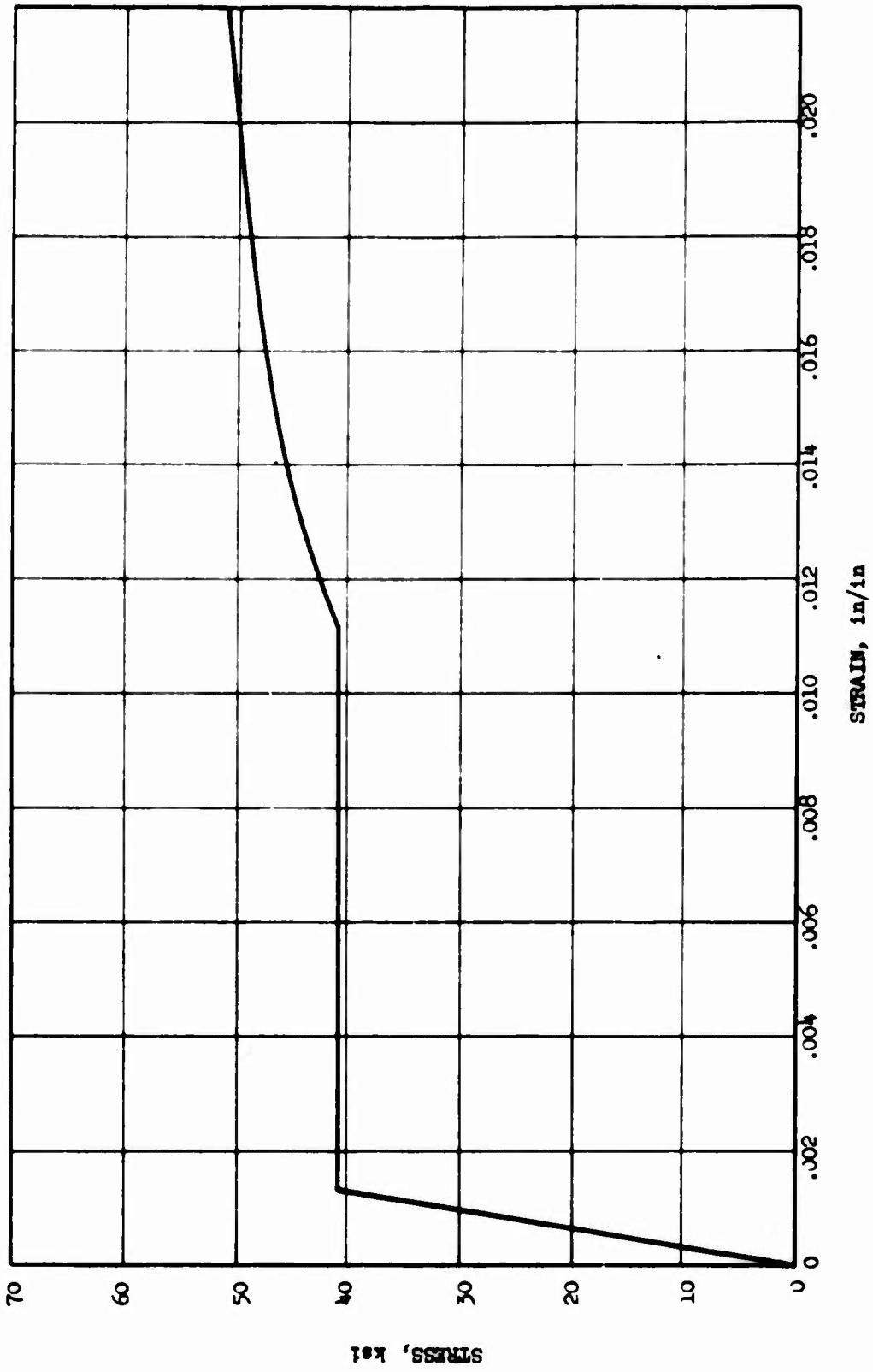


FIG. 4.20 TYPICAL STRESS-STRAIN CURVE, $\frac{1}{8} \times \frac{1}{8}$ REINFORCING BARS

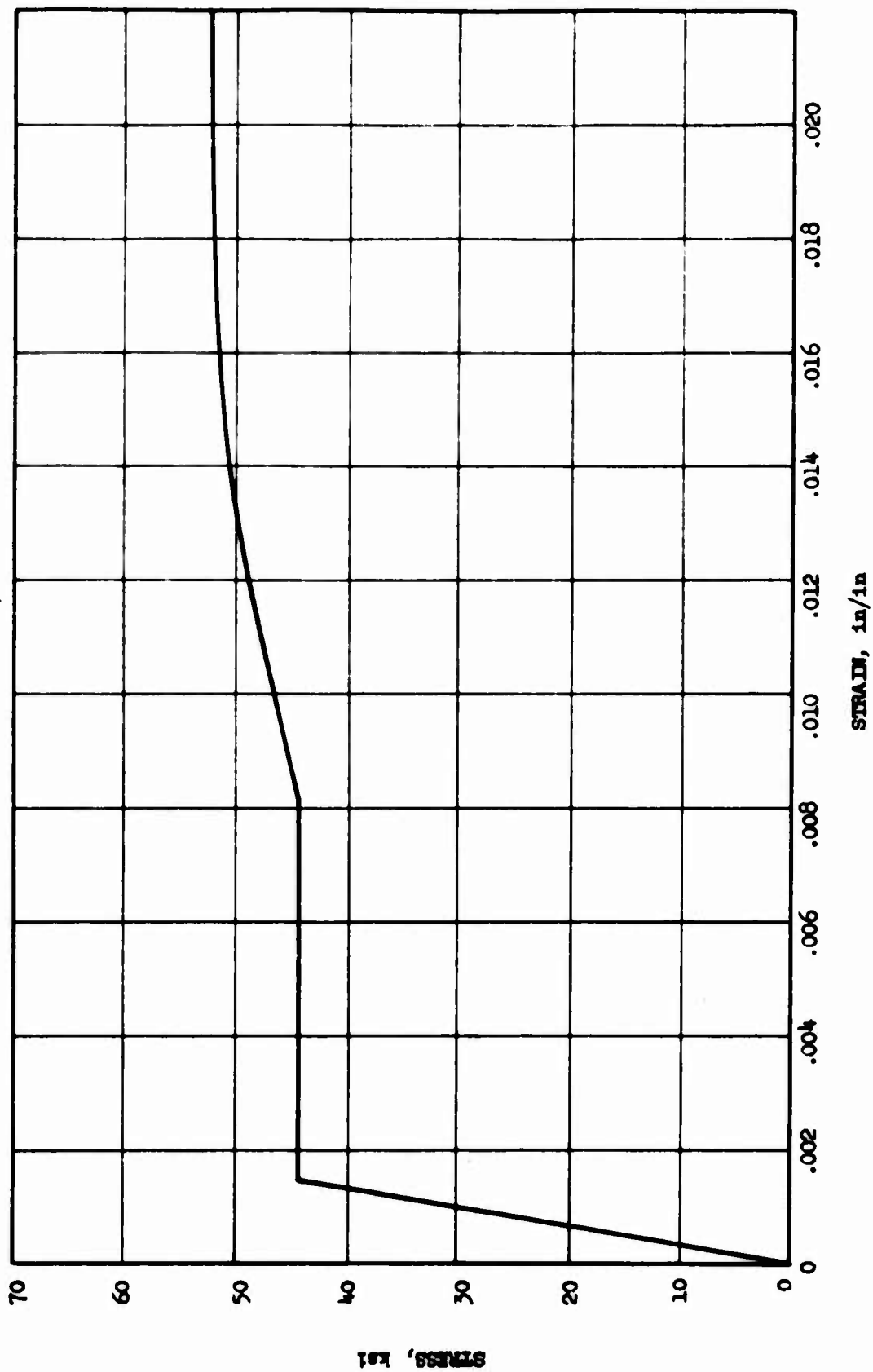


Fig. 4.21 TYPICAL STRESS-STRAIN CURVE, 16 GA. PLATE

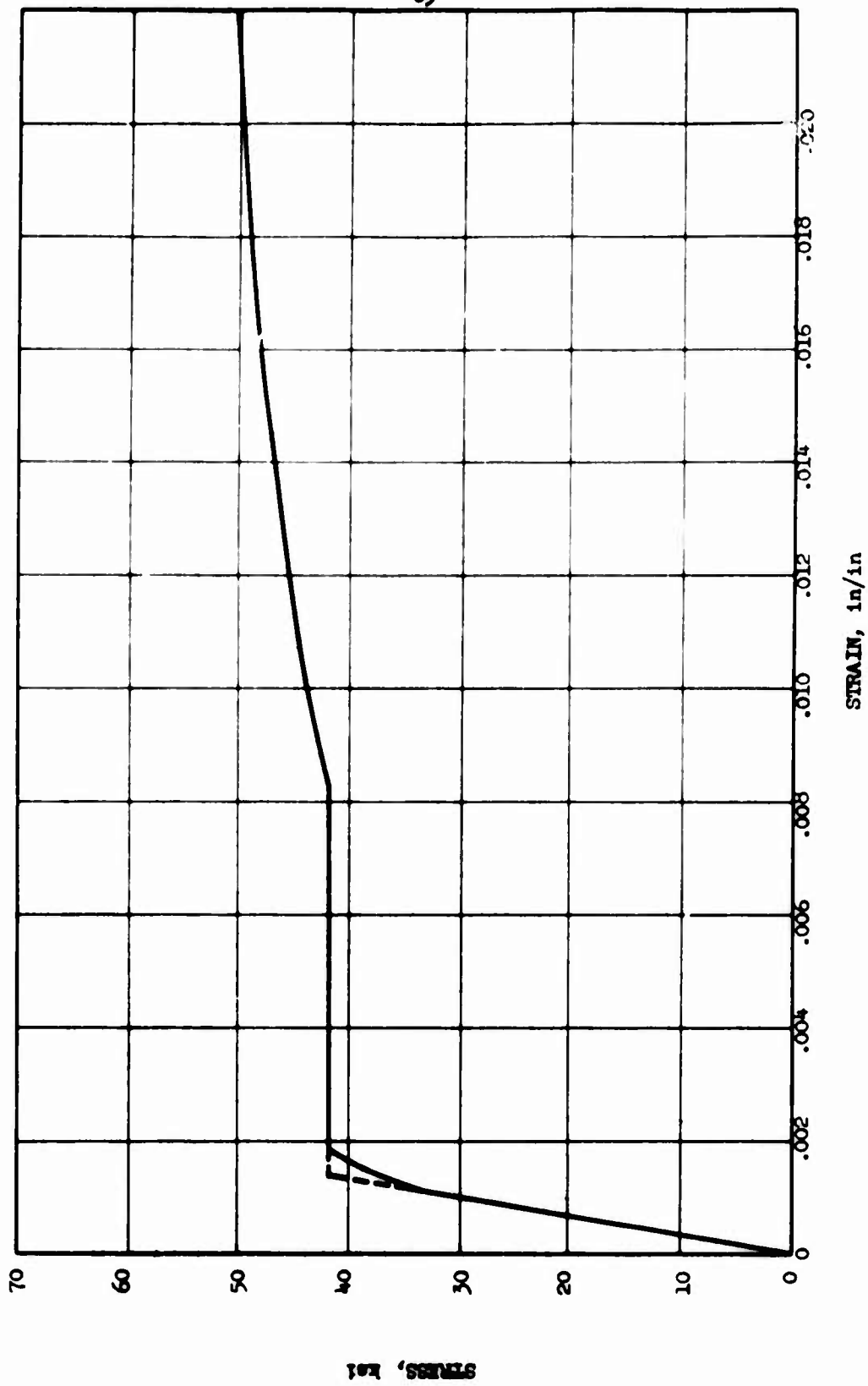


Fig. 4.22 TYPICAL STRESS-STRAIN CURVE, 24 GA. PLATE

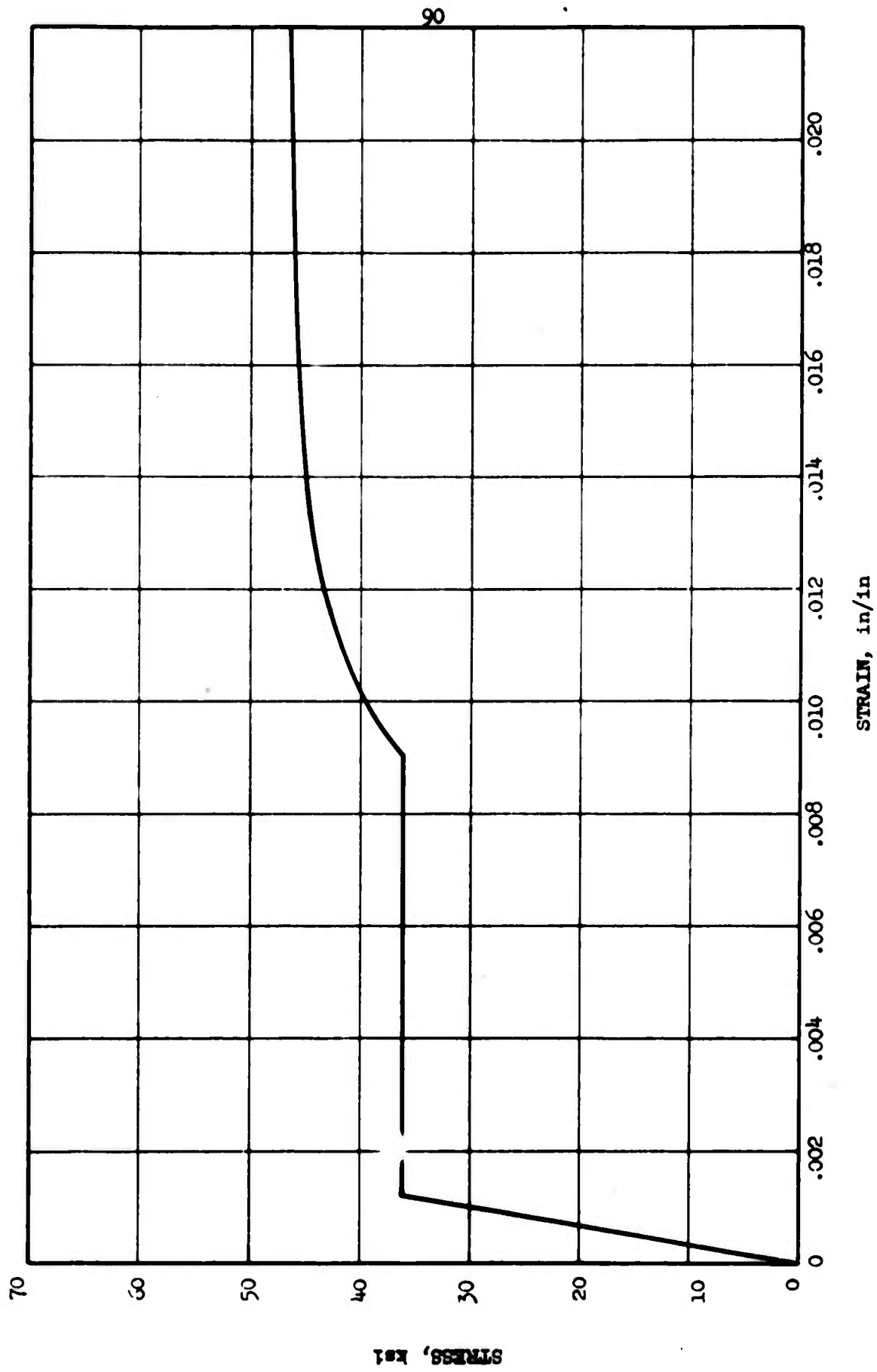
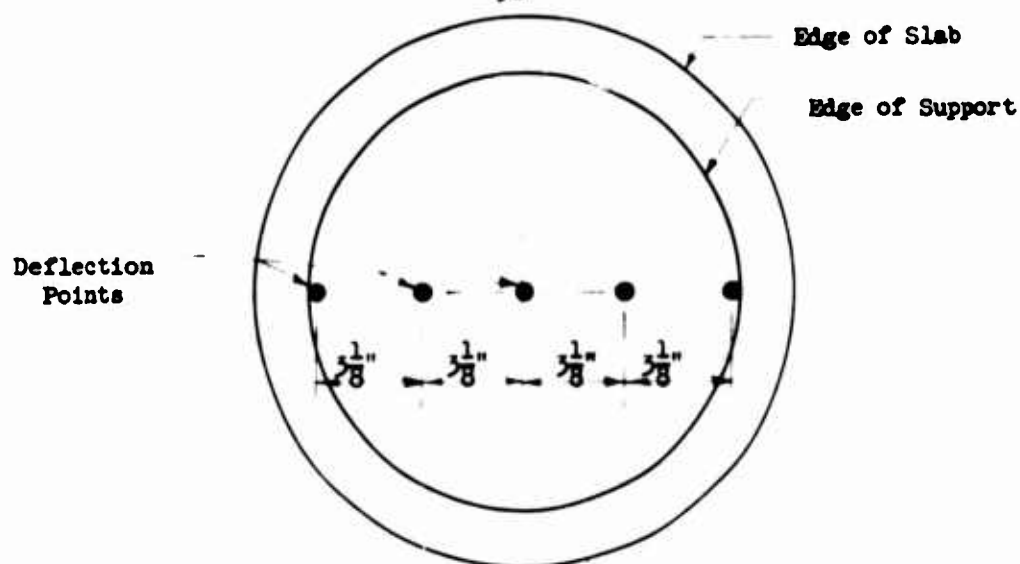
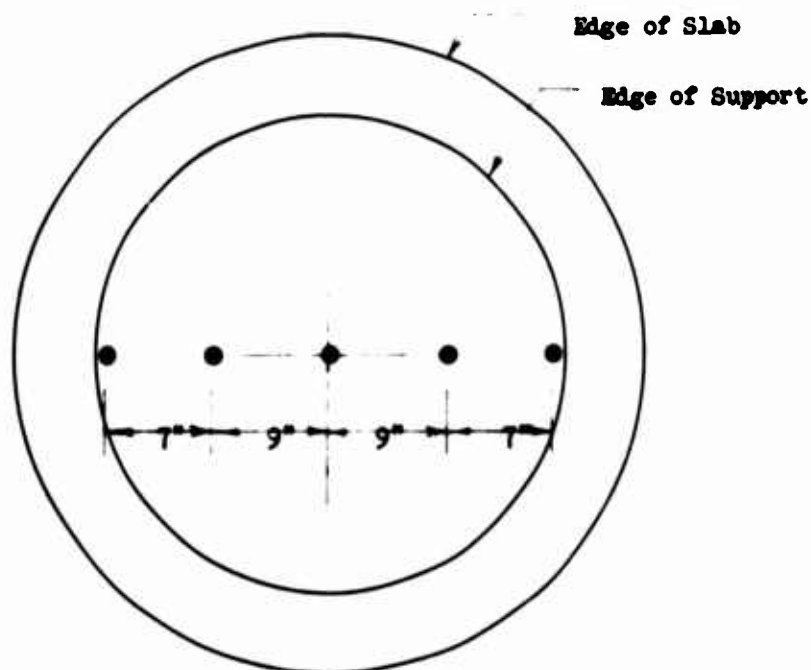


FIG. 4.25 TYPICAL STRESS-STRAIN CURVE, VERTICAL STEEL

91



(a) 1/4-th Scale Models



(b) 1/5-th Scale Models

Fig. 4.24 Locations of Deflection Gages

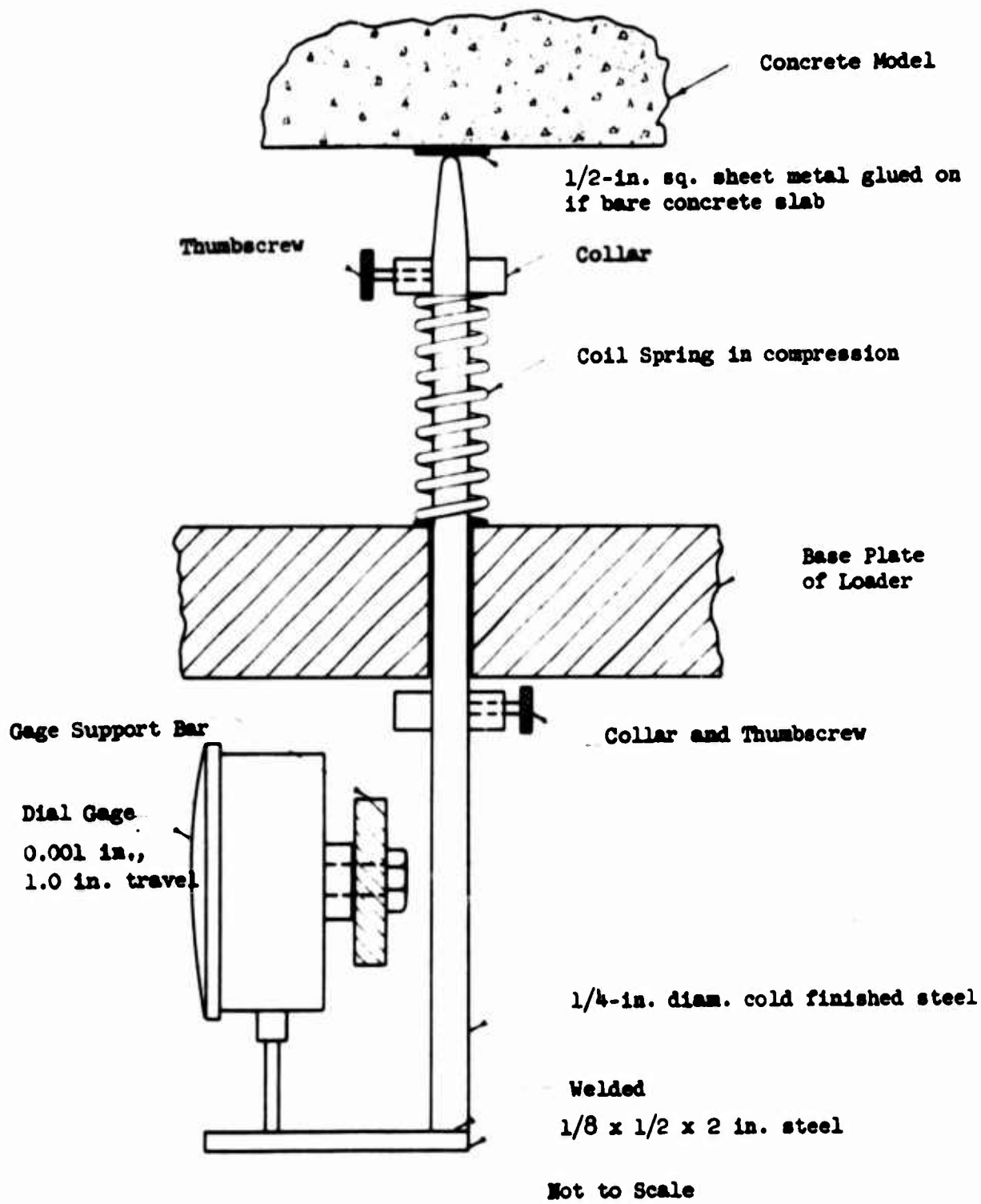


Fig. 4.25 DEFLECTION INSTRUMENTATION, 1/14-th SCALE MODELS

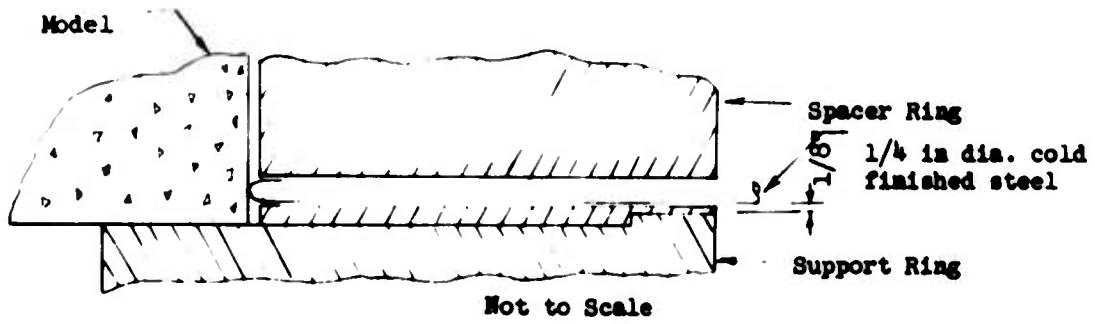
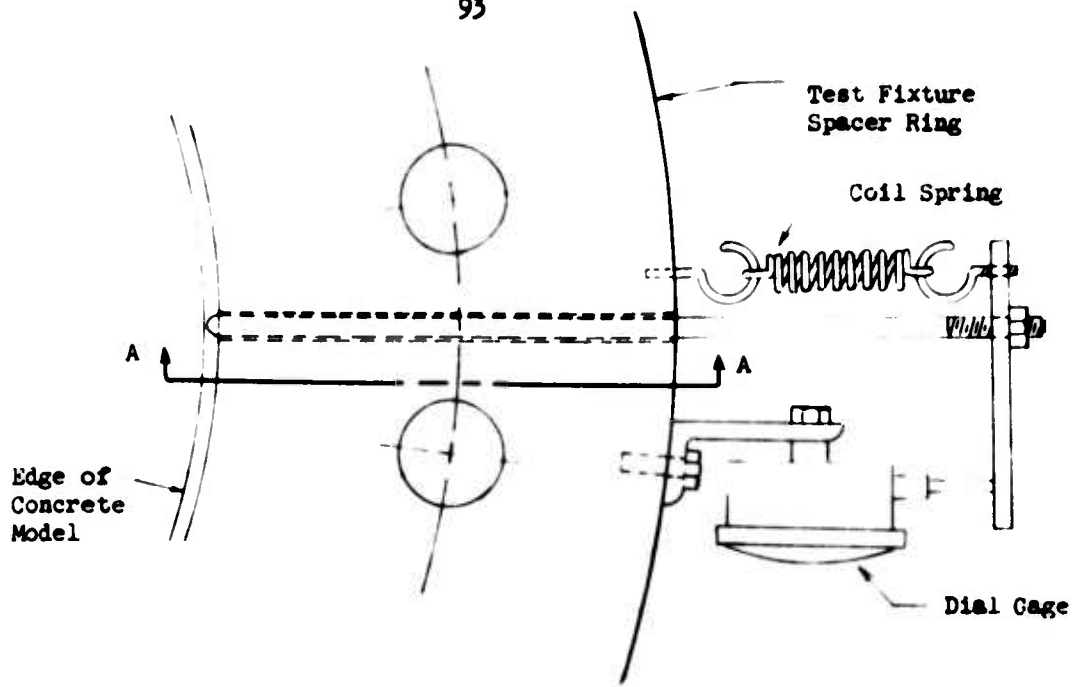
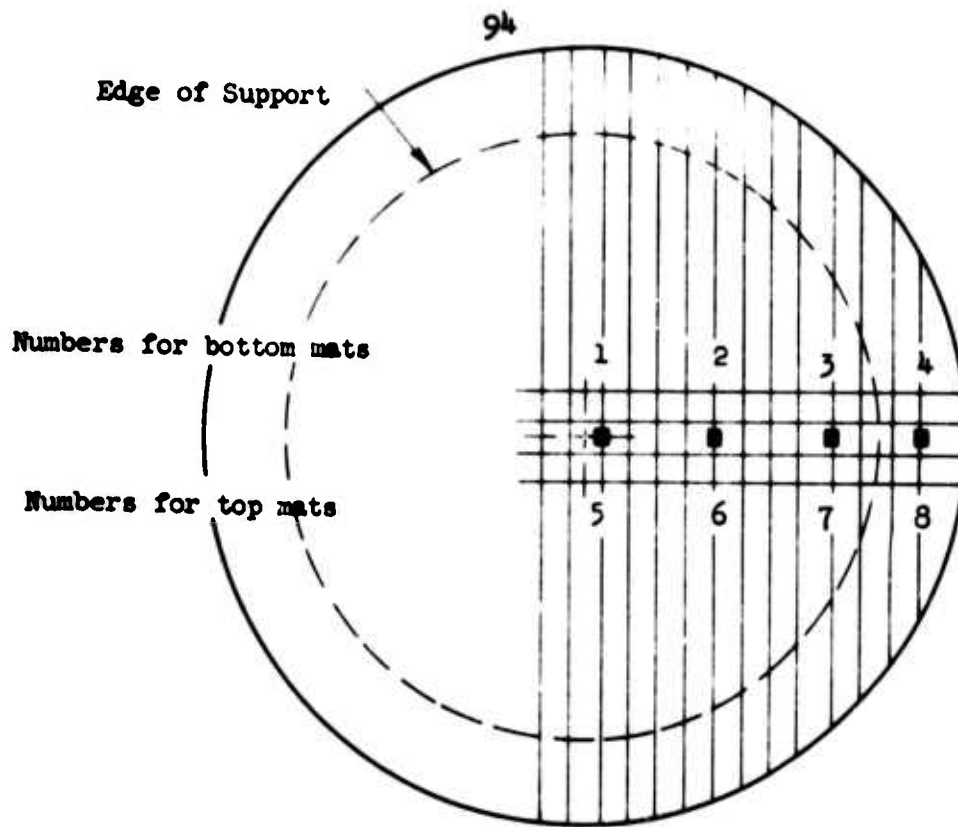
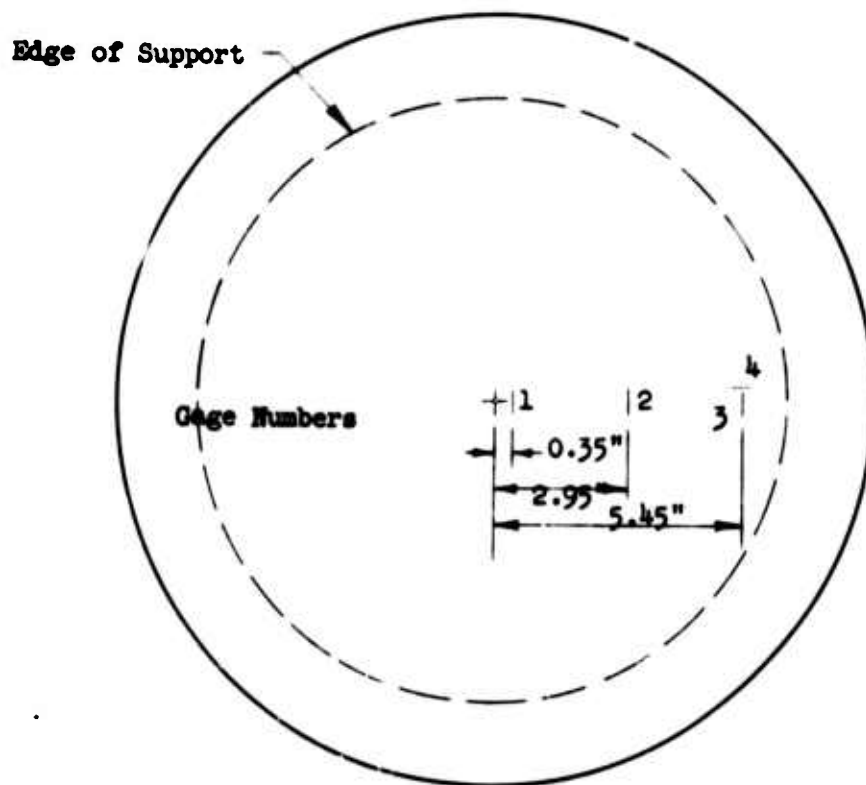


Fig. 4.26 Lateral Deflection Gage, G-Series Models



a) Gages on Bar Mats



b) Gages on Plate Reinforcement

Fig. 4.27 Strain Gage Locations and Numbering

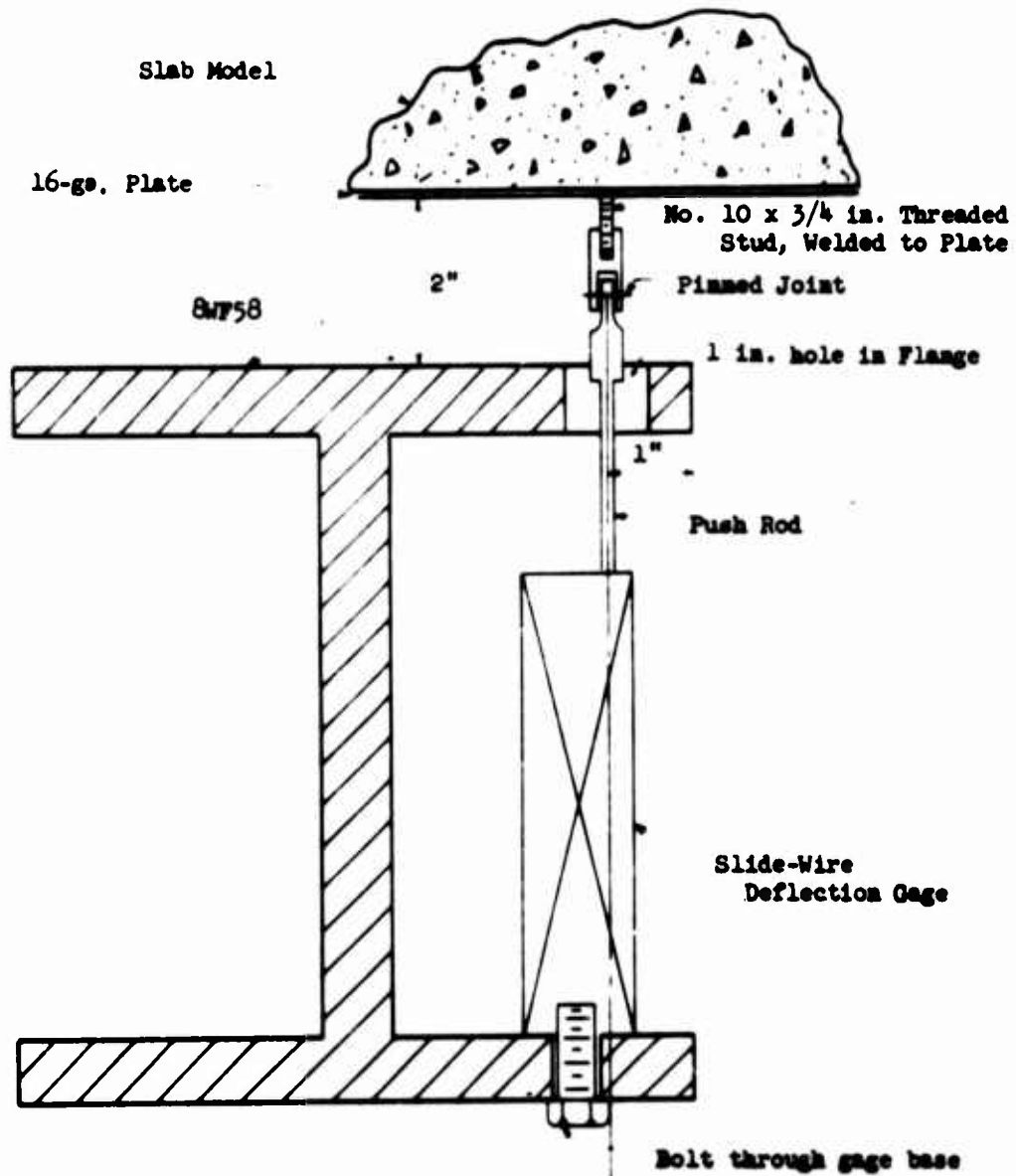
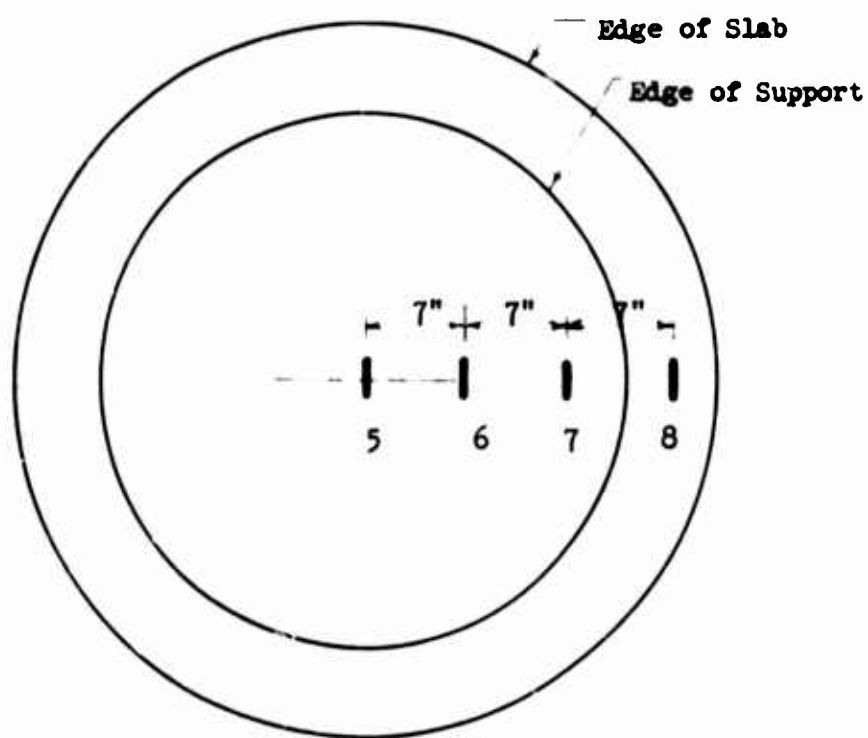
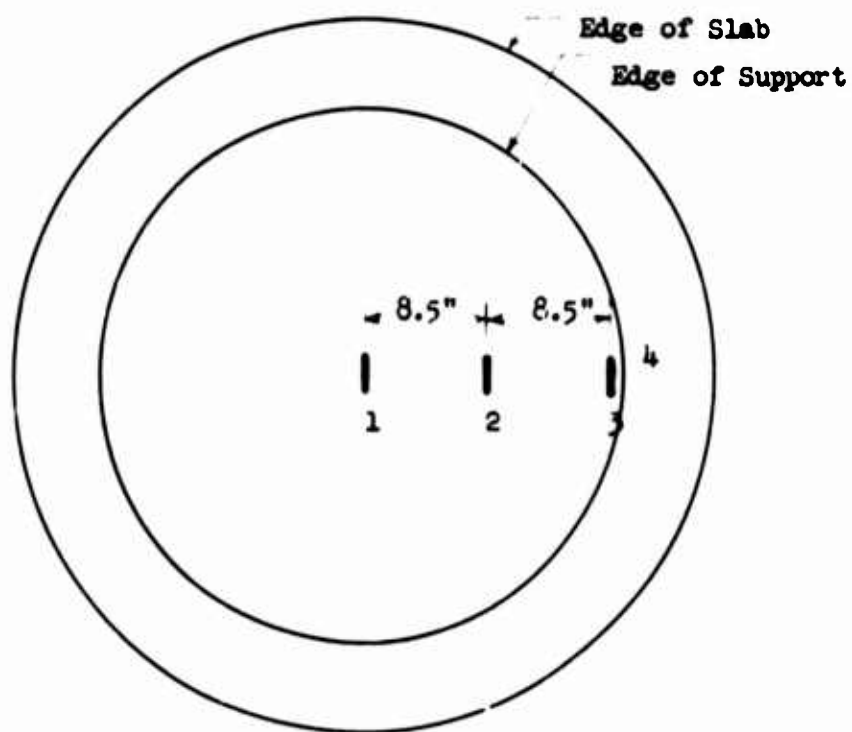


Fig. 4.28 Arrangement of Deflection Gages
1/5-th Scale Models



(a) Gages on Compression Steel



(b) Gages on Tension Steel (Plate)

Fig. 4.29 LOCATIONS AND NUMBERING OF STRAIN GAGES, 1/5-th SCALE MODELS

CHAPTER 5
TEST RESULTS

5.1. General

The instrumentation used in the program of model closure tests reported in this paper was described in Chapter 4. The measurements of deflection, pressure and strain taken at various stages of loading for each model constitute the test data for this program. The same measurements, plotted as load-deflection curves, deflection profiles and load-strain curves, will be referred to in this report as test results. The behavior of the model closure slabs, as indicated by the test results, is discussed in this chapter.

Test results for K-Series and J-Series models totaling 105 figures, have been presented in SAMSO TR-67-15 (1). To avoid unnecessary duplication those figures have not been included in this report. Figures representing all of the results of the later G-Series of model tests are incorporated in this chapter.

The maximum loads sustained by the model slabs constitute a concise and valuable set of test data. These have been reported in Tables 4.1 and 4.3 of the preceding chapter. The appearance and condition of each model after failure contribute to a second significant set of observations. Photographs of failed G-Series models are included with this chapter, and photographs of K-Series and J-Series models may be found in Ref. 1.

Several important conclusions can be drawn from the maximum load figures and from visual inspection of the test specimens. First,

the failure loads were in all cases significantly higher than the design loads. Second, the mode of failure was not flexural as assumed in the yield-line method used for design. This was true in all cases except, perhaps, G-4. In most cases a punching shear failure was observed. A failure crack started on the lower surface of the slab and sloped upward toward the center of the slab, where its projection on the upper surface formed the boundary of a circular depression. The slope of the failure crack was very nearly 45° for all of the 3.68-in. thick slabs and was steeper for the thicker slabs.

Several of the G-Series specimens appeared to have suffered bearing failures. In some of these cases the failed slab continued to deform until it was confined by the spacer rings of the test fixture. It then accepted additional load until a second maximum was reached, apparently indicating a shear failure at that point.

A detailed examination of the test data is not required to explain the absence of flexural failures. The yield-line theory used for design assumed simple supports at the boundary of the clear span, whereas the models were actually supported over an annular area. The clamping action of the load on the area of slab over the support must reduce the maximum positive moment. Furthermore, the same clamping action may be expected to provide a frictional restraining force on the lower surface of the slab. Test results are available to support these qualitative assertions. These results are discussed further in later sections of this chapter. In general, it may be concluded that the simple yield-line theory used for design in Chapter 3 errs on the side of conservatism for predicting failure loads for closure slabs loaded and supported in the same manner as were the models in these tests.

The behavior of the 34 model slabs tested can best be described and compared with reference to the load-deflection curves. As previously stated, only the G-Series load-deflection curves are presented with this report. All of the curves obtained are similar in some respects, however. The initial portion, reasonably linear, is followed by a portion of decreasing slope to the maximum load. An unloading portion to failure follows, except in the case of K-15, K-17 and several G-Series models in which a second maximum load was observed. The shape and length of the unloading portion after the final maximum load was reached varied considerably from model to model.

In order to avoid discussing 34 individual curves on a purely subjective basis, the writer has assigned stiffness and ductility values, deduced from the curves, to each of the models tested. The method of assigning these values was entirely arbitrary, though consistent. The numbers assigned are therefore reported as "relative stiffness" and "relative ductility" in Table 5.1.

The method of obtaining stiffness and ductility values is illustrated on Fig. 5.1, the load-deflection curve for model slab G-1. The linear portion of the curve is extended to the point at which it is separated from the actual curve by a distance of 0.01 in. (abscissa scale). The load at that point is considered the "apparent yield" load. The abscissa is the yield deflection. The quotient of the yield load divided by the yield deflection is the "relative stiffness." The second intersection of the actual curve with the yield load is the maximum deflection (for that load). Division of the maximum deflection by the yield deflection gives the "relative ductility." The ratio of

apparent yield load to maximum load is included in Table 5.1 as an indicator of the bias introduced by the arbitrariness of the system.

The stiffnesses of the model slabs were straightforwardly determined in most cases and the values reported deserve some confidence. The ductilities found by this method are extremely sensitive to several factors, and should be used with caution. The stiffness and ductility data are explored further in the next chapter.

The following sections describe the behavior of the model slabs tested in this program. Each section considers a group of related closure models.

Test results in graphical form are presented for the G-Series of model slabs at the end of the chapter. The figures are arranged numerically by model number. For each model number the load-deflection curve is presented first, followed by the deflection profiles and load-strain curves. The following notes apply to the load-strain curves:

- (1) Curves identified with a plus (+) report tension strains positive. Compressions are plotted as positive strains where the curves are marked with a (-).
- (2) The word "out" terminating a curve indicates that the gage ceased to provide satisfactory information at that point.
- (3) An arrowhead terminating a curve indicates that the gage continued to provide data exceeding the limits of the plot.

Photographs of the specimens after testing are presented, in numerical order by model number, after the graphical data.

5.2. Bar-Reinforced Slabs

Five of the 1/14th-scale models tested contained mats of 1/8-in. square bars as the only tension reinforcement. Models K-1 and

K-2 had no shear reinforcing, models K-5 and K-6 had three rings of vertical steel and model K-13 was provided with six rings of vertical steel. Models K-1, K-2 and K-5 were loaded and unloaded once before being loaded to failure. The stiffnesses reported in Table 5.1 for those models were computed from the second loading, though in all cases the first-loading stiffnesses appeared to be about the same.

Tables 5.2 and 5.3 were prepared to show the effect if any, of shear reinforcement on stiffness and ductility, respectively. No relation between shear reinforcement and the stiffness of bar-reinforced slabs seems to exist, nor is there any obvious explanation for the two magnitudes of stiffness exhibited by the five models. There does appear to be an improvement in ductility when shear reinforcement is added.

Maximum loads (see Table 5.4) ranged from 2450 psi for K-2 to 2710 psi for K-5 and did not appear to be significantly improved by the addition of shear reinforcement.

Strains were measured in all of the bar-reinforced slabs except K-1. None of the strains measured in any of the tension steel indicated yielding except those in K-13. The measured tension steel strains were in most cases lower than the compression strains measured at corresponding locations in the section. Consequently, the neutral axis position was lower in the section than would be expected. For instance, the strains measured by gage 1 (tension) and gage 5 (compression) in model slab K-2 at 2000 psi indicate a neutral axis position about $0.57d$ from the top surface. For a section with the properties of K-2, just before yielding, the location of the neutral

axis should be about $0.35d$ from the compression face. Thus the measured strain data for this group of models tend to support the earlier assumption of a frictional restraining force acting on the lower surface of the slab.

5.3. Plate-Reinforced 1000-psi Slabs

The slabs discussed in this section include K-3, K-8, K-12, K-14, G-1, G-2, G-3, G-9 and G-11. All of these slabs except G-11 were reinforced with a 16-gage plate. The reinforcing plate of G-11 was 14-gage. Nominal concrete cylinder strengths were 5000 psi except for slabs G-1 and G-3 with nominal compressive strengths of 7000 psi and 3000 psi, respectively. Model K-8 had three rings of shear reinforcement and model K-12 was provided with six rings. Model G-11 contained one row of threaded rods for shear reinforcement. No shear reinforcement was used in any of the other models of the group.

The maximum loads resisted by this set of slabs varied from 1575 psi (G-3) to 2480 psi (G-11). When the load is divided by the square root of the corresponding concrete strength (see parenthetical numbers in Table 5.4), the variation is largely eliminated. The loads normalized in this manner show no significant improvement due to the addition of shear reinforcement. There does seem to be an indication that the maximum loads resisted by the plate-reinforced slabs are consistently less than the loads taken by bar-reinforced slabs of the same nominal design pressure.

The stiffnesses reported in Table 5.2 are similarly unaffected by the addition of shear reinforcement. Neither is there any consistent

difference in stiffnesses between the bar-reinforced models discussed in the previous section and the plate-reinforced models of this group. The stiffness reported for G-3 is obviously anomalous, as is the initial part of the load deflection curve for that model (see Fig. 5.12). This discrepancy has not been explained.

Table 5.3 indicates that the ductilities for the plate-reinforced model slabs are consistently and significantly higher than those found for the bar-reinforced models. The tabulated values also show a slight increase in ductility when shear reinforcement is added, as was the case for the bar reinforced slabs.

At least one strain gage on the tension reinforcement of each model in the group showed yielding. With the exception of the gages on model K-14, which is a special case, and two other gages, yielding consistently occurred at or very near (within 10 percent) the maximum load.

Model slabs G-1, G-2, G-3 and K-12 each produced compression gage records indicating yielding at one or more gage locations. When yielding was observed, it first occurred at a load equal or nearly equal (within 10 percent) to the maximum load. Yielding of the compression reinforcement in the bar-reinforced slabs, on the other hand, occurred at somewhat lower loads.

Pairs of strain gage records, i.e., records from tension and compression gages at corresponding locations in the section, are available for slabs K-3, K-8, K-12, K-14, G-1 and G-2. Strain profiles constructed from these records, except in the case of model K-14, consistently indicate neutral axis locations greater than $0.5d$ from the

compression face. In slab G-1 at 2000 psi the midspan gages suggest a neutral axis position at about $0.72d$ from the upper surface.

Model closure K-14, which was otherwise identical to K-3, was specially treated before testing in an attempt to reduce the frictional restraint available from the test fixture. The matching surfaces of the model and test device were polished and the test fixture bearing surface was sprayed with a Teflon* compound and greased. The maximum load, stiffness and ductility were similar to other models of the group, but differences were noted in the strain gage records. The tension reinforcement at all four gage locations yielded at 80% of maximum load. Tension gages on the other models of the group generally did not indicate initiation of yielding until a load greater than 90% of maximum had been reached. The strain profile from the midspan gages at 2000 psi suggests a neutral axis position at about $0.37d$ from the compression face, considerably higher than for any of the similar slabs.

Model slab G-9 was subjected to repeated loadings to 2000 psi. After five cycles of loading to that level had produced no significant permanent deformation, the load was increased to 2300 psi. Failure occurred at 2300 psi on the second cycle to that load. The stiffness reported in Table 5.1 for G-9 was computed for the third cycle of loading, and is higher than that displayed on the first cycle. Strain measurements were taken on the first two cycles of loading. Gage No. 3 indicated yielding at 1880 psi load on the first cycle.

* An E. I. DuPont de Nemours and Co. trademark.

The "welded wire fabric" used for shear reinforcing in the K-Series models was manufactured by spot-welding the annealed 16-gage wires. During the difficult task of fitting the shear reinforcement to the "studded" bottom plate and the compression mat, quite a few welds were broken. Difficulty was also encountered with weld breakage in assembling models G-7 and G-10. The shear reinforcement scheme of G-11 was designed to minimize this problem. On a maximum-load basis (see Table 5.4), its behavior was slightly better than that of its counterparts. Ductility was comparable to other models with shear reinforcement. The choice of a 14-gage tension plate for model G-11 was unfortunate, since it introduced another difference and made comparison with the other models more difficult.

Models G-1, G-2 and G-3 were cast of three different concrete strengths to test the effect of that parameter on load resistance. The maximum load, which may be considered a direct measure of the ultimate shear stress for models of identical dimensions, was found to be an almost constant function of the square root of the concrete compressive strength. Maximum load data are reported in Table 5.4.

5.4. Plate-Reinforced 300-psi Slabs, 1/14th Scale

Model slabs J-1 and J-2 were 1/14th-scale reproductions of closures designed for a nominal load resistance of 300 psi. The two models were identical, except for the unavoidable variation in concrete strength, and their behavior was comparable. The maximum loads are essentially equal. The stiffnesses reported in Table 5.1, compared to the 1000 psi slabs, are lower than would be expected. Based on the

ratio of the cube of the depth, one would expect a flexural stiffness about one-fourth that of the 3.68-in. slabs. The actual stiffness ratio is much less.

Models J-1 and J-2 exhibited the least ductility (as defined herein) of any of the models tested except G-5. An explanation has not been found. Reinforcement strains in both slabs were large, and tensile yielding was observed at loads as low as 300 psi. Strain profiles at loads near the maximum place the neutral axis high on the section, indicating that frictional restraint was not an important factor in these two tests.

5.5. Plate-Reinforced 300-psi Slabs, 1/5th Scale

Three 1/5th-scale models designed for a nominal 300 psi collapse load were tested at the University of Illinois Structural Dynamics Laboratory. Slab J-5 was tested to failure at 560 psi under a slowly applied load. Slab J-6 was subjected to four rapidly applied loadings with rise times from zero load to maximum load of 2.3 to 2.5 milliseconds. Several different decay rates were used. In the fourth test the model withstood a load of 592 psi without failure. Slab J-8 was subjected to five rapidly applied loadings with a peak pressure of 675 psi in the last test. The slab did not collapse.

The bottom plates of the 1/5th-scale slabs were slightly warped by the welding of the 3/16-in. diameter shear studs. In order to provide uniform support, the bearing surface was greased and then coated with an epoxy paste. The lower surface of the slab was wiped clean and set down in the soft epoxy.

Slab J-5 was loaded to failure in a short term static test. The maximum load of 560 psi was reached in about 11.5 minutes. When the maximum load was reached the specimen collapsed completely and violently as the energy stored in the compressed gas was released. Photographs of the damage can be seen in SAMSO TR 67-15 (1). A truncated cone of concrete was punched out of the slab and half of the cone was blown to the bottom of the support structure, leaving only the compression steel spanning the opening. The 16-gage plate was torn and several pieces of it were ripped completely free. A large number of shear studs were pulled from the plate, pulled from the concrete or severely bent.

The stiffness and ductility of J-5, computed from the load-deflection curve, are reported in Table 5.1. The stiffness, scaled to compare with the 1/14th-scale models, is slightly higher than the values found for J-1 and J-2. The ductility of J-5 was considerably higher than the values found for J-1 and J-2 and comparable to the ductilities of the deeper plate-reinforced slabs.

The load-strain records for J-5 indicate that most of the area of the reinforcing plate had yielded at the 500 psi load level. None of the compression steel yielded. The strain profiles indicate a high neutral axis position, as was true for models J-1 and J-2.

Slab J-6 was subjected to four dynamic loadings. Five dynamic loadings were applied to J-8. The maximum pressures and load decay rates are listed in Table 5.5. In each case the rise time from zero to maximum load was between 2.3 and 2.5 milliseconds. The word "dwell" in the table refers to the length of time between reaching maximum load and opening the load decay valves. In the tests with dwell time the

loading was a step pulse followed by a pressure decay. In the other cases the pressure decay followed the peak pressure.

The dynamic tests are discussed in detail in SAMSO TR 67-15 (1) and the load-time and load-strain records are included with that report. In the present report only the highlights of the results of those tests are presented. The most important finding from the dynamic tests is that the response of the model slabs was essentially static. No large amplifications of motion were caused by the rapidly applied loadings. Apparently the slab response time was short compared to the load rise time and the "dynamic" tests were effectively short-term (tenths of seconds) static tests. Both data and theory lend support to this conclusion.

The period of vibration of the slabs was short enough that the measured strains appeared to follow the variations of the load in every detail. Every major variation in the load-time curve for a given test was reproduced in the load-strain records, though with a time lag of one to two milliseconds.

If Eq. (3.11) is applied to the geometry of the model slab, the period of vibration is found to be about 1.55 milliseconds. Though the actual period may be longer due to shear deformation and vertical compression effects, it is probably shorter than the rise time of 2.3 to 2.5 milliseconds.

Slab J-6 was removed from the test fixture after test D-4, which was effectively a step pulse of 520 psi applied for one minute. The upper surface of the slab was intact, with only minor cracking. The lower surface was bulged downward. An area about 20 in. in diameter

in the central portion of the bottom plate had apparently separated from the concrete. Within this area there were holes left by shear studs pulled loose from the plate. The plate in the area was dimpled, indicating that it had been subjected to substantial forces by the shear studs. This damage is believed to have been caused by leakage of helium into the slab during test D-4.

Model slab J-8 had not collapsed when testing was terminated after five loadings, but the measured strains after the last test indicated that failure was imminent. Loads of 640 and 675 psi were reached in tests D-8 and D-9, respectively. The slab, when it was removed from the test device, did not appear to be badly damaged. The residual deflection at the center of the slab was only one percent of the clear span. There was some cracking on the upper surface near the supports and cracks up to $1/32$ in. in width were noticed on the edges. The lower surface was intact and the plate was in good contact with the concrete over most of the area of the slab.

Deflection records were not obtained on any of the dynamic tests.

5.6. Plate-Reinforced 2000-psi Slabs

The group of specimens discussed in this section includes model slabs G-5, G-7 and G-10. Slabs G-7 and G-10 each contained three rows of vertical 11-gage wires for shear reinforcement. Model G-5 had no shear reinforcement. Slab G-10 was provided with one mat of tension steel in addition to the 14-gage steel plate. Other differences make direct comparison of these models difficult. The height of G-5 was

0.1 in. less than the thickness of the spacer rings, which affected the manner of failure. A different method was used for designing the shear studs for G-5 than for G-7 and G-10. More than twice as many shear studs were used in G-5 as in G-7 and G-10.

Model slab G-5 failed at 2800 psi in bearing. Shortly after the maximum load was reached the pressure dropped to zero. The difference in thickness of the slab and the test fixture caused the aluminum ring of the seal assembly to deform. The inner edge of the ring pressed into the upper surface of the slab, near its edge, and the concrete was broken away from the edge at one point. The neoprene membrane followed the aluminum ring into the gap and the oil seal was broken. The failure of the upper surface may be seen in the photograph, Fig. 5.63. The vertical deformations of the upper and lower surfaces were small for this specimen.

Closure model G-7 failed at 2800 psi and unloaded to 2425 psi. The outer edge of the specimen engaged the spacer rings of the test fixture at that point and became confined. The slab then accepted additional load, reaching a maximum of 2925 psi. A shear failure was underway at the time the pressure was lost, but an oil seal failure may have hastened the end of G-7. The model was tightly wedged in the spacer rings and force was required to remove it. The failed model showed considerable distress around the edges due to the bearing failure, in addition to the deformations associated with the shear failure. The 14-gage steel reinforcing plate was sheared through in the test.

Model G-10 behaved in essentially the same manner as G-7. Stronger concrete and additional tension steel contributed to the higher loads withstood by model G-10. The initial failure in bearing occurred at 3350 psi. The load then dropped to 3000 psi, at which point the concrete had deformed outward far enough to contact the spacer rings of the test device. The model then reloaded to 3400 psi, where a shear failure occurred. Jacking was required to separate the failed specimen from the test fixture spacer rings. The appearance of the slab after removal from the fixture was similar to that of model G-7.

In the tests of models G-7 and G-10 the pressure fell off while the model was on an ascending portion of the load-deflection curve, which was not generally the case with the models tested in this program. One possible explanation is that the sealing membranes failed before the shear failures in the models could develop fully. This hypothesis would also explain the relatively low deflections observed when these models failed, compared to other models tested.

The normalized maximum loads, in terms of $\sqrt{f'_c}$, reported in Table 5.4 for the slabs in this group are of about equal magnitude. When these values are multiplied by the ratio 3.68/5.47, values of 25.2, 28.8, and 30.8 are obtained for models G-5, G-7 and G-10, respectively. The latter numbers are in good agreement with the normalized maximum loads reported for the 3.68-in. plate-reinforced models. This indicates that the maximum average shear stresses at the edge of the support, in terms of the square root of the concrete strength, were approximately the same.

Stiffnesses computed for the slabs of this group are shown in Table 5.2. The difference between stiffnesses of G-7 and G-10 reflects the difference in amount of tension steel. The lower value for G-5 is believed due to the improper test set-up.

Two ductilities were reported for models G-7 and G-10 in Table 5.3. The first value shown is based on a maximum deflection that coincides with the deflection at the low point on the load-deflection curve between the two maximum loads. Thus, it reflects the ductility if the model slab could not have been confined as it was. The second value considers an actual maximum deflection at the apparent yield load, thus reflecting the ductility where confinement is permitted. In either case the ductilities are lower than those reported for thinner plate-reinforced models with shear reinforcement.

The ductility of model slab G-5 was quite low, indicating the effect of the early pressure loss due to the deformation of the aluminum ring in the loading fixture.

All of the strain gages on slab G-5 survived the entire test. Gage No. 2 indicated yielding at 46 percent of the maximum load. None of the other tension gages reached yield strains. All of the strain gages on the compression steel reported tensile strains, an anomaly which has not been explained. Gage No. 8 indicated tensile yielding at 94 percent of maximum load.

The strain gages on models G-7 and G-10 behaved more predictably. Four tension gages on G-7 and three on G-10 showed yielding initiated at or very near maximum load. Gage No. 3 on G-10 failed to function. Gage 5 on G-7 indicated yielding at the maximum load. The

remaining compression gages were lost before reaching yield strain. Three G-10 compression gages functioned throughout the test and none indicated yielding.

5.7. Plate-and-Bar-Reinforced Slabs

Two pairs of slabs were reinforced with both a mat of 1/8-in. square bars and a steel plate. Models K-10 and K-11 were designed for a nominal load of 1000 psi and models G-6 and G-8 were each designed for 2000 psi. Slabs K-10 and K-11 were 3.68 in. thick, and slabs G-6 and G-8 were 4.47 in. thick.

The maximum loads resisted by models K-10 and K-11, as shown in Table 5.4, are comparable to those resisted by all the other plate-reinforced 3.68-in. thick slabs. The lower concrete strength of K-11 (see Table 4.1) provided an unintentional variation of that parameter. The normalized maximum load was not affected by the addition of three rings of shear reinforcement in model K-11.

Normalized maximum loads are shown in Table 5.4 for models G-6 and G-8. Multiplication of the reported values by the ratio $3.68/4.47$ yields scaled loads for comparison with the thinner specimens. Values of 29.1 and 32.3 are obtained for G-6 and G-8, respectively. These numbers are comparable to the maximum loads found for the 3.68-in. plate-reinforced slabs.

The load-deflection curves of G-6 and G-8 are of the Bactrian variety, similar to G-7 and G-10, as opposed to the Dromedary curves exhibited by most of the other models tested. In the cases of G-6 and G-8, though, the first peaks on the curves, i.e., the bearing failures,

were the maximum loads. Models G-7 and G-10 sustained greater loads on the second peaks, after confinement of the models in the spacer rings had occurred. Both G-6 and G-8 were wedged into the spacer rings after failure, requiring jacking to remove them. The appearance of the failed models was similar to that of G-7 and G-10, with evidence of the bearing failure apparent on the edges of the specimens.

The relative stiffnesses shown in Table 5.2 for K-10 and K-11 are roughly comparable to one another but much lower than the values listed for other slabs of the same thickness. The bar mats in these models were placed directly on the steel plate. This procedure may have limited the bond available to develop the strength of the bars and thus reduced the stiffness.

Model slabs G-6 and G-8 were identical except for concrete strengths, which were 5000 psi and 7000 psi, respectively. The higher stiffness reported for G-8 may be due in part to the stronger concrete, though G-1 and G-2 had nearly equal stiffness with different concrete strengths. The stiffnesses of G-6 and G-8 are of the expected magnitude, lying between those reported for the 3.68-in. slabs and those observed for the 5.47-in. models.

The ductilities shown in Table 5.3 for K-10 and K-11 are comparable to those reported for the slabs discussed in Section 5.3. Model slab K-11, with three rings of shear reinforcement, was significantly more ductile than K-10. The ductilities of G-6 and G-8 are of about the same magnitude as those of most other plate-reinforced slabs without shear reinforcement.

The tension strain gage records from K-10 and K-11 are complete and all show that yielding occurred at or within three percent of the maximum load. One compression gage on K-10 functioned, indicating yielding had begun at 88 percent of maximum load. On model K-11, gages 5 and 6 showed yielding at 95 and 76 percent of maximum load, respectively, and gage 7 indicated no yielding.

The strain gage behavior for model slabs G-6 and G-8 was similar. All of the tension gages worked, and all reported yielding at 98-100 percent of maximum load. Gage 5 on the compression reinforcement of each model showed yielding at 97 percent of maximum load. The other compression gages either did not function or were lost before they reached yield strain.

It may be generally concluded that closure slabs reinforced with both plates and bars will behave in about the same way as those reinforced with plates only.

5.8. Miscellaneous Slabs

The slabs included in this section are K-4, K-7, K-9, G-4 and G-12. Model K-4 was designed for 500 psi and reinforced with a 24-gage steel plate. Closure models K-7 and G-4 were plain concrete specimens, 3.68-in. and 5.47-in. thick, respectively. Slabs K-9 and G-12 represented attempts to obtain greater strengths by confining the concrete.

The maximum load taken by model K-4 was 1735 psi, or $24\sqrt{f'_c}$. The normalized maximum is only slightly less than the maximum values reported for 1000-psi plate-reinforced slabs, though K-4 contained

only 40 percent as much tension steel. The relative stiffness of K-4 was equal to or greater than the values computed for several 1000-psi models. The ductility at the apparent yield load was comparable to that observed for all plate-reinforced models without shear reinforcement.

Three tensile strain gages on K-4 indicated yielding at loads very near the maximum. Two compression strain gages also reported yielding at loads within a few percent of the maximum load. The other three gages did not produce complete records.

Model K-4 failed in shear in a manner similar to most of the 3.68-in. thick specimens.

Model slab K-7 failed in shear at 2120 psi. The specimen collapsed completely at the failure load. A truncated cone of concrete extending through to the top surface of the slab was punched out of the remaining part of the model. The maximum load, normalized maximum load (28.7) and stiffness were all higher than those found for some of the reinforced 3.68-in. models. The stiffness, in particular, is of about the same magnitude as the stiffnesses reported for the bar-reinforced slabs discussed in Section 5.2. Apparently more friction was available at the concrete-to-steel interfaces of these tests than at the steel-to-steel interfaces of the plate-reinforced slab tests.

Model closure G-4 failed at a lower load (1940 psi) and in an entirely different manner. The deflections were small and there was no evidence of a punching shear failure. Though it was 50 percent thicker than K-7, model G-4 appeared to have failed in flexure. The specimen after testing exhibited a system of radial cracks suitable for a textbook illustration. Part of the explanation lies in the fact that G-4

was 0.1 in. thinner than the spacers of the loading fixture. The aluminum ring did not deform as it did at the higher loads of the G-5 test. The portion of the upper surface outside the inner edge of the ring was not loaded and the model was essentially simply-supported. The behavior of the model was also affected by non-uniform bearing, as evidenced by the low slope of the initial portion of the load-deflection curve, Fig. 5.16.

Model K-9 was provided with a circular steel angle retaining ring as the only tension reinforcement. The model carried a maximum load of 2140 psi and then collapsed completely. A truncated cone of concrete extending up to the level of the compression steel fell completely free of the slab.

Compression strain gages 5 and 6 reported yielding at loads equal to 60 and 70 percent, respectively, of the maximum load. Gage 9 on the circular retaining ring indicated yielding at the maximum load, and gage 10, also on the ring, reported a strain of 0.001 at the maximum load.

One can account, in an approximate way, for the fact that K-9 failed at the same load as K-7, which was not reinforced. Comparison of the performance of the bar-reinforced models with the plate-reinforced models suggests that a concrete-to-steel interface provides more frictional restraint than a steel-to-steel interface. Apparently the confinement provided by the retaining ring of K-9 was about equal to the difference in frictional confinement provided by the two types of interface.

Considering the vertical leg of the retaining ring only (the circumferential deformation of the horizontal leg cannot be appreciable), and using an average stress of 35,000 psi, as suggested by the strain gages, we obtain a force of 9500 pounds in the retaining ring. This is equivalent to a horizontal line load of 1480 pounds/in. applied at the edge of the support. The maximum applied load of 2140 psi is equivalent to a vertical line load of 11,000 pounds/in. applied at the edge of the support. Thus, the effect of the K-9 confining ring, by this simple analysis, is equivalent to a change in friction coefficient of 0.135. This appears to be a reasonable figure. Friction coefficients will be discussed further in the next chapter.

Model G-12 was reinforced with an 11-gage steel tension plate and provided with an 11-gage confining ring that extended the full height of the slab. The model reached a first maximum load of about 3900 psi when a failure, apparently in bearing, caused the load to drop to 3150 psi. The steel confining ring had by then partially contacted the test fixture spacer rings and the specimen began to reload, reaching a second maximum load of about 4100 psi. The slab failed abruptly at that load. The failed model was very tightly pressed into the spacer rings, and considerable force and ingenuity were required to remove it. The confining ring of the model was uniformly barrel-shaped after the test, with a maximum diameter at a point located about one-fourth of the slab thickness from the bottom edge of the slab.

The behavior of model G-12, as indicated by the load-deflection curve, is similar to that of G-7 and G-10. There were two peaks on the curve, with the second higher than the first. The pressure

fell off abruptly after the second peak in all three cases. The higher load taken by G-12 was due to the confining ring, the threaded rod shear reinforcement or the increased area of tension steel, or to a combination of these factors. Based on the results of the other tests in the series, the confining ring is believed to have had the greatest influence in producing the additional load capacity.

The ductilities reported for G-12 are higher than those shown for G-7 and G-10 and about comparable to those of other plate-reinforced models with shear reinforcement.

Strain gage performance on G-12 was not very satisfactory. Gage 4 was the only tension gage to function throughout the test or until yield strain was reached. It indicated yielding at 84 percent of maximum load. Two compression gages functioned long enough to provide information on yielding. Gage 5 indicated yielding at 93 percent of maximum load and gage 8 showed no yielding. Gage 9, on the confining ring, failed at a load of 3800 psi. The strain at that load was 0.00125. The nature of the confining ring deformation was such that a single gage could not provide much information.

5.9. Randomly-Reinforced Slabs

Slabs K-15 and K-17 were randomly reinforced with short lengths of small wire. The behavior of these models was somewhat similar to that of the G-Series 2000-psi models. An initial maximum was followed by an unloading, during which the slab deformed outward until it contacted the spacer rings of the test fixture. The structure then reloaded to a second, higher peak load. Failed specimens were

jammed into the test fixture and required force for removal. The chopped wire models failed first in flexure, and finally in shear.

Models K-15 and K-17 were both loaded to failure. Slab K-15 supported 1230 psi at the first peak and 2100 psi at the maximum load. Model K-17 withstood 1455 psi at the first peak and eventually reached a maximum load of 2850 psi. In terms of the square root of the cylinder strength, the first peak values were 16.0 for K-15 and 17.1 for K-17. The maximums were 27.3 for K-15 and 33.5 for K-17. The ductilities reported in Table 5.1 for these specimens are essentially identical, both for the case where confinement is not allowed and for the case in which confinement is permitted.

Loading of slab K-16 was stopped before jamming occurred so that the model could be examined. The first peak load had been reached. Its value was 1205 psi or, in terms of $\sqrt{f'_c}$, 14.3. The stiffnesses shown in Table 5.1 for the initial loading of all three slabs are essentially equal.

After these slabs were tested the support surface of the loading fixture showed many radial scratch marks caused by the slab sliding on the support. No evidence of such movement was found in any of the other tests. The friction between slab and support was apparently low enough to allow significant sliding to occur. Numerous wire surfaces coincide with the surface of the chopped-wire concrete, and this was evidently responsible for the reduced friction.

The relatively low load capacities, before jamming, can be traced to the lower friction between the slab and the support. The lower friction leads to lower forces in the plane of the slab, which

result in lower flexural strengths. However, the random reinforcement was effective in preventing a shear failure.

This completes the presentation of the results of the model tests. These results are discussed further in the next chapter.

TABLE 5.1. STIFFNESS AND DUCTILITY OF MODEL SLABS

Model No.	Apparent Yield Load (psi)	Apparent Yield Load Max. Load	Yield Defl. (in.)	Max. Defl. (in.)	Relative Stiffness 1000	Relative Ductility
K-1	2320	.94	.026	.082	89.5	3.15
K-2	2320	.95	.027	.056	86.0	2.07
K-3	1600	.74	.027	.216	59.2	8.0
K-4	1500	.87	.038	.219	39.5	5.77
K-5	2360	.87	.029	.147	81.3	5.07
K-6	1900	.82	.036	.157	52.8	4.37
K-7	1950	.92	.026	.061	75.0	2.35
K-8	1550	.72	.031	.51	50.0	16.45
K-9	1920	.90	.033	.078	58.2	2.37
K-10	1800	.83	.064	.24	28.1	3.75
K-11	1120	.68	.052	.465	21.6	8.93
K-12	1740	.79	.041	.44	42.5	10.7
K-13	2180	.84	.038	.176	57.4	4.63
K-14	1600	.74	.043	.38	37.2	8.85
K-15	1110	.90*	.033*	.173	33.6	5.23
		.53**	.033**	.475		14.4
K-16	1190	.99	not failed		34.0	
K-17	1190	.82	.037*	.186	32.2	5.03
		.42	.037**	.53		14.3
J-1	695	.89	.151	.283	4.6	1.88
J-2	710	.99	.205	.25	3.5	1.22
J-5	435	--	.23	1.48		6.43
J-5***	435	.78	--	--	5.3	--
G-1	2000	.88	.05	.29	40.0	5.8
G-2	1800	.83	.05	.34	36.0	6.8
G-3	1580	1.0	no ductility		316.0	1.0
G-4	1600	.84	no ductility		57.6	1.0
G-5	2580	.92	.0425	.090	60.7	2.12
G-6	2360	.85	.05	.465	47.2	9.3
G-7	2440	.87*	.032	.152	76.2	4.75
		.83**	.032	.308	--	9.6
G-8	3020	.89	.045	.23	67.1	5.1
G-9	2000	--	no ductility		59.8	--
(cycle #3)			determined			
G-10	3000	.90*	.034	.14	88.3	4.1
		.88**	.034	.205	--	6.0
G-11	2180	.88	.06	.635	36.3	10.6
G-12	3150	.81*	.035	.29	90.0	8.3
		.77**	.035	.58	--	16.6

* Confinement not allowed.

** Confinement permitted.

*** Scaled.

TABLE 5.2. EFFECT OF SHEAR REINFORCEMENT ON STIFFNESS

"Relative Stiffness"/1000

No Shear Reinforcement	Three Rings 16-ga. Wire	Six Rings 16-ga. Wire	One Ring 1/4" Threaded Rods
Bar- (K-1) 89.5	(K-5) 81.3	(K-13) 57.4	
Reinforced (K-2) 86.0	(K-6) 52.8		
Plate- (K-3) 59.2	(K-8) 50.0	(K-12) 42.5	(G-11) 36.3
Reinforced (G-1) 40.0			
1000 psi (G-2) 36.0			
(G-3) 31.6			
(G-9) 59.8			
(K-14) 37.2			
Plate-and- (K-10) 28.1	(K-11) 21.6		
Bar-Reinforced			
1000 psi			
	<u>Three Rings</u> <u>11-ga. Wire</u>		
Plate-Reinf (G-5) 60.7	(G-7) 76.2		
2000 psi	(G-10) 88.3		
Plate-and- (G-6) 47.2			
Bar-Reinforced			
2000 psi (G-8) 67.1			

TABLE 5.3. EFFECT OF SHEAR REINFORCEMENT ON DUCTILITY

		"Relative Ductility"			
No Shear Reinforcement		Three Rings 16-ga. Wire	Six Rings 16-ga. Wire	One Ring 1/4" Threaded Rods	
Bar-	(K-1) 3.15	(K-5) 5.07	(K-13) 4.63		
Reinforced	(K-2) 2.07	(K-6) 4.37			
Plate-	(K-3) 8.0	(K-8) 16.45	(K-12) 10.7	(G-11) 10.6	
Reinforced	(G-1) 5.8				
1000 psi	(G-2) 6.8				
	(G-3) None				
	(G-9) ---				
	(K-14) 8.85				
Plate-and-	(K-10) 3.75	(K-11) 8.93			
Bar-Reinforced					
1000 psi					
	Three Rings 11-ga. Wire				
Plate-	(G-5) 2.12	(G-7) 4.75/9.6*			
Reinforced	(G-10) 4.1/6.0				
2000 psi					
Plate-and-	(G-6) 9.3				
Bar-	(G-8) 5.1				
Reinforced					
2000 psi					

* Confinement not allowed/confinement permitted.

TABLE 5.4. EFFECT OF SHEAR REINFORCEMENT ON MAXIMUM LOAD

		Max. Load (Max. Load/ $\sqrt{f'_c}$)		
No Shear Reinforcement		Three Rings 16-ga. Wire	Six Rings 16-ga. Wire	One Ring 1/4" Threaded Rods
Bar-	(K-1) 2460 (32.2)	(K-5) 2710 (36.0)	(K-13) 2610 (34.7)	
Reinforced	(K-2) 2450 (30.6)	(K-6) 2310 (32.6)		
Plate-	(K-3) 2150 (28.1)			
Reinforced	(G-1) 2280 (27.2)	(K-8) 2150 (31.0)	(K-12) 2200 (28.5)	(G-11) 2480 (34.6)
1000 psi	(G-2) 2175 (26.5)			
	(G-3) 1575 (28.7)			
	(G-9) 2300 (31.7)			
	(K-14) 2170 (26.8)			
Plate-and-	(K-10) 2160 (28.0)	(K-11) 1655 (26.0)		
Bar-Reinforced				
1000 psi				
				Three Rings 11-ga. Wire
Plate	(G-5) 2800 (37.4)			(G-7) 2925 (42.8)
Reinforced				(G-10) 3400 (45.8)
2000 psi				
Plate-and-	(G-6) 2775 (36.5)			
Bar-	(G-8) 3400 (40.5)			
Reinforced				
2000 psi				

TABLE 5.5. TESTS ON 1/5-th SCALE SLABS

Test No.		Slab	Maximum Load psi	Decay or Dwell
S-1	10 Jan. 1967	J-5	560	Static
D-1	27 Feb.	J-6	258	0.045 sec to 1/2 load
D-2	27 Feb.	J-6	414	0.018 sec to 1/2 load
D-3	27 Feb.	J-6	410	0.060 sec dwell
D-4	27 Feb.	J-6	592	1 min. dwell
D-5	14 Apr.	J-8	380	0.029 sec to 1/2 load
D-6	2 May	J-8	435	0.060 sec dwell
D-7	2 May	J-8	550	0.021 sec to 1/2 load
D-8	10 May	J-8	640	0.029 sec to 1/2 load
D-9	12 May 1967	J-8	675	0.061 sec dwell

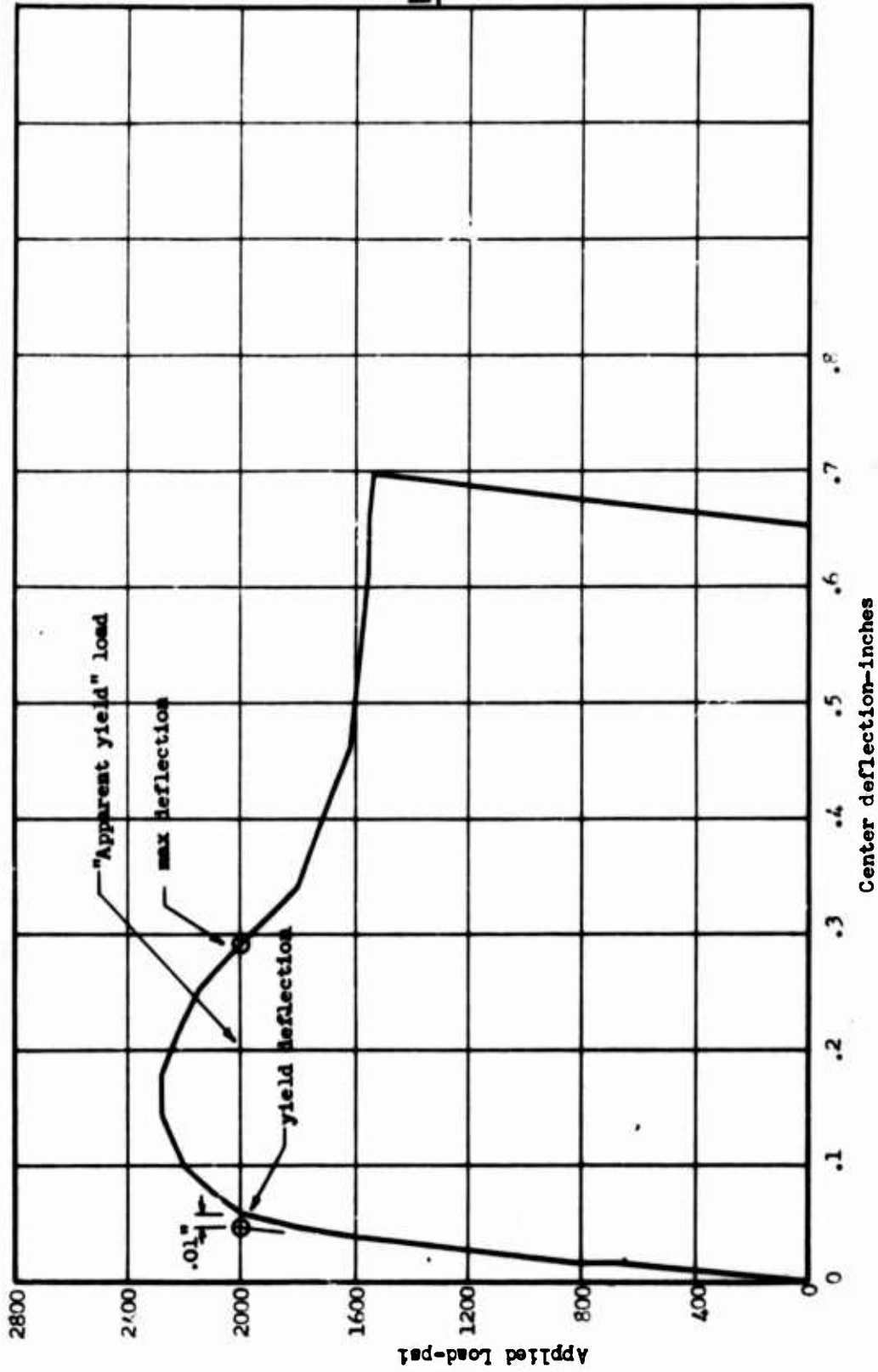


Fig. 5.1 Load-Deflection Curve, Slab G-1

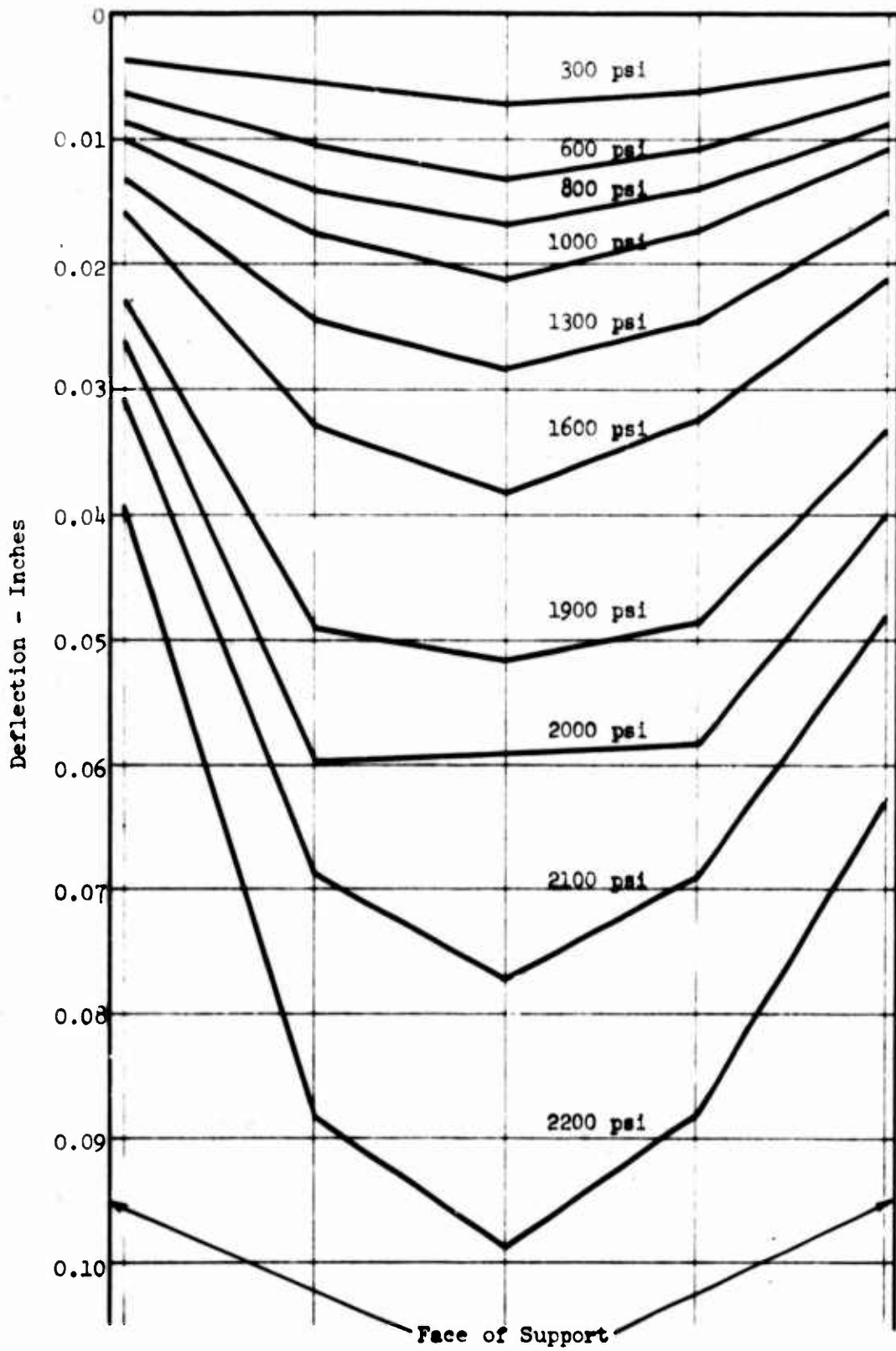
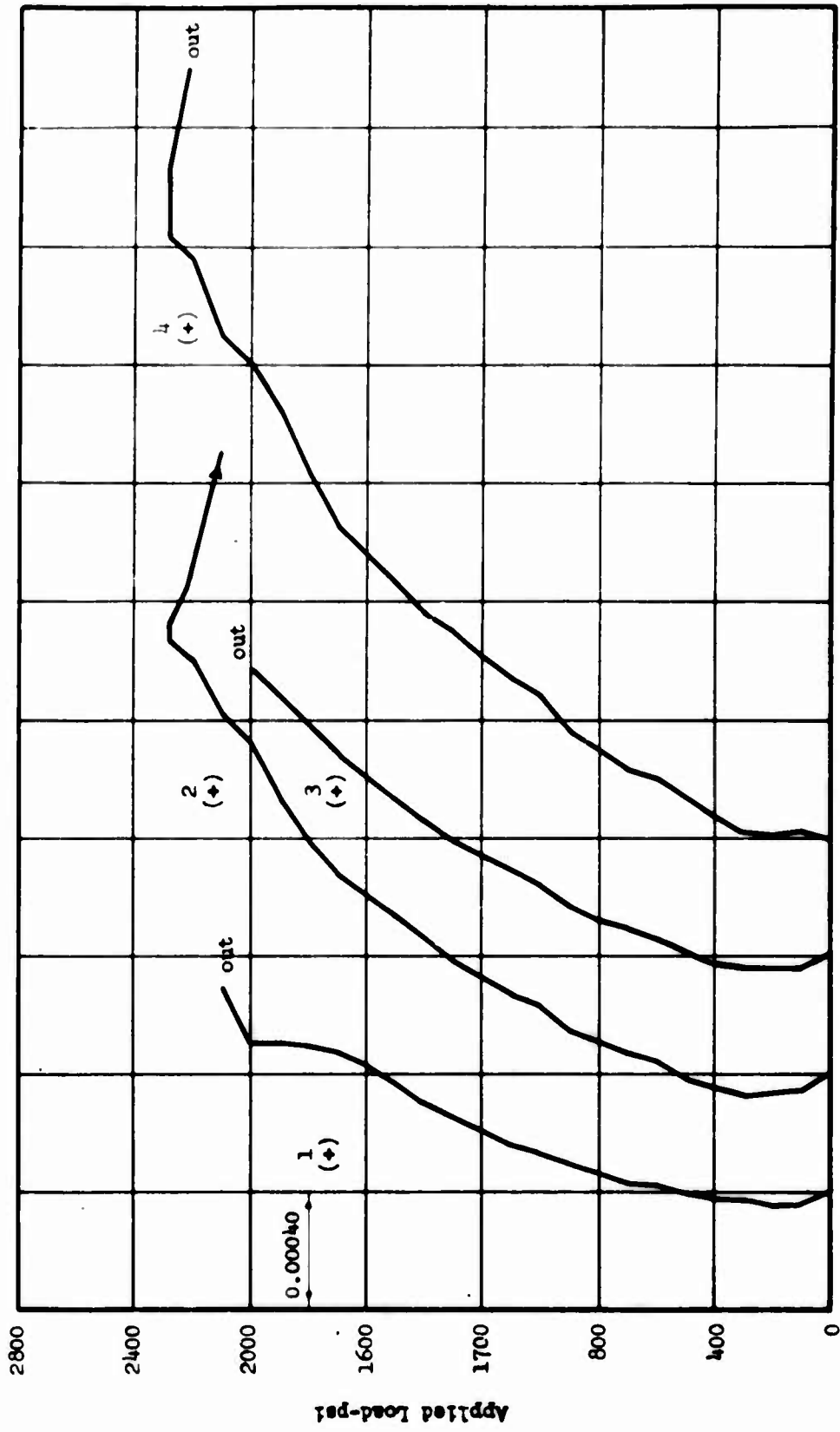
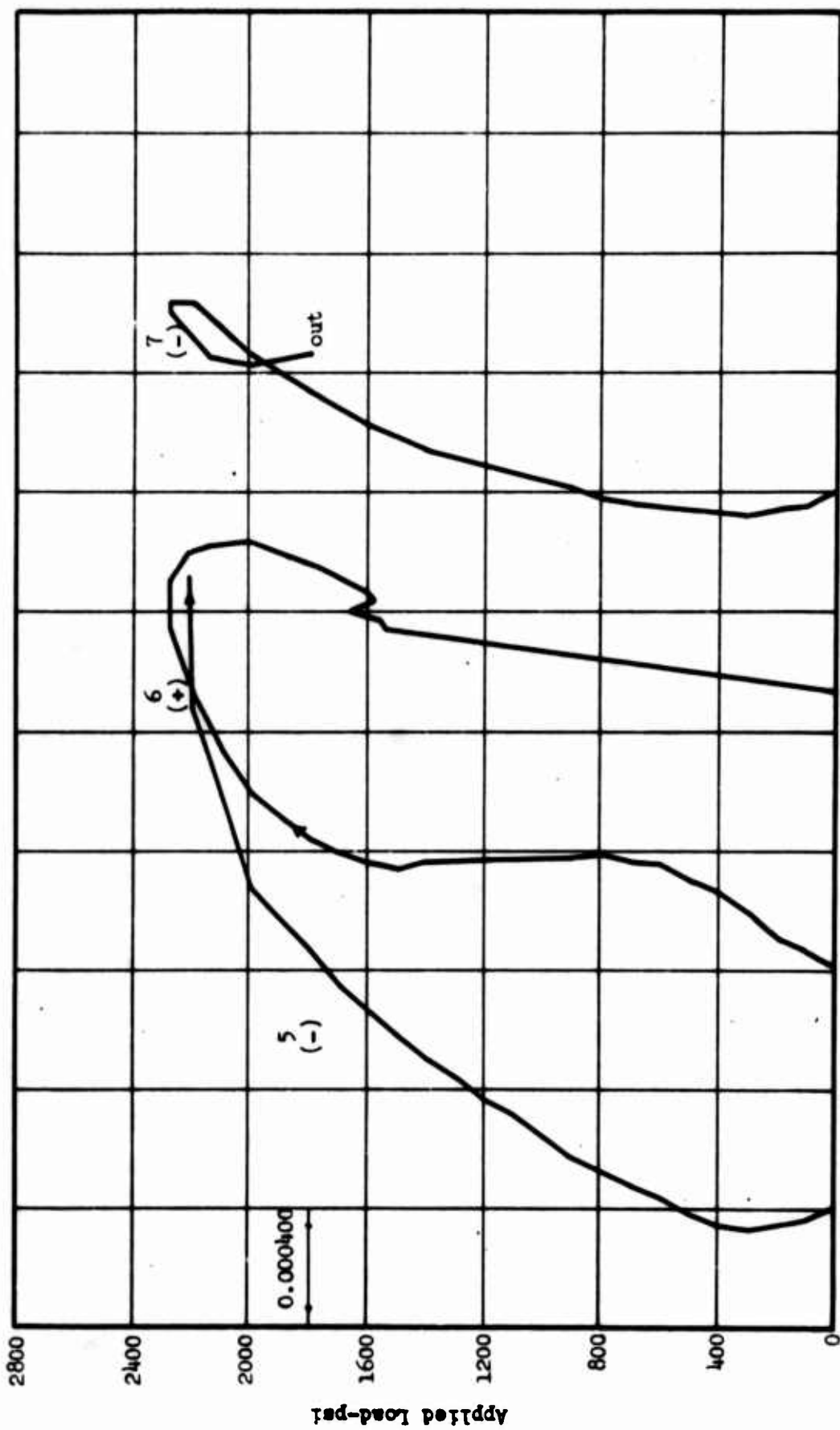


Fig. 5.2 Deflection Profiles, Slab G-1



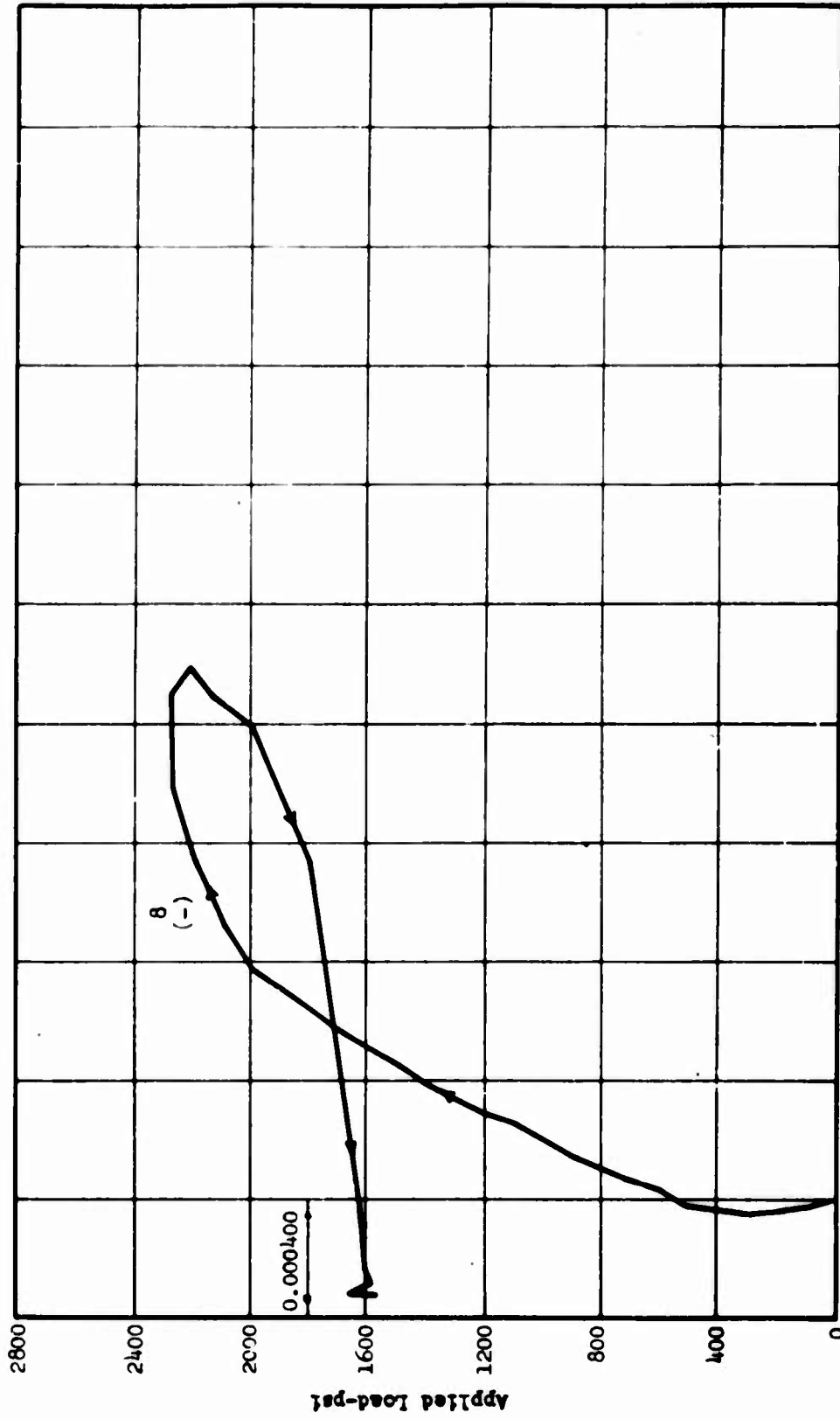
Reinforcement Strain

Fig. 5.3 Load-Strain Curves, Slab G-1



Reinforcement Strain
Fig. 5.4 Load-Strain Curves, Slab G-1





Reinforcement Strain
Fig. 5.5 Load-Strain Curves, Slab G-1

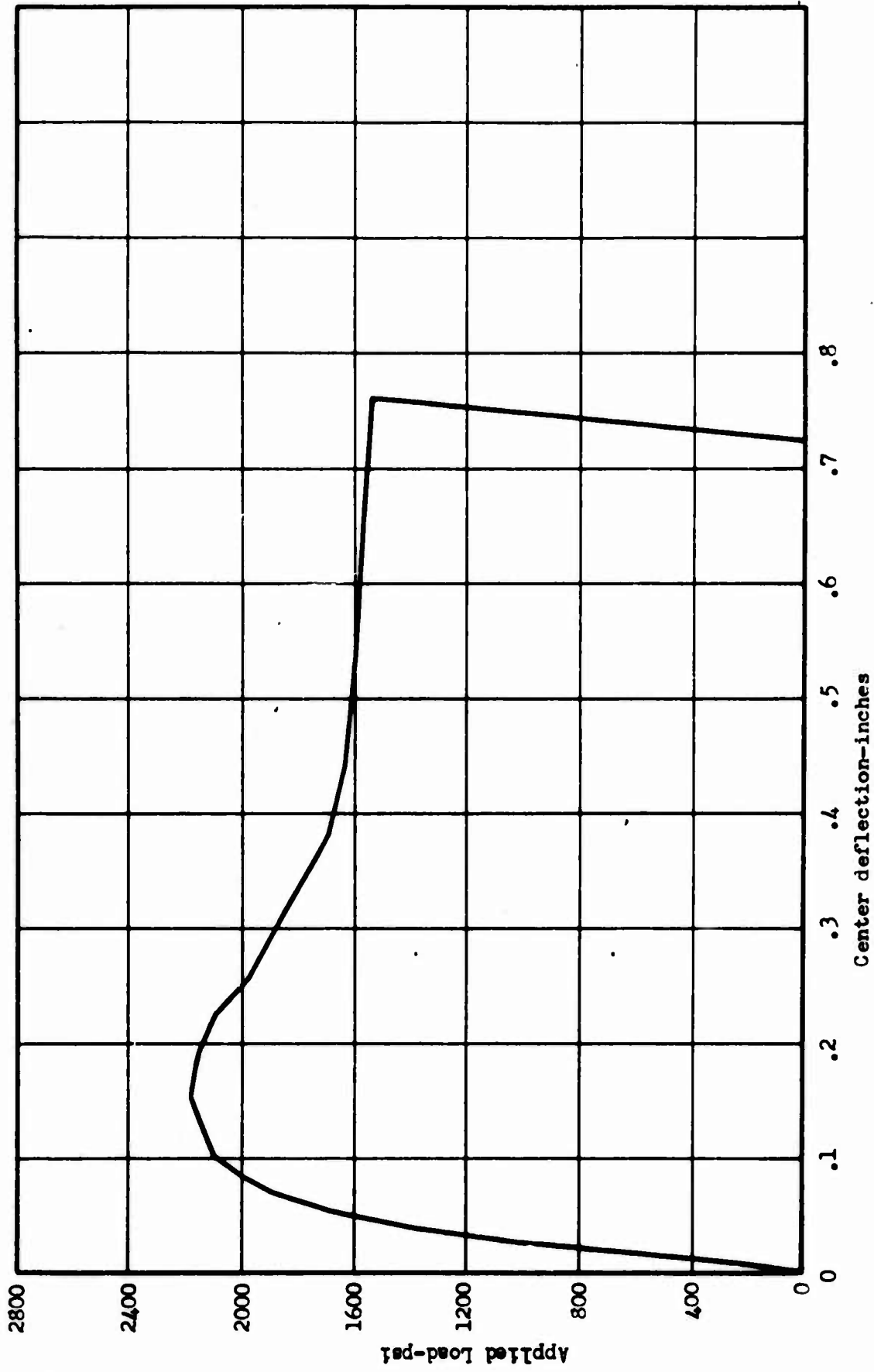


Fig. 5.6 Load-Deflection Curve, Slab G-2

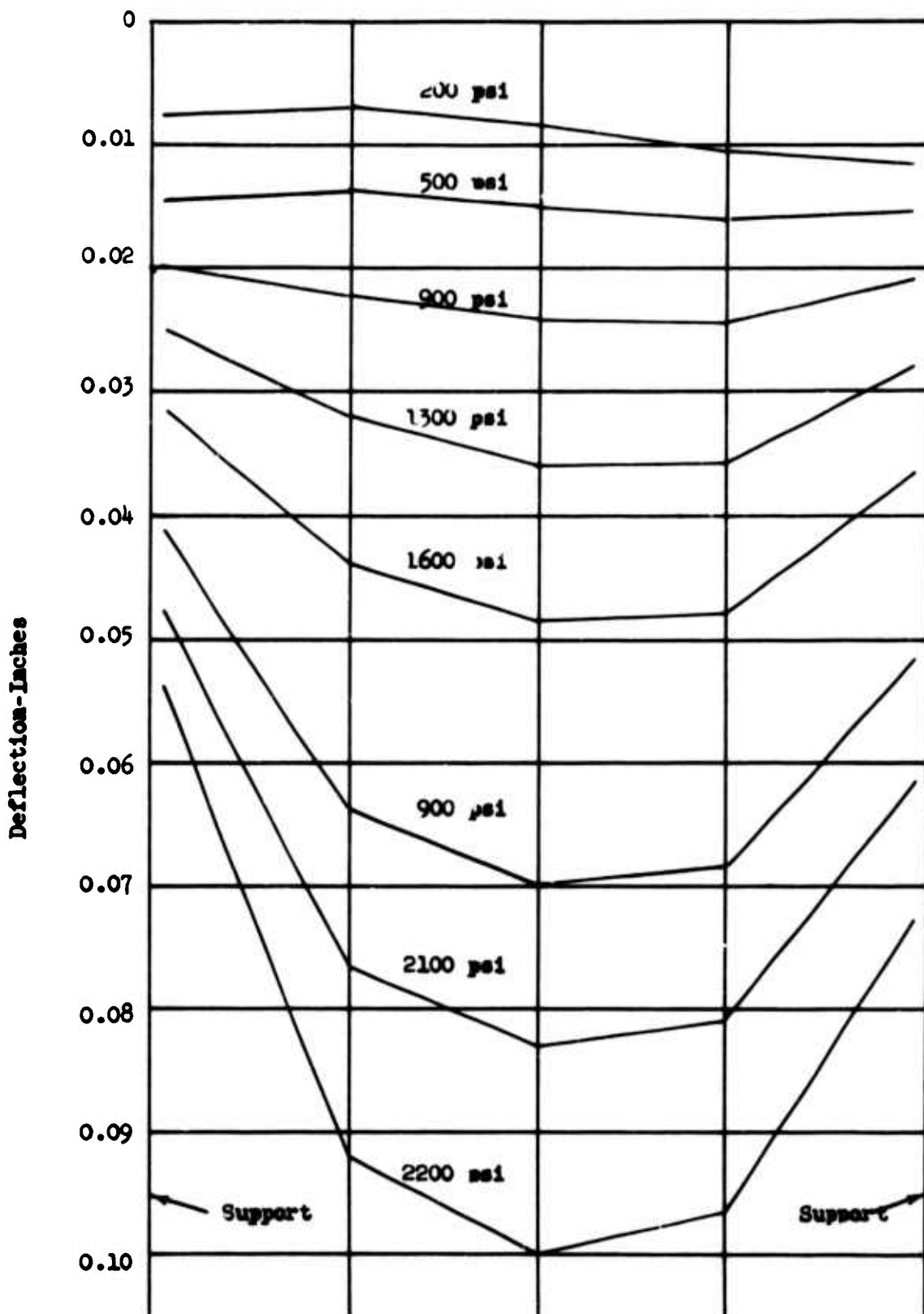
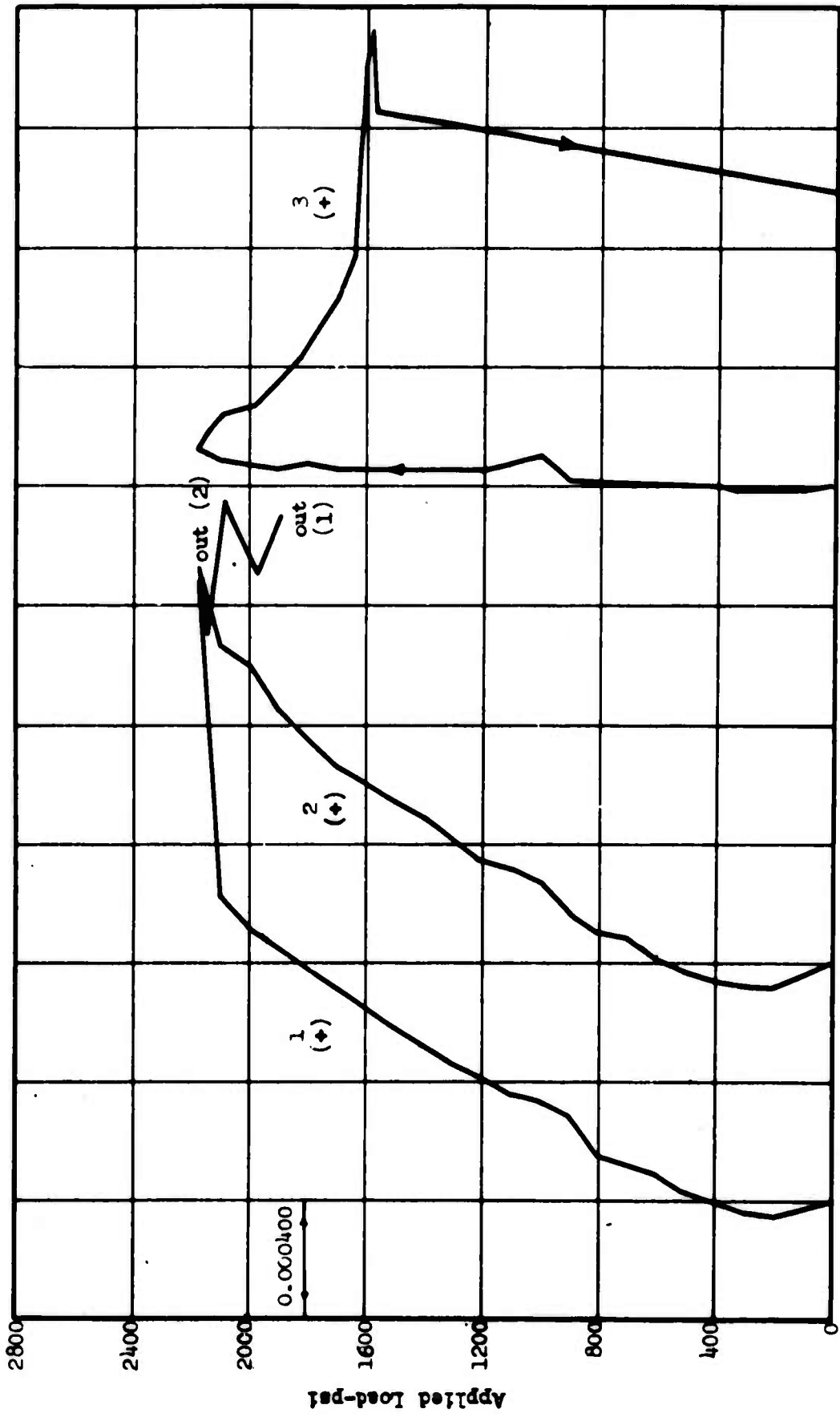
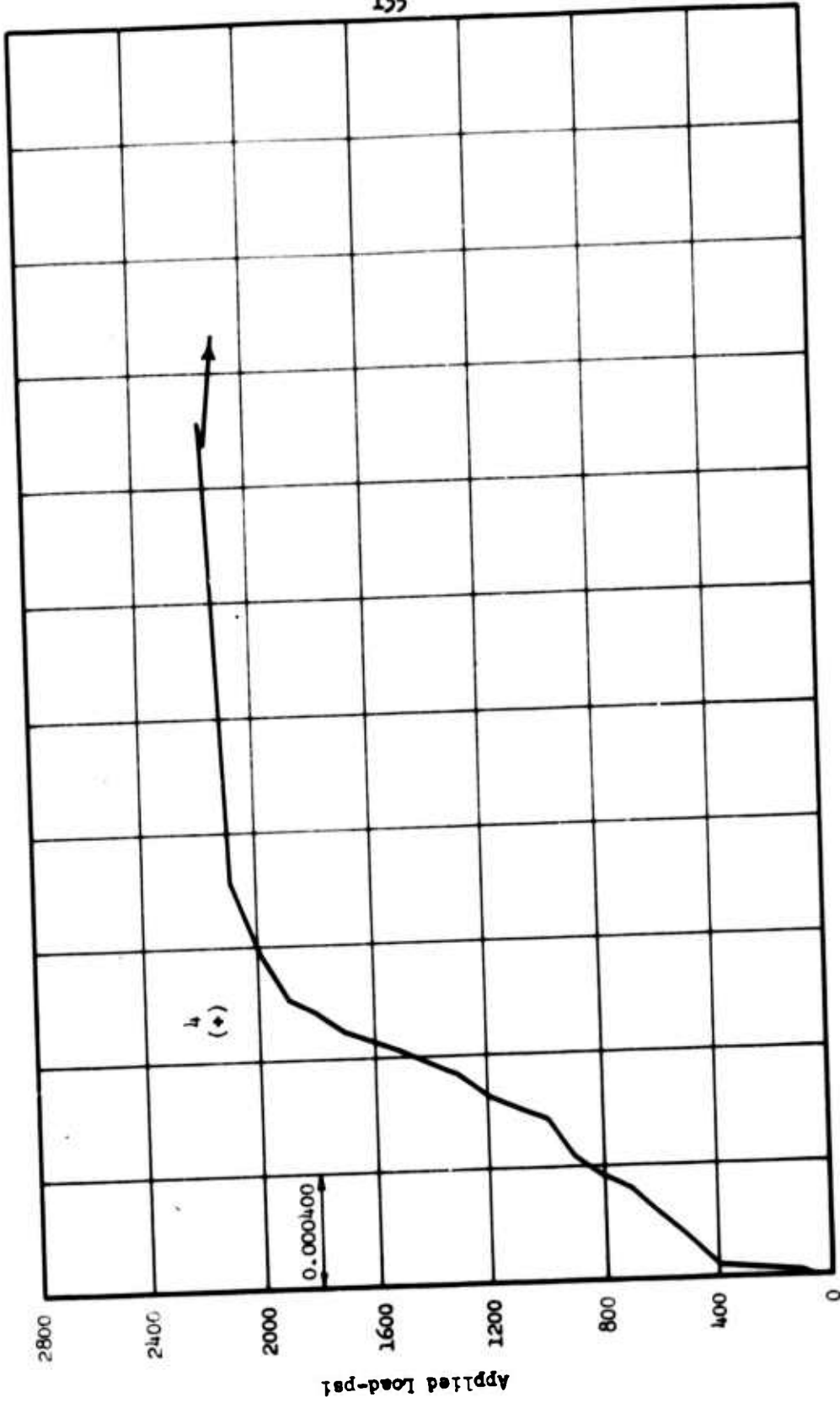


Fig. 5.7 Deflection Profiles Slab G-2



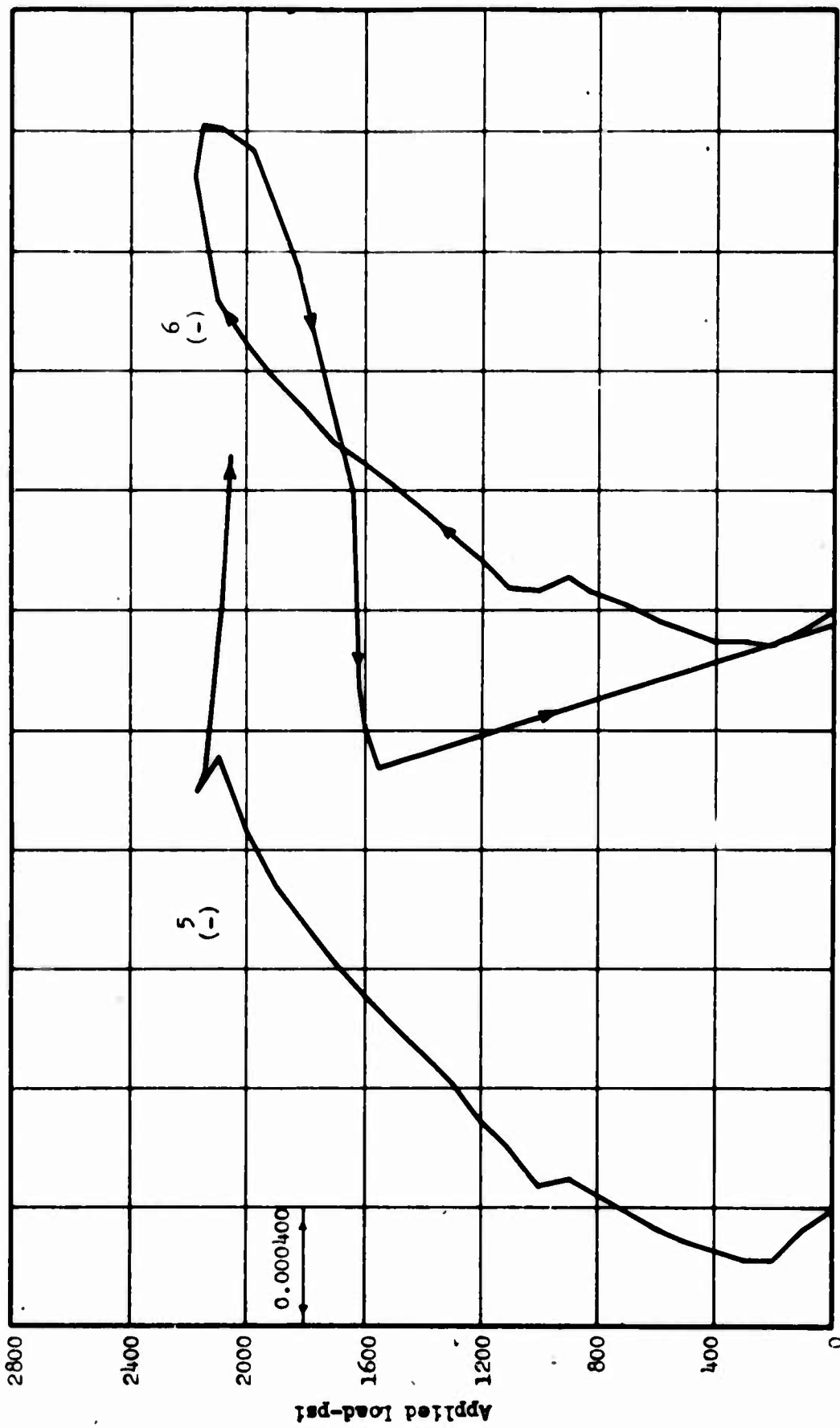
Reinforcement Strain

Fig. 5.8 Load-Strain Curves, Slab C-2



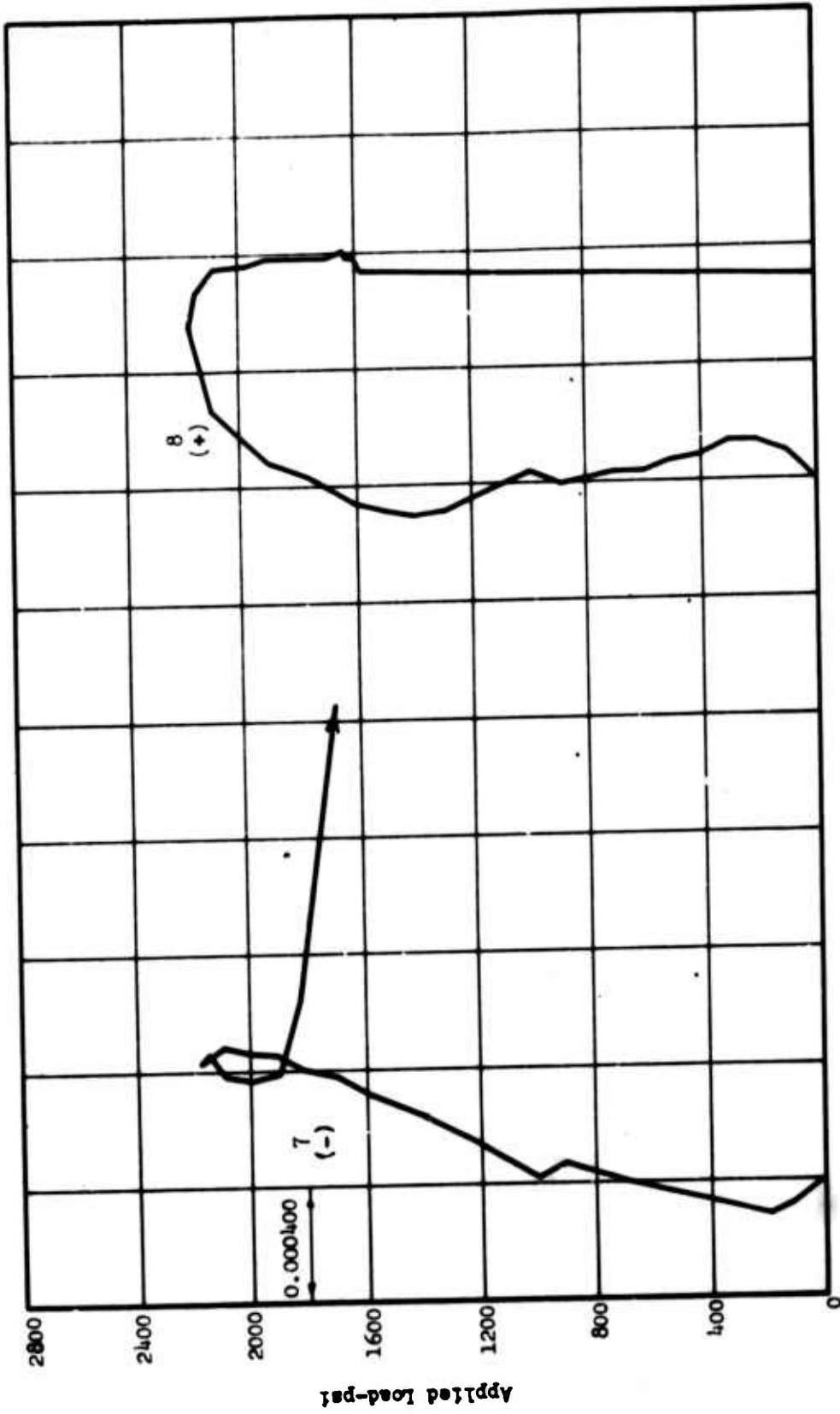
Reinforcement Strain

Fig. 5.9 Load-Strain Curves, Slab G-2



Reinforcement Strain

Fig. 5.10 Load-Strain Curves, Slab G-2



Reinforcement Strain
Fig. 5.11 Load-Strain Curves, Slab G-2

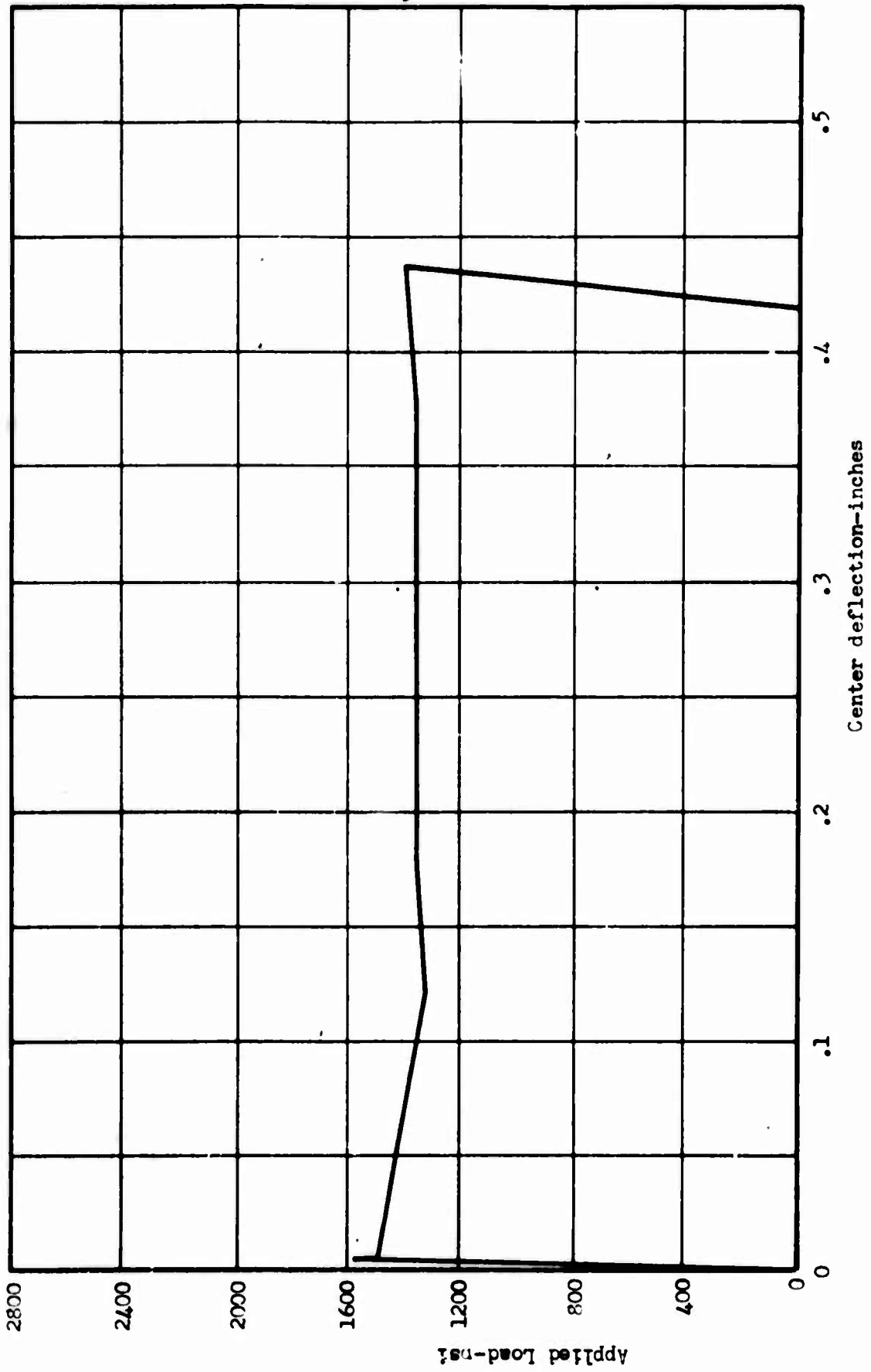


Fig. 5.12 Load-Deflection Curve, Slab G-3

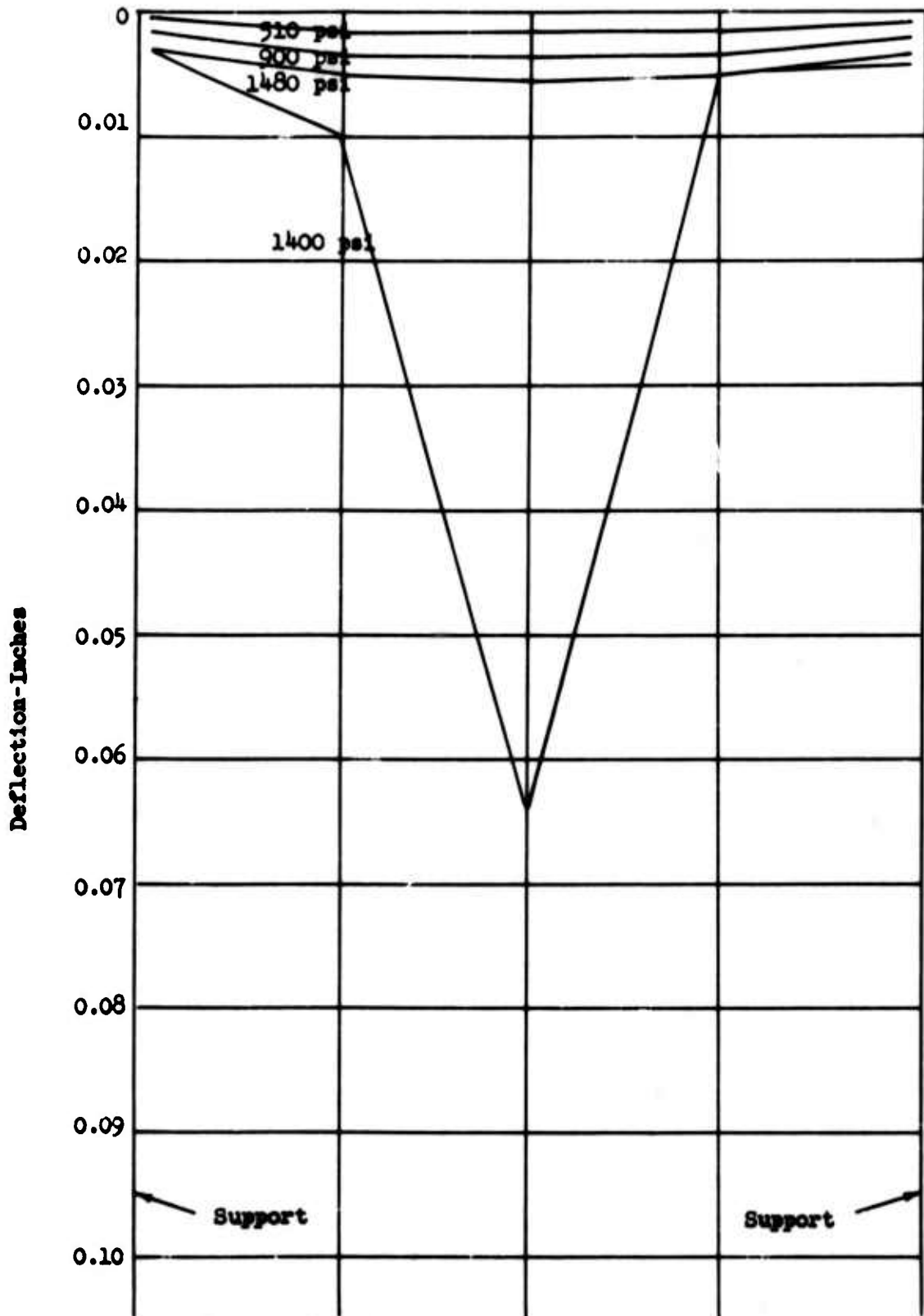
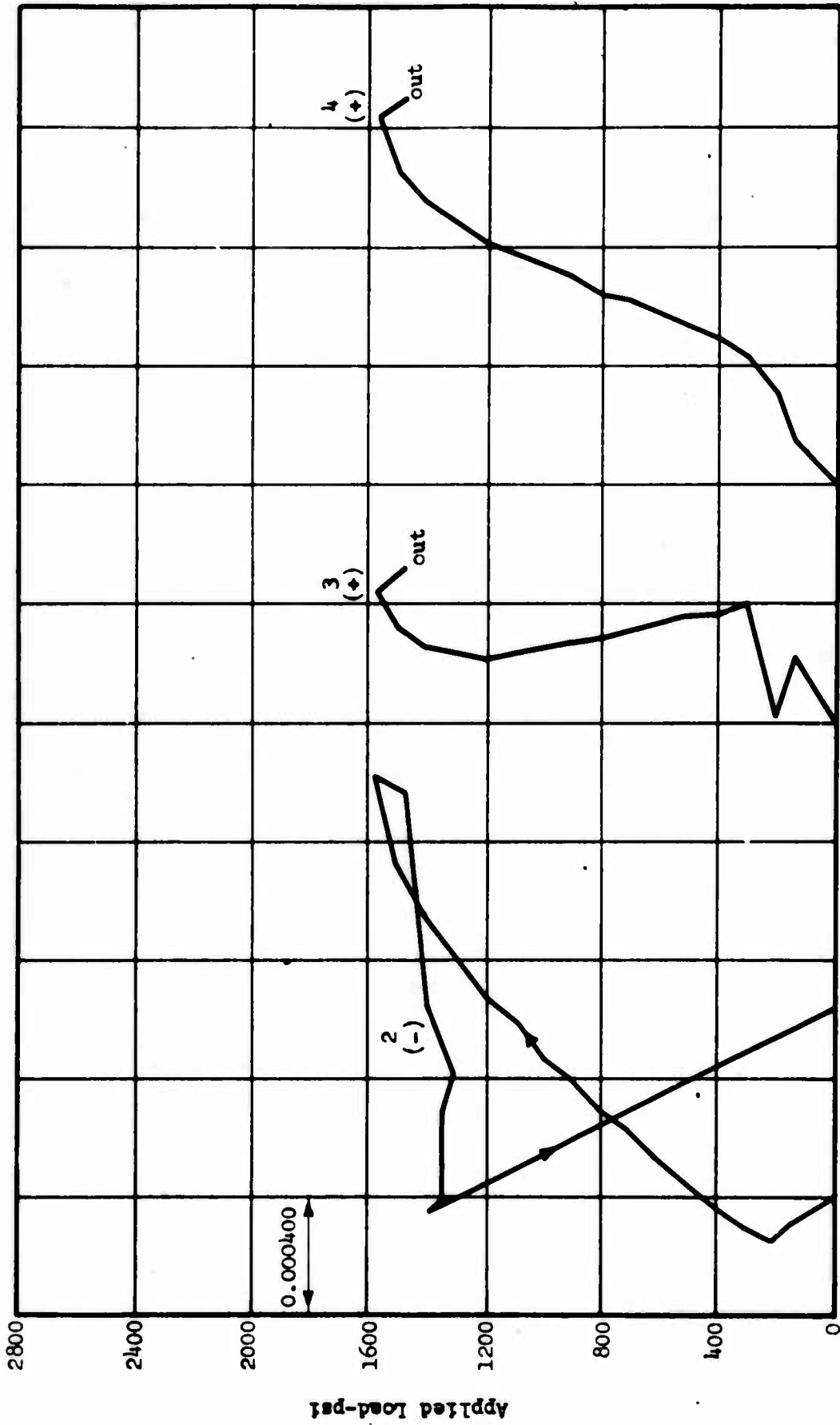


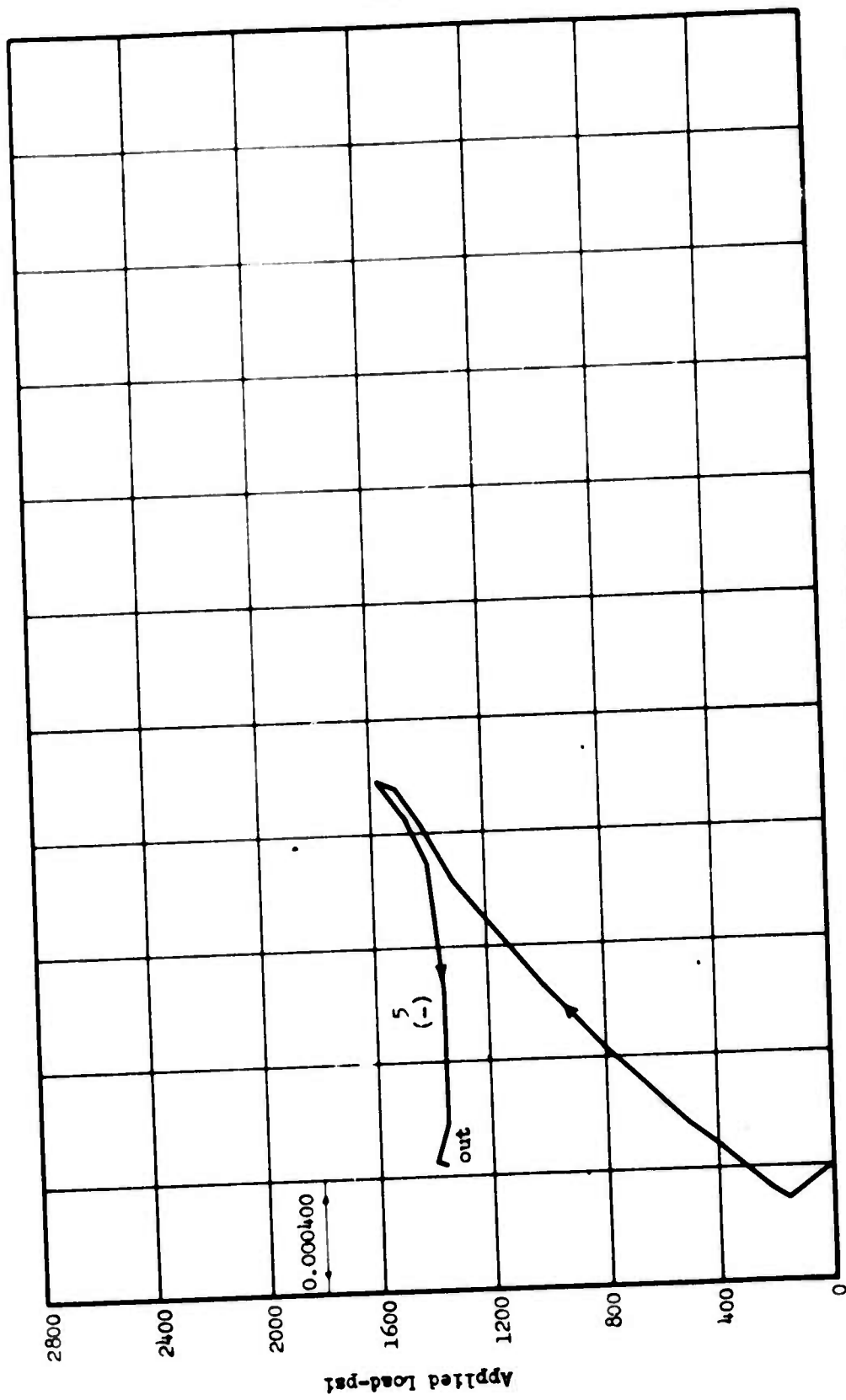
Fig. 5.13 Deflection Profiles, Slab G-3



Reinforcement Strain

Fig. 5.14 Load-Strain Curves, Slab G-3





Reinforcement Strain
Fig. 5.15 Load-Strain Curves, Slab G-3

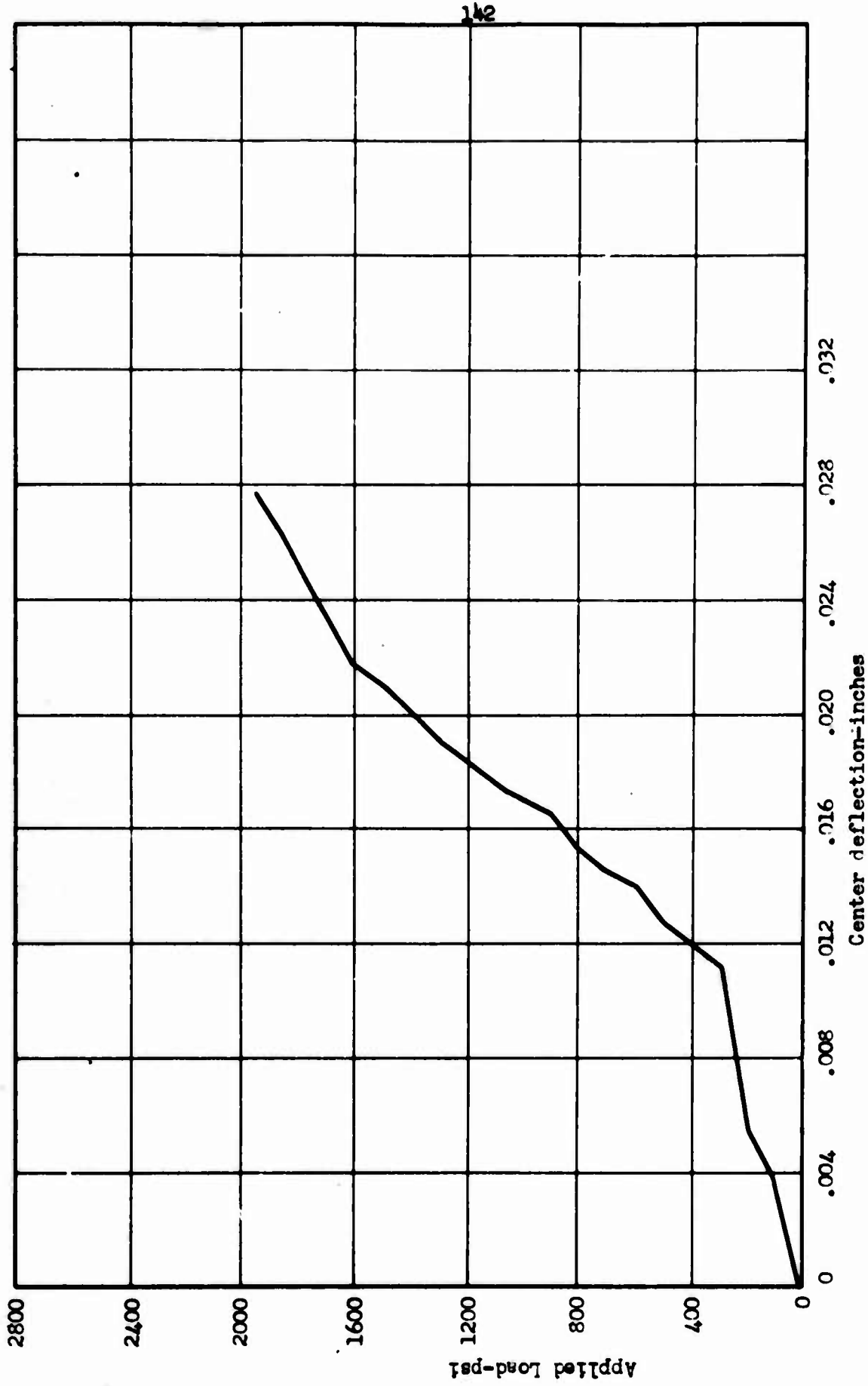


Fig. 5.16 Load-Deflection Curve, Slab G-4

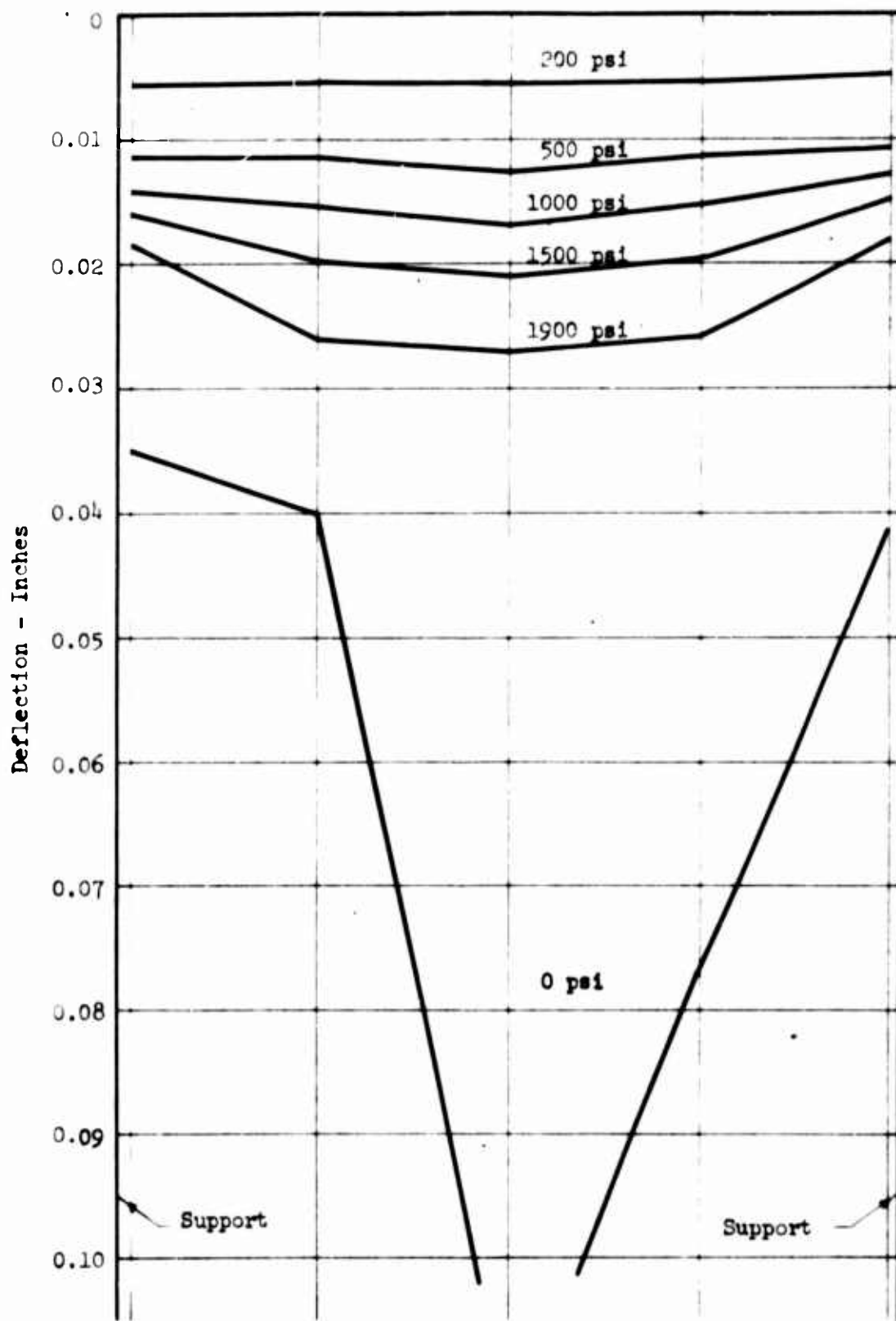


Fig. 5.17 Deflection Profiles, Slab G-4

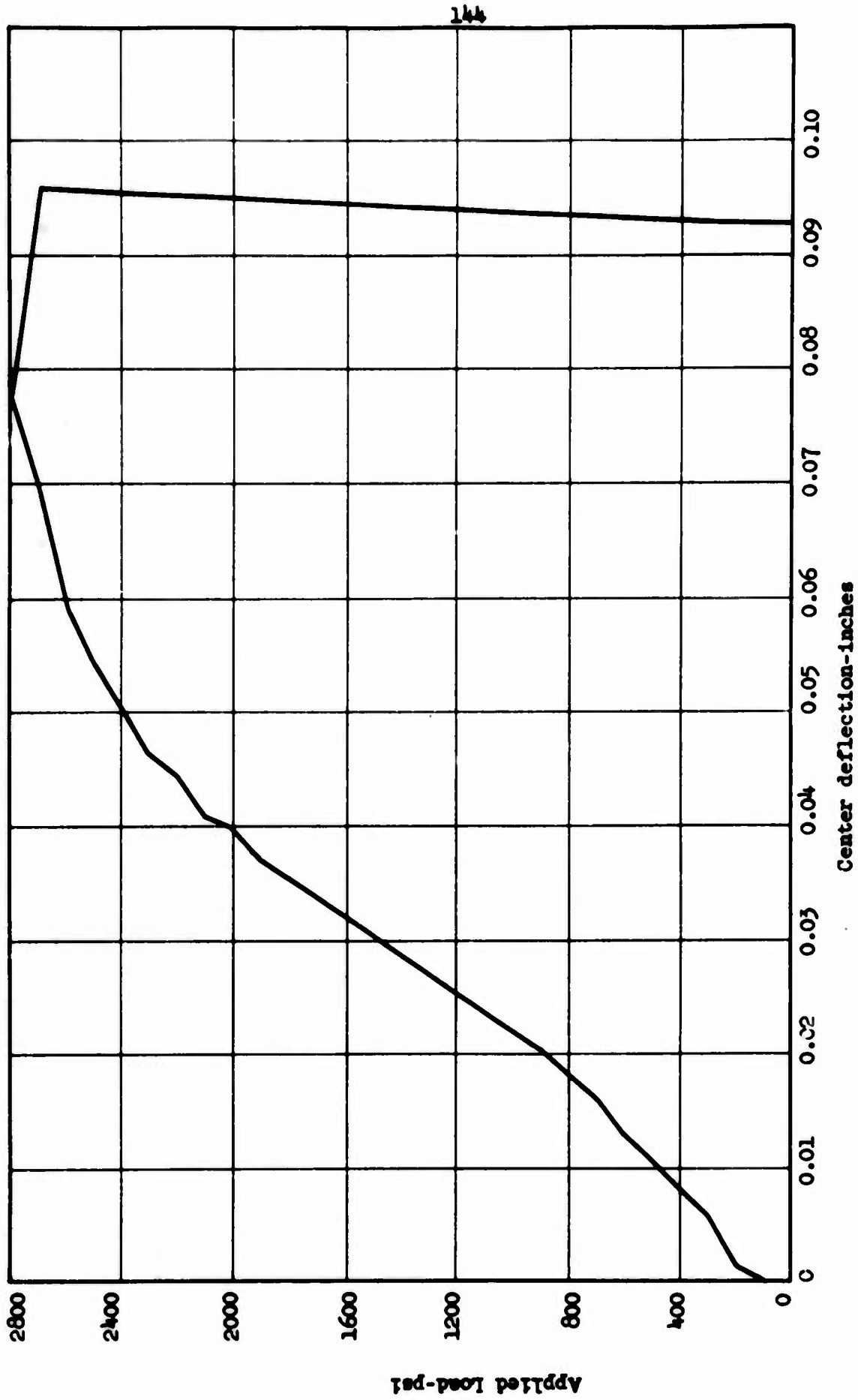


Fig. 5.18 Load-Deflection Curve, Slab G-5

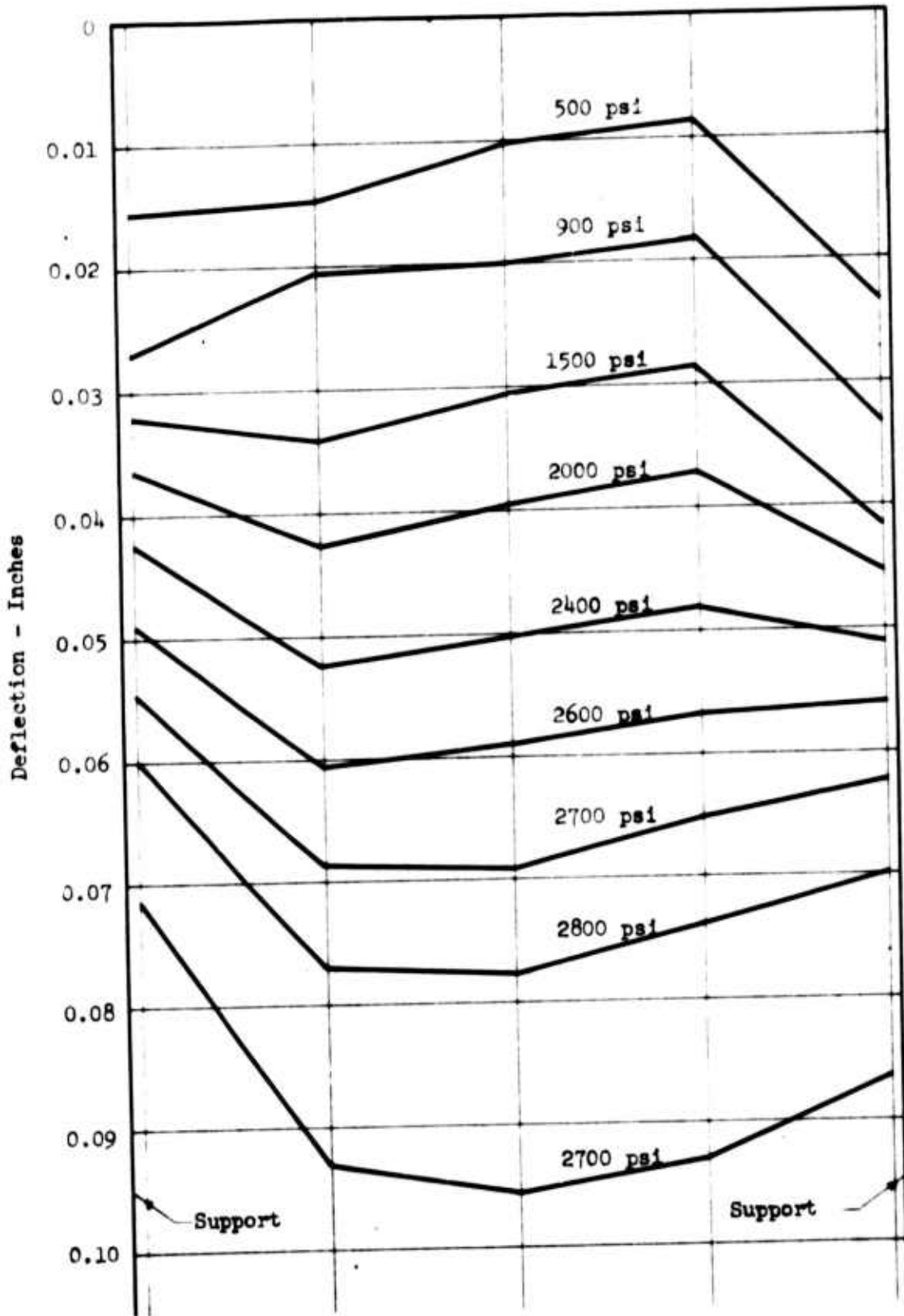
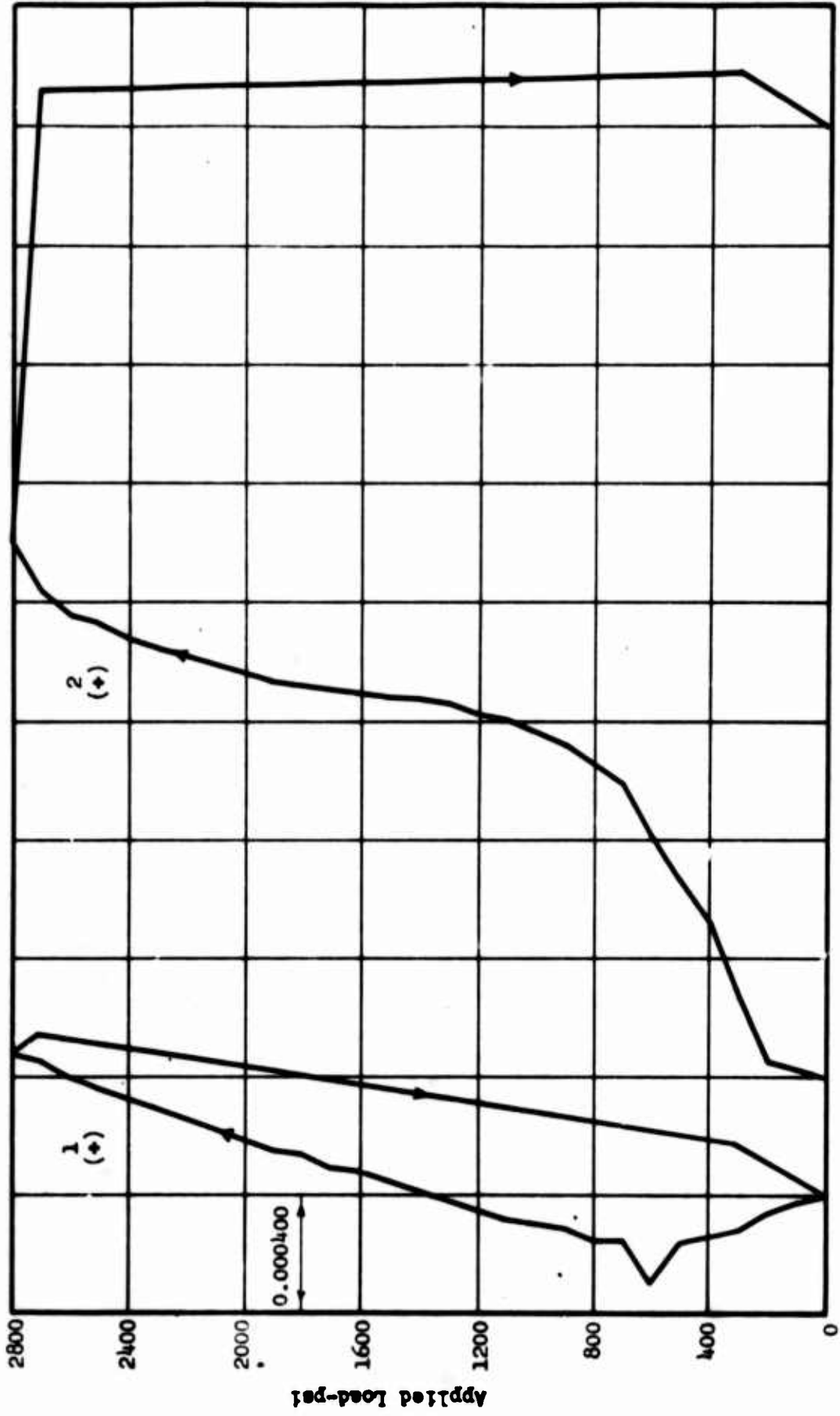
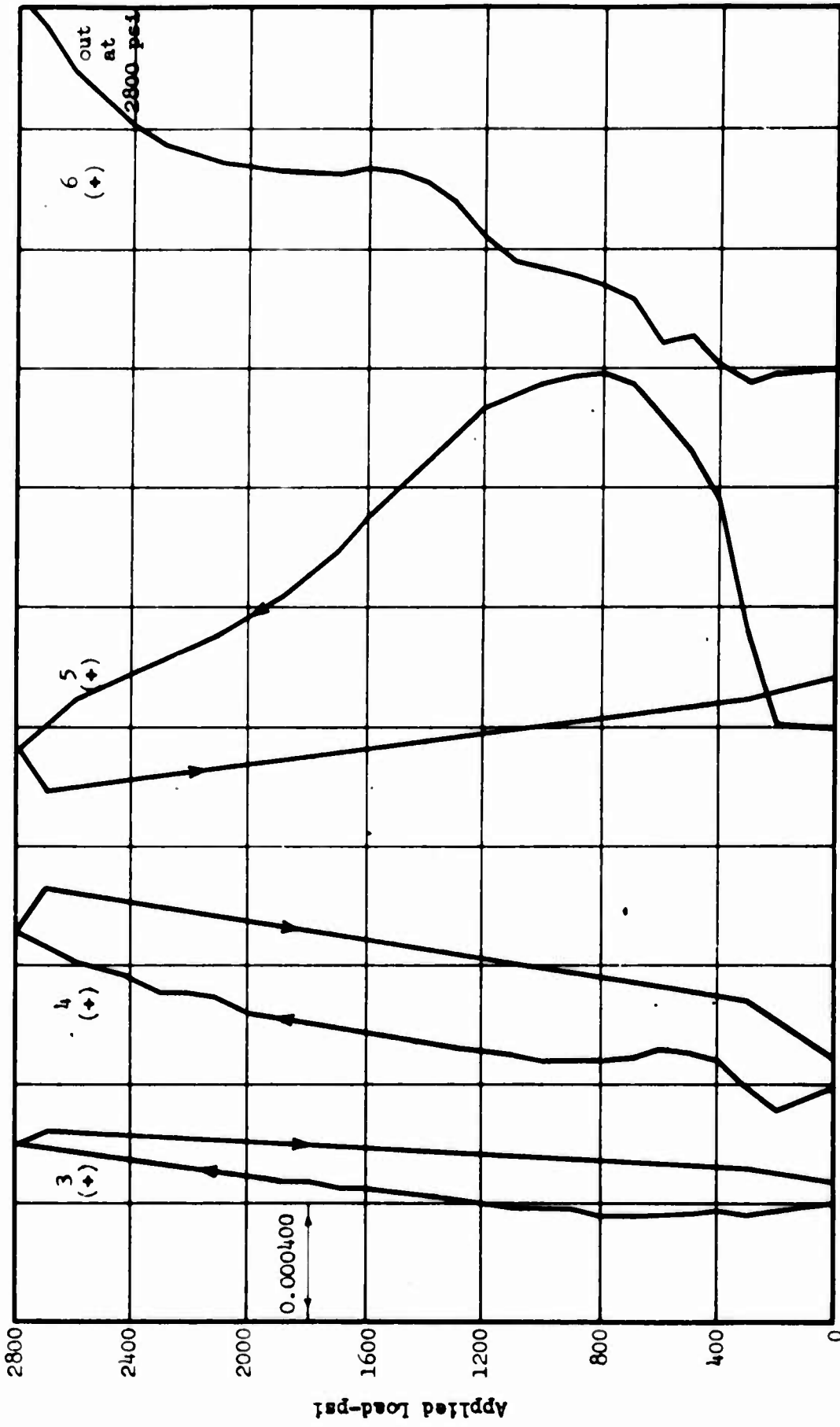


Fig. 5.19 Deflection Profiles, Slab G-5

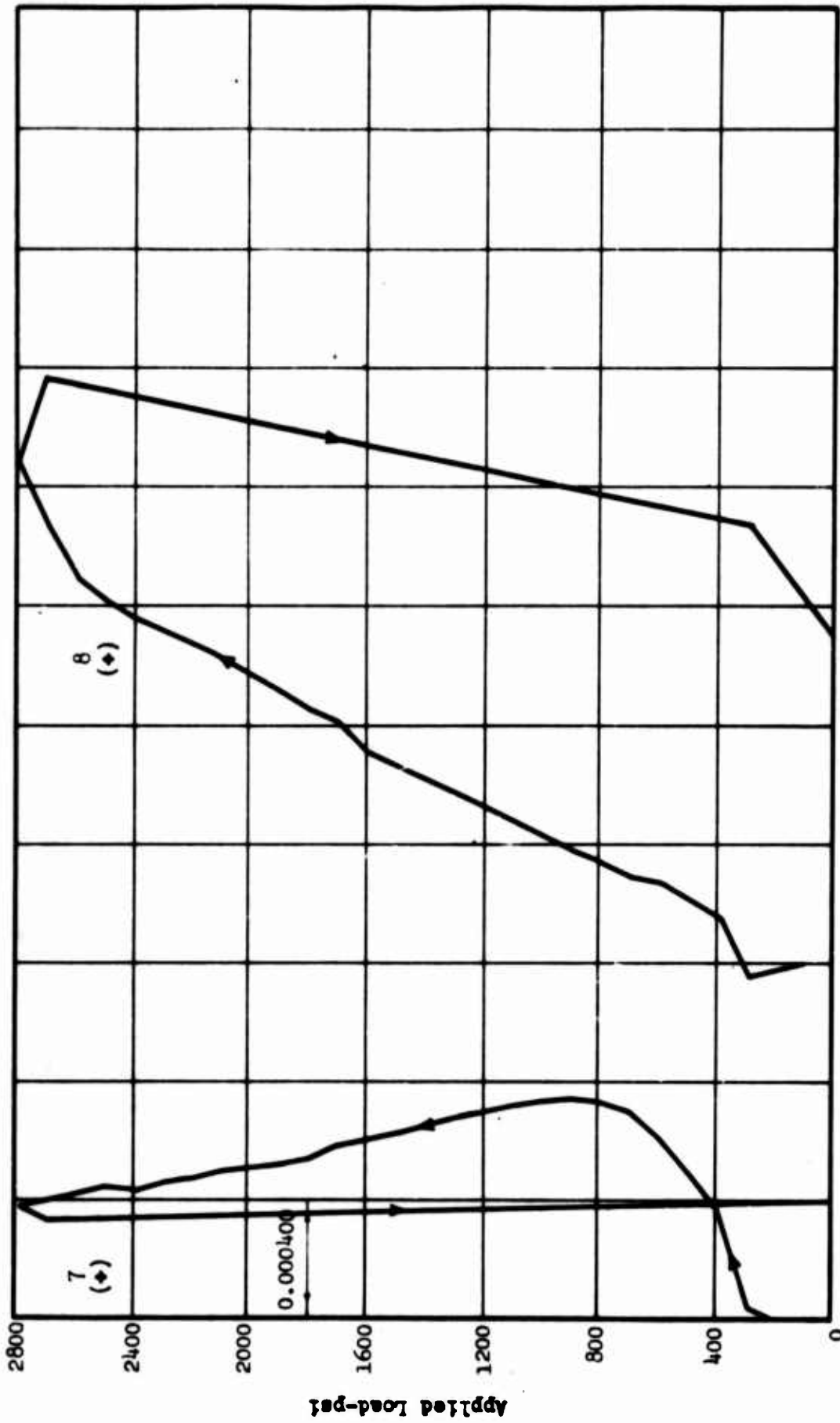


Reinforcement Strain
Fig. 5.20 Load-Strain Curves, Slab G-5

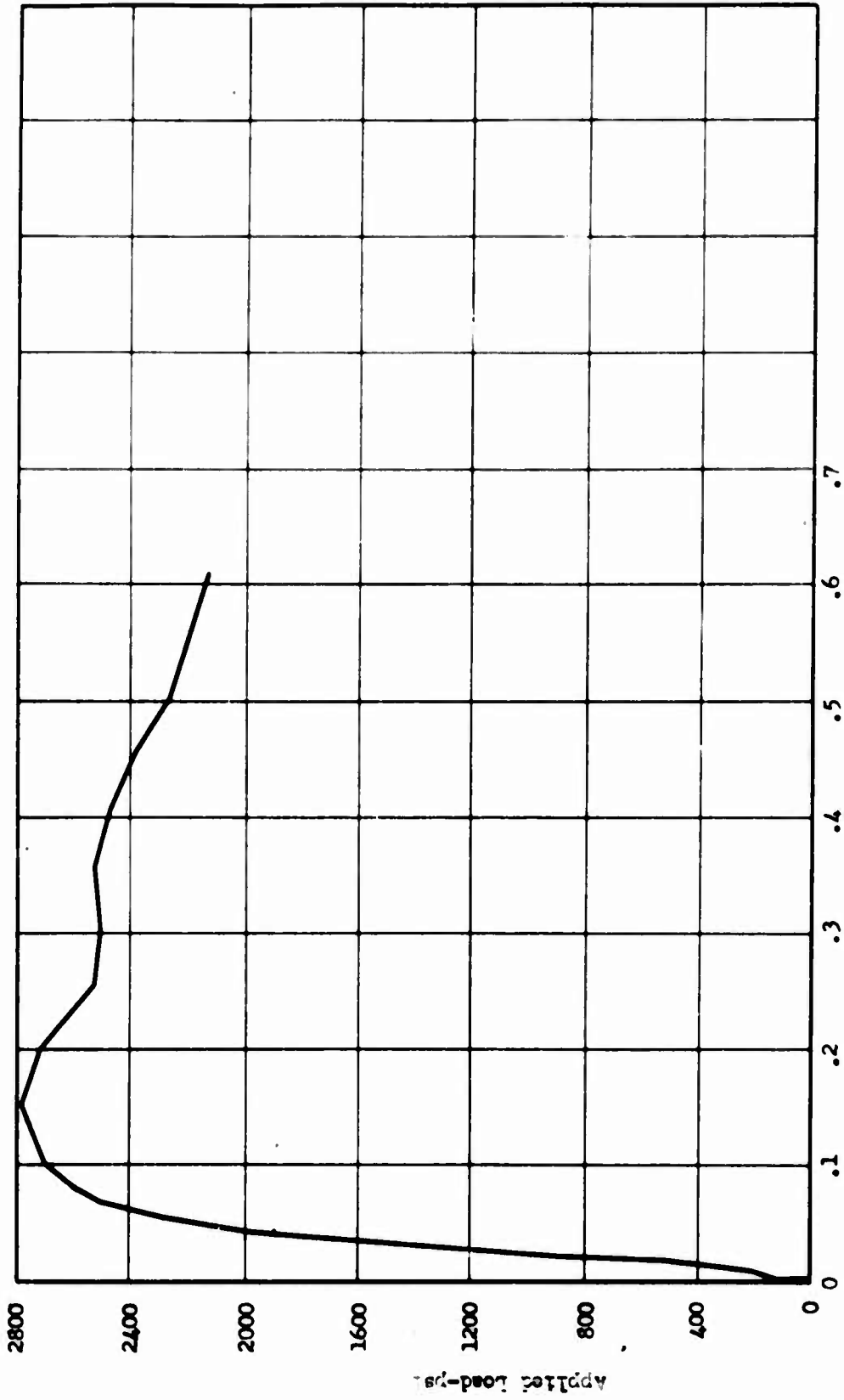


Reinforcement Strain

Fig. 5.21 Load-Strain Curves, Slab G-5



Reinforcement Strain
 Fig. 5.22 Load-Strain Curves, Slab G-5



Center deflection-inches

Fig. 5.23 Load-Deflection Curve, Slab G-6

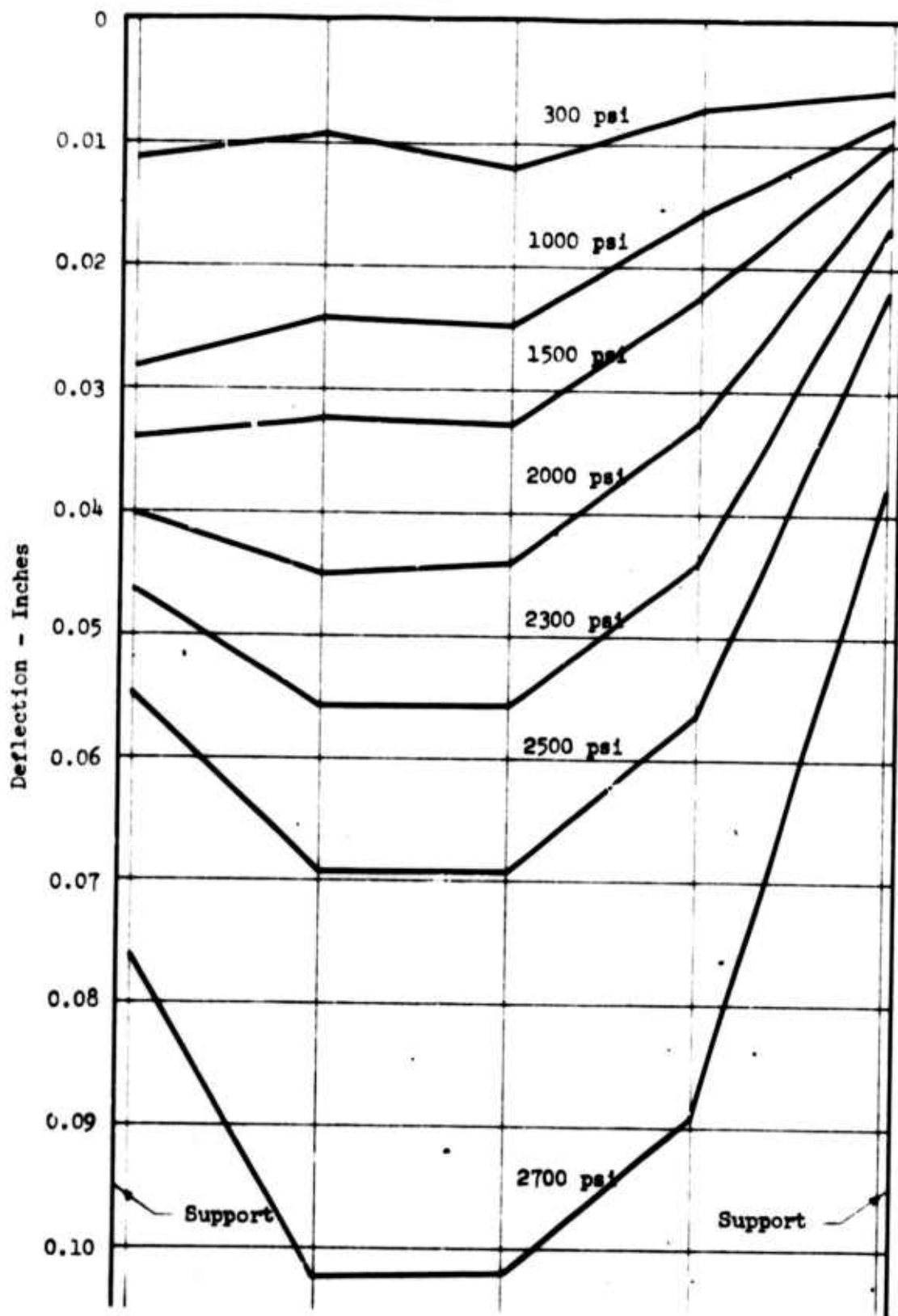
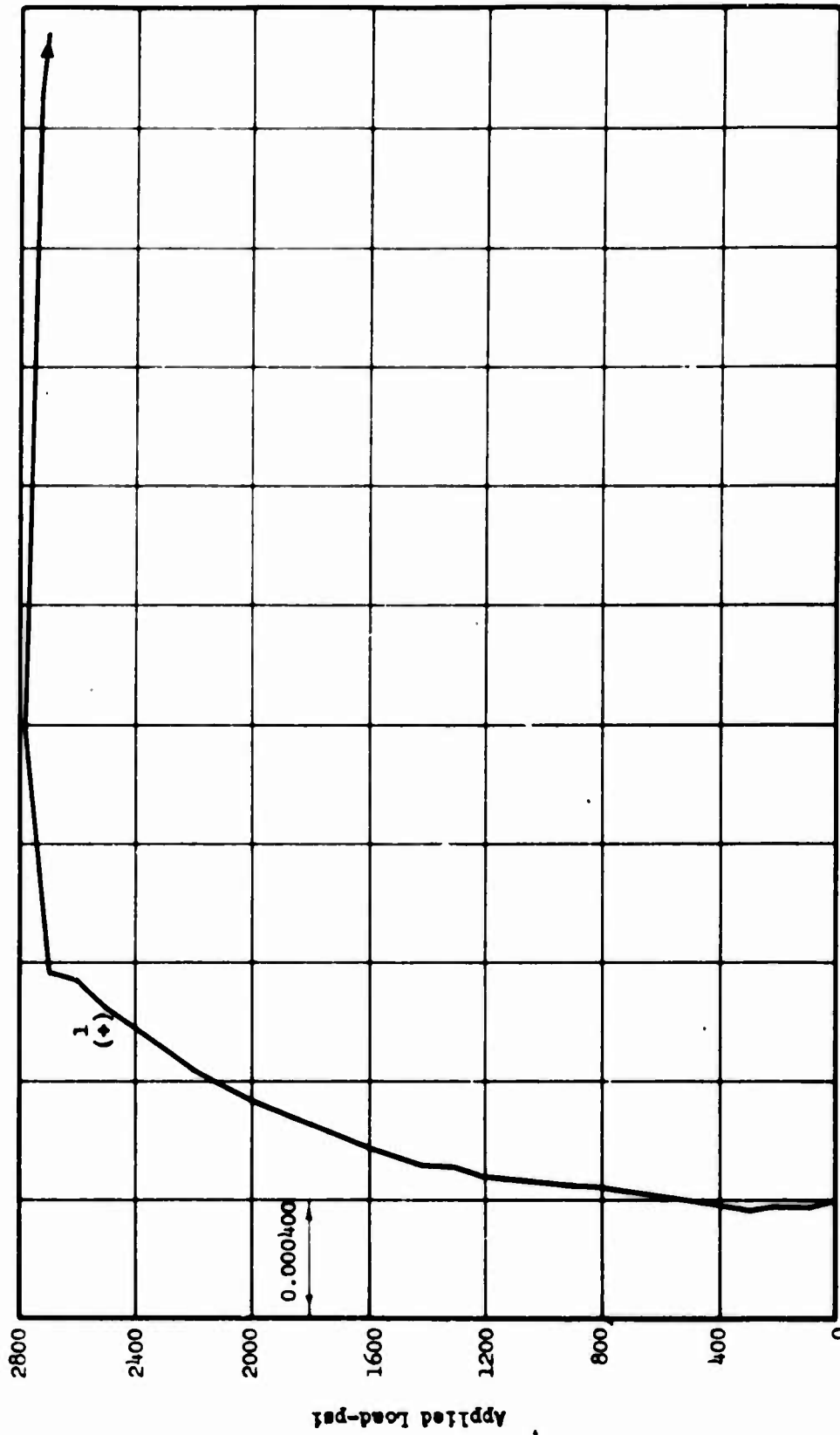
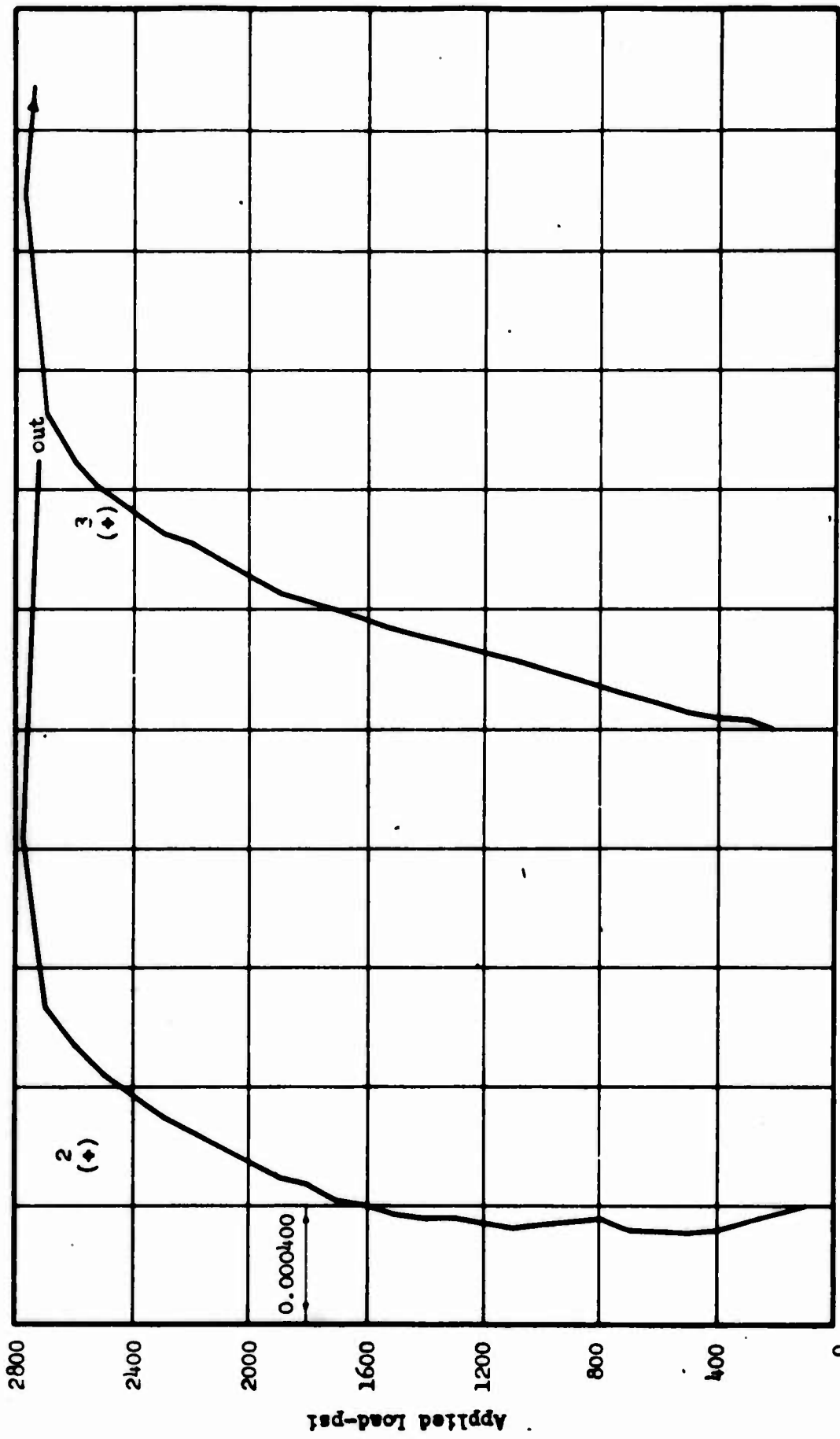


Fig. 5.24 Deflection Profiles, Slab G-6



Reinforcement Strain
Fig. 5.25 Load-Strain Curves, Slab G-6



Reinforcement Strain
Fig. 5.26 Load-Strain Curves, Slab G-6



Reinforcement Strain
Fig. 5.27 Load-Strain Curves, Slab G-6

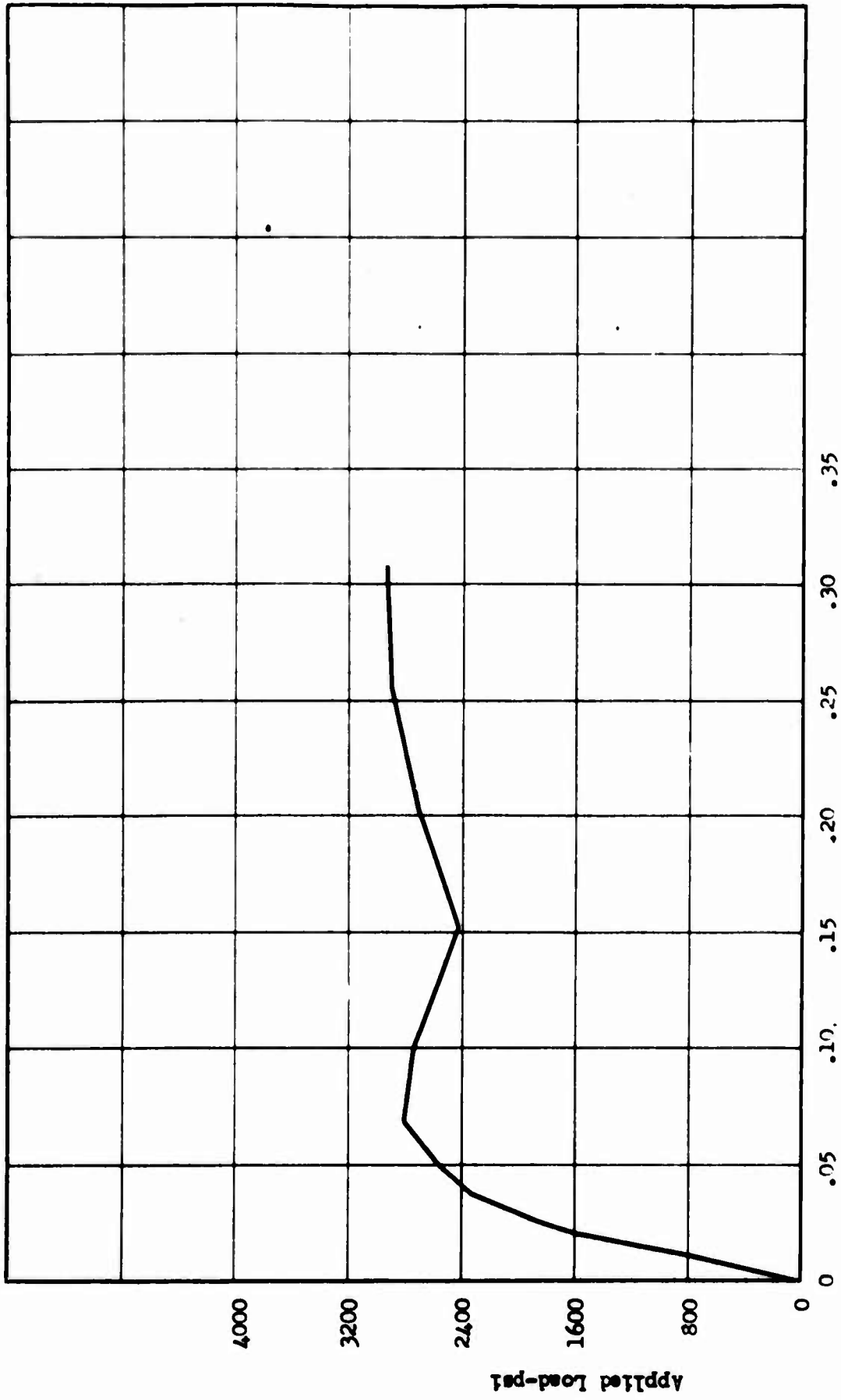


Fig. 5.28 Load-Deflection curve, Slab G-7

Center Deflection-inches

Applied Load-psi

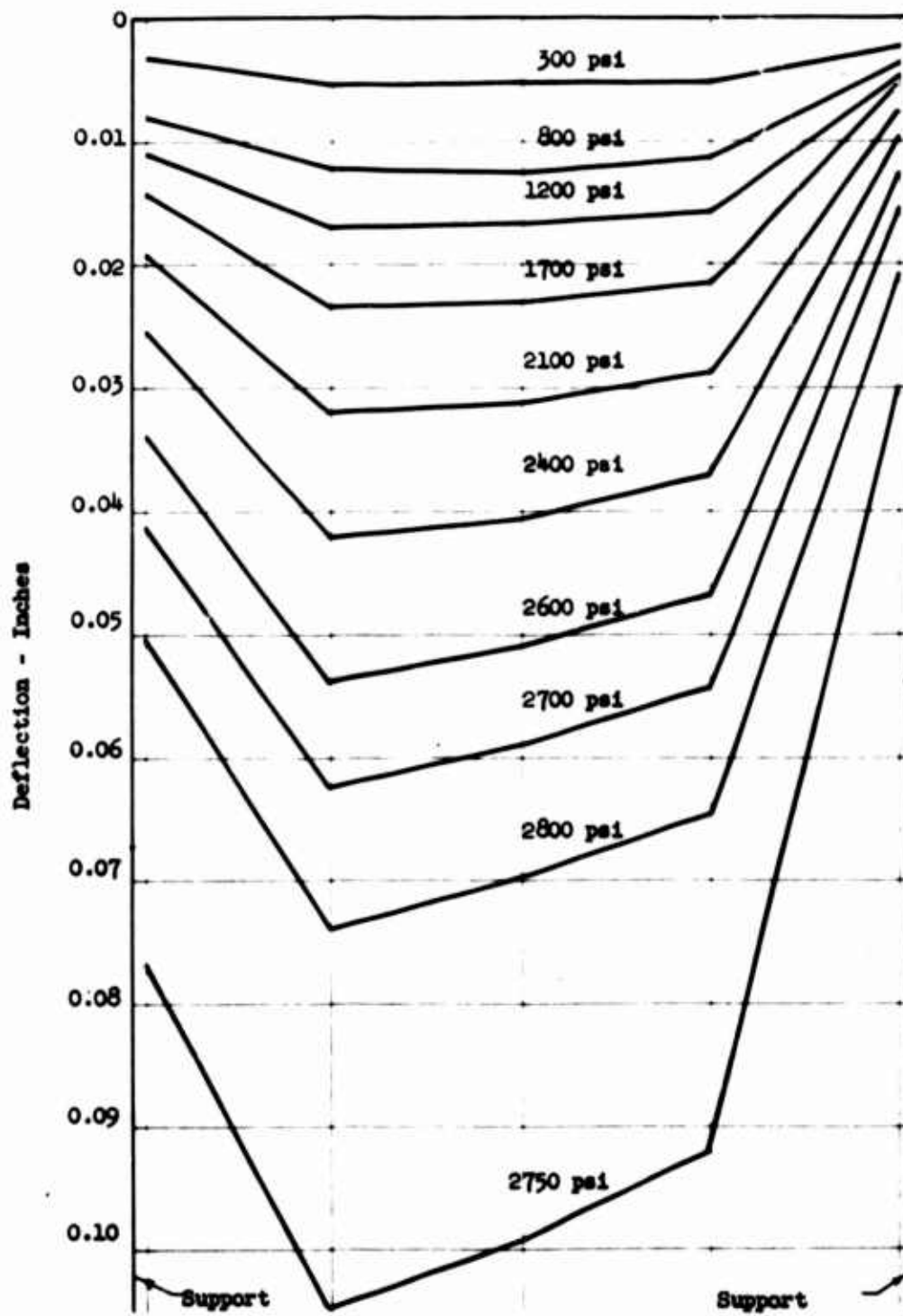
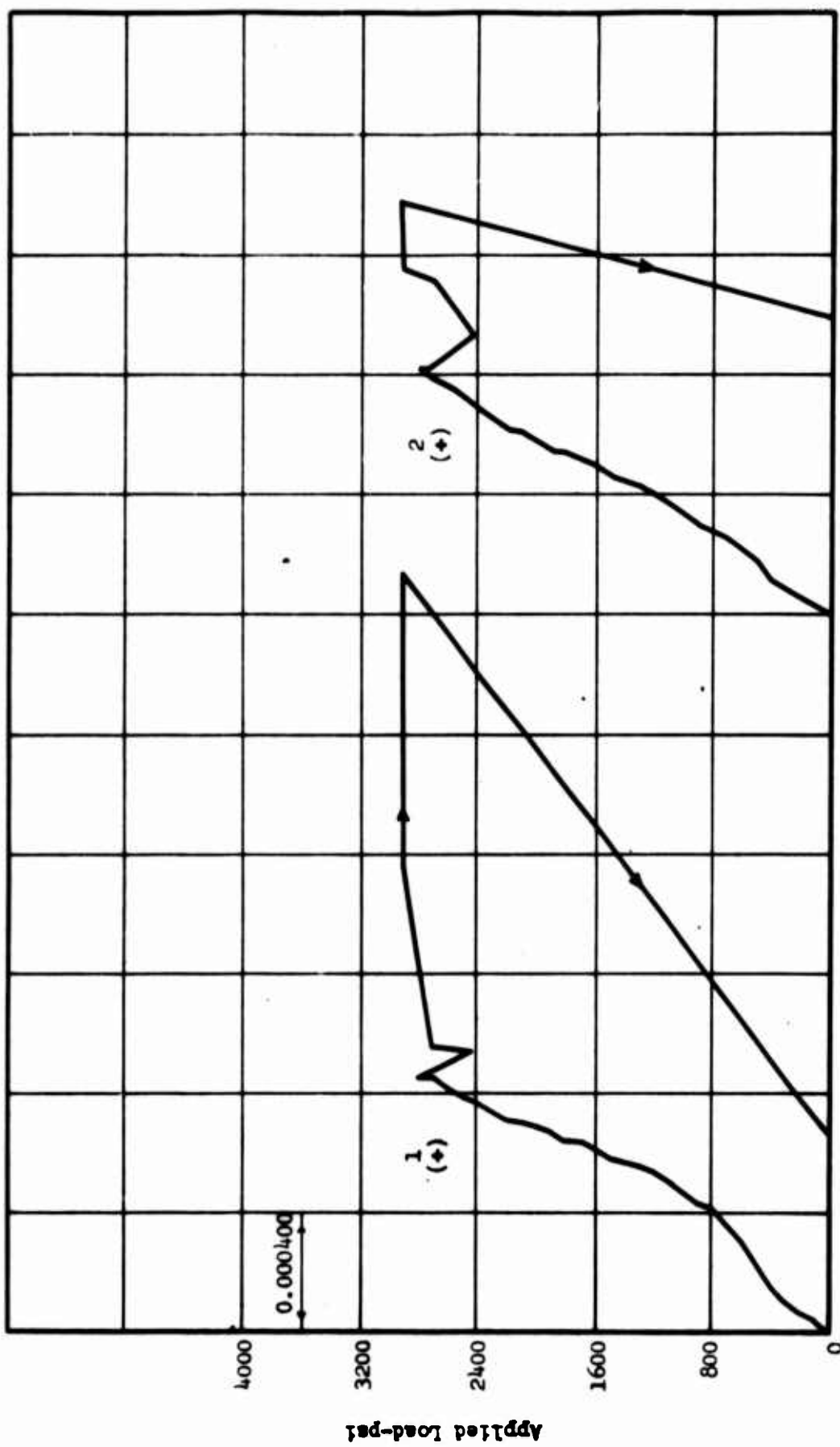
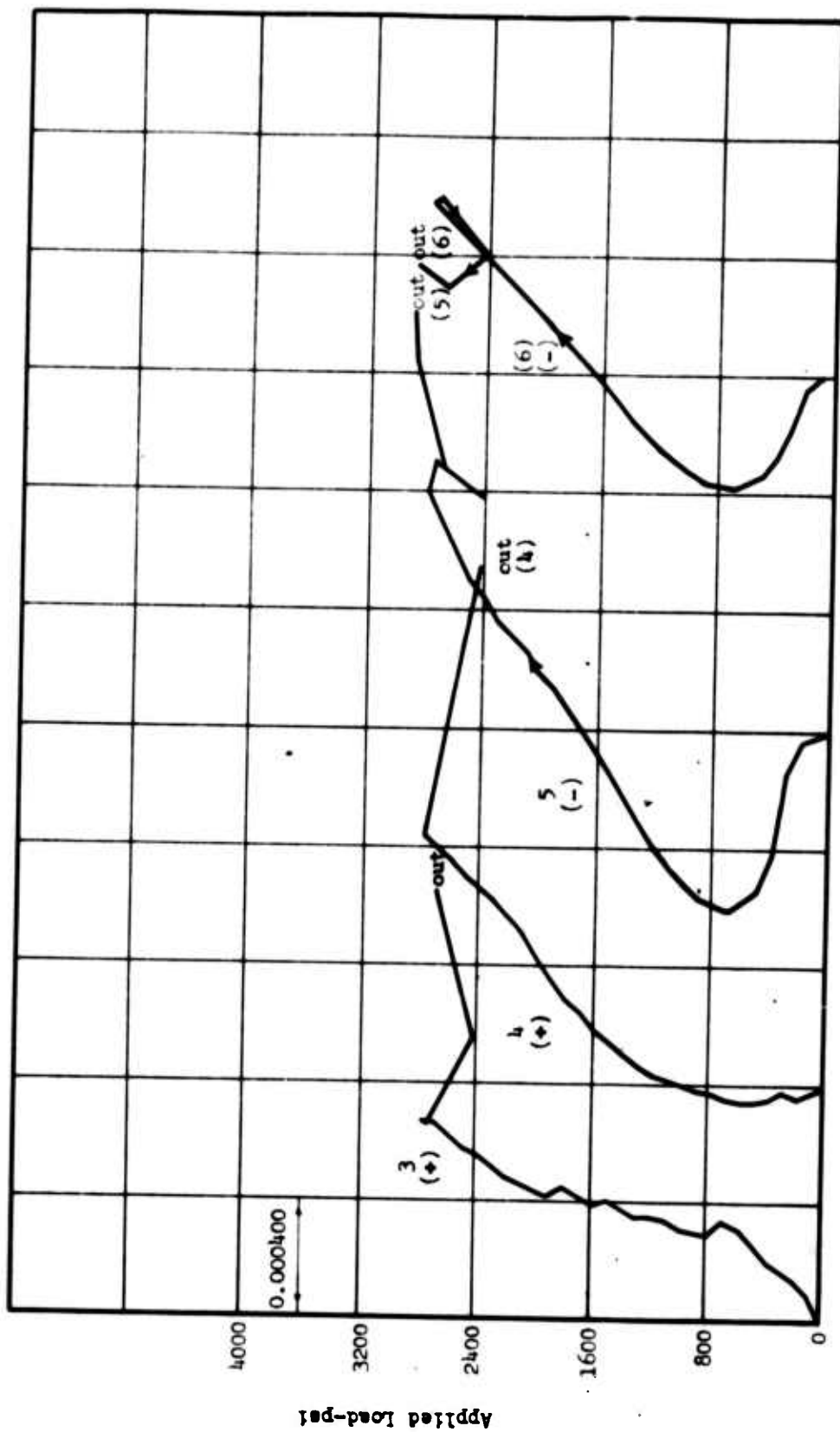


Fig. 5.29 Deflection Profiles, Slab G-7

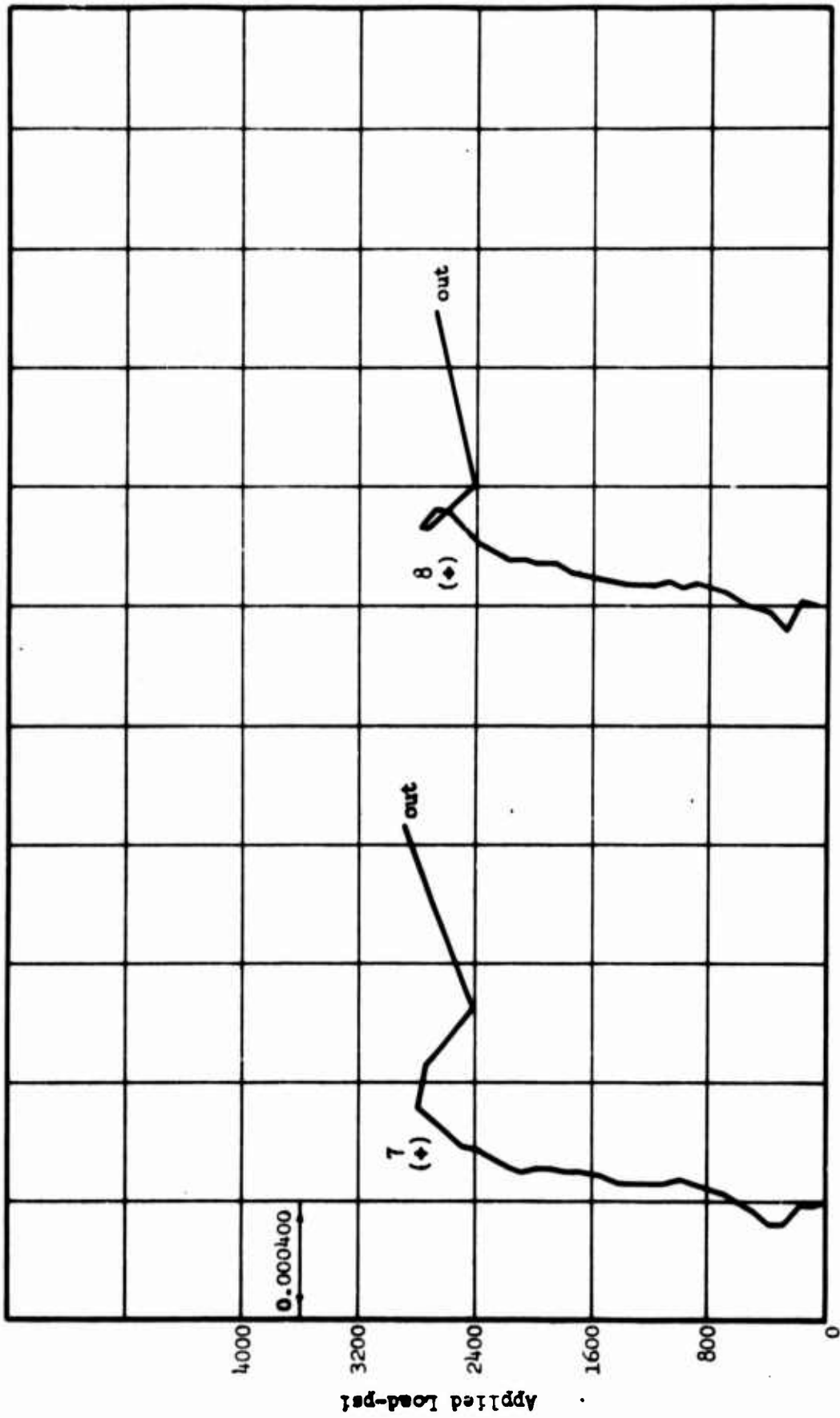


Reinforcement Strain
Fig. 5.30 Load-Strain Curves, Slab G-7



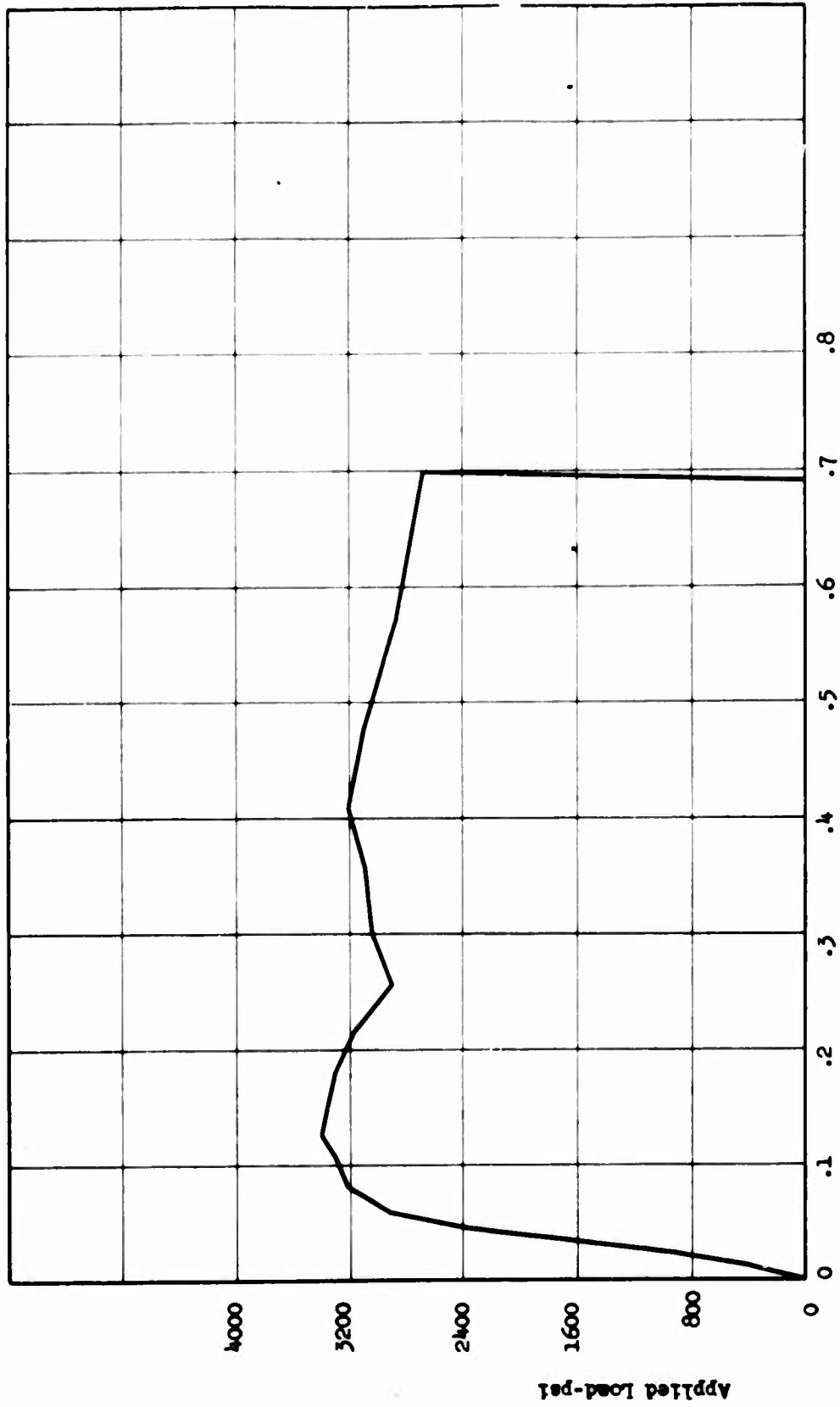
Reinforcement Strain

Fig. 5.31 Load-Strain Curves, Slab G-7



Reinforcement Strain

Fig. 5.32 Load-Strain Curves, Slab G-7



Center deflection-inches

Fig. 5.33 Load-Deflection Curve, Slab G-8

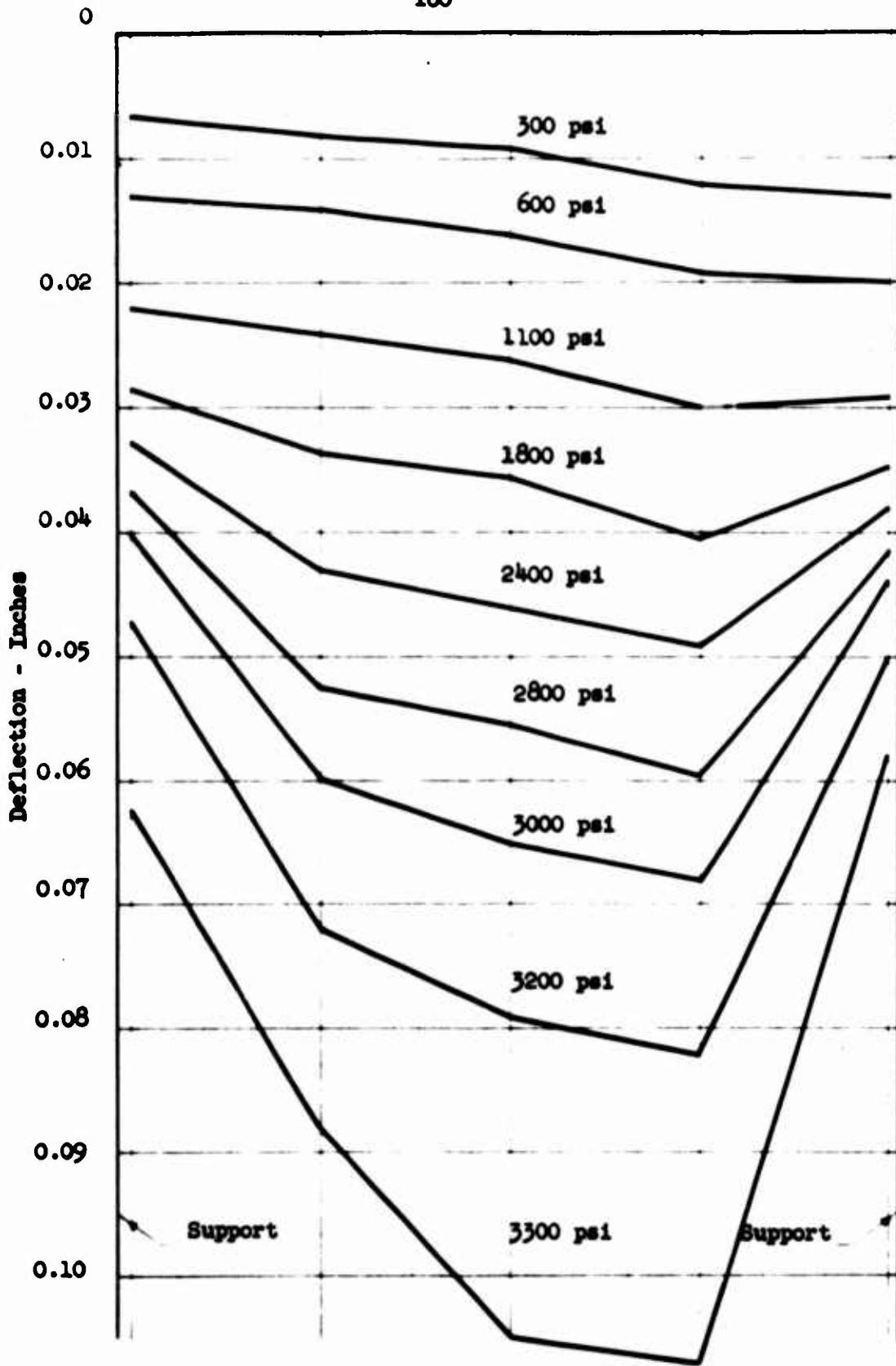
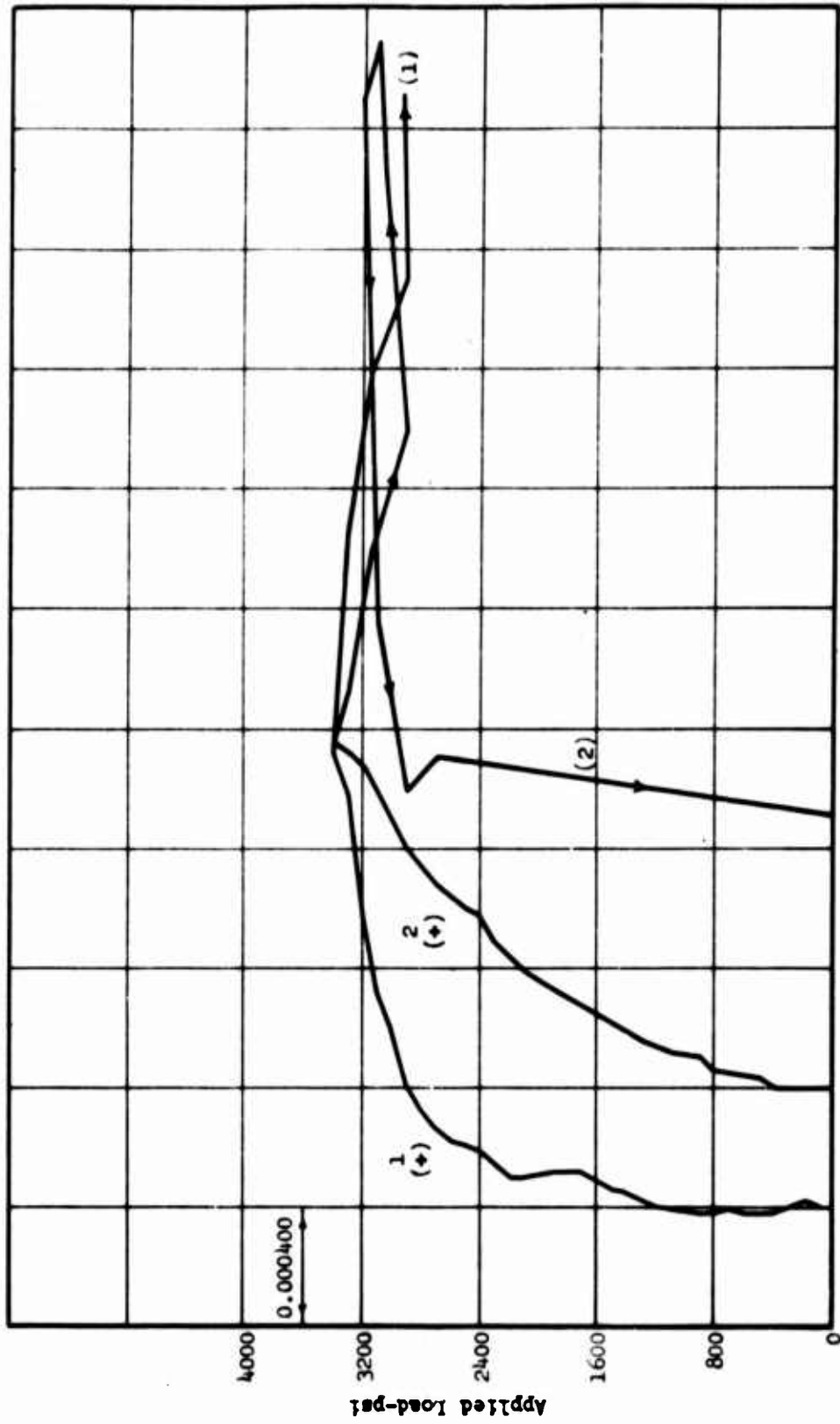
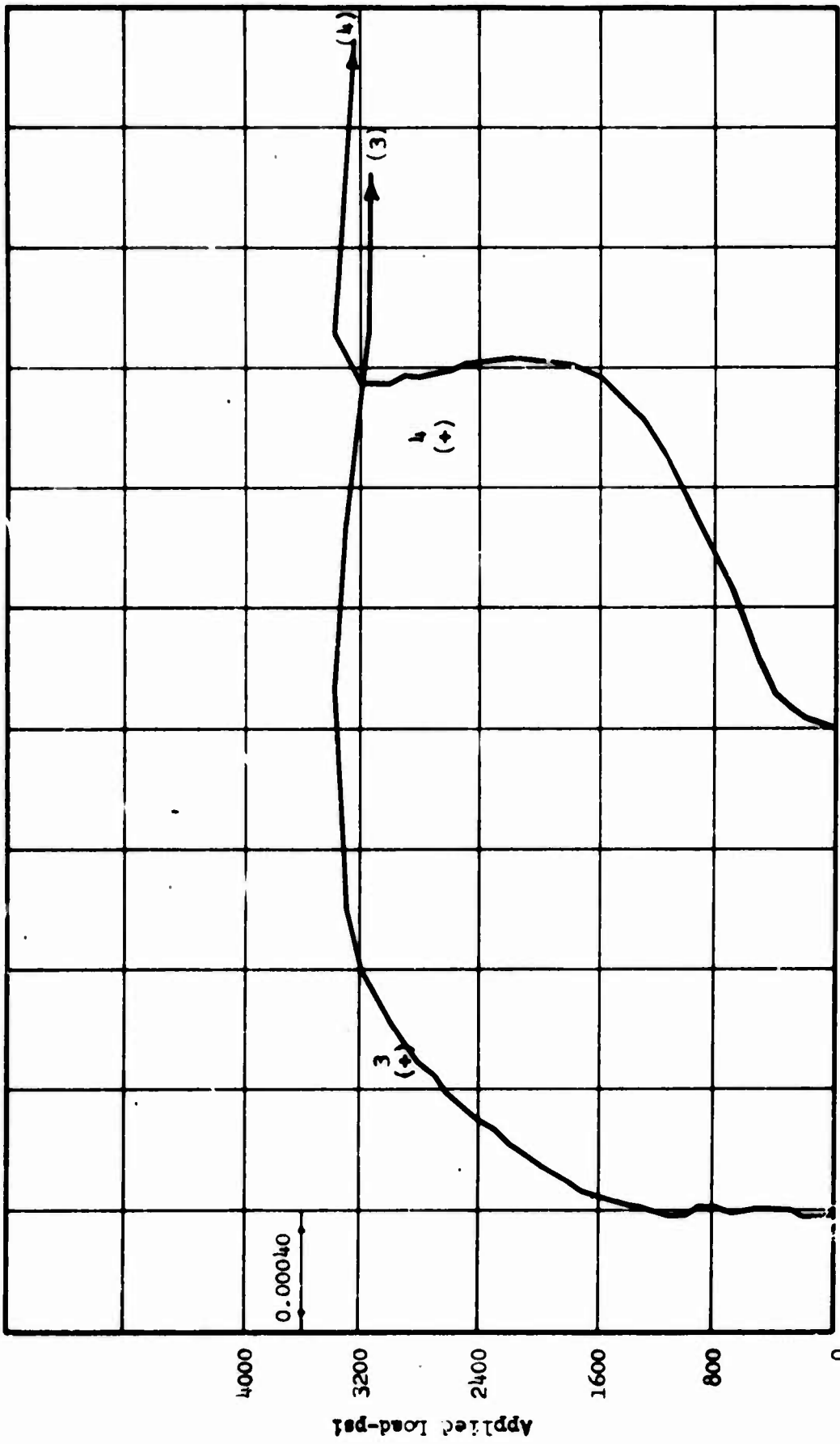


Fig. 5.34 Deflection Profiles, Slab G-8



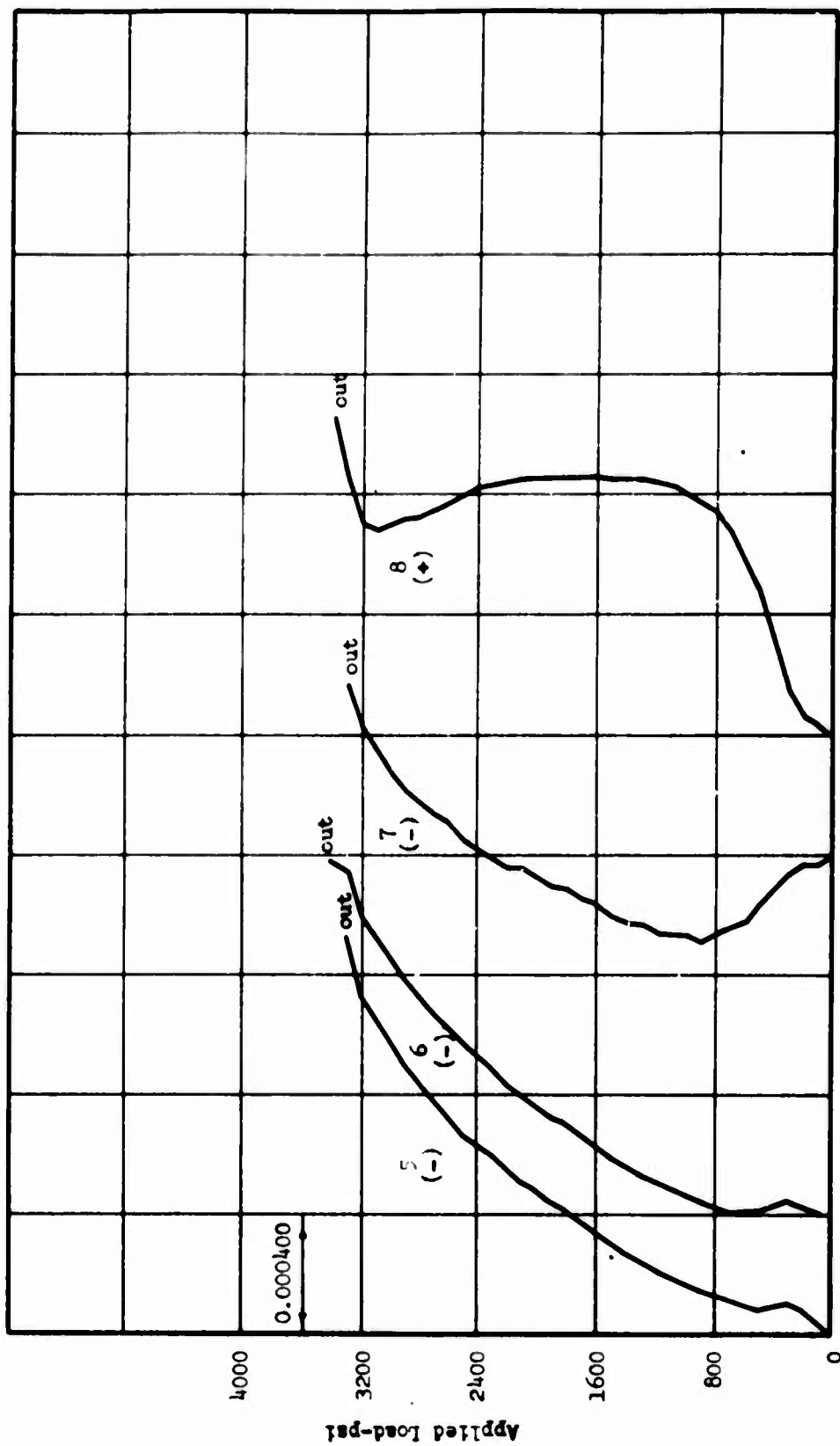
Reinforcement Strain

Fig. 5.35 Load-Strain Curves, Slab G-8



Reinforcement Strain

Fig. 5.36 Load-Strain Curves, Slab G-8



Reinforcement Strain

Fig. 5.37 Load-Strain Curves, Slab G-8

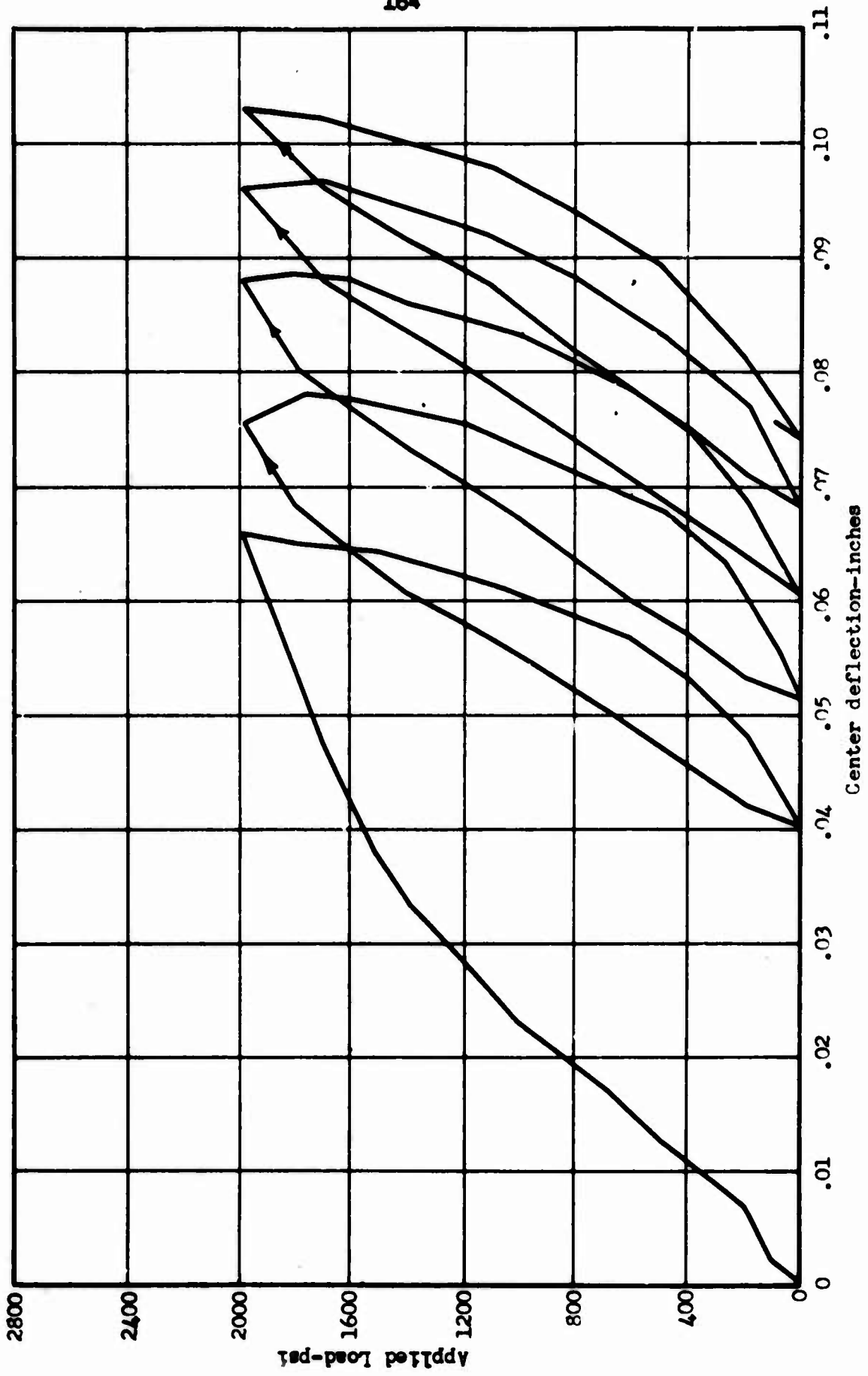


Fig. 5.38 Load-Deflection Curve, Slab G-9, Cycles 1-5

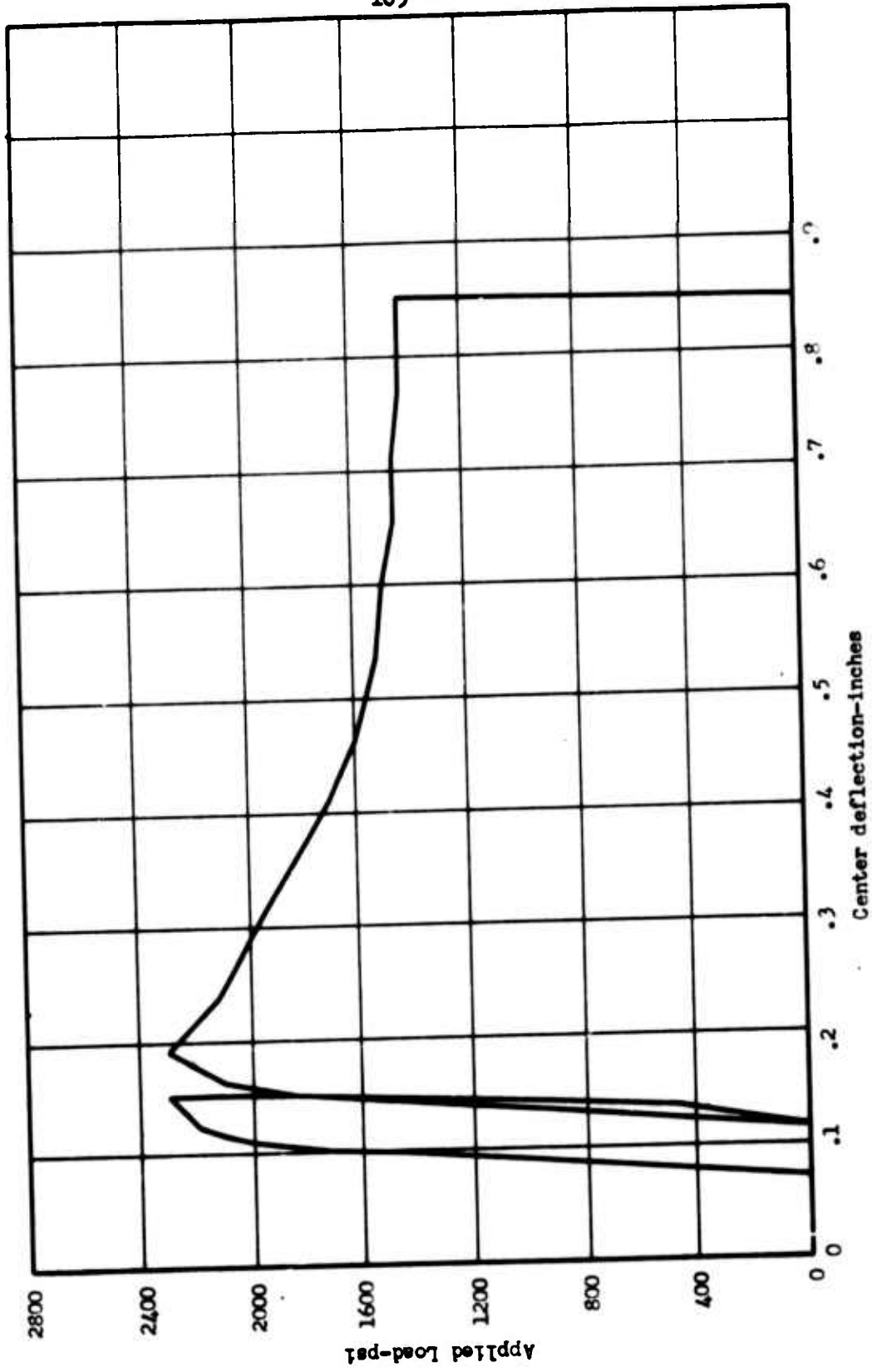


Fig. 5.39 Load-Deflection Curve, Slab G-9, Cycles 6&7

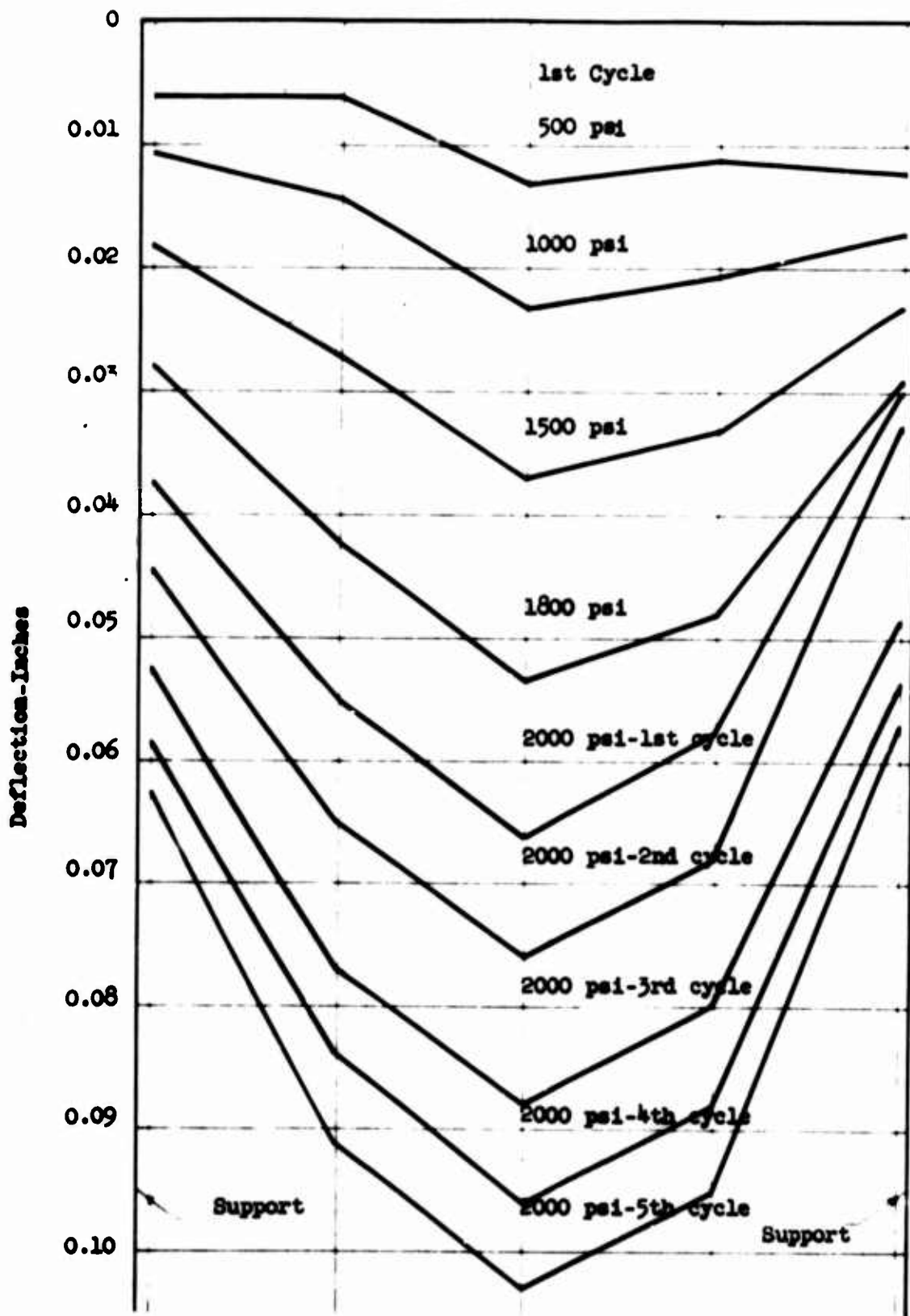
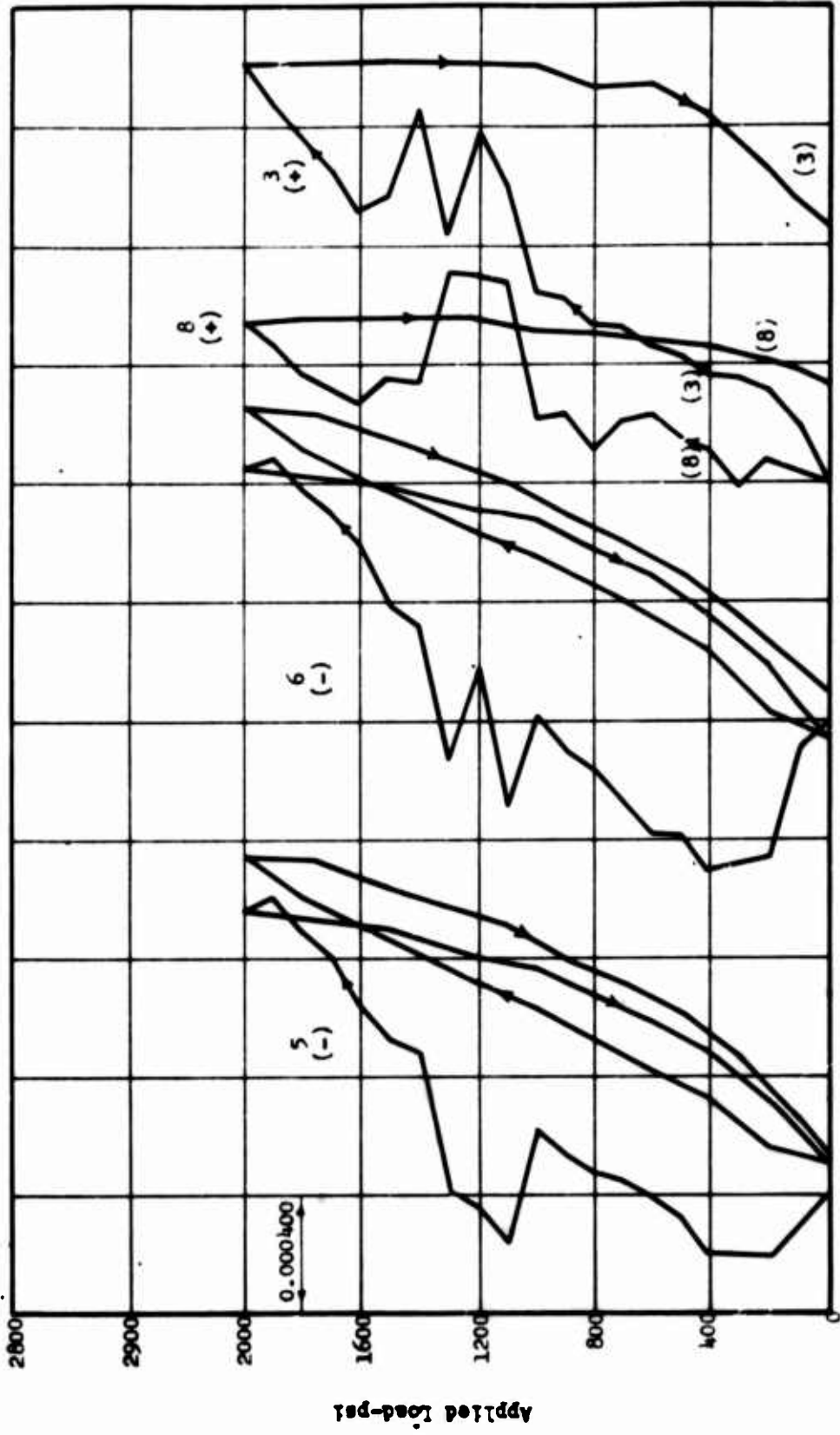


Fig. 5.40 Deflection Profiles Slab G-9



Reinforcement Strain

Fig. 5.41 Load-Strain Curves, Slab G-9

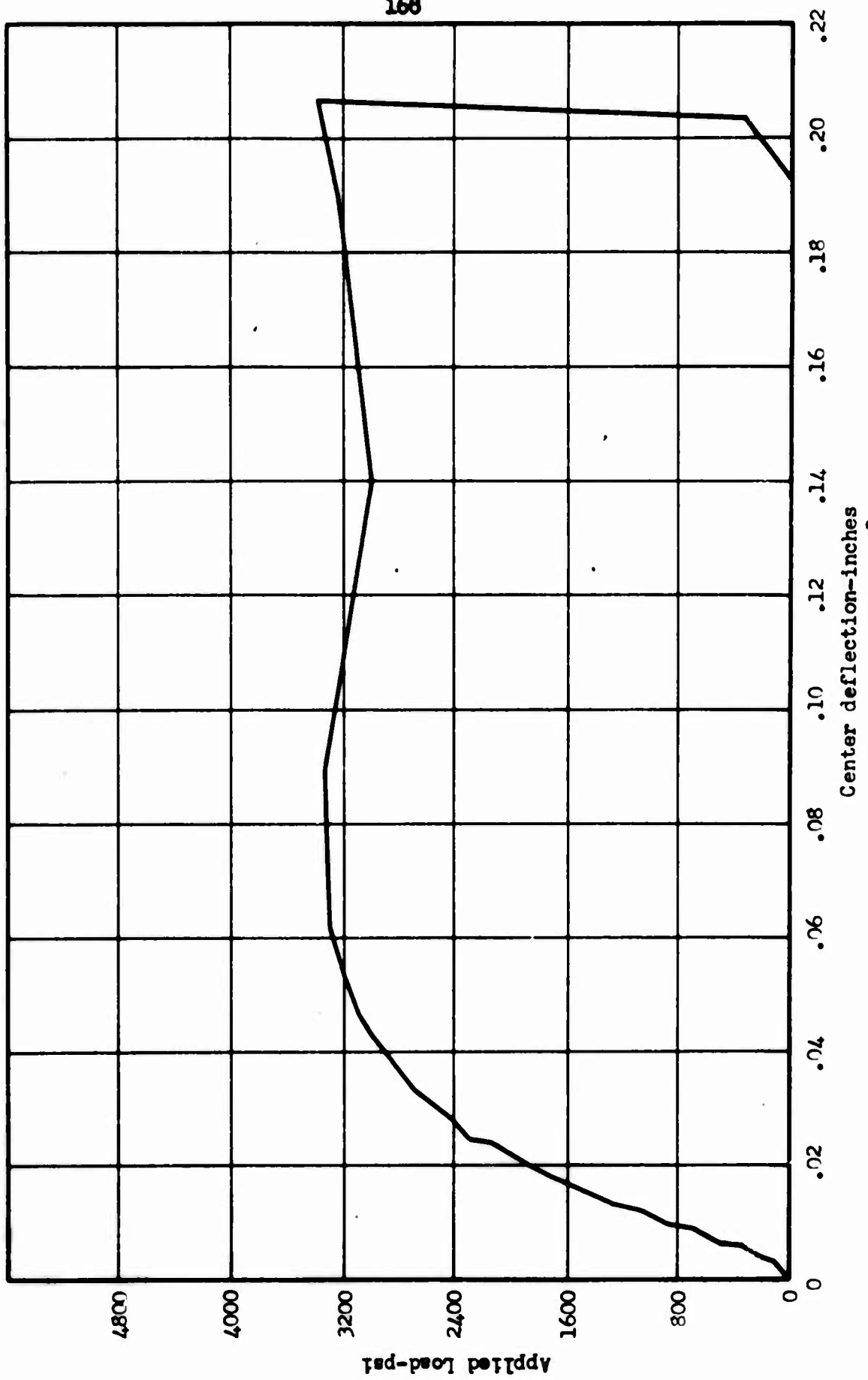


Fig. 5.42 Load-Deflection Curve, Slab G-10

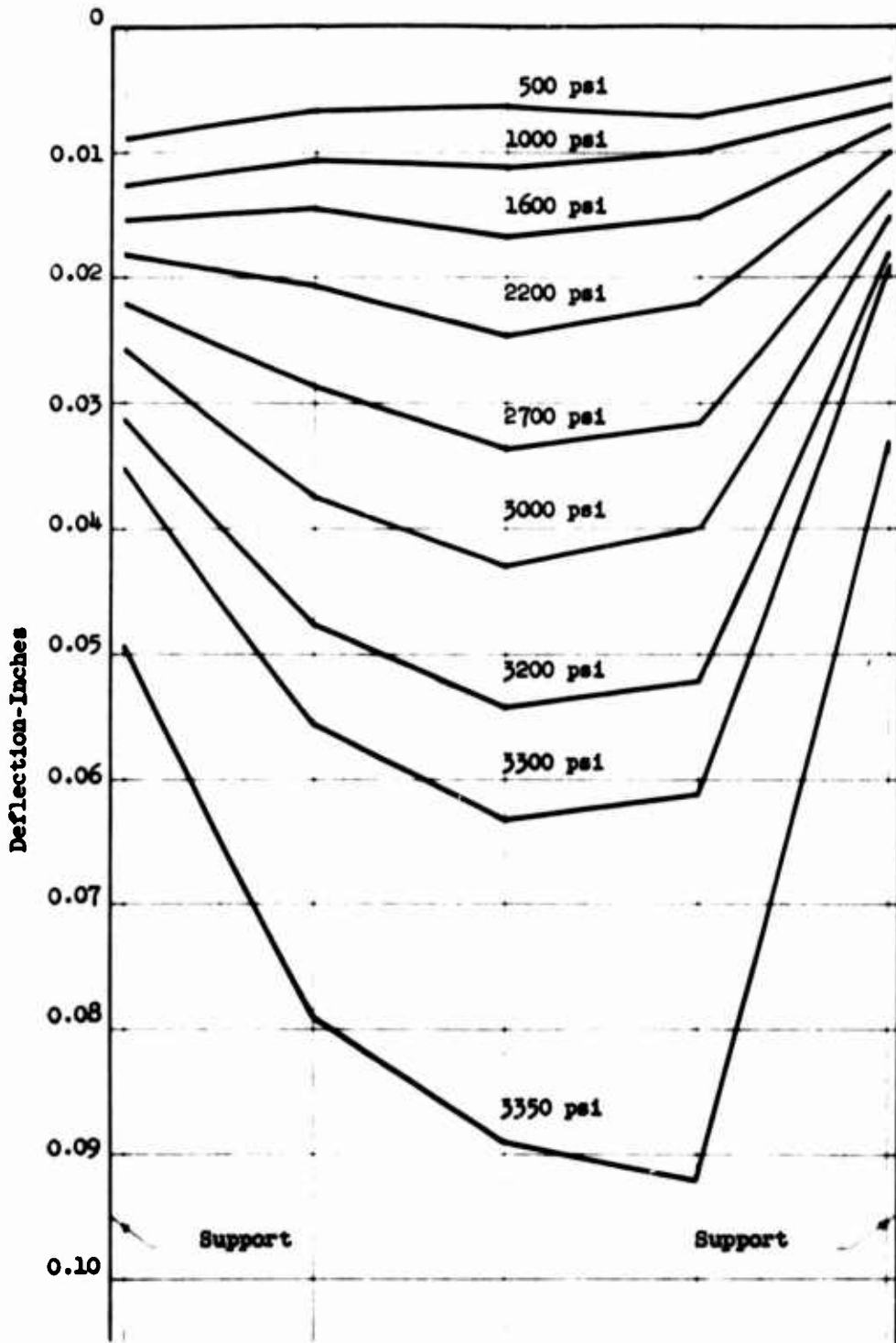
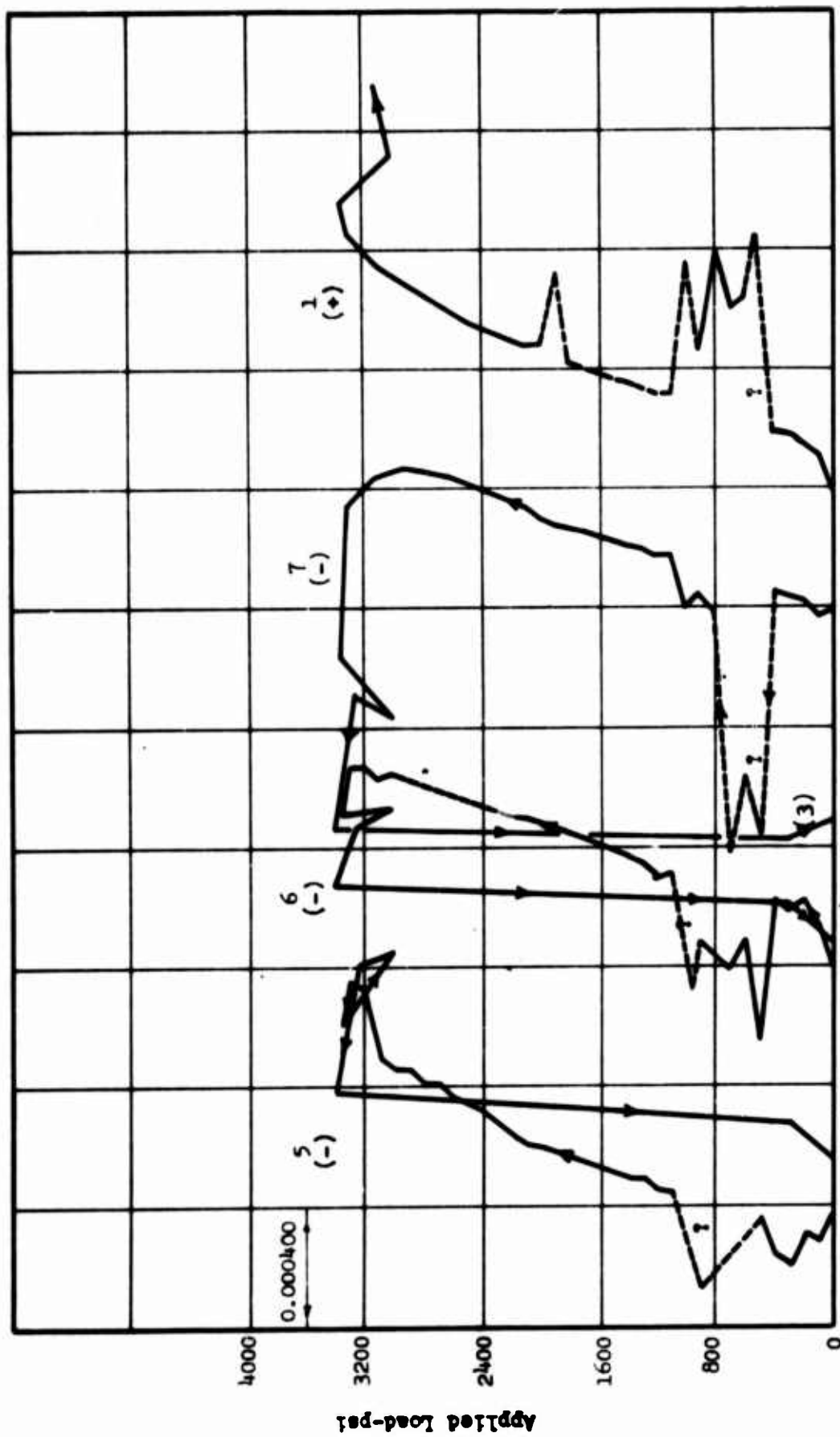
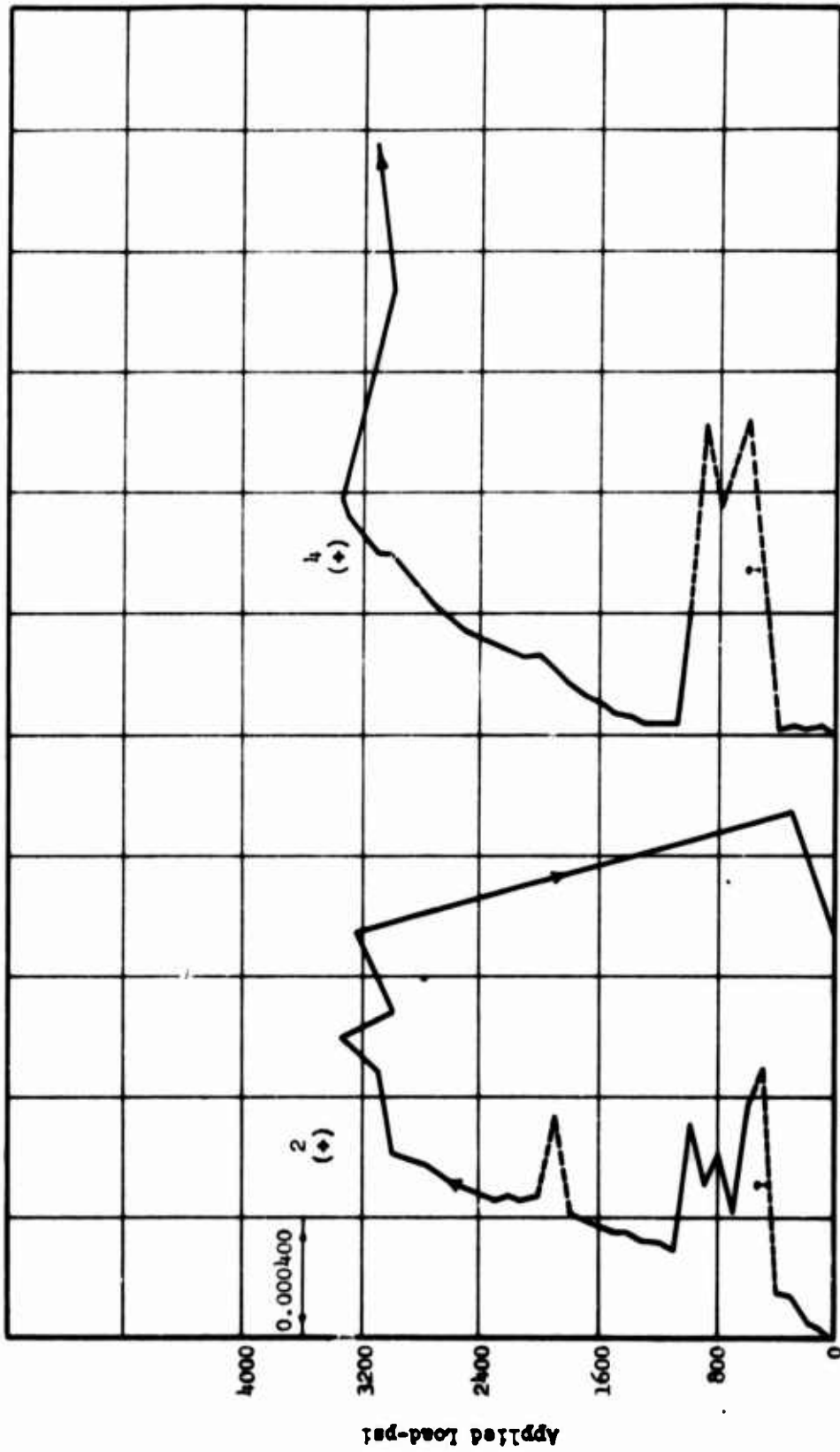


Fig. 5.43 Deflection Profiles, Slab G-10



Reinforcement Strain

Fig. 5.44 Load-Strain Curves G-10



Reinforcement Strain
Fig. 5.45 Load-Strain Curves, Slab G-10

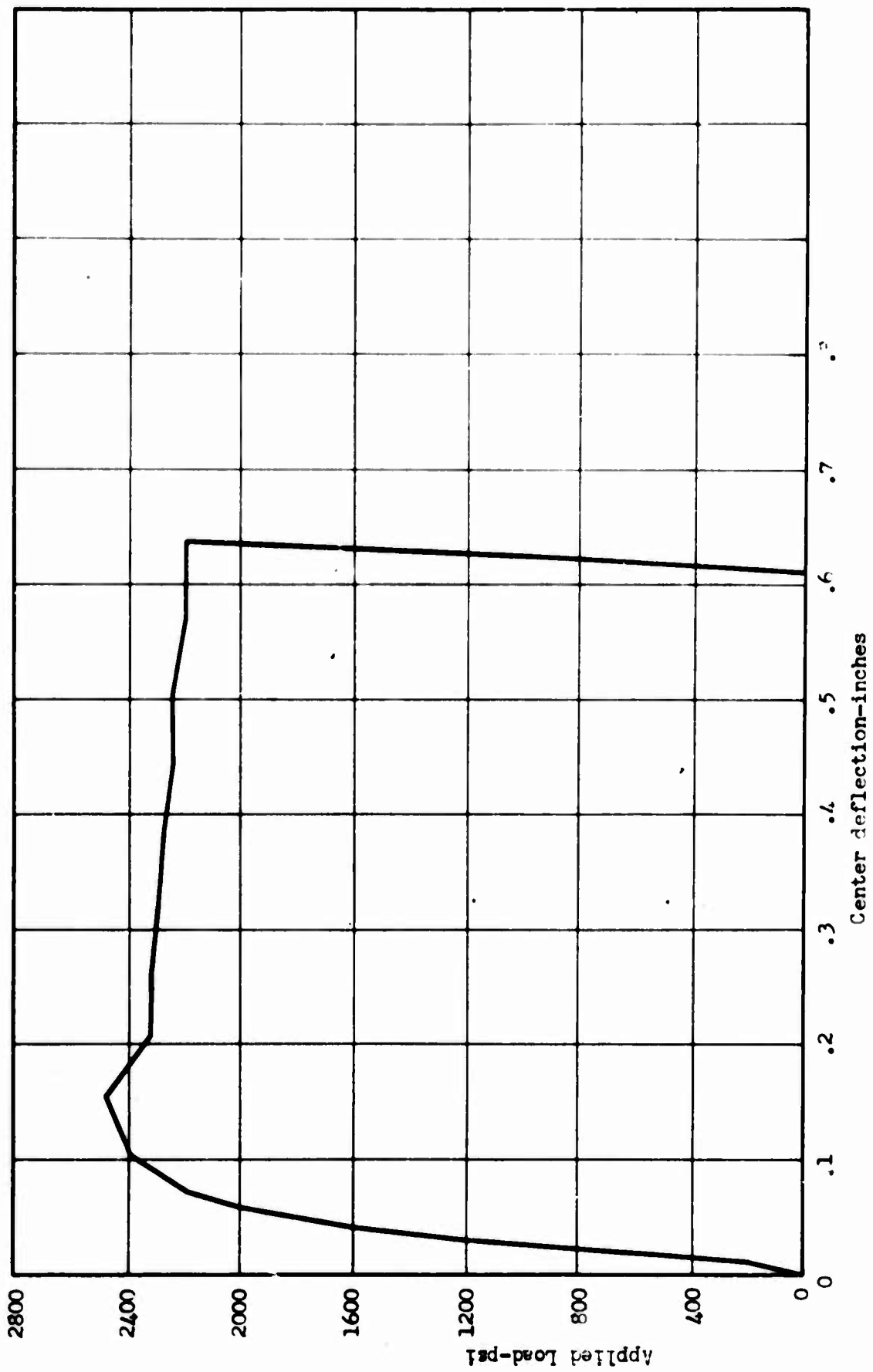


Fig. 5.46 Load-Deflection Curve, Slab G-11



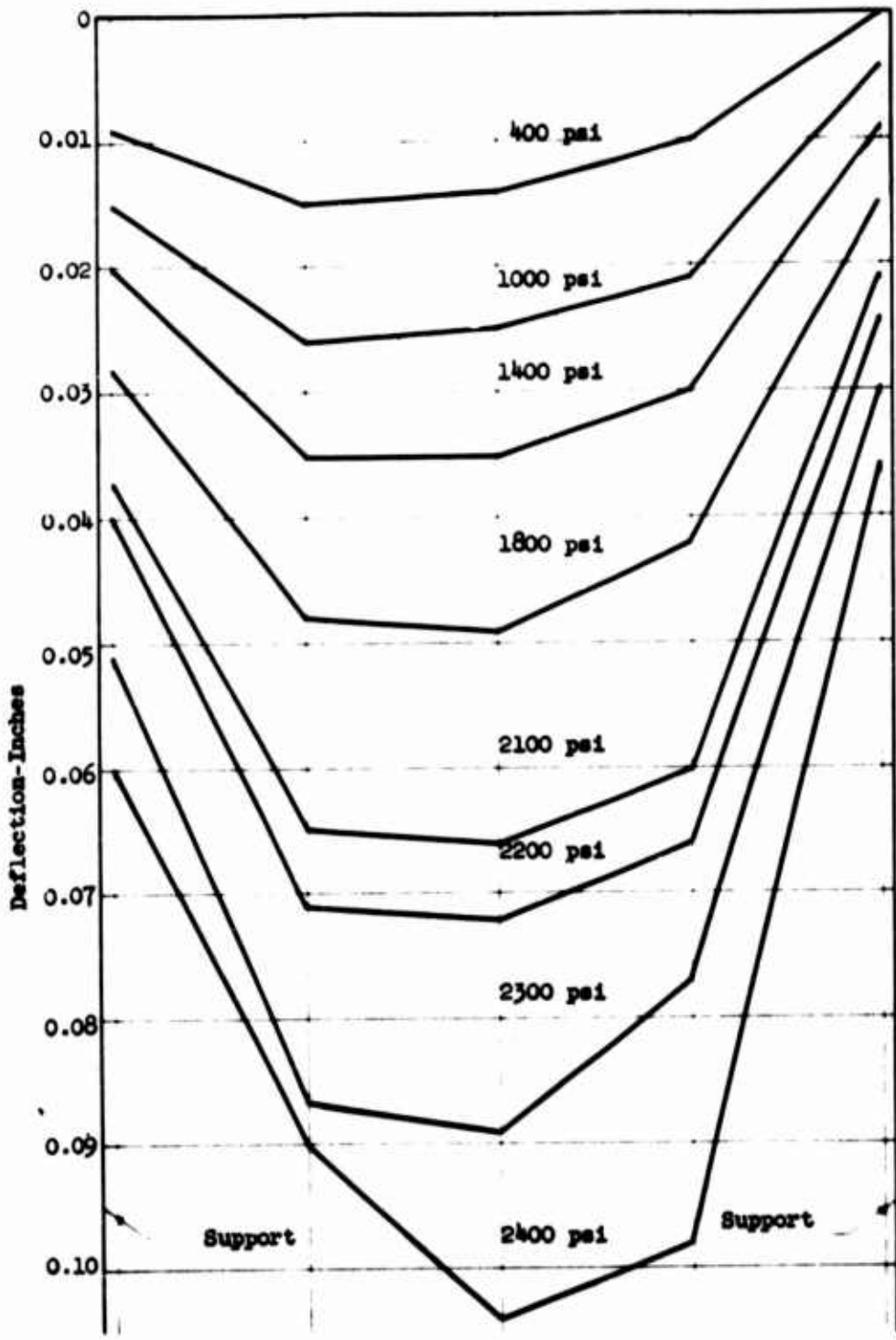
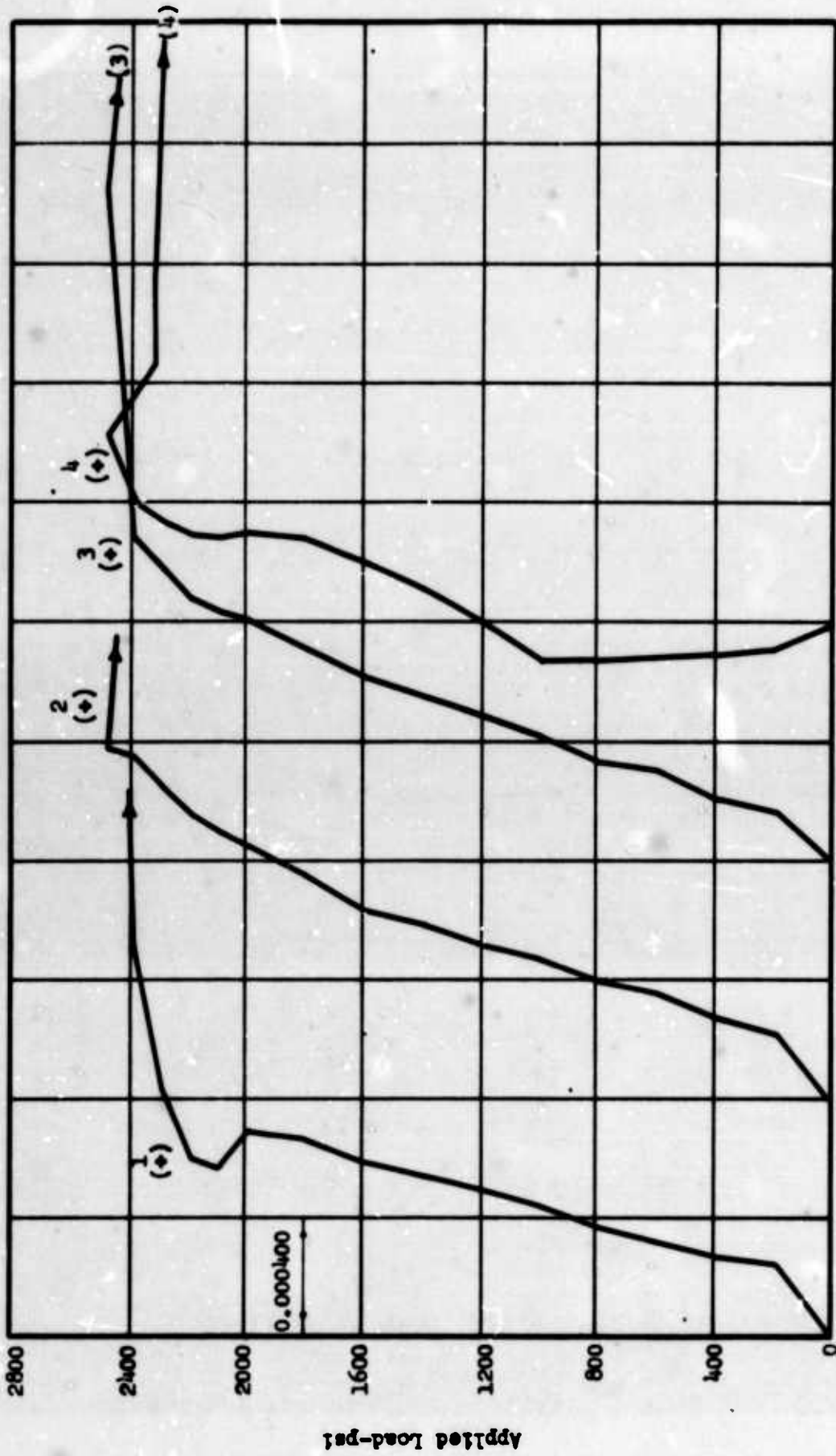


Fig. 5.47 Deflection Profiles, Slab 6-11



Reinforcement Strain

Fig. 5.48 Load-Strain Curves, Slab G-11

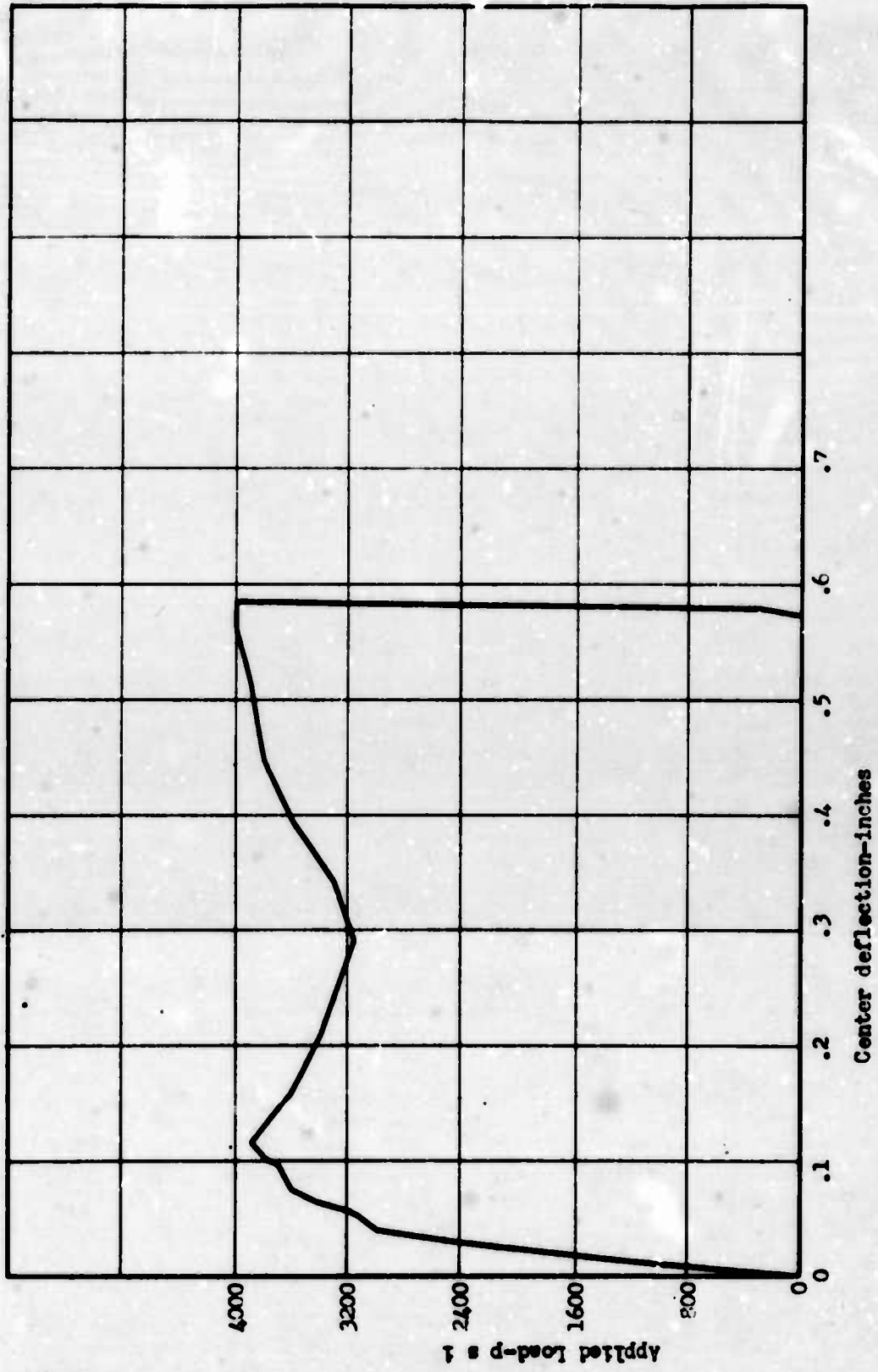


Fig. 5.49 Load-Deflection Curve, Slab C-12

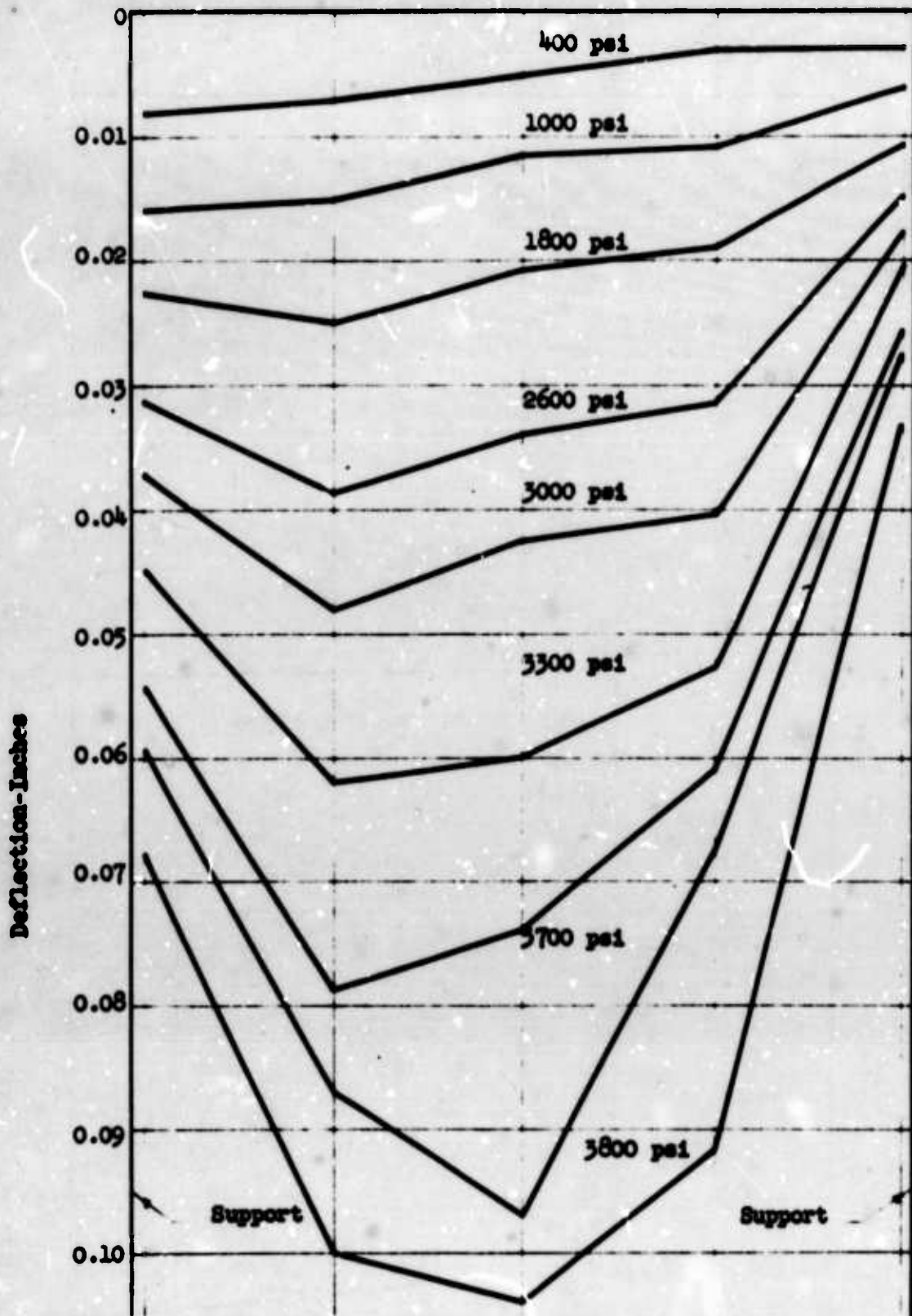
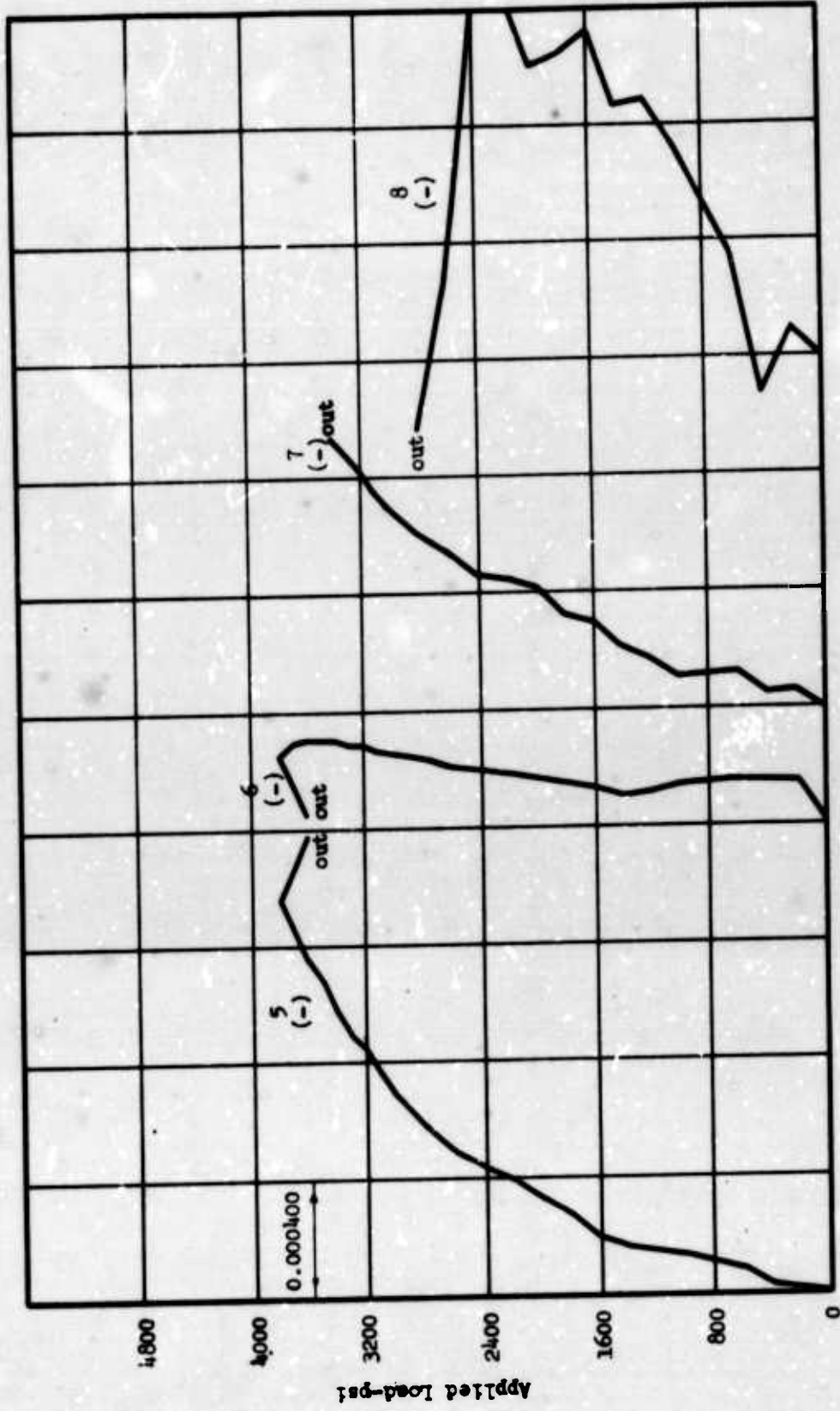


Fig. 5.50 Deflection Profiles, Slab G-12



Reinforcement Strain
 Fig. 5.51 Load-Strain Curves, Slab G-12



Reinforcement Strain

Fig. 5.52 Load-Strain Curves, Slab G-12



Fig. 5.53 Slab G-1. Deformation of Top Surface

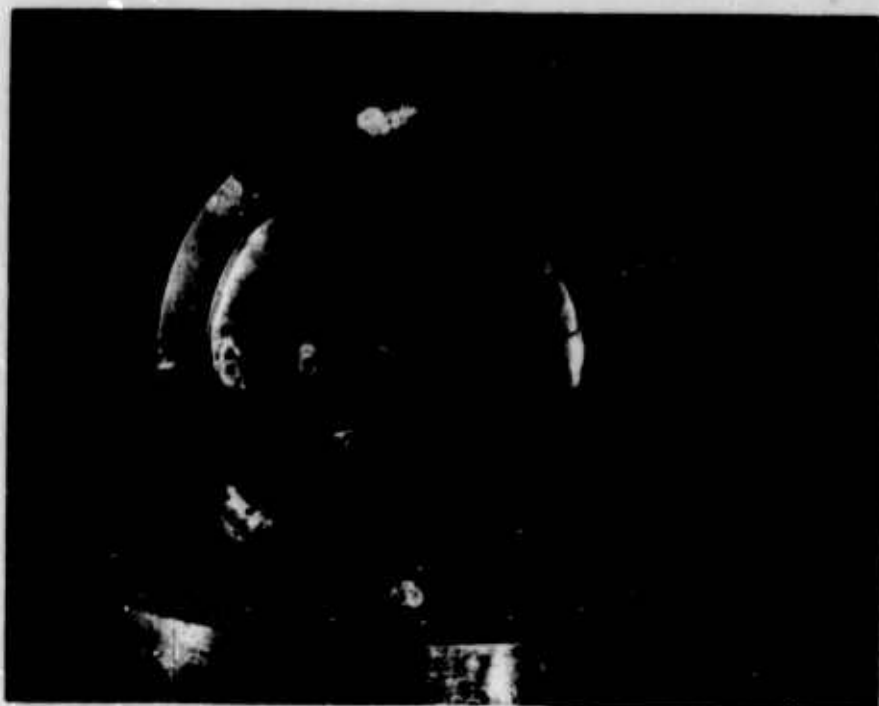


Fig. 5.54 Slab G-1, Deformation at Bottom Surface

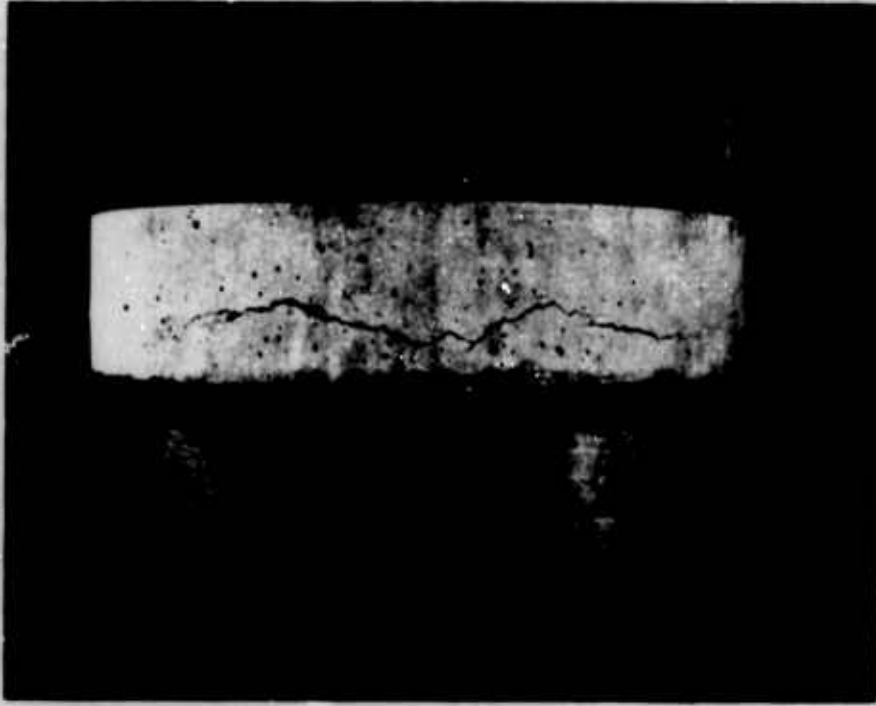


Fig. 5.55 Slab G-1, Profile

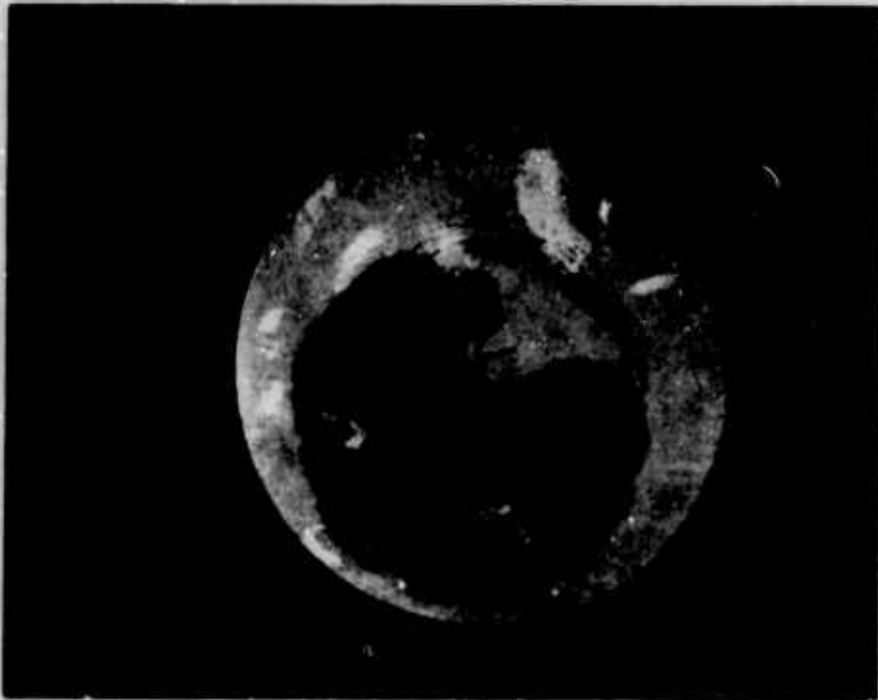


Fig. 5.56 Slab G-2, Deformation of Top Surface



Fig. 5.57 Slab G-2, Deformation of Bottom Surface

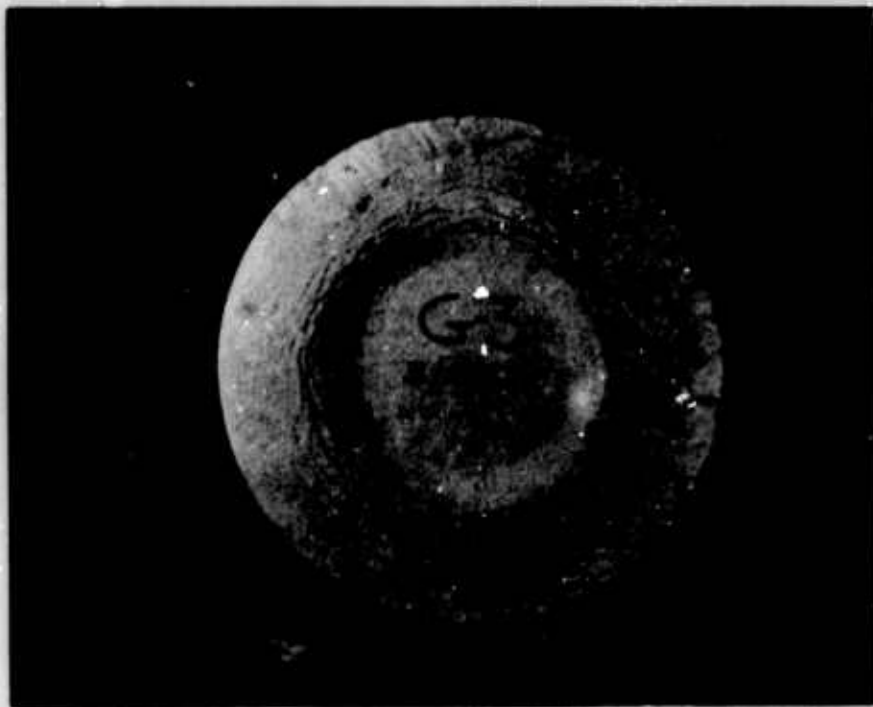


Fig. 5.58 Slab G-3, Deformation of Top Surface

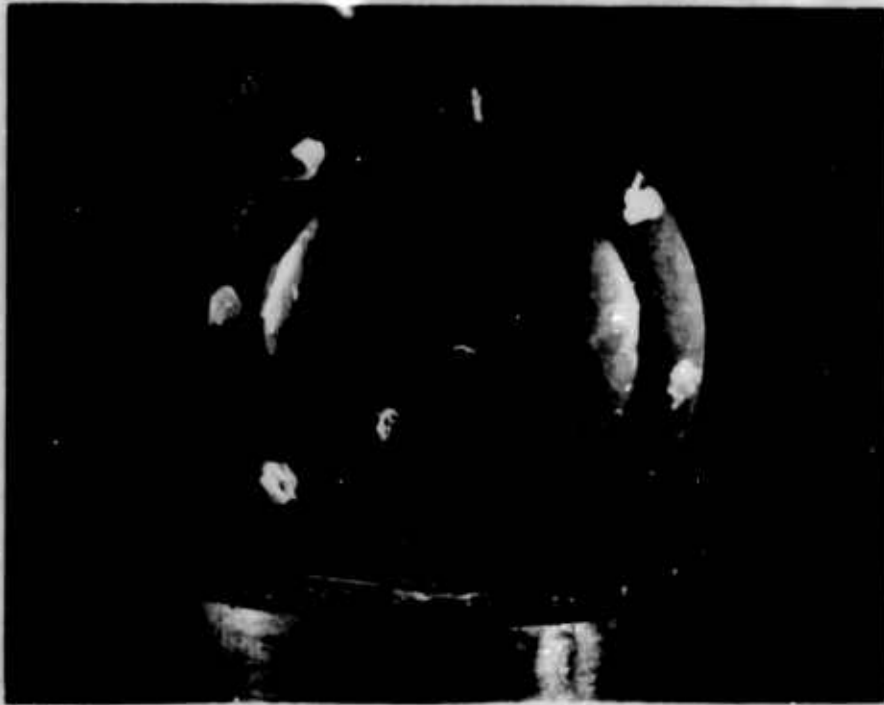


Fig. 5.59 **Slab G-3, Deformation of Bottom Surface**

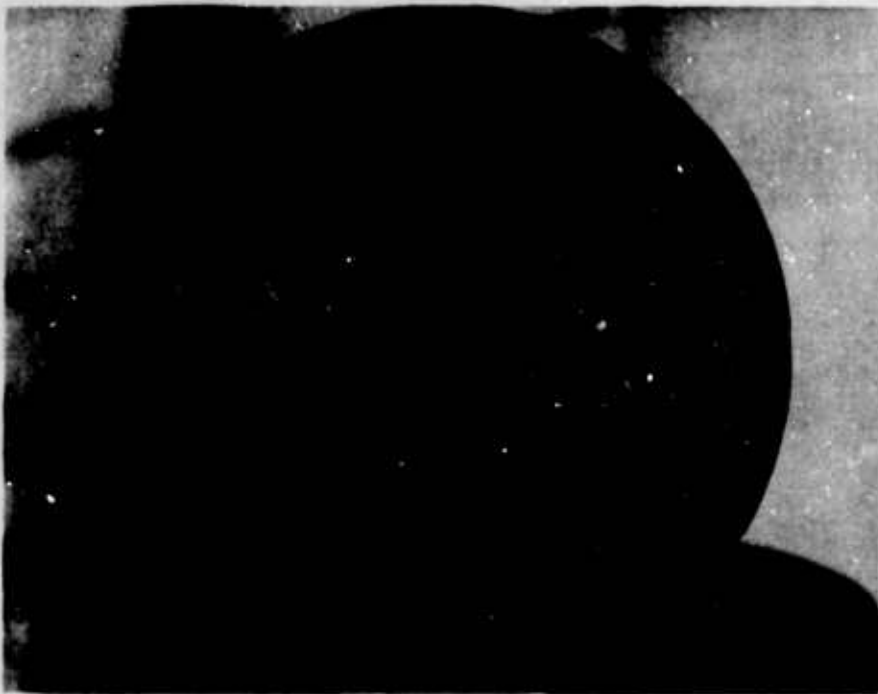


Fig. 5.60 **Slab G-4, Deformation of Top Surface**



Fig. 5.61 Slab G-4, Deformation of Bottom Surface



Fig. 5.62 Slab G-4, Profile

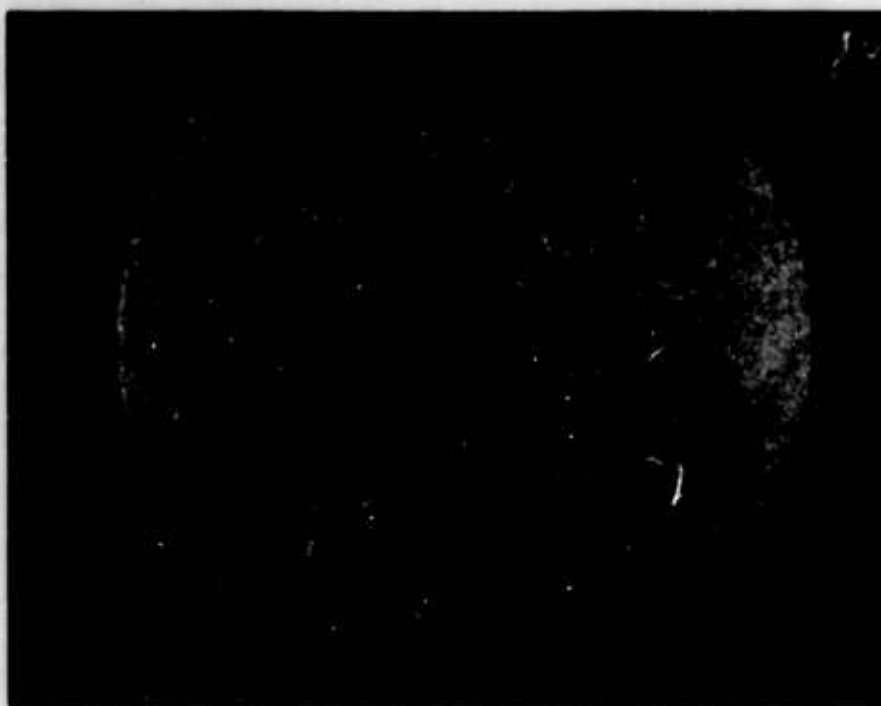


Fig. 5.63 Slab G-5, Deformation of Top Surface

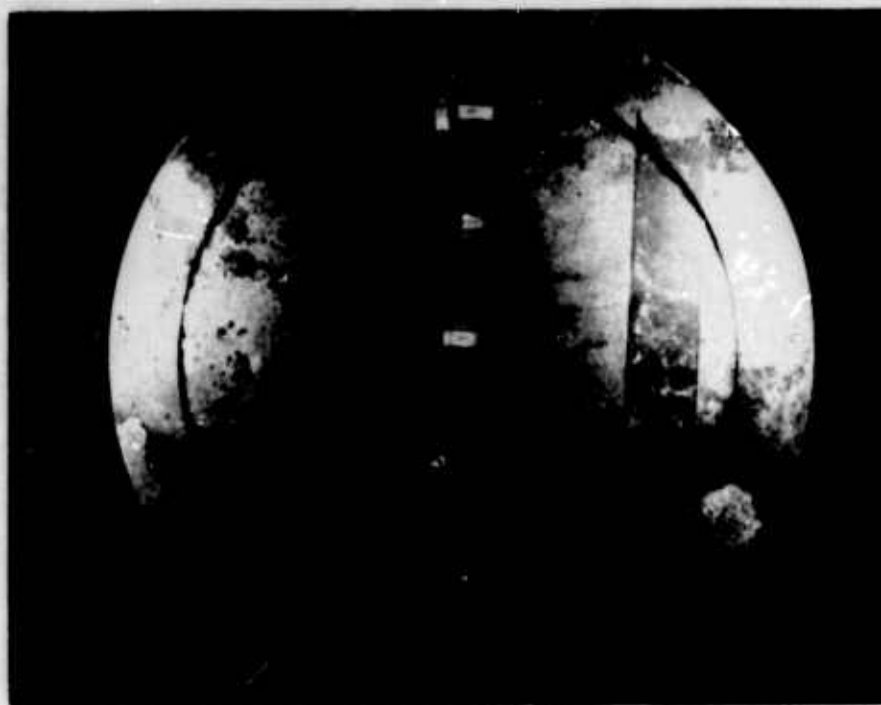


Fig. 5.64 Slab G-5, Deformation of Bottom Surface



Fig. 5.65 Slab G-5, Profile



Fig. 5.66 Slab G-6, Deformation of Top Surface

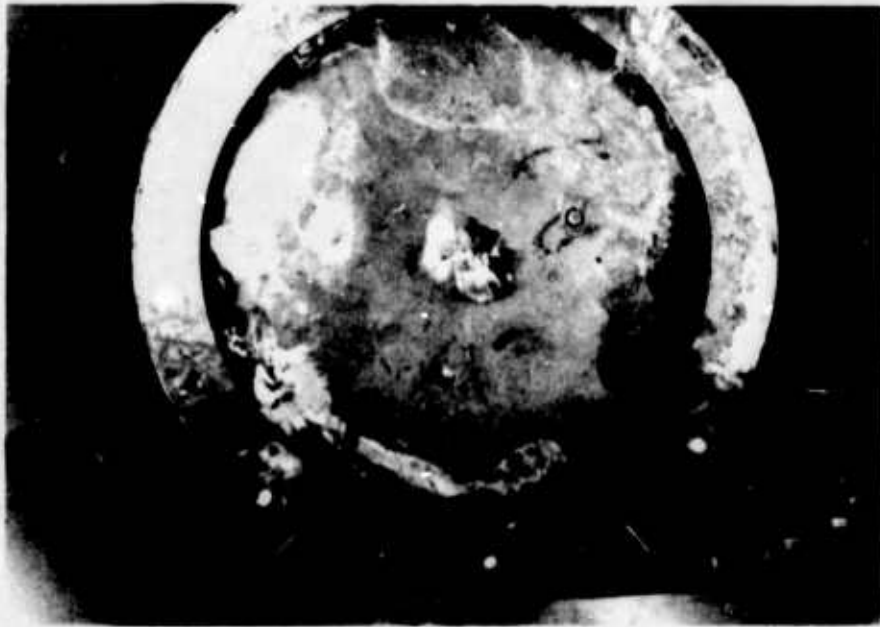


Fig. 5.67 Slab G-6, Deformation of Bottom Surface



Fig. 5.68 Slab G-6, Profile

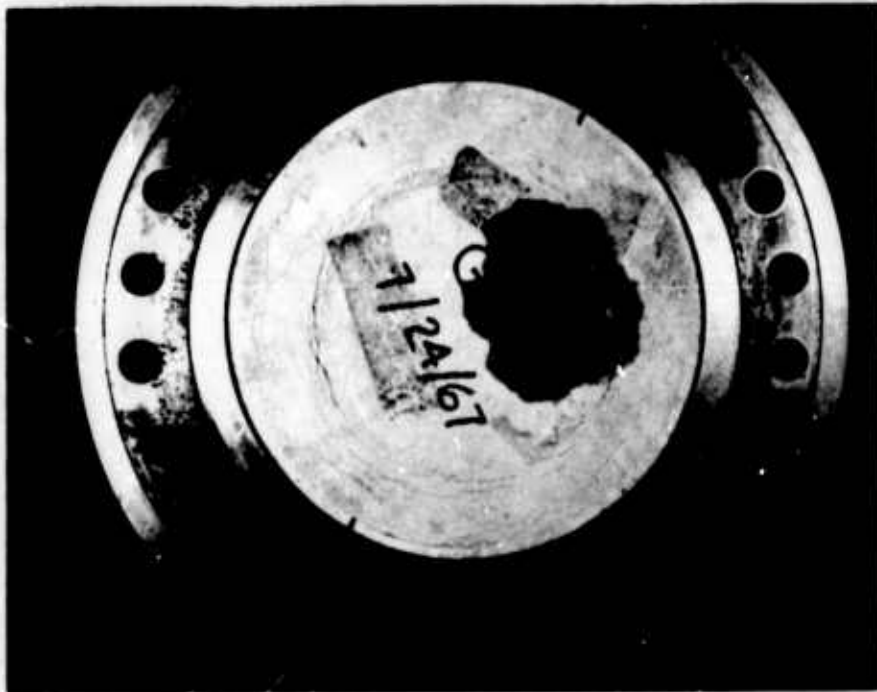


Fig. 5.69 Slab G-7, Deformation of Top Surface

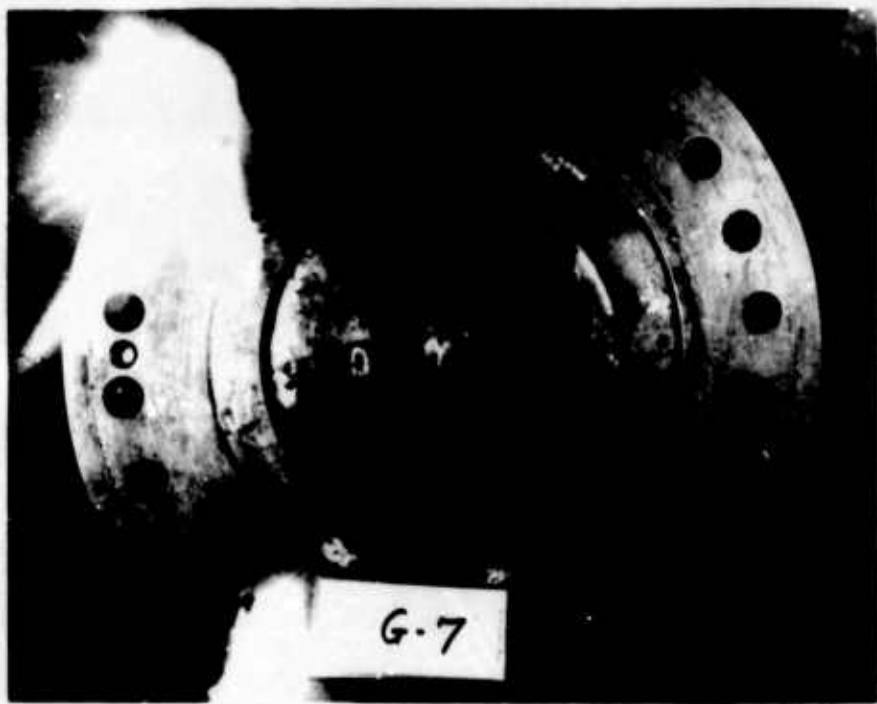


Fig. 5.70 Slab G-7, Deformation of Bottom Surface



Fig. 5.71 Slab G-7, Profile

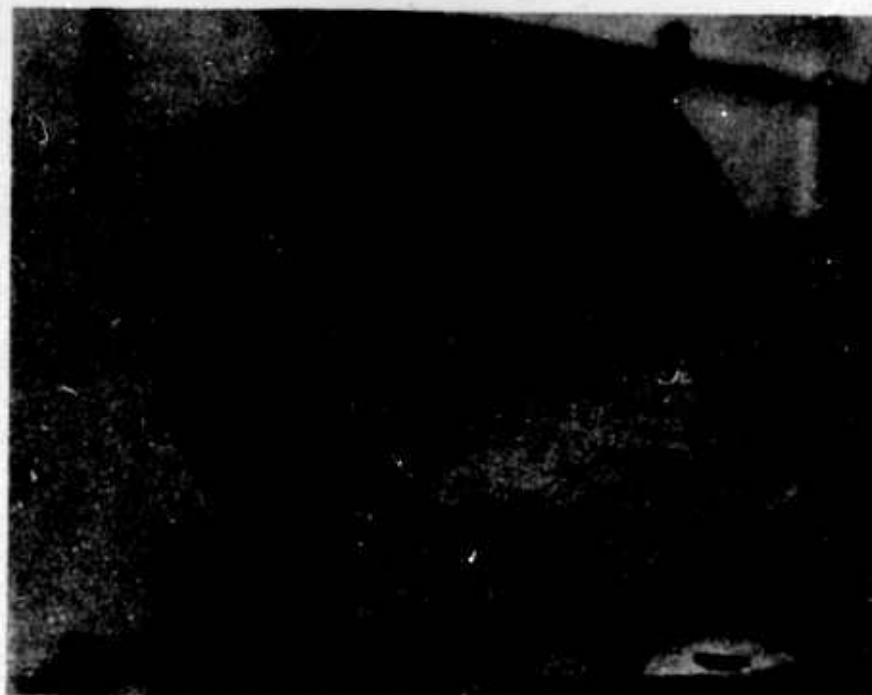


Fig. 5.72 Slab G-8, Deformation of Top Surface



Fig. 5.73 Slab G-8, Deformation of Bottom Surface

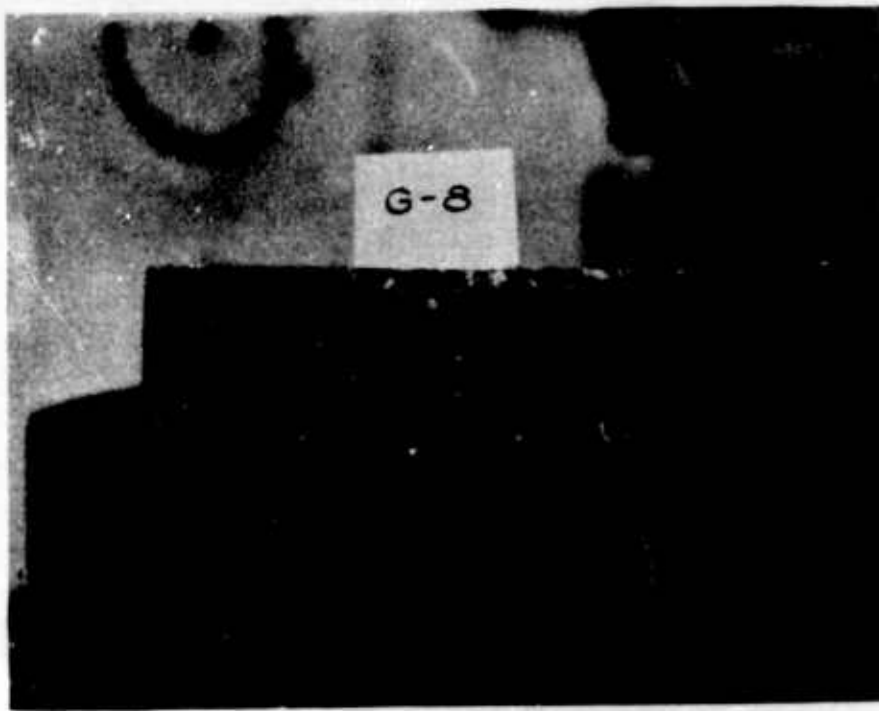


Fig. 5.74 Slab G-8, Profile



Fig. 5.75 Slab G-9, Deformation of Top Surface



Fig. 5.76 Slab G-9, Deformation of Bottom Surface

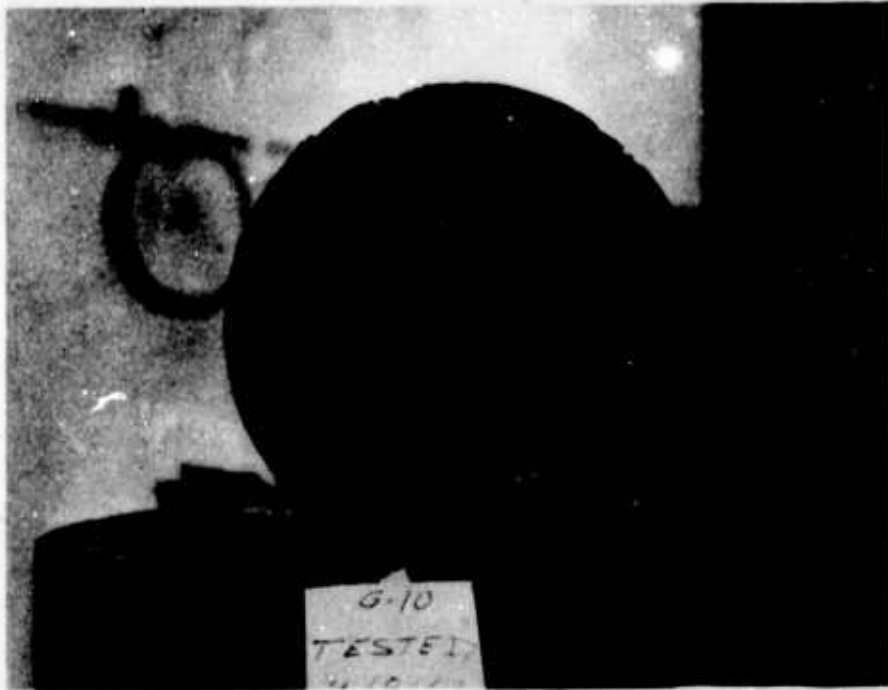


Fig. 5.77 Slab G-10, Deformation of Top Surface



Fig. 5.78 Slab G-10, Deformation of Bottom Surface



Fig. 5.79 Slab G-10, Profile

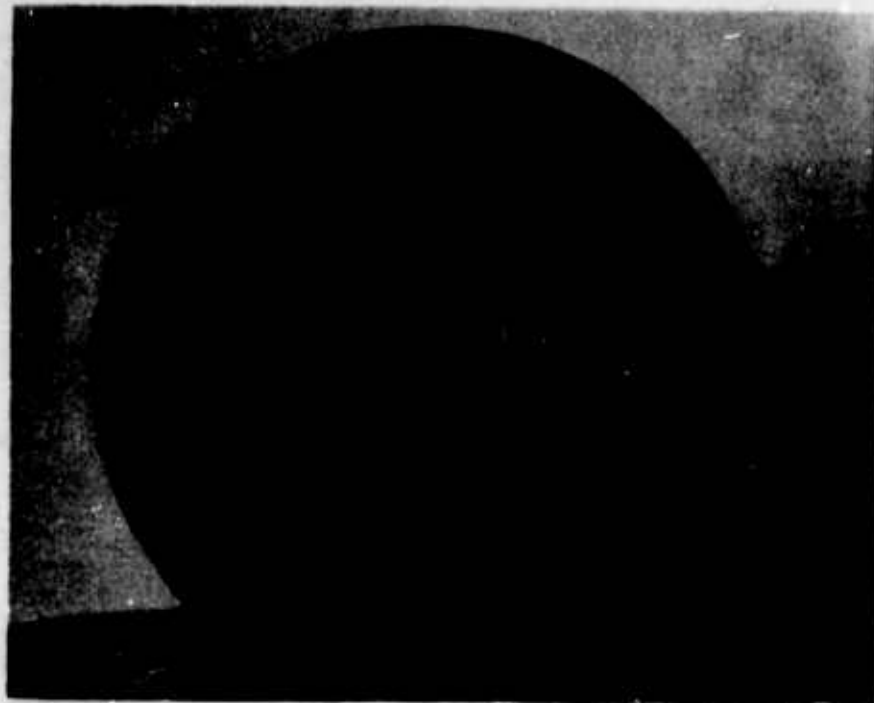


Fig. 5.80 Slab G-11, Deformation of Top Surface

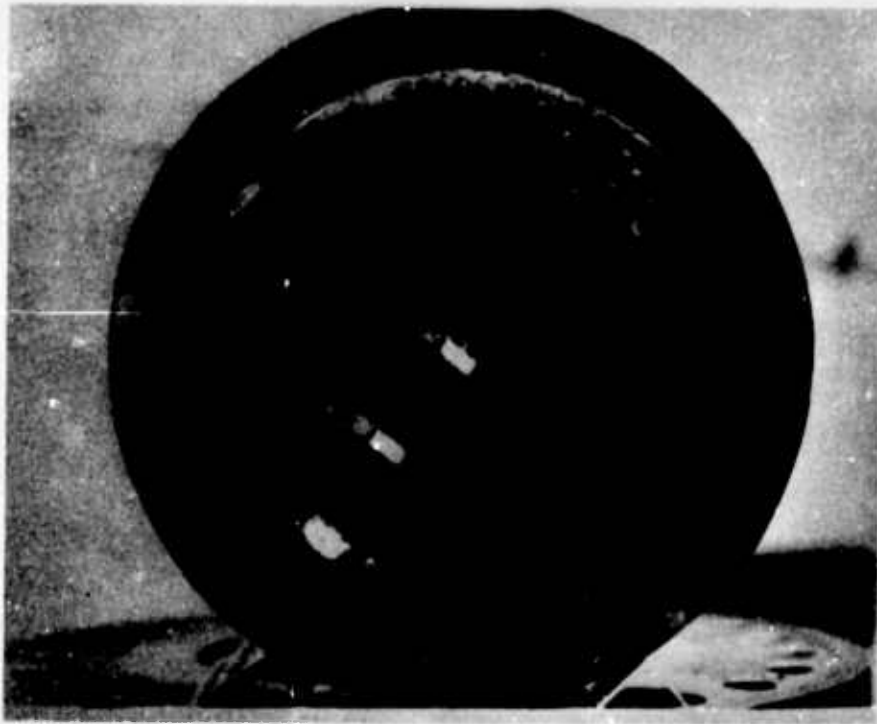


Fig. 5.81 **Slab G-11, Deformation of Bottom Surface**

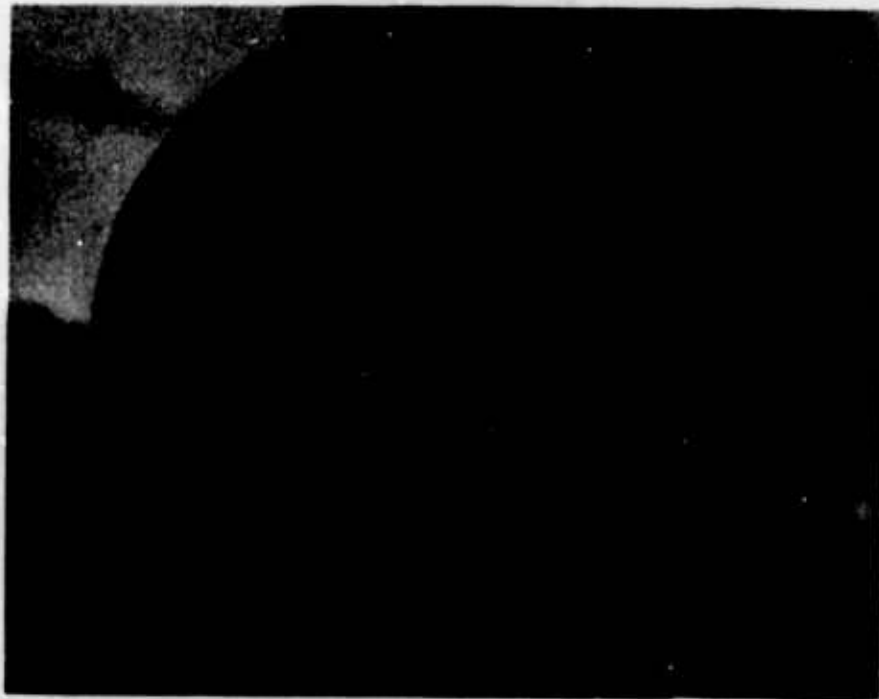


Fig. 5.82 **Slab G-12, Deformation of Top Surface**



Fig. 5.83 Slab G-12, Deformation of Bottom Surface



Fig. 5.84 Slab G-12, Profile

CHAPTER 6

DISCUSSION OF TEST RESULTS

6.1. General

The results of the model test series, presented in Chapter 5, have shown that the primary objectives of this research have been fulfilled. Silo closures can be designed to withstand overpressure loadings of 1000 and 2000 psi. The test results have further shown that model closures designed to fail in flexure at these loadings actually failed in shear and/or bearing at substantially greater overpressures. The added load capacity was attributed to thrust against the lower surface of the slab due to friction between the slab and the supporting structure.

The model tests have demonstrated that closure slabs using steel plates for tension reinforcement are comparable to bar-reinforced slabs in load-carrying capacity and provide somewhat greater ductility. The addition of shear reinforcement to the models was found to consistently improve ductility. Shear steel had no effect on load-carrying capacity, however.

In this chapter methods of computing friction forces and friction coefficients from the model test results are described. Results of such computations are presented for two representative models to explain the high flexural load-carrying capacity of the closure structures. Bearing stresses are examined and a limiting bearing stress is recommended. The shear strength of the model slab is examined on an empirical basis and a design expression is presented.

6.2. Friction Forces

In the previous chapter strain profiles were cited to show, qualitatively, the presence of lateral forces acting on the lower surfaces of the model slabs. Gamble, et al, in SAMSO-TR-67-15 (1) have developed a procedure for computing the friction forces acting at a given load level. In their procedure each pair (top and bottom) of strain gages in the cross-section of a bar-reinforced model is arbitrarily assigned a "tributary area" of the cross-section. The strain registered by a gage is assumed to exist across the width of the tributary area at the level of the gage. Elasto-plastic stress-strain curves are assumed for both the concrete and the steel and strains are assumed to vary linearly across the height of the section. Forces in the concrete, tension steel and compression steel are then computed for each tributary area and the friction force is obtained as the force required to balance the tensions and the compressions. The thrusts for the four tributary areas are totaled and the sum is divided by the clear span radius to determine the average thrust per unit length of clear span. By analogy to a hoop-stress analysis, this unit force is equal to the horizontal thrust, per unit length of circumference, acting radially at the support. If the overpressure is expressed as a unit vertical line load acting at the edge of the support, then a coefficient of friction can be obtained by dividing the unit thrust by the unit vertical load.

Plate-reinforced models require an additional assumption, since no strain gage was placed on the tension plate in the zone over the support. Gamble used model slab K-6, a bar-reinforced slab, as a

reference, and assumed that the ratio of the coefficient of friction in a plate-reinforced slab to that of slab K-6 would be equal to the ratio of total thrusts for the three interior zones. Friction coefficients were computed for model slabs K-6 and K-8 at four load levels. Friction coefficients ranging from 0.36 to 0.6 for K-6 and from 0.3 to 0.38 for K-8 were found. The results are plotted versus applied load in Fig. 6.1.

The writer has extended Gamble's method and programmed it for computer solution. In the writer's method the strains are assumed to vary continuously from gage to gage. A third-degree curve is fitted to the four strain readings from the compression steel and the four strain readings from the tension bars of a bar-reinforced slab. A second-degree curve is fitted to the three circumferential strains registered by the tension gages of a plate-reinforced slab. The stress-strain curve for the steel is elasto-plastic and the concrete stress-strain curve is the parabola recommended by Hognestad (22). Strains are assumed to vary linearly across the height of the section. The computational procedure is the same as Gamble's, except that the "tributary areas" can be made as narrow as is desired.

Friction coefficients computed for slabs K-6 and K-8 using the writer's techniques are shown in Fig. 6.2. The agreement with Gamble's results is reasonably good. The friction coefficients found range from 0.45 to 0.7 for K-6 and from 0.17 to 0.52 for K-8. The dashed portion of the K-8 plot indicates that the computed thrusts are too low by an unknown amount. The curve fitting procedure predicted strains of the

same sign (top and bottom) at a section near the edge of the slab. The program recognizes and reports this situation but cannot handle it.

6.3. Bearing Capacity

The average bearing stress at maximum load, normalized in terms of f'_c , is listed in Table 6.1 for each slab tested. The average stress is found by Eq. (3.5) to be 2.65 times the applied load. (For slabs J-5, J-6, and J-8, the bearing stress was 2.35 times the applied load.)

The normalized bearing stress was greater than unity for many of the slabs. Bearing capacity failures were observed in all six of the 4.47-in. and 5.47-in. thick G-Series slabs. The average normalized bearing stress for the group of six models was at least 1.28. Similar values were obtained for K-5, K-6, K-13, G-3 and G-11, but no bearing distress was observed in these 3.68-in. thick slabs. Of the latter group, all but G-3 contained shear reinforcement.

The failure loads, slab thicknesses, average bearing stresses, cylinder strengths and normalized bearing stresses are tabulated below for each of the six slabs that suffered bearing failures.

Slab	Thickness in.	Applied Load At Bearing Failure psi	Bearing Stress f'_b psi	f'_c psi	Normalized Bearing Stress f'_b/f'_c
G-5	5.47	2800	7420	5600	1.33
G-6	4.47	2775	7350	5750	1.28
G-7	5.47	2800	7420	4670	1.59
G-8	4.47	3400	9010	7030	1.28
G-10	5.47	3350	8880	5500	1.61
G-12	5.47	3900	10330	5100	2.03

These results seem quite consistent. Slabs G-5, G-6 and G-8 contained no shear reinforcement and failed at normalized bearing stresses of 1.28 to 1.33. Slabs G-7 and G-10 each contained three rings of shear reinforcement, and the average normalized bearing stresses at failure were 1.59 and 1.61, respectively. Slab G-12 was provided with heavy shear reinforcement and a confining ring and failed at an average normalized bearing stress of 2.03.

The failure loads reported above for G-7, G-10 and G-12 are the loads at which bearing failure occurred. These three slabs each withstood slightly higher maximum loads.

There appears to be an enhancement of bearing capacity in those slabs where shear steel is present, but no explanation for this has been found. Model slabs G-7 and G-10 were also considerably stiffer (see Table 5.1) than G-5, suggesting greater friction between slab and support, and therefore higher confining stresses.

It is reasonable to expect bearing stresses greater than f'_c , since frictional restraining forces act on the lower surfaces of the slabs at the support. One would further expect the improvement in bearing capacity to increase as the ratio of slab thickness to the width of the bearing surface decreases. This appears to be the case, since slabs K-5, K-6, K-13, G-3 and G-11 resisted bearing stresses as high as those that caused failure in G-5, G-6 and G-8.

Based on the available test data, it is recommended for design purposes, where supplementary confinement is not provided, that bearing stresses be restricted to $1.25 f'_c$. For 5000-psi concrete and the support geometry considered in this study, this recommendation

limits the design overpressure to a maximum of 2360 psi. If a greater design overpressure is to be considered, then it is recommended that a confining ring be designed in accordance with the procedure described in Chapter 4, for the design of model G-12. The procedure is briefly restated:

- (1) Calculate the confining pressure (σ_3) needed to produce the additional bearing capacity required, using Richart's (21) formula for concrete in triaxial compression. The required increase in bearing capacity is

$$\Delta\sigma_1 = f_b - 1.25f'_c$$

where f_b is the total bearing stress required. From Richart's equation,

$$\Delta\sigma_1 = 4.1\sigma_3$$

Therefore, the required confining stress is

$$\sigma_3 = \frac{f_b - 1.25f'_c}{4.1}$$

The thickness of the hoop needed to provide the required confining pressure is given by

$$t = \frac{D_c}{8.2f_y} (f_b - 1.25f'_c) \quad (6.1)$$

Equation (6.1) requires a hoop 1-5/16 in. thick for an overpressure of 3000 psi ($f_b = 7950$) when $D_o = 228$ inches, $f_y = 36,000$ psi and $f'_c = 5000$ psi. It is recommended that the height of the hoop be made equal to the width of the bearing area.

6.4. Shear Strength

In Chapter 5 it was shown that the maximum loads resisted by slabs of equal depth, when normalized in terms of $\sqrt{f'_c}$, were reasonably constant. The consistency is believed due to the fact that the loads are actually multiples of the average shear stress at a given section, since the failures are shear failures. Gamble, et al, (1) explored this relationship in some detail for the K-Series and J-Series models. Average shear stresses, over the effective depth (d) and over the total thickness (t) of the section, were computed. Computations were made for sections at the support, at $d/2$ (or $t/2$) away from the support, and at d (or t) away from the support. The shear stresses at each section were normalized both in terms of the compressive stress, f'_c , and in terms of $\sqrt{f'_c}$. The computations have since been extended to include the G-Series of models. Tables 6.2 and 6.3 list shear stresses computed over sections t in thickness for all of the statically tested models.

Sections at $d/2$ or $t/2$ from the support were chosen in an attempt to find a "critical section." Presumably, sections at these locations cross the failure planes and may reflect the highest diagonal tension stresses. The writer has also computed average shear stresses at 1.83 in. from the support, a distance equal to half the thickness of the K-Series slabs. These computations were based on the observation that the diameter of the depressed portion of the upper slab surface appeared to remain approximately constant, regardless of the slab depth. This indicated that the slopes of the failure cracks depended on the span/thickness ratios of the slabs.

Since the average stresses normalized in terms of $\sqrt{f'_c}$ seemed more nearly constant than those expressed in terms of f'_c , two other exponents of f'_c were investigated. Coefficients of variation were calculated for each set of normalized stresses investigated, and these coefficients are tabulated below for comparison. Model slabs K-4, K-7, K-9, the randomly-reinforced models, the J-Series slabs, and models G-4 and G-12 were omitted from the calculations of these coefficients. The coefficient of variation of a set of numbers is defined as the standard deviation divided by the mean, and is a measure of the dispersion of the set.

Section Location	Section Thickness	Stresses Normalized in Terms of	Exponent "m"	Coefficient of Variation	Mean Value $\frac{v_u}{(f'_c)^m}$
At Support	t	$\sqrt{f'_c}$	0.5	0.096	26.5
At t/2	t	$\sqrt{f'_c}$	0.5	0.131	18.3
At 1.83"	t	$\sqrt{f'_c}$	0.5	0.096	19.2
At Support	t	f'_c	1.0	0.147	0.366
At 1.83"	t	f'_c	1.0	0.148	0.257
At Support	t	$(f'_c)^{0.4}$	0.4	0.099	62.8
At Support	t	$(f'_c)^{0.6}$	0.6	0.116	11.1

The stresses calculated at the support in terms of $\sqrt{f'_c}$ are as closely arrayed as any and have the added advantage of being simply found. Some of the dispersion in these numbers can be eliminated by taking into account the obvious difference in friction between the bar-reinforced models and plate-reinforced models. An equation of the form

$$\frac{v_u}{\sqrt{f'_c}} = Ae^{f_r} \quad (6.2)$$

where f_r is a "relative" friction factor, should account for differences in support friction. The writer chose $A = 12.4$, representing the average stress in a 3.68-in. slab with a load of 1000 psi applied. This implies a flexural failure at the design load when the friction vanishes. The observed shear stresses for bar-reinforced and plate-reinforced slabs were then averaged separately, and the ratio of the two averages was used to determine the difference between the friction coefficients. The magnitude of the friction coefficients was determined by the constant A and the average of the normalized stresses for one of the group of models. The resulting equations were

$$\begin{aligned} \frac{v_u}{\sqrt{f'_c}} &= 12.4e^{0.85} && \text{for bar-reinforced slabs} \\ \frac{v_u}{\sqrt{f'_c}} &= 12.4e^{0.73} && \text{for plate-reinforced slabs} \end{aligned} \quad (6.3)$$

Shear stresses normalized in terms of $\sqrt{f'_c}$ and Ae^{f_r} were found to have a coefficient of variation of only 0.08. A still further improvement would be obtained by substituting a function of slab thickness for the constant A . However, without a better basis for assigning values of f_r , and without some physical justification for the form of the equation, further refinement would be a meaningless algebraic exercise.

A more acceptable expression can be found by considering more of the variables that appear to affect the shear strength. The span/thickness ratio, L/t , would be expected to be a factor, and Fig. 6.3 shows that a relation between the normalized shear stress and the L/t ratio exists. Figure 6.4 indicates that the ultimate shear stress is governed in part by the amount of flexural reinforcement provided. The steel is believed to act as shear reinforcement and/or as a tensile membrane to provide this enhancement.

The reliability of the yield-line method of analysis has been confirmed for slabs of normal proportions. Hence, an expression for the shear strength of the deep slabs of interest might be found by starting with the yield-line analysis. By equating the expressions for yield moment (Eq. 3.1) and resistance moment (Eq. 3.2) we can obtain an expression for allowable (yield) load

$$w = \frac{24f_y p j d^2}{L^2} \quad (6.4)$$

where L is the clear-span diameter. The average shear stress on a section at the edge of the support is

$$v_u = \frac{wL}{4d} \quad (6.5)$$

and, by substitution, and letting $j = 0.9$, we obtain

$$v_u = \frac{5.4 p f_y}{(L/d)} \quad (6.6)$$

Equation 6.6 predicts an average shear stress at the support based on the yield-line analysis. This equation will be used as a framework, in the discussion that follows, for the derivation of a formula to fit the observed data. Since the exercise is empirical, and since the slab thickness and the effective depth are nearly identical for most of the models tested, the span/thickness ratio (L/t) will be substituted for the span/depth ratio (L/d) in the remainder of the discussion. The average shear stresses considered are those over the full thickness of the section, t , rather than those averaged over the effective depth. Shear stresses for slabs K-4, J-1 and J-2, which were omitted from the computation of coefficients of variation, are included in the data considered in the following paragraphs.

The basic equation (Eq. 6.6) was altered in a series of steps in order to find a normalizing function which would reduce the dispersion of the normalized data. The constants carried forward or introduced in these steps have no meaning other than to make the numbers manageable. The steps taken are now described.

The shear stresses observed in the test specimens were divided by those predicted by the Eq. (6.6) and the quotients were normalized by dividing by $\sqrt{f'_c}$. The normalized results appear in Column 4 of Table 6.4. The figures thus obtained show a marked inconsistency for different L/t ratios. Therefore, each number in Column 4 was divided by $\sqrt{L/t}$. The results, listed in Column 5, are better correlated than the Column 4 figures, but an inconsistency remains. Values shown for K-4, J-1 and J-2, which had the lowest steel content of all the models tested, are considerably higher than those of the

other plate-reinforced slabs. To improve the dependence on steel content, the Column 5 entries were multiplied by $10\sqrt{p}$ and the products were entered in Column 6. The coefficient of variation for the Column 6 array is 0.123.

The steps described above suggest an equation of the form

$$v_u = C \frac{f_y \sqrt{pf'_c}}{\sqrt{L/t}} \quad (6.7)$$

where C is a constant. Equation (6.7) includes all of the parameters expected to be important except the friction between slab and support. In order to determine the magnitude of the constant the steps were repeated, as shown in Table 6.5. The shear stresses were multiplied by $1000\sqrt{L/t}/f_y\sqrt{pf'_c}$. The average value of "C" was found to be 9.24, and the coefficient of variation for the numbers shown in Column 4 of Table 6.5 is 0.119. The slight improvement over the coefficient for Table 6.4 is attributed to the elimination of two steps of computation, and attendant round-off errors, and to the use of more precise figures for f_y and p.

The shear strength of the model slabs can now be expressed by the formula

$$v_u = (0.00924 \pm n\sigma) \times f_y \frac{\sqrt{pf'_c}}{\sqrt{L/t}} \quad (6.8)$$

where $n\sigma$ is an error term, expressed as a multiple of the standard deviation. The normalized shear stress, $1000 v_u/f_y\sqrt{pf'_c}$, is plotted versus L/t in Fig. 6.5. Equation (6.8) is shown as a solid line and

confidence limits of σ and 2σ are represented by dashed lines. All of the available test results are bounded by a line representing a deviation of 1.5σ below the mean. A conservative design expression is then

$$v_u = 0.0076 \epsilon_y \sqrt{\frac{pf'_c}{L/t}} \quad (6.9)$$

It is now desirable to determine whether the present expression (Eq. 6.8), which was originally based on a yield-line analysis, will still produce satisfactory results for thin slabs. We can do this by equating Eq. (6.8) (without the $n\sigma$ term) and (6.6) (in terms of L/t) and solving for the span/thickness ratio at which they are equal. We obtain the expression

$$L/t = 342,000 p/f'_c \quad (6.10)$$

which, for $f'_c = 5000$, $p = 0.02$, gives $L/t = 1.37$. At higher span/thickness ratios the two equations (6.6 and 6.8) will diverge considerably. Therefore, Eq. (6.8) cannot be expected to give dependable results as L/t is increased to the point that flexural strength becomes critical.

Another check that can be performed is to compare the shear strengths of these slabs, as represented by Eq. (6.8), with the shear strengths of deep beams. Albritton (8) has proposed the simple formula

$$v_u = f'_c/(L/d) \quad (6.11)$$

for the average ultimate shear stress at the support of a simply-supported, uniformly loaded deep beam. If this expression is equated to Eq. (6.8) (without the error term) we obtain, for $L/t = L/d$,

$$L/t = \frac{11,700f'_c}{pf_y^2} \quad (6.12)$$

For $f'_c = 5000$, $p = 0.02$ and $f_y = 40,000$, the two expressions agree at $L/t = 1.83$. Using Eq. (6.9) rather than Eq. (6.8), the curves will intersect at a higher L/t , and if p is taken as 0.01, then L/t becomes 5.45. Thus, comparable results are obtained for the span/thickness ratios of interest in this study, as would be expected.

It would be possible to "polish" Eq. (6.8) a bit more by adding a term to account for differences in support friction, as was discussed earlier. Such a refinement, even if it could be physically justified, would not lead to a more economical design expression, however, since prototype closures will probably be supported on steel-to-steel interfaces. Similarly, a better fit to the data might be obtained by adjusting the exponents of p and L/t in Eq. (6.8), but the number of available data points at L/t ratios other than 3.5 are too few to justify such adjustments.

6.5. Ductility

It was shown in Chapter 3 that the ratio P_m/Q_y is a function of both the ductility ratio, μ , and the ratio t_d/T , where t_d is the duration of an initially peaked triangular pressure pulse. P_m is the peak value of the loading function and Q_y is the yield resistance of an assumed elasto-plastic resistance function. Table 3.1 lists values of P_m/Q_y for three values of t_d/T and for ductilities from 1.3 to 15.

The model structures tested in this program did not, as a general rule, exhibit perfect elasto-plastic behavior. The real load-deflection curves were, however, idealized as elasto-plastic curves in the method described in Chapter 5 for computing relative ductilities. In the discussion that follows we will let Q_y represent the "apparent yield load" defined in Chapter 5, and Q_m represent the maximum load. Values of the ratio Q_y/Q_m , also defined in Chapter 5, and the ductility, μ , are listed in Table 5.1.

One expects a relation to exist between the ratio Q_y/Q_m and the ductility μ . It can be shown, in fact, that if the load-deflection curve is parabolic, the ductility can be found from the expression

$$\mu = \frac{1 + \sqrt{\frac{1 - Q_y}{Q_m}}}{1 - x_0 - \sqrt{\frac{1 - 2Q_y}{Q_m}}} \quad (6.13)$$

where x_0 is the arbitrary offset, taken as 0.01 in. in Chapter 5.

The values of μ and of Q_y/Q_m from Table 5.1 are plotted in Fig. 6.6. The data are well-behaved and seem to obey a simpler relation than that indicated by Eq. (6.13). A good representation of the data is given by

$$\frac{Q_y}{Q_m} = \mu^{-0.12} \quad (6.14)$$

The values of P_m/Q_y from Table 3.1 are shown as dashed lines on Fig. 6.7 for each of the three values of t_d/T . The real points cannot be connected by straight lines of normal width, but good

approximations for the range $2 < \mu < 10$ are obtained by the expressions

$$\begin{aligned} P_m/Q_y &= 1.42\mu^{0.547} & \text{for } t_d/T = 0.3 \\ P_m/Q_y &= 0.78\mu^{0.301} & \text{for } t_d/T = 1.4 \\ P_m/Q_y &= 0.72\mu^{0.120} & \text{for } t_d/T = 80 \end{aligned} \quad (6.15)$$

The peak dynamic load, P_m , can now be related to the observed maximum static resistance, Q_m , by combining Eq. (6.14) with each of Eq. (6.15). The resulting expressions are

$$\begin{aligned} P_m/Q_m &= 1.42\mu^{0.427} & \text{for } t_d/T = 0.3 \\ P_m/Q_m &= 0.78\mu^{0.181} & \text{for } t_d/T = 1.4 \\ P_m/Q_m &= 0.72 & \text{for } t_d/T = 80 \end{aligned} \quad (6.16)$$

Equations (6.16) are plotted as solid lines on Fig. 6.7. The model test results have demonstrated that ductilities in the range 2-10 for which Eqs. (6.15) are valid can be dependably obtained. When t_d/T is reasonably well known, Eqs. (6.16) may be used to select P_m/Q_m . When t_d/T is not well known, conservatism will require the use of the lower bound $P_m/Q_m = 0.72$.

6.6. Confinement

The beneficial effects of confining the concrete in a closure slab against lateral expansion have been demonstrated repeatedly in the model test series, though not always intentionally. Partial confinement by frictional restraint on the bearing surface is believed responsible for the high bearing stresses observed in many of the tests. The "second peaks" obtained in the tests of the randomly-reinforced

slabs and several of the G-Series models are due to confinement in the relatively rigid test device. The added load capacity of model slab G-12, as compared to, say, G-10, was about equal to that predicted in the calculations described in Chapter 4.

The model tests described in this report probably represent the upper limit to the loads that can be obtained with unconfined closure structures. The attainment of higher maximum loads may require the use of confining rings either to prevent failure of the concrete in the structure, or to limit the outward thrust on the supporting structure, or both.

It is probable that leakage of the blast overpressure around the edges of the closure will provide enough confining force to greatly improve its strength. A system of seals adequate to keep the pressure out is difficult to envision. The effect of confinement by the blast pressure has not been investigated and no additional strength will be assigned to the structure because of it. Some additional factor of safety should exist because of this effect.

6.7. Recommended Design Procedure

Equation (6.9) is recommended for the computation of maximum shear stress at the support from a statically applied load. Equation (6.9) forms a lower bound to all the data used in deriving it, i.e., data from 24 of the 34 models tested. The applied static overpressure load which will produce the shear stress given by Eq. (6.9) is

$$w = 0.0304f_y \sqrt{pf'_c} / (L/t)^{1.5} \quad (6.17)$$

The design dynamic load may be taken equal to the static load if we let the ductility $\mu = 4$ and apply the second of Eqs. (6.16), for $t_d/T = 1.4$. This suggests a period of, say, 10 milliseconds and an effective duration, t_ω , of about 15 milliseconds, as would be expected from a weapon of one megaton yield.

The lower bound for the dynamic load, found from the last of Eq. (6.16), is taken as 72 percent of the static maximum.

$$w_{\text{minimum}} = 0.021f_y \sqrt{pf'_c} / (L/t)^{1.5} \quad (6.18)$$

Equation (6.17), with the stipulation suggested in Section 6.3, that the bearing stress be limited to $1.25f'_c$ or that additional confinement be provided, form the writer's recommendations for design of closure slabs. A conservative approach has been taken throughout in arriving at Eq. (6.17). Even so, its use is recommended only for the conditions for which it was derived. All of the models tested were under-reinforced, with steel ratios no greater than about two percent. The span/depth ratios varied only from 2.35 to 5.6. Most importantly, appreciable restraint was provided by friction between the slab and its support.

This concludes the discussion of the test results. The conclusions are summarized and recommendations for further study are presented in the next chapter.

TABLE 6.1. BEARING STRESSES AT FAILURE*

Slab No.	Bearing Stress/ f'_c	Slab No.	Bearing Stress/ f'_c
K-1	1.11	J-1	0.38
K-2	1.01	J-2	0.31
K-3	0.99	J-5	0.24
K-4	0.86	J-6	0.24
K-5	1.27	J-8	0.30
K-6	1.22	G-1	0.85
K-7	1.04	G-2	0.94
K-8	1.19	G-3	1.38
K-9	1.13	G-4	0.95
K-10	0.96	G-5	1.33
K-11	1.08	G-6	1.28
K-12	0.98	G-7	1.61
K-13	1.22	G-8	1.28
K-14	0.88	G-9	1.16
K-15	0.52	G-10	1.59
K-16	0.48	G-11	1.29
K-17	0.55	G-12	2.03

* The bearing stress at the maximum load reached is tabulated for slabs that were not actually failed.

TABLE 6.2. ULTIMATE SHEAR STRESSES ON SECTION t IN THICKNESS, K AND J-SERIES MODELS

$$v_u = V_u / b_o t$$

Slab	At Support			At $t/2$ Away			At t Away		
	v_u psi	$\frac{v_u}{f'_c}$	$\frac{v_u}{\sqrt{f'_c}}$	v_u psi	$\frac{v_u}{f'_c}$	$\frac{v_u}{\sqrt{f'_c}}$	v_u psi	$\frac{v_u}{f'_c}$	$\frac{v_u}{\sqrt{f'_c}}$
K-1	2150	0.366	28.1	1530	0.261	20.0	920	0.157	12.0
K-2	2140	0.334	26.8	1520	0.237	19.0	915	0.143	11.4
K-5	2370	0.420	31.5	1690	0.299	22.5	1015	0.180	13.5
K-6	2020	0.401	28.5	1440	0.286	20.3	865	0.172	12.2
K-13	2290	0.405	30.5	1620	0.287	21.6	975	0.173	13.0
K-3	1880	0.329	24.8	1340	0.234	17.7	805	0.141	10.6
K-14	1890	0.288	23.3	1350	0.206	16.7	810	0.123	10.0
K-8	1880	0.392	27.1	1340	0.279	19.3	805	0.168	11.6
K-12	1920	0.322	24.9	1370	0.230	17.7	825	0.138	10.7
K-10	1890	0.316	25.7	1350	0.226	18.3	810	0.136	10.5
K-11	1450	0.358	22.8	1030	0.254	16.2	620	0.153	9.7
K-4	1510	0.287	20.8	1080	0.206	14.9	650	0.124	9.0
J-1	1100	0.199	14.8	900	0.163	12.1	705	0.127	9.5
J-2	1010	0.161	12.8	820	0.132	10.4	650	0.104	8.2
J-5	780	0.140	10.5	640	0.115	8.6	490	0.088	6.6
J-6	820	0.142	10.8	670	0.116	8.8	525	0.091	6.9
J-8	935	0.176	12.8	765	0.144	10.5	595	0.112	8.2

TABLE 6.3. ULTIMATE SHEAR STRESSES ON SECTION t IN THICKNESS, G-SERIES MODELS

$$v_u = V_u / b_o t$$

Slab	w_u	f'_c	$\sqrt{f'_c}$	At Support			At $t/2$ Away			At t Away		
				v_u	$\frac{v_u}{f'_c}$	$\frac{v_u}{\sqrt{f'_c}}$	v_u	$\frac{v_u}{f'_c}$	$\frac{v_u}{\sqrt{f'_c}}$	v_u	$\frac{v_u}{f'_c}$	$\frac{v_u}{\sqrt{f'_c}}$
G-1	2280	7050	84.0	1990	.282	23.8	1420	.202	16.95	850	.121	10.15
G-2	2175	6130	78.5	1900	.311	24.2	1360	.222	17.3	812	.133	10.35
G-3	1575	3030	55.1	1380	.455	25.1	980	.324	17.8	590	.194	10.7
G-4	1940	5400	73.5	1142	0.212	15.5	660	0.122	9.0	177	0.033	2.41
G-5	2800	5600	74.8	1650	.295	22.1	955	.170	12.8	255	.0445	3.42
G-6	2775	5750	75.8	2000	0.348	26.4	1315	0.231	17.4	620	0.108	8.17
G-7	2925	4670	68.4	1725	0.369	25.3	995	0.213	14.4	266	0.057	3.89
G-8	3400	7030	84.0	2450	0.349	29.2	1610	0.229	19.2	760	0.108	9.05
G-9	2300	5250	72.5	2010	.384	27.8	1435	0.274	19.8	860	0.164	11.8
G-10	3300	5500	74.2	2005	.365	27.0	1155	.210	15.6	296	.0535	3.99
G-11	2480	5100	71.5	2170	.425	30.4	1550	.304	21.7	948	.186	13.25
G-12	4100	5100	71.5	2420	.475	33.9	1390	.273	19.5	359	.075	5.02

TABLE 6.4. ULTIMATE SHEAR STRESSES AT SUPPORT
IN TERMS OF p , L/t AND $\sqrt{f'_c}$

Slab No.	(1) v_u At Support	(2) $\frac{5.4pf_y}{(L/t)}$	(3) $\frac{v_u}{(5.4pf_y/L/t)}$	(4) $\frac{100}{\sqrt{f'_c}} \left(\frac{v_u}{5.4pf_y/L/t} \right)$	(5) $\frac{(4)}{\sqrt{L/t}}$	(6) $(5) \times 10 \sqrt{p}$
K-1	2150	1010	2.13	2.78	1.49	1.89
K-2	2140	1010	2.12	2.65	1.42	1.80
K-3	1880	1110	1.69	2.23	1.19	1.52
K-4	1510	420	3.60	4.97	2.66	2.15
K-5	2370	1010	2.35	3.12	1.67	2.12
K-6	2020	1010	2.0	2.82	1.51	1.91
K-8	1880	1110	1.69	2.44	1.31	1.68
K-10	1890	870	2.17	2.81	1.50	1.75
K-11	1450	870	1.67	2.62	1.40	1.63
K-12	1920	1110	1.73	2.24	1.20	1.54
K-13	2290	1010	2.27	3.02	1.61	2.04
K-14	1890	1110	1.70	2.10	1.12	1.43
J-1	1100	360	3.06	4.11	1.73	1.77
J-2	1010	360	2.81	3.55	1.50	1.53
G-1	1990	1110	1.79	2.14	1.14	1.46
G-2	1900	1110	1.71	2.18	1.17	1.50
G-3	1555	1110	1.40	2.54	1.36	1.74
G-5	1650	1195	1.38	1.85	1.21	1.42
G-6	2000	1550	1.29	1.73	1.02	1.49
G-7	1725	1195	1.44	2.11	1.38	1.62
G-8	2450	1550	1.58	1.88	1.11	1.63
G-9	2010	1110	1.81	2.50	1.34	1.72
G-10	2005	1550	1.29	1.74	1.14	1.51
G-11	2170	1210	1.71	2.39	1.28	1.85

Avg. of Col. 6 = 1.70
 Std. Dev. = 0.209
 Coeff. of Variation = 0.123

TABLE 6.5. ULTIMATE SHEAR STRESSES AT SUPPORT
 IN TERMS OF \sqrt{p} , $\sqrt{(L/t)}$ and $\sqrt{f'_c}$

Slab No.	(1) v_u At Support	(2) $\sqrt{pf'_c}$	(3) $\frac{1000 v_u}{f_y \sqrt{pf'_c}}$	(4) $\frac{1000 v_u \sqrt{L/t}}{f_y \sqrt{pf'_c}}$
K-1	2150	9.70	5.40	10.08
K-2	2140	10.10	5.17	9.65
K-3	1880	9.70	4.42	8.25
K-4	1510	5.85	6.15	11.50
K-5	2370	9.50	6.10	10.40
K-6	2020	9.00	5.48	10.23
K-8	1880	8.90	4.80	8.95
K-10	1890	9.00	5.07	9.45
K-11	1450	7.40	4.73	8.83
K-12	1920	9.90	4.42	8.25
K-13	2290	9.50	5.90	11.00
K-14	1890	10.40	4.14	7.74
J-1	1100	7.60	4.02	9.53
J-2	1010	8.05	3.48	8.25
G-1	1990	10.57	4.84	9.04
G-2	1900	10.05	4.85	9.05
G-3	1555	7.05	5.66	10.57
G-5	1650	8.75	4.97	7.60
G-6	2000	11.10	4.56	7.75
G-7	1725	8.00	5.68	8.68
G-8	2450	12.30	5.03	8.55
G-9	2010	9.30	5.55	10.36
G-10	2005	9.83	5.17	7.90
G-11	2170	10.3	5.55	10.36

Avg. of Col. 4 = 9.24
 Std. Dev. = 1.1
 Coeff. of Variation = 0.119

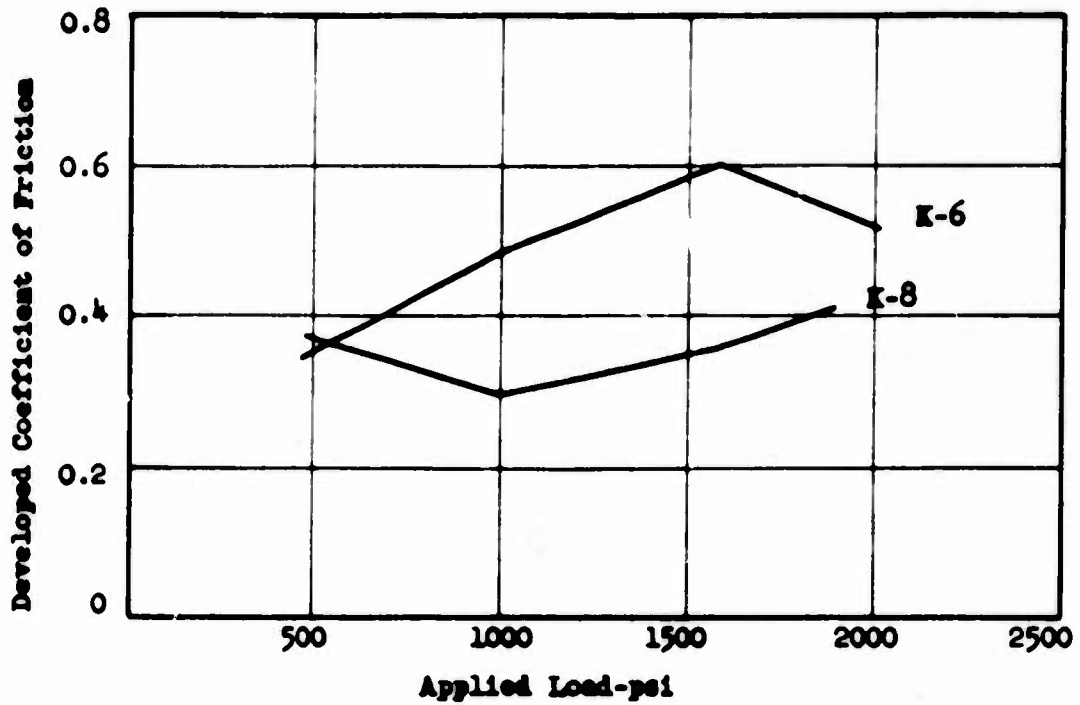


Fig. 6.1 Variation of Support Friction with Load (Gamble's Method)

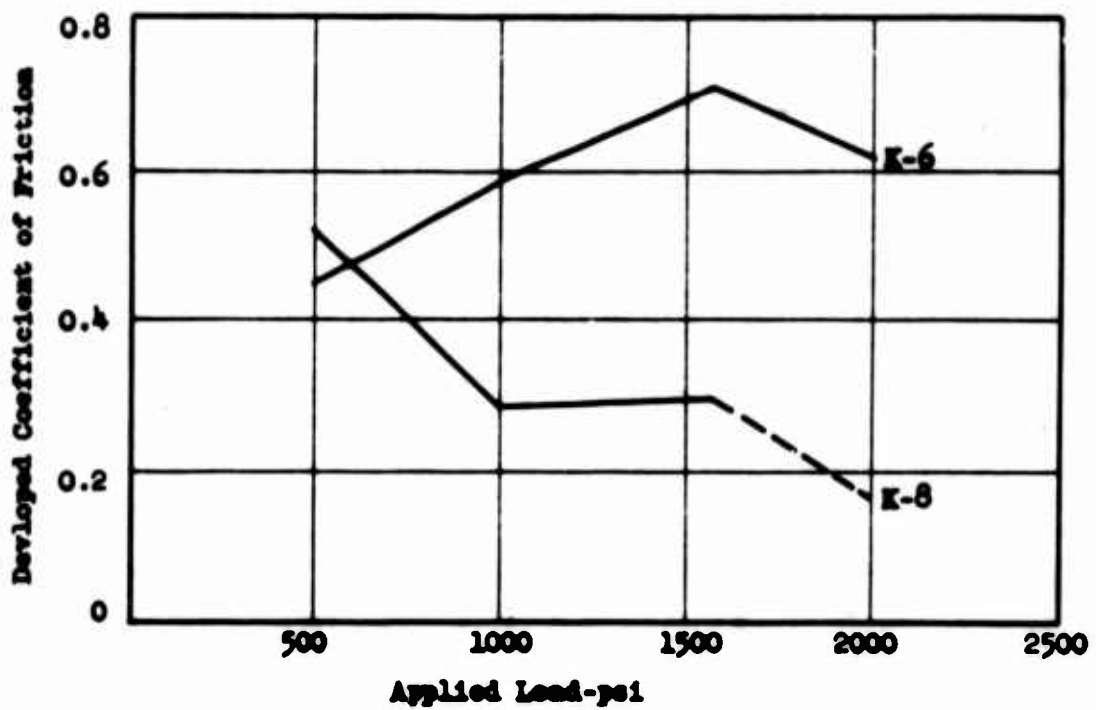


Fig. 6.2 Variation of Support Friction with Load (Iten's Method)

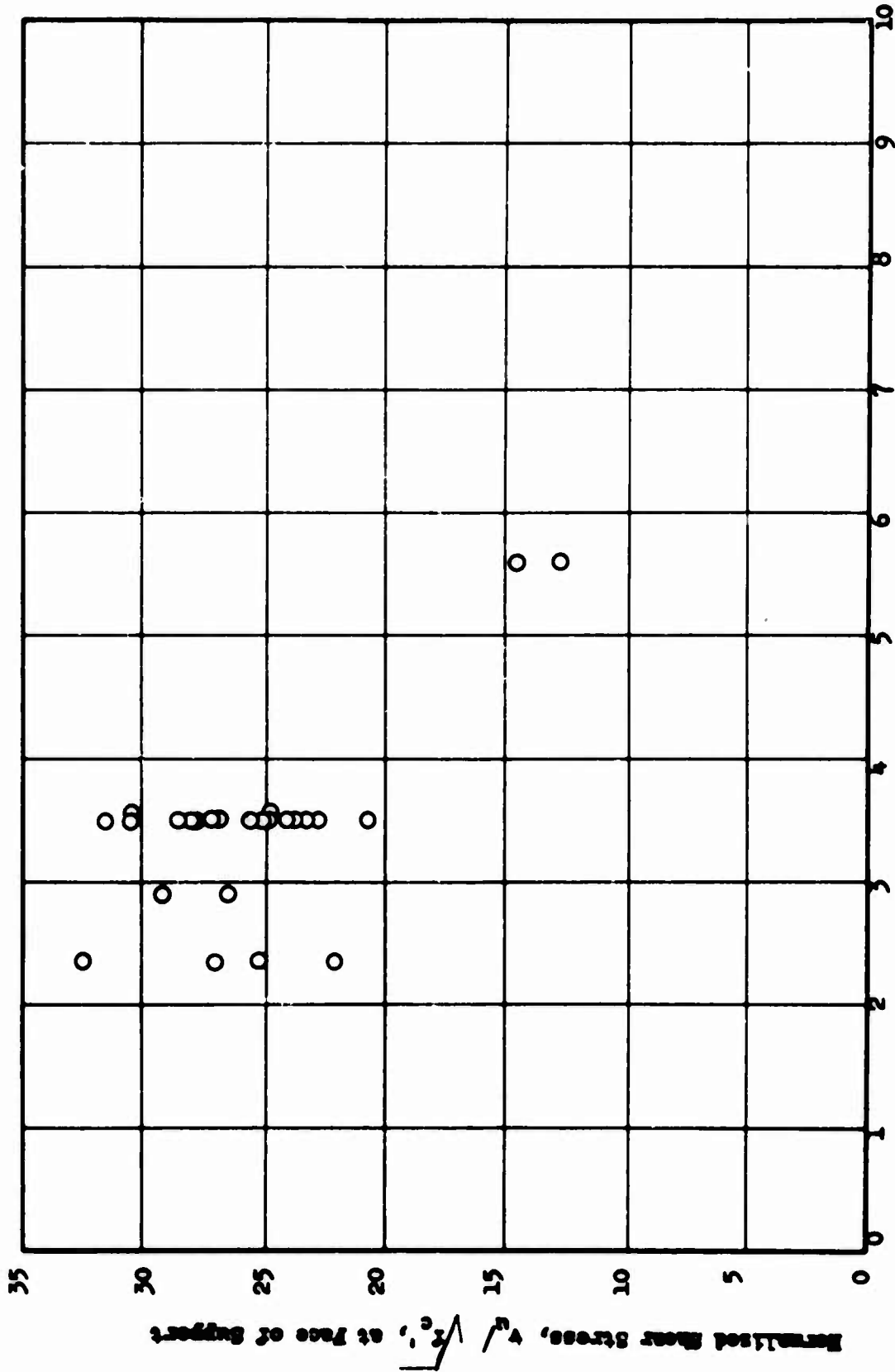


Fig. 6.3 Variation of Normalized Shear Stress with Span/Thickness Ratio

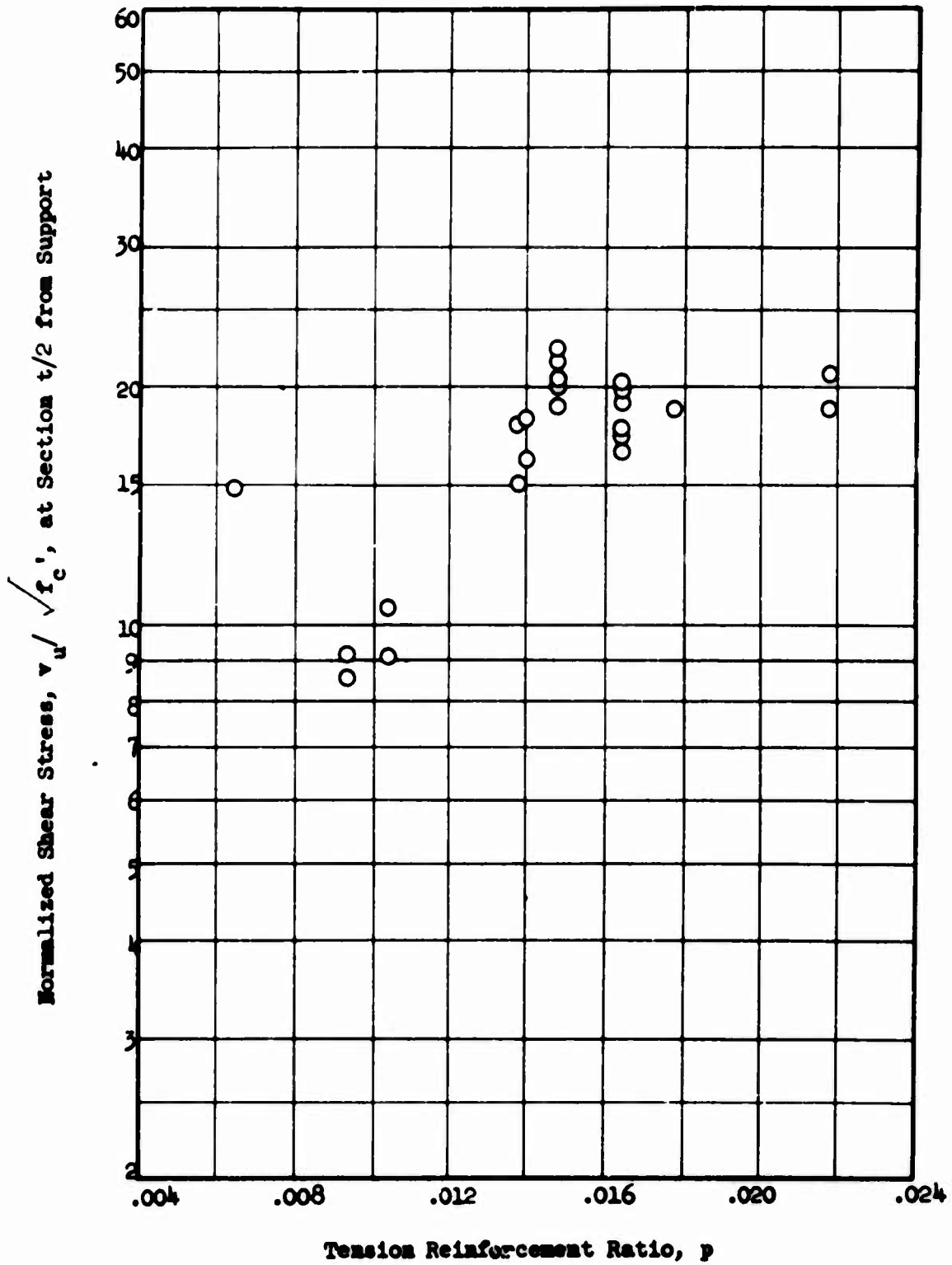


Fig. 6.4 Variation of Normalized Shear Stress with Reinforcement Ratio

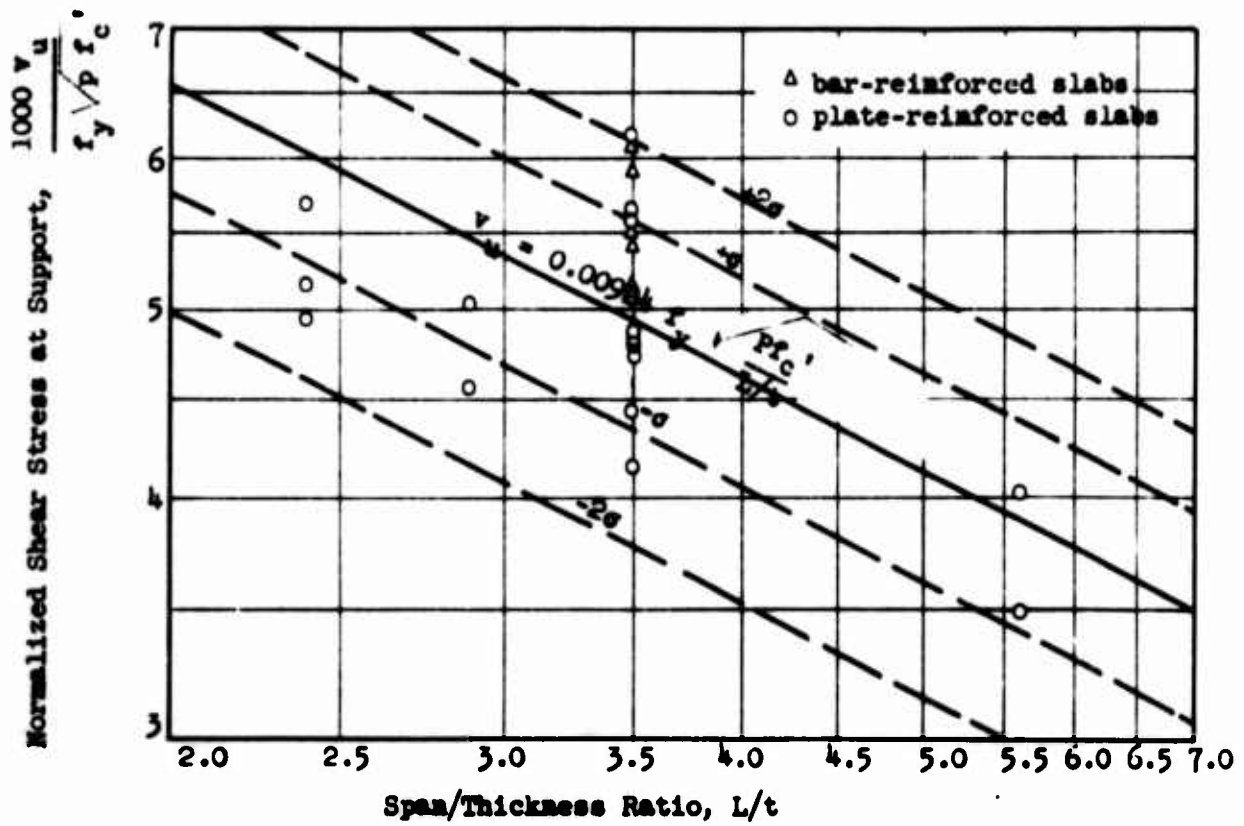


Fig. 6.5 Ultimate Shear Stress vs. Span/Thickness Ratio

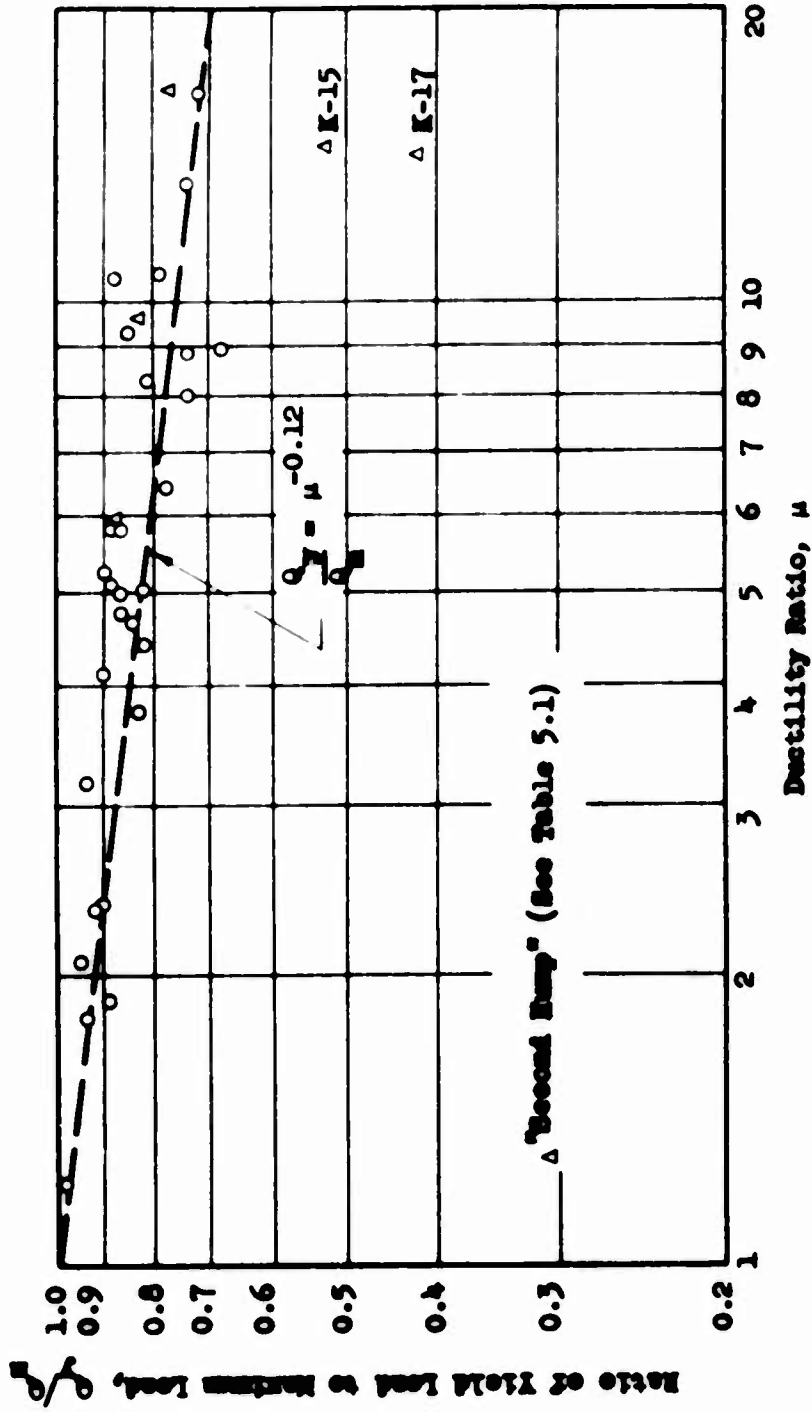


Fig. 6.6 Variation of Q_y/Q_m with Ductility in Model Test Series

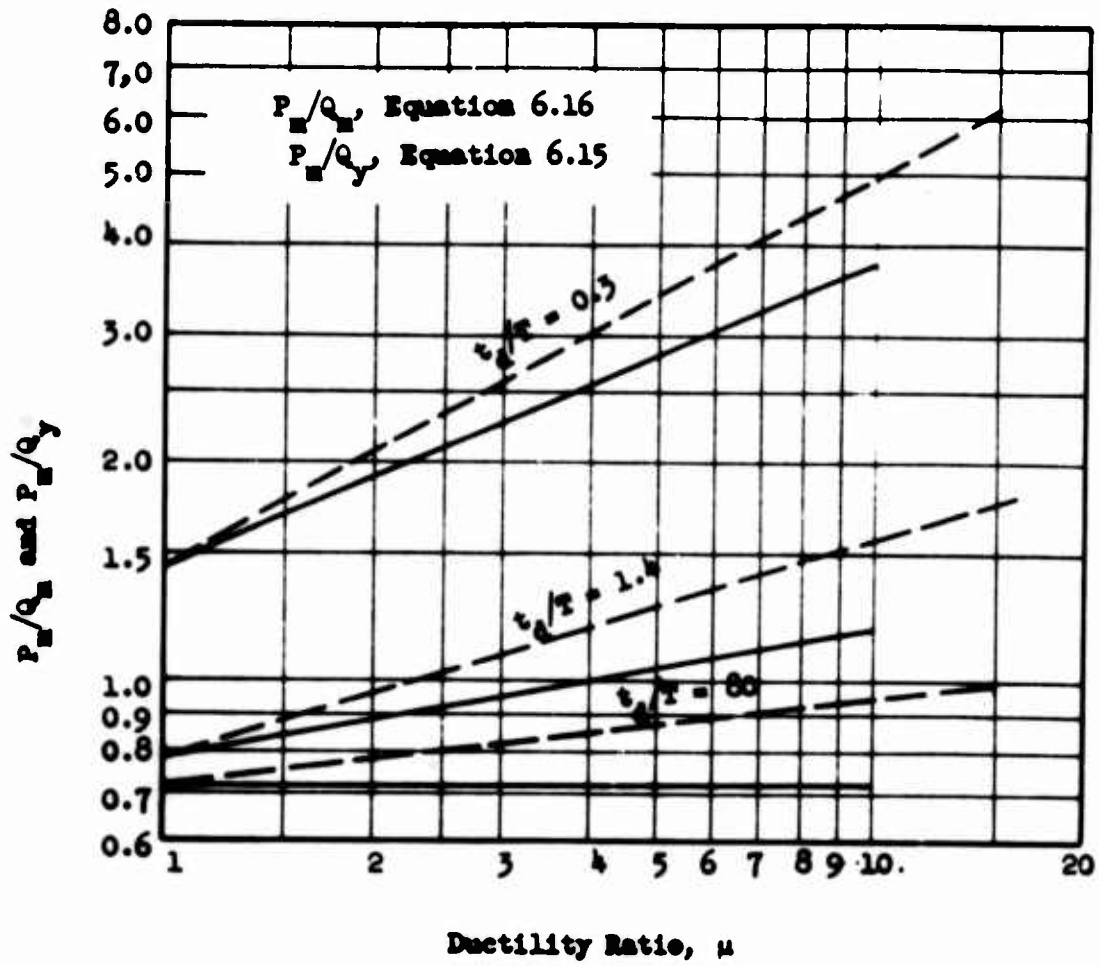


Fig. 6.7 Variation of P_m/Q_m with Ductility

CHAPTER 7

CONCLUSIONS AND RECOMMENDATIONS

7.1. Conclusions

From the results of the model tests described and discussed in this report, one can conclude that it is entirely feasible to build missile silo closures with a high probability of surviving blast overpressures of 1000 and 2000 psi. In fact, it appears that significantly higher overpressures can be resisted by reinforced concrete slabs.

Composite slabs reinforced with steel tension plates are completely satisfactory and exhibit more ductility than bar-reinforced structures. Thus, the steel plates required for EMP protection (see Chapter 2) can be made to do double duty as structural reinforcement.

The addition of shear reinforcement to either plate or bar reinforced slabs adds ductility, though the amount of ductility added cannot be related to the amount of shear steel provided, based on the results of these tests.

The ductility required to resist dynamic loads can be provided by plate-reinforced slabs with or without shear reinforcement or by bar-reinforced slabs with shear reinforcement.

The enhancement of flexural resistance by friction forces acting on the lower surface of the slab has been demonstrated in the test series and can be theoretically explained. Because of this enhancement of flexural resistance, slabs of the proportions considered in this program will generally fail in shear or in bearing.

Lateral restraint of closures slabs appears to improve both their bearing capacity and shear strength, as well as improving flexural resistance. Steel rings, or hoops, can be successfully used to increase the lateral restraint and load-carrying capacity.

7.2. Recommended Additional Tests

An additional series of static model tests is recommended, in order to confirm the conclusions of this study and to gain a still better understanding of thick slab behavior. All are to be conducted in the existing 1/14th scale test fixture. Several areas of investigation are proposed. They are: (1) A variational study of the material property and geometric parameters of Eq. (6.17), in order to confirm the equation. (2) An investigation of shear stud requirements. (3) An examination of the effect of base restraint on slab behavior. (4) A determination of the relation between shear steel and ductility. (5) An examination of the bearing strength of thick slabs.

The list above suggests eight parameters, including four for item (1). If each parameter were allowed to take on three values, all of the possible combinations could be represented by about 6500 models. The program proposed here is somewhat less comprehensive, though a fairly large number of tests is still proposed.

Only plate-reinforced models need to be tested. Therefore, the examination of shear stud behavior should be given priority, as this could lead to economy in later prototype construction. A series of tests on prisms attached by shear studs to greased steel plates should precede, and govern the design of the model tests. Twenty-four

prism tests, comprising three variations of concrete strength, four variations of stud diameter and two stud lengths are suggested. Three additional specimens will be required to demonstrate repeatability at one combination of stud diameter, stud length and concrete strength. A similar program involving prototype-size specimens should also be considered.

A series of eight model slab tests is recommended to apply the information gained from the prism tests. Two values of the ratio of diameters (D_o/D_i) should be employed to determine the effect of clamping due to the overhang on the need for shear studs. One combination of shear stud length and diameter is recommended, to be tested in these four configurations: (1) Optimum number (from results of prism tests) with ungreased plate, (2) Optimum number with greased plate, (3) Fifty percent of optimum number with ungreased plate, and (4) No shear studs at all (except a few for attachment) with an ungreased plate. A high L/t ratio is suggested for this test series. It is believed that the number of shear studs required in tests to follow might be reduced as a result of the tests just described.

A series of tests to determine the effect of material and geometrical properties is proposed. The parameters to be investigated and the number of variations suggested for each are: (1) The span/thickness ratio, L/t (four values), (2) the tension reinforcement ratio, p (three values), (3) the concrete strength, f'_c (three values), and (4) the yield strength of the reinforcing steel, f_y , (three values). Table 7.1 shows all the possible combinations, which total 108. A suggested series of twenty-four tests, comprising five casts of four

models each, is indicated, by letters identifying the casts, on the table. One combination is circled, to show that an additional cast of four identical models of that configuration is required for control. Additional control casts may be needed to differentiate between the effects of parameter variation and normal scatter in the results.

The form of Table 7.1 can be extended to show combinations of the material properties with variations in base restraint, shear reinforcement and bearing configuration. An additional 20-30 models may be required. It is recommended that base restraint be varied by the use of ball bearings (on special bearing rings, to prevent damage to the test fixture), glass filled Teflon^{*} bearing surfaces to reduce friction, and/or crushable bearing surfaces, such as plywood or hard-board. Shear reinforcement of the type used in models G-7 and G-10 is recommended, with careful attention to be given to weld quality.

A better understanding of the bearing strength of deep slabs might be gained by casting models of low L/t ratio with high-tensile-strength "micro-concrete" in an attempt to force the bearing strength to be critical. Other possibilities suggest themselves, such as the testing of thin models with and without confining rings on a narrow (low D_o/D_1), lubricated bearing area.

In order to conduct a large number of tests in a reasonable time period, some changes in fabrication and testing techniques will be required. It is recommended that compression reinforcement and supplementary tension bars (as in models G-6 and G-8) not be used.

* Trademark of the E. I. DuPont de Nemours Company.

Additional forms should be built so that specimens can be cast in groups of four. These changes, and some minor modifications to the loading fixture, its supporting stand and its auxiliary equipment can provide the additional efficiency needed for an expanded program of testing.

7.3. Analytical Study

An analytical study of the closure slab problem is recommended, to proceed concurrently with the experimental program suggested above. The finite-element approach to the numerical solution of the problem is believed to be a reasonable method, and one that is capable of representing the boundaries in a satisfactory manner. In order to be of value to the experimental effort, the computer program should be put into operation as soon as possible. Thus, it is recommended that no time be spent in either developing automatic problem-describing routines or in striving for the high degree of generality sought by many investigators.

TABLE 7.1. VARIATIONS OF MATERIAL PROPERTY AND GEOMETRIC PARAMETERS

Parameter No. 1 has 4 possible values. Parameters Nos. 2, 3 and 4 each have 3 possible values. (Letters indicate casts, at four models per cast. Circle indicates control specimen.)

1st Parameter, L/t		1			2			3			4		
		1	2	3	1	2	3	1	2	3	1	2	3
2nd Parameter, p		1	2	3	1	2	3	1	2	3	1	2	3
3rd Parameter, f' _c		1	2	3	1	2	3	1	2	3	1	2	3
4th Parameter f' _y	1st Value					D			D				
	2nd Value	E	C	A	E	C	A	B	C	A	B	C	A
	3rd Value					D			D				

LIST OF REFERENCES

1. Gamble, W. L., A. J. Hendron, J. H. Rainer and W. C. Schnobrich, "A Study of Launch Facility Closures," SAMSO-TR-67-15, November, 1967.
2. Ang, Alfredo H.-S., and Johann H. Rainer, "Model for Wave Motions in Axi-Symmetric Solids," Proc. ASCE, Vol. 90, EM2, April 1964, pp. 195-223.
3. Brotchie, John F., Amnon Jacobson and Sadaji Okubo, "Effect of Membrane Action on Slab Behavior," Massachusetts Institute of Technology Dept. of Civil Engineering, Report R65-25, August, 1965, 100 pages.
4. Gregory, R. K., R. C. DeHart, and W. J. Austin, "Response of Deep Reinforced Concrete Slabs," Air Force Weapons Laboratory Report WL-TDR-64-54, February, 1965, 138 pages.
5. Beadle, C. W., J. W. Dally and W. F. Riley, "Experimental Determination of the Rigidity and Load-Carrying Capacity of Circular Steel and Concrete Plates," IIT Research Institute Report, undated, 45 pages.
6. Menza, Thomas F., "Cadet Research - Missile Silo Closures," Air Force Civil Engineer, Vol. 8, No. 3, August, 1967, pp. 26-28.
7. Burgess, Danny N., unpublished notes, Department of Civil Engineering, U. S. Air Force Academy, Colorado, July-August, 1967.
8. Albritton, G. E., "Static Tests of Reinforced Concrete Deep Beams," Technical Report No. 1-676, U. S. Army Waterways Experiment Station, Vicksburg, Mississippi, June, 1965, 125 pages.
9. Albritton, "Review of the Literature Pertaining to the Analysis of Deep Beams," Technical Report No. 1-701, U. S. Army Waterways Experiment Station, Vicksburg, Mississippi, November, 1965, 80 pages.
10. dePaiva, H. A. R. and C. P. Seiss, "The Investigation of Deep Reinforced Concrete Beams Under Static and Dynamic Loading, Vol. II, Strength and Behavior in Shear," AFSWC-TR-61-47, July, 1961 (Also Civil Engineering Studies, Structural Research Series No. 231, Dept. of Civil Engineering, University of Illinois, Urbana), 252 pages.
11. dePaiva, H. A. R. and W. J. Austin, "Behavior and Design of Deep Structural Members, Part 3, Tests of Reinforced Concrete Deep Beams," AFSWC-TR-59-72, March 1960 (Also Civil Engineering Studies,

- Structural Research Series No. 194, Department of Civil Engineering, University of Illinois, Urbana), 126 pages.
12. Brode, H. L., "A Review of Nuclear Explosion Phenomena Pertinent to Protective Construction," Rand Corporation Report R-425-PR, May 1964, 65 pages.
 13. Newmark, N. M. and J. D. Haltiwanger, "Air Force Design Manual, Principles and Practices for Design of Hardened Structures," AFSWC-TDR-62-138, December, 1962.
 14. Glasstone, Samuel (ed.), "The Effects of Nuclear Weapons," rev. ed., U. S. Department of Defense, U. S. Atomic Energy Commission, April, 1962, 730 pages.
 15. Wood, R. H., "Plastic and Elastic Design of Slabs and Plates," The Ronald Press, New York, 1961, 344 pages.
 16. Casillas G. de L., Juan, N. Khachaturian and C. P. Siess, "Studies of Reinforced Concrete Beams Reinforced with Steel Plates," Civil Engineering Studies, Structural Research Series No. 134, University of Illinois, Urbana, 1957.
 17. Viest, Ivan M., "Investigation of Steel Shear Connectors for Composite Concrete and Steel T-Beams," Journal ACI, April, 1956, Proceedings Volume 52, p. 875-891.
 18. Melin, J. W., and S. Sutcliffe, "Development of Procedures for the Rapid Computation of Structural Response," Civil Engineering Studies, Structural Research Series No. 171, University of Illinois, Urbana, 1958.
 19. Timoshenko, S., "Vibration Problems in Engineering," 3rd Edition, D. Van Nostrand Co., Inc., 1955.
 20. Mattock, Allan H., "Structural Model Testing-Theory and Applications," Journal of the PCA Research and Development Laboratories, Vol. 4, No. 3, September, 1962, pp. 12-23.
 21. Richart, Frank E., Anton Brantzaeg and Rex L. Brown, "A Study of the Failure of Concrete Under Combined Compressive Stresses," Bulletin No. 185, Engineering Experiment Station, University of Illinois, November, 20, 1928.
 22. Hognestad, Eivind, "A Study of Combined Bending and Axial Load in Concrete Members," University of Illinois Engineering Exp. Sta. Bulletin No. 399, 1951.
 23. Agbabian, M. S., "Survival Requirements for Underground Structures," from class notes for UCLA Extension Course X430, "Design of Underground Protective Structures," University of California at Los Angeles, January 8, 1965.

Unclassified

Security Classification

DOCUMENT CONTROL DATA - R & D

Security classification of title, body of abstract and indexing annotation must be entered when the overall report is classified

1. ORIGINATING ACTIVITY (Corporate author) Department of Civil Engineering University of Illinois Urbana, Illinois		2a. REPORT SECURITY CLASSIFICATION Unclassified	
		2b. GROUP	
3. REPORT TITLE Behavior of Missile Silo Closures Designed to Resist High Overpressures			
4. DESCRIPTIVE NOTES (Type of report and, inclusive dates) Final Report			
5. AUTHOR(S) (First name, middle initial, last name) Robert M. Iten and William L. Gamble			
6. REPORT DATE March 1968		7a. TOTAL NO. OF PAGES 232	7b. NO. OF REFS 23
8a. CONTRACT OR GRANT NO. AF04-694-796		9a. ORIGINATOR'S REPORT NUMBER(S)	
b. PROJECT NO.		9b. OTHER REPORT NO(S) (Any other numbers that may be assigned this report)	
c.			
d.			
10. DISTRIBUTION STATEMENT Distribution of this document is unlimited			
11. SUPPLEMENTARY NOTES		12. SPONSORING MILITARY ACTIVITY Space and Missile Systems Organization Air Force Systems Command Norton Air Force Base, California	
13. ABSTRACT In this study of the strength and behavior of thick, simply supported circular slabs, the tests of 12 slabs representative of possible missile silo closures are described in detail. In addition, the results of 22 other tests are summarized. A design procedure leading to the required proportions of slabs which must resist given overpressures is outlined. In all of the tests, the models failed by a shear mode at loads considerably in excess of the flexural capacities predicted by means of a simple yield-line analysis. This discrepancy is traced to the development of very large compression forces in the plane of the slabs because of friction between the base of the slab and the supporting structure. Using the test data, an empirical relationship is developed relating the shear strength of such thick slabs to the strength of the concrete, the reinforcement ratio, the reinforcement strength, and the ratio of span to slab thickness. The expression leads to a reasonable estimate of the shear strength of reinforced concrete slabs which are simply supported over circular openings, within the limits of the Diameter/Thickness ratio of 2.35 to 5.6.			

Unclassified

Security Classification

14 KEY WORDS	LINK A		LINK B		LINK C	
	ROLE	WT	ROLE	WT	ROLE	WT
Reinforced Concrete Slabs; Thick Slabs; Shear Failures; Protective Construction; Composite Slabs; Weapons Effects; Dynamic Loading; Missile Silo Closures						

DD FORM 1473 (BACK)

NOV 68
S/N 0101-507-6921

Unclassified

Security Classification

A-31409